BEILSTEIN JOURNAL OF ORGANIC CHEMISTRY

Cyclodextrins as building blocks for new materials

Edited by Sophie Fourmentin and Miriana Kfoury



Generated on 02 November 2026, 02:53

Imprint

Beilstein Journal of Organic Chemistry
www.bjoc.org
ISSN 1860-5397
Email: journals-support@beilstein-institut.de

The *Beilstein Journal of Organic Chemistry* is published by the Beilstein-Institut zur Förderung der Chemischen Wissenschaften.

Beilstein-Institut zur Förderung der Chemischen Wissenschaften
Trakehner Straße 7–9
60487 Frankfurt am Main
Germany
www.beilstein-institut.de

The copyright to this document as a whole, which is published in the *Beilstein Journal of Organic Chemistry*, is held by the Beilstein-Institut zur Förderung der Chemischen Wissenschaften. The copyright to the individual articles in this document is held by the respective authors, subject to a Creative Commons Attribution license.

The cover image, copyright 2023 Miriana Kfoury, Marc Fourmentin and Sophie Fourmentin, is licensed under the Creative Commons Attribution 4.0 license (https://creativecommons.org/licenses/by/4.0). The reuse, redistribution or reproduction requires that the author, source and license are credited.

BEILSTEIN JOURNAL OF ORGANIC CHEMISTRY

Cyclodextrins as building blocks for new materials

Miriana Kfoury and Sophie Fourmentin*

Editorial

Open Access

Address:
Université du Littoral Côte d'Opale, Unité de Chimie Environnementale et Interactions sur le Vivant (UCEIV, UR 4492), 59140 Dunkerque, France

Email:
Sophie Fourmentin* - lamotte@univ-littoral.fr

* Corresponding author

Keywords:
building blocks; cyclodextrins; new materials

Beilstein J. Org. Chem. **2023,** *19,* 889–891.
https://doi.org/10.3762/bjoc.19.66

Received: 01 June 2023
Accepted: 12 June 2023
Published: 19 June 2023

This article is part of the thematic issue "Cyclodextrins as building blocks for new materials".

Guest Editor: S. Fourmentin



© 2023 Kfoury and Fourmentin; licensee Beilstein-Institut.
License and terms: see end of document.

The continuous increase in the number of publications carried out on cyclodextrins (CDs) and their market growth are clear evidence of the undying interest in these macrocycles discovered in 1891 [1]. It seems that these supramolecules still have not revealed all their secrets and are still stimulating curiosity in fundamental and applied research. CDs are the most studied supramolecular hosts. They provide the most extensive database on molecular recognition in the literature, with more than 100,000 publications [2]. CDs owe their success not only to the unique molecular structure [3], which allows them to act as host compounds, but also to their biodegradability [4], negligible toxicity, and excellent safety profile [5]. In addition, CDs offer a further step towards sustainability, making them suitable for a wide range of uses in various fields. Accordingly, the global market size of CDs is expected to grow to nearly US$ 390 million by 2027, registering consequently a compound annual growth rate of 5.5% from 2021. The CD market was not affected by the COVID-19 pandemic and had in fact experienced a strong increase. This was due to the favorable environment for the CD market created by the increasing demand for pharmaceuticals containing CDs. Three clinical trials have demonstrated the use of CDs in the treatment of COVID-19. Two of them use the sulfobutyl ether β-CD/remdesivir inclusion complex and the third applies the α-CD/sulforaphane inclusion complex called Sulforadex® [6]. The approved Janssen vaccine against SARS-CoV-2 infection (Ad26.COV2.S) was also a milestone for CD research and has served as a large-scale safety test for 2-(hydroxypropyl)-β-CD (HP-β-CD). CDs have also been used to functionalize face mask textiles to block and inactivate bacteria and viruses [7].

Apart from the COVID-19 pandemic, CDs are well represented in the pharmaceutical market, in at least 130 marketed products [2]. Examples of the use of CDs in medicines are β-CD in cetirizine tablets and cisapride suppositories, γ-CD in a minoxidil solution, HP-β-CD in itraconazole antifungal, in intravenous and oral solutions, sulfobutyl ether β-CD in intravenous voriconazole antimycotic, and randomly methylated β-CD in a nasal spray for hormone replacement therapy with 17β-estradiol.

Yet, the current interest goes far beyond the simple use of CDs as a delivery system for therapeutic agents. Current research interests focus on the intrinsic activity of CDs as well as their derivatives and polymers. One of the biggest discoveries in this field is the observation that the solubilizer HP-β-CD is effec-

tive against Niemann–Pick type C disease (NPC) and is in phase 2b/3 clinical trials [8]. It has also been suggested that CDs may have beneficial effects on other neurodegenerative diseases, such as Alzheimer's, Parkinson's, and Huntington's diseases. Due to their ability to extract cholesterol, treatment with CDs could reduce atherogenesis and atherosclerotic plaque size by solubilizing cholesterol crystals [9]. In addition, CDs can sequester cholesterol and lipids from viruses and envelopes and provide virucidal and bactericidal activity against a wide range of microorganisms [10]. Altogether, these findings highlight the ability of CDs to act as potential active pharmaceutical ingredients, which may influence the current regulatory framework for the use of CDs and further stimulate their market.

The exploration of the potential of inclusion complexation is not limited to the biomedical field. CDs are renewable and biodegradable materials that enable green and environmental biotechnologies for all applications [11]. The ability of CDs to act as solubilizers, stabilizers, permeation enhancers, cryoprotectors, sequestrants of toxic compounds, taste and odor maskers, coating materials of solid surfaces, and chiral receptors has been successfully explored in food, packaging, cosmetics, textiles, separation processes, environmental remediation, extraction, and catalysis [2,5,12].

Molecular encapsulation is not the only application area for these macrocyclic components at present. CDs are versatile molecules. Their 3D structure makes them exceptional building blocks for the design of innovative supramolecular architectures due to the differential reactivity of their alcohol functions. This allows regioselective chemical modification at either the primary or secondary rim [13]. As a result, these molecular hosts can be specifically linked either covalently or noncovalently to a wide variety of ligands. CDs are a significant part of almost all areas of science that require high performance with minimal environmental impact. They are involved in the construction of interlocked molecules (rotaxanes and catenanes), supramolecular polymers, artificial enzymes, hydrogels, metal–organic frameworks, supramolecular solvents, fibers, nanotubes, nanoparticles, and so on [14-17]. In addition to bearing a rigid skeleton, CDs act as versatile multitasking agents. They add value to these composites as their cavities remain generally available to accommodate active substances, or they work as supramolecular catalysts or molecular concealers.

Due to the fact that CDs are nontoxic to humans and to the environment and used to develop greener synthetic routes and strategies, CD-based materials are considered safe and environmentally friendly [18]. This includes, among other characteristics, that they are edible, biodegradable, ecological, and biocompatible. Thus, these supra-architectures have a multitude of uses in food, biomedicine, regenerative medicine, cosmetics, molecular electronics, polymer chemistry, gold recovery, gas absorption, depollution, biochemical material sciences, nanotechnology, self-healing materials, 3D printing, and so on [19-21].

We hope that you will enjoy consulting the articles in this thematic issue and that you will gain new insights to help advance CD-based materials, which are burgeoning on several fronts and are likely to continue to push the boundaries in all areas of applications and beyond. We are extremely grateful to all the researchers who contributed to this issue and thankful to the Editorial Team at the Beilstein-Institut for their kind assistance and support.

Miriana Kfoury and Sophie Fourmentin

Dunkerque, June 2023

ORCID® iDs

Miriana Kfoury - https://orcid.org/0000-0003-3436-6943
Sophie Fourmentin - https://orcid.org/0000-0002-4334-0051

References

1. Morin-Crini, N.; Fourmentin, S.; Fenyvesi, É.; Lichtfouse, E.; Torri, G.; Fourmentin, M.; Crini, G. *Environ. Chem. Lett.* **2021,** *19,* 2581–2617. doi:10.1007/s10311-020-01156-w
2. Loftsson, T.; Sigurdsson, H. H.; Jansook, P. *Materials* **2023,** *16,* 2223. doi:10.3390/ma16062223
3. Crini, G. *Chem. Rev.* **2014,** *114,* 10940–10975. doi:10.1021/cr500081p
4. Verstichel, S.; De Wilde, B.; Fenyvesi, E.; Szejtli, J. *J. Polym. Environ.* **2004,** *12,* 47–55. doi:10.1023/b:jooe.0000010050.52967.94
5. Trotta, F.; Loftsson, T.; Gaud, R. S.; Trivedi, R.; Shende, P. *Carbohydr. Polym.* **2022,** *295,* 119880. doi:10.1016/j.carbpol.2022.119880
6. Almeida, B.; Domingues, C.; Mascarenhas-Melo, F.; Silva, I.; Jarak, I.; Veiga, F.; Figueiras, A. *Int. J. Mol. Sci.* **2023,** *24,* 2974. doi:10.3390/ijms24032974
7. Maton, M.; Gabut, S.; Neut, C.; Odou, P.; Sacareau, C.; Pinon, A.; Vialette, M.; Gerber, G.; Martel, B.; Blanchemain, N. *Biomater. Sci.* **2023,** *11,* 3502–3511. doi:10.1039/d2bm01988d
8. Davidson, C. D.; Ali, N. F.; Micsenyi, M. C.; Stephney, G.; Renault, S.; Dobrenis, K.; Ory, D. S.; Vanier, M. T.; Walkley, S. U. *PLoS One* **2009,** *4,* e6951. doi:10.1371/journal.pone.0006951
9. Agnes, M.; Pancani, E.; Malanga, M.; Fenyvesi, E.; Manet, I. *Macromol. Biosci.* **2022,** *22,* 2200090. doi:10.1002/mabi.202200090
10. Braga, S.; Barbosa, J.; Santos, N.; El-Saleh, F.; Paz, F. *Pharmaceutics* **2021,** *13,* 409. doi:10.3390/pharmaceutics13030409
11. Fenyvesi, É.; Sohajda, T. *Environ. Sci. Pollut. Res.* **2022,** *29,* 20085–20097. doi:10.1007/s11356-021-18176-w
12. Crini, G.; Cosentino, C.; Bradu, C.; Fourmentin, M.; Torri, G.; Ruzimuradov, O.; Alaton, I. A.; Tomei, M. C.; Derco, J.; Barhoumi, M.; Prosen, H.; Malinović, B. N.; Vrabeľ, M.; Huq, M. M.; Soltan, J.; Lichtfouse, E.; Morin-Crini, N. *Environ. Chem. Lett.* **2022,** *20,* 2597–2628. doi:10.1007/s10311-022-01438-5

13. Liu, J.; Wang, B.; Przybylski, C.; Bistri-Aslanoff, O.; Ménand, M.; Zhang, Y.; Sollogoub, M. *Angew. Chem., Int. Ed.* **2021,** *60,* 12090–12096. doi:10.1002/anie.202102182
14. Roy, I.; Stoddart, J. F. *Acc. Chem. Res.* **2021,** *54,* 1440–1453. doi:10.1021/acs.accounts.0c00695
15. Kfoury, M.; Landy, D.; Fourmentin, S. *Curr. Opin. Green Sustainable Chem.* **2022,** *36,* 100630. doi:10.1016/j.cogsc.2022.100630
16. Hashidzume, A.; Yamaguchi, H.; Harada, A. *Eur. J. Org. Chem.* **2019,** 3344–3357. doi:10.1002/ejoc.201900090
17. Jain, M.; Nowak, B. P.; Ravoo, B. J. *ChemNanoMat* **2022,** *8,* e202200077. doi:10.1002/cnma.202200077
18. Cecone, C.; Hoti, G.; Krabicová, I.; Appleton, S. L.; Caldera, F.; Bracco, P.; Zanetti, M.; Trotta, F. *Green Chem.* **2020,** *22,* 5806–5814. doi:10.1039/d0gc02247k
19. Ponchel, A.; Monflier, E. *Nat. Commun.* **2023,** *14,* 1283. doi:10.1038/s41467-023-36700-z
20. Velessiotis, D.; Maffeo, D.; Millios, C.; Makarona, E.; Viswanathan, C.; Yannakopoulou, K.; Mavridis, I.; Pikramenou, Z.; Glezos, N. *Phys. Status Solidi A* **2008,** *205,* 2532–2535. doi:10.1002/pssa.200780194
21. Alvarez-Lorenzo, C.; García-González, C. A.; Concheiro, A. *J. Controlled Release* **2017,** *268,* 269–281. doi:10.1016/j.jconrel.2017.10.038

License and Terms

This is an open access article licensed under the terms of the Beilstein-Institut Open Access License Agreement (https://www.beilstein-journals.org/bjoc/terms), which is identical to the Creative Commons Attribution 4.0 International License (https://creativecommons.org/licenses/by/4.0). The reuse of material under this license requires that the author(s), source and license are credited. Third-party material in this article could be subject to other licenses (typically indicated in the credit line), and in this case, users are required to obtain permission from the license holder to reuse the material.

The definitive version of this article is the electronic one which can be found at:
https://doi.org/10.3762/bjoc.19.66

BEILSTEIN JOURNAL OF ORGANIC CHEMISTRY

Cyclodextrin-based Schiff base pro-fragrances: Synthesis and release studies

Attila Palágyi[1], Jindřich Jindřich[*1], Juraj Dian[2,3] and Sophie Fourmentin[4]

Full Research Paper

Open Access

Address:
[1]Department of Organic Chemistry, Faculty of Science, Charles University, Hlavova 8, CZ-128 43 Prague, Czech Republic, [2]Department of Chemical Physics and Optics, Faculty of Mathematics and Physics, Charles University, Ke Karlovu 3, 121 16, Prague 2, Czech Republic, [3]Department of Analytical Chemistry, Faculty of Science, Charles University, Hlavova 8, CZ-128 43, Prague, Czech Republic and [4]Unité de Chimie Environnementale et Interactions sur le Vivant (UCEIV), UR 4492 SFR Condorcet FR CNRS 3417, Université du Littoral-Côte d'Opale (ULCO), Dunkerque, France

Email:
Jindřich Jindřich[*] - jindrich.jindrich@natur.cuni.cz

* Corresponding author

Keywords:
aldehyde; controlled release; cyclodextrin; imine; kinetics; pro-fragrance; Schiff base

Beilstein J. Org. Chem. **2022,** *18,* 1346–1354.
https://doi.org/10.3762/bjoc.18.140

Received: 29 July 2022
Accepted: 06 September 2022
Published: 28 September 2022

This article is part of the thematic issue "Cyclodextrins as building blocks for new materials".

Associate Editor: H. Ritter

© 2022 Palágyi et al.; licensee Beilstein-Institut.
License and terms: see end of document.

Abstract

A simple method for the preparation of β-cyclodextrin derivatives containing covalently bonded aldehydes via an imine bond was developed and used to prepare a series of derivatives from 6^{I}-amino-6^{I}-deoxy-β-cyclodextrin and the following volatile aldehydes – cinnamaldehyde, cyclamen aldehyde, lilial, benzaldehyde, anisaldehyde, vanillin, hexanal, heptanal, citral, and 5-methylfurfural. Subsequently, the rate of release of the volatile compound from selected pro-fragrances, as a function of the environment (solvent, pH), was studied by ^{1}H NMR spectroscopy (for benzaldehyde) and static headspace-gas chromatography (for benzaldehyde, heptanal, and 5-methylfurfural). The aldehyde release rate from the imine was shown to depend substantially on the pH from the solution and the air humidity from the solid state.

Introduction

The fragrance and flavor industry is one of the most intensively developing sectors of the chemical industry. Encapsulation techniques are widely used in both food and cosmetic industries to control the delivery of the encapsulated guest molecules and protect those agents from environmental degradation [1,2]. Cyclodextrins (CDs) serve as one of the simplest encapsulating systems. CDs are cyclic oligosaccharides composed of 1→4 linked α-D-glucopyranose units (6, 7, and 8 for the most common α-, β-, and γ-CD). CDs are well known for their hydrophilic outer surface and hydrophobic cavity. This cavity can

encapsulate another lipophilic guest molecule and thus form an inclusion complex [3,4]. This phenomenon is reversible and leads to an equilibrium between encapsulated and free guest.

A staggering number of inclusion complexes of CDs with various organic molecules have been described so far. It was proved that the complexation of volatile organic compounds, such as aldehydes, into the CD's cavity reduces the volatility and increases the solubility and bioavailability of these compounds [5-14]. The release of the included molecule from the CD's cavity takes from minutes to hours, depending on the environmental conditions as well as on the structure of the molecule. The prolongation of the release time of the complexed compounds would make significant progress in fragrance delivery as well as in an odor and flavor control; it could be used to improve the stabilization, quality, efficiency and persistence of repellents, disinfectants, perfumes, laundry detergents and flavoring agents [15,16].

Another strategy to prolong the longevity of the fragrance and, as an additional benefit, to increase the stability of labile compounds is to prepare pro-fragrances in analogy with the concept of pro-drugs developed for pharmaceutical applications. The fragrance is linked covalently to a substrate that will release the fragrance under defined chemical conditions. For applications in the fragrance and flavor industry, the covalent bond that links the fragrance to its substrate must be cleaved under environmental conditions found in everyday life, and the substrate should be non-volatile and non-toxic [17]. Typical triggers that may be used for mild chemical reactions are temperature, enzymatic or pH-dependent hydrolysis, oxidation, or light (Figure 1) [18]. Different substrates were used to synthesize pro-fragrances, like polymers [19], ionic liquids [20], rotaxanes [21], or saccharides [22].

To the best of our knowledge, no studies investigate the use of CDs as substrate. Linking the fragrance to CDs could present an advantage compared to simple encapsulation and to other substrates as they will not only ensure very low volatility of the obtained pro-fragrance but also be able to encapsulate the guest after the cleavage of the covalent bond, leading to a two-in-one system. Indeed, encapsulation in CDs is known to modify and/or improve the physical and chemical properties of the included guest, ensuring the protection of labile molecules from photodegradation or oxidation [3,6,23]. Moreover, many CD derivatives are available, opening the possibility of using different chemical functions (ester, imine…) to attach the fragrance covalently with various functional groups. Additionally, CDs already occur in many daily products [16] and fulfill the requirements of biocompatibility and cost for designing pro-fragrances that could find applications in the flavor and fragrance industry [18].

In this article, we describe the synthesis of ten pro-fragrances – Schiff bases prepared from amino-β-cyclodextrin and common volatile aldehydes. Aldehydes constitute a prominent class of molecules broadly used as food product additives and are also key components of perfumes [24]. They were therefore chosen as an example of flavor compounds. The imine bond was chosen for its relative stability; on the other hand, it can be readily hydrolyzed forming the starting non-volatile amine and releasing the aldehyde. The kinetics of the aldehyde release was studied by ^{1}H NMR techniques in buffers with different pH values. The aldehyde release itself from the buffers and by humidity was followed by static headspace-gas chromatography (SH-GC).

Results and Discussion

Synthesis of pro-fragrances

6^I-Amino-6^I-deoxy-β-cyclodextrin (amino-β-CD, **1**) was chosen as the most appropriate amino-cyclodextrin derivative due to its easiest accessibility; besides, β-CD forms usually the strongest inclusion complexes compared to α-CD and γ-CD. The amino-β-CD was prepared according to published procedures [25-27].

Common commercially available volatile aldehydes **2a–j** (Figure 2) were chosen as the aldehyde reactants. Some of the aldehydes were mixtures of isomers, but it was acceptable for our intended purpose – to study the controlled release of the aldehydes, i.e., volatile organic compounds (VOCs).

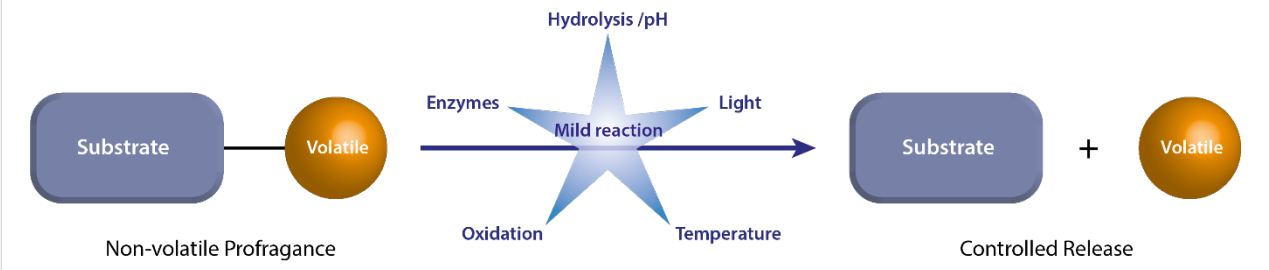


Figure 1: Concept of the controlled release of volatile organic molecules from pro-fragrances [18].

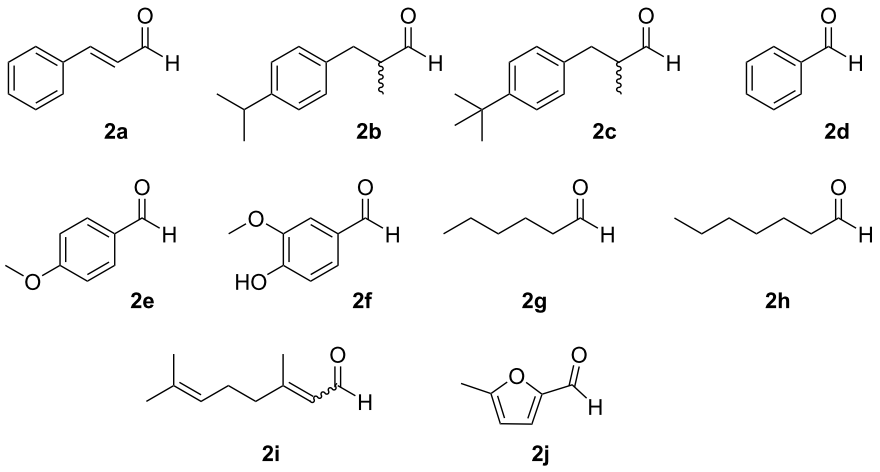


Figure 2: The common commercially available aldehydes used for binding to amino-β-CD (**1**): *trans*-cinnamaldehyde (**2a**), cyclamen aldehyde (**2b**), lilial (**2c**), benzaldehyde (**2d**), anisaldehyde (**2e**), vanillin (**2f**), hexanal (**2g**), heptanal (**2h**), citral (**2i**), 5-methylfurfural (**2j**).

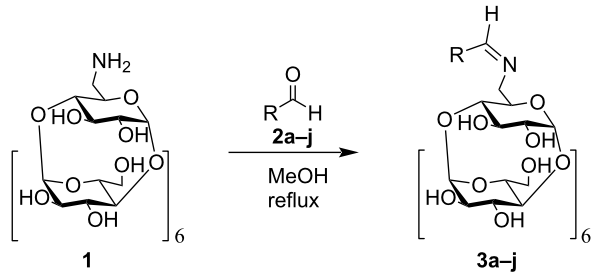
The aldehyde selected for the optimization of reaction conditions was cinnamaldehyde (**2a**), as it is strongly UV absorbing, i.e., easy to follow by TLC. But in the end, the reaction progress was monitored by MS due to the fast hydrolysis of the imine even during the chromatography on TLC plates. Methanol was chosen as a solvent because it dissolves the aldehydes well and sufficiently (≈5 mg/mL) amine **1**.

At first, we studied the influence of adding hygroscopic salts ($MgSO_4$, $LiClO_4$, or $Ca(ClO_4)_2$), triethyl orthoformate, or activated molecular sieves to the reaction. These compounds could function as desiccants removing the water formed during the reaction, as well as catalysts; nevertheless, the conversion to the final imine needed, in all cases, a large excess of an aldehyde.

Finally, the best reaction conditions for the large-scale preparation of target compounds proved to be just refluxing of amine **1** with up to 30-fold excess of the aldehydes **2a**–**j** in methanol (Scheme 1), which afforded the final imines **3a**–**j** in high yields (80–97%).

This method allows for easy recovery of the unreacted aldehyde as well as separation of the product (just by extraction by hexane and drying under reduced pressure) without its decomposition. The structure of the final imines was confirmed by ^{1}H NMR, ^{13}C NMR, ESI–MS, and the release of the VOCs was next studied by ^{1}H NMR and SH-GC for selected imino-β-CD.

The prepared imines could also be mixtures of *E*/*Z* isomers, but no attempts were made to isolate them for the reason metioned above. Also, the prepared imines proved to be difficult to purify by chromatographic methods due to their low stability towards hydrolysis.



Scheme 1: Preparation of the Schiff bases from amino-β-CD **1** and aldehydes **2a–j**. Yields: **3a**, 96%; **3b**, 83%; **3c**, 91%; **3d**, 86%; **3e**, 82%; **3f**, 96%; **3g**, 89%; **3h**, 97%; **3i**, 80%; **3j**, 83%.

Kinetic studies of the imine hydrolysis by NMR

For the kinetic studies of the hydrolysis of imino-CDs, we selected the pro-fragrance **3d** made from the most common aldehyde – benzaldehyde. The release of the benzaldehyde (**2d**) was studied by ^{1}H NMR spectroscopy. Aqueous 0.1 M phosphate buffer solutions of pH 1.08, 2.00, 3.00, 4.00, 5.00, 6.00, 7.00, 8.00, 9.00, 10.00 11.00, 12.00, and 12.80 were prepared (see Experimental section) using deuterium oxide instead of water to facilitate NMR spectroscopy experiments. Because of the low solubility of the pro-fragrance in water, it had to be dissolved in deuterated dimethyl sulfoxide. Then, the buffer solution was added and mixed in a 1:1 (v/v) ratio just before starting the measurements. The samples were kept at ambient temperature (20–25 °C).

All measurements for a given pH value were repeated at least three times with about 10 mg of the pro-fragrance **3d**. For the pH in the range 1.08–4.00, the samples were taken and measured in intervals from 2 min up to 24 h for several days, the remaining samples with higher pH were measured in 2 h to several day intervals for up to three months. The integrals of the signal at 8.30 ppm (hydrogen of the imine group of Schiff base) were compared to the integral of the signal belonging to the same proton of the starting compound **3d** measured in DMSO-d_6 (without a buffer) used as a blank.

We note that the experiment was conducted in a closed system with a 50% content of DMSO-d_6 to enable dissolution of the pro-fragrance, which influenced the equilibrium between dissociation and formation reactions. The integrals of the imine group signal at 8.30 ppm measured at various time intervals were depicted as a function of time for all the samples with pH from 3 to 12.8. Data were fitted by a nonlinear regression method (Levenberg–Marquardt algorithm) using both mono- and double-exponential functions (Microcal Origin software). In most cases, the double-exponentials described the observed behavior much better (see Supporting Information File 1, Figures S1–S11). Experimental data were fitted with the double-exponential function of the form:

$$I = I_0 + I_1 e^{-((t-t_0)/t_1)} + I_2 e^{-((t-t_0)/t_2)} \quad (1)$$

where I_0, I_1, and I_2 are fitting parameters corresponding to the integrated areas of the background and corresponding time components, t_0 is a parameter related to the correction of zero time, and t_1 and t_2 are time constants of the slow and fast components of the double-exponential decay curve.

A typical example of the time decay of the integral of the imine signal area for the sample at pH 9 is depicted in Figure 3.

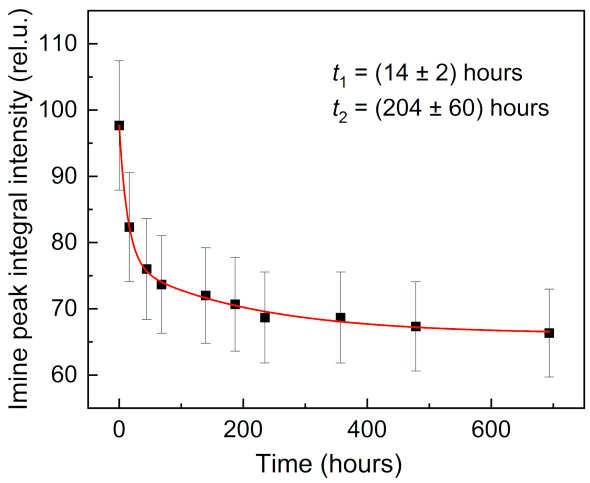


Figure 3: The integrals of the imine group proton signal at 8.30 ppm in the acquired ^{1}H NMR spectrum of compound **3d** at pH 9 as a function of time. Time constants t_1 and t_2 correspond to the fast and slow components of the double-exponential decay function. The red line is the corresponding fit of the experimental data by Equation 1.

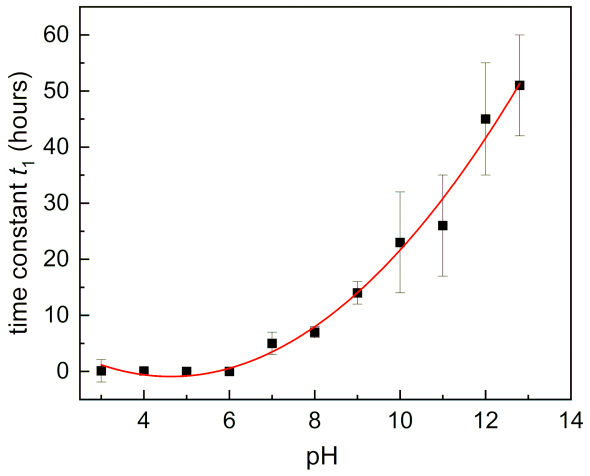


Figure 4: pH behavior of the time constant t_1 of the fast component in the time evolution of the NMR signal of the imine group of the compound **3d**. Error bars correspond to the regression error; red line corresponds to the polynomial fit of the experimental data.

For lower pH values (pH 1 and 2), the hydrolysis was too fast to be investigated by ^{1}H NMR spectroscopy; the experimental data are summarized in Table S1 in Supporting Information File 1. To visualize the pH dependence of the time decay of the integral of the imine group, we chose the time constant of the fast component t_1 and depicted it as a function of pH (Figure 4).

Figure 4 shows that the pH behavior of t_1 component is nearly monotonic (except for low pH values). A substantial difference is seen between acidic conditions, under which the imino-β-CD is unstable, and the benzaldehyde releases fast over the time course investigated, and basic conditions, under which the benzaldehyde is released slowly. In all cases, equilibrium between the hydrolyzed and the non-hydrolyzed pro-fragrance is obtained – the more acidic the solution is, the equilibrium is reached faster, and the imine is hydrolyzed to a higher degree. For pH 1 and 2 the hydrolysis degree is about 90%, which decreases with the pH rising.

It has to be noted that during the NMR studies, no degradation of the cyclodextrin was detected with the available methods. At pH of 11.00, 12.00 and 12.80, a decrease and later (in the case of pH 12.80) a total disappearing of the hydrogen signal of the aldehyde group of benzaldehyde at 10.06 ppm was observed

due to Cannizaro's reaction. At pH 12.80, the benzaldehyde was fully converted to benzyl alcohol and benzoic acid after 5 days.

Static headspace analysis

We first determined the Henry law constants and the formation constants with β-CD of three selected aldehydes (Table 1). As can be seen from Table 1, the studied aldehydes exhibit Henry law constant <1. The obtained formation constants are in good agreement with values obtained for aromatic or linear flavors [28].

Multiple headspace extraction experiments were performed to follow the release of the aldehydes. This technique was already successfully used to follow the release of flavor in solution or solid state [29-31]. The aldehyde release was studied using three different sampling time intervals corresponding to three time regions I, II, and III, in Figures 5–7. This experiment mode enabled better observation of the trends in the change of the aldehyde headspace concentrations at different sampling times and pH.

First, we follow the release of heptanal in aqueous buffer solutions (Figure 5A). We can observe a decrease of the area due to the depletion of the aldehyde in the aqueous solution after successive extractions, while the release of heptanal from heptanylimino-β-CD is more sustained (Figure 5B). Similar behavior at various pH conditions could be observed in the case of the release of benzaldehyde (**2d**) from the phosphate buffer (Figure 6A) and benzylimino-β-CD (**3d**, Figure 6B) and 5-methylfurfural (**2j**) from the phosphate buffer (Figure 7A) and 5-methylfurfurylimino-β-CD (**3j**, Figure 7B).

Figures 5–7 show that the aldehyde release from the β-CD imino derivatives was slower than the release from the corresponding aldehyde aqueous phosphate buffers. This observation is consistent with the role of the physicochemical barrier that slows down the release of aldehyde due to the supramolecular interaction between aldehyde and β-CD cavity.

It follows from Figures 5–7 that heptanal (**2h**) is released faster with lower pH values, whereas benzaldehyde (**2d**) and 5-methylfurfural (**2j**) show opposite trends. It can be attributed to the lower boiling point (153 °C) and lower hydrophilicity (log*P* 2.5) of the aliphatic heptanal compared to the two aromatic aldehydes with higher boiling points (179 °C, 187 °C) and more than an order of magnitude higher hydrophilicity

Table 1: Henry law constants and formation constants with β-CD (M^{-1}) of the three selected aldehydes (30 °C, aqueous solution).

aldehyde	benzaldehyde (**2d**)	heptanal (**2h**)	5-methylfurfural (**2j**)
H_c	0.10	0.16	0.02
K_f	103	452	61

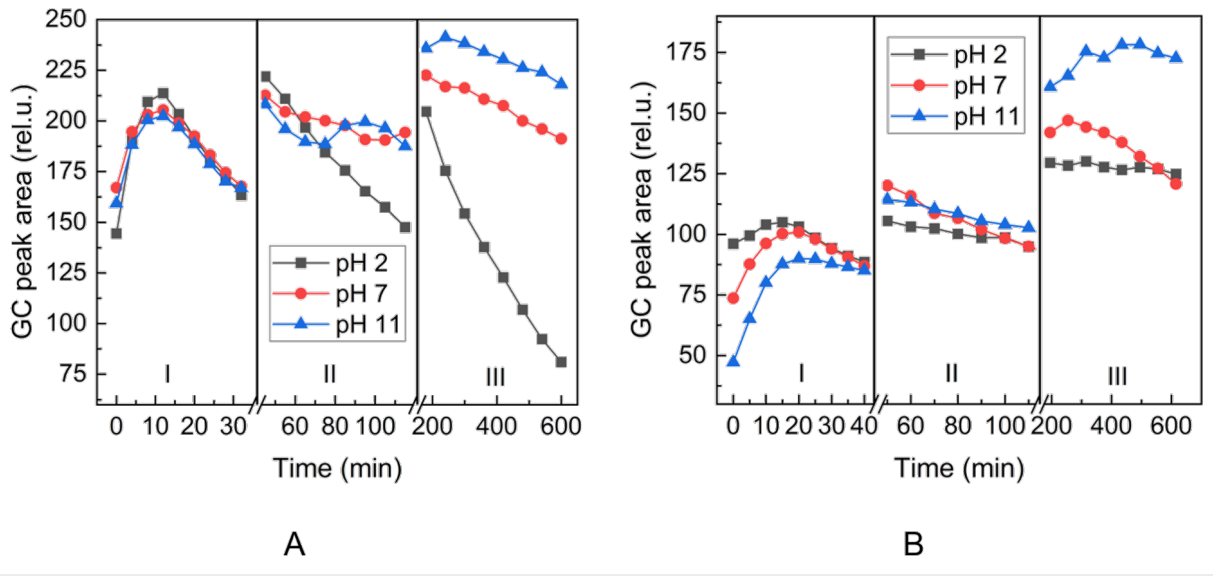


Figure 5: Time evolution of the headspace concentration of heptanal (**2h**) after successive extractions from the gaseous phase above (A): heptanal (**2h**) in aqueous phosphate buffers and (B): heptanylimino-β-CD (**3h**) in aqueous phosphate buffers. Sampling intervals in the corresponding regions: I – 4 min (A) or 5 min (B), II – 10 min, III – 60 min.

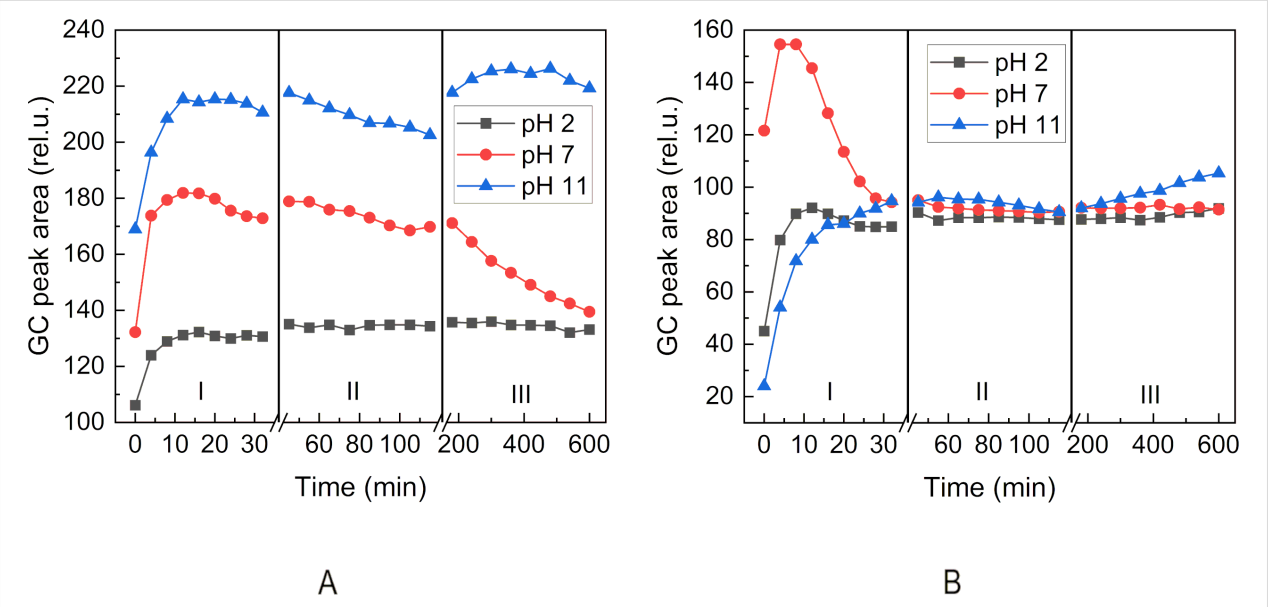


Figure 6: Time evolution of the headspace concentration of benzaldehyde (**2d**) after successive extractions from the gaseous phase above (A): benzaldehyde (**2d**) in aqueous phosphate buffers and (B): benzylimino-β-CD (**3d**) in aqueous phosphate buffers. Sampling intervals in the corresponding regions: I – 4 min, II – 10 min, III – 60 min.

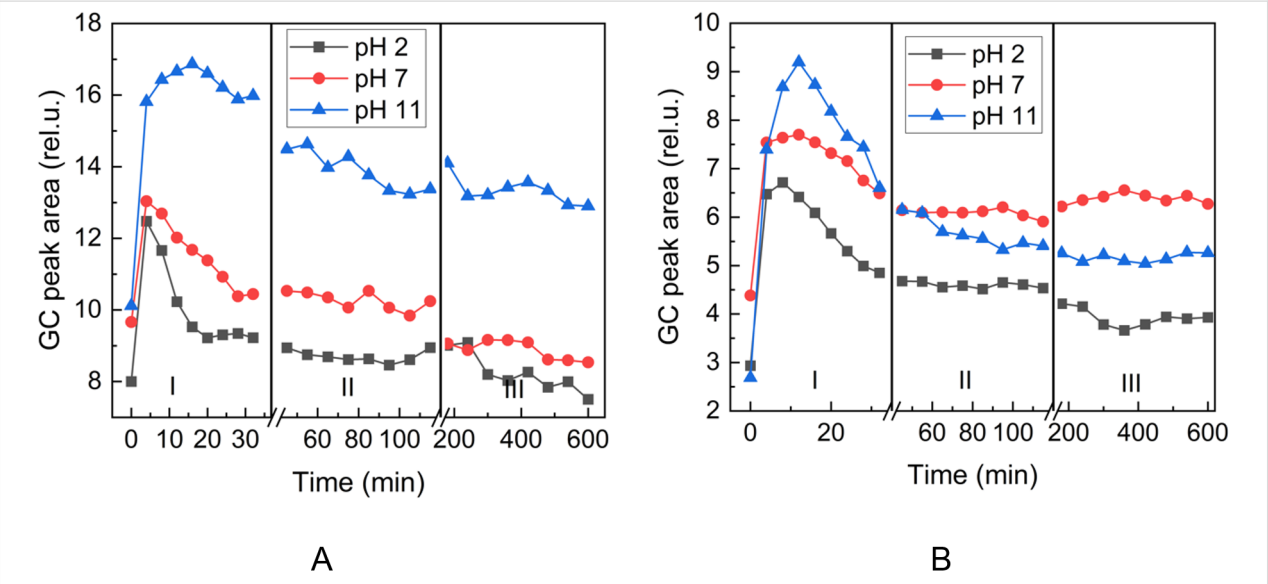


Figure 7: Time evolution of the headspace concentration of 5-methylfurfural (**2j**) after successive extractions from the gaseous phase above (A): 5-methylfurfural (**2j**) in aqueous phosphate buffers and (B): 5-methylfurfurylimino-β-CD (**3j**) in aqueous phosphate buffers. Sampling intervals in the corresponding regions: I – 4 min, II – 10 min, III – 60 min.

(log*P* 1.48, 0.654) (physical properties values taken from chemspider.com).

Finally, the release of 5-methylfurfural (**2j**) from 5-methylfurfurylimino-β-CD (**3j**) was monitored at different humidity (RH%). In this case, a powder of 5-methylfurfurylimino-β-CD (**3j**) was placed in a small vial and exposed to different RH%. As we can see from Figure 8, humidity is necessary to trigger the release of the volatile aldehyde as the amount of released volatile increased with the RH%. In this experiment, we also observed a sustained release of the volatile compound from the imino-β-CD.

Conclusion

Here a new family of pro-fragrances using CD as substrate was prepared for the first time. A general, simple, and high-yielding

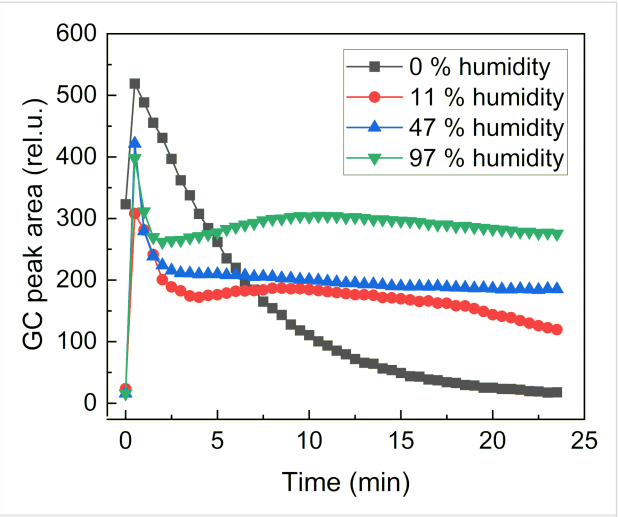


Figure 8: Evolution of the area of 5-methylfurfural released from 5-methylfurfurylimino-β-CD (**3j**) upon time after successive extractions of the gaseous phase at different RH% values.

method for their preparation was developed – Shiff base pro-fragrance is formed by refluxing amino-β-CD with an excess of a volatile aldehyde in methanol and purified just by extraction. The use of CD is interesting as it acts as a double barrier carrier for fragrance aldehyde molecules. We illustrated that CD-based pro-fragrances combine a chemical barrier, as the aldehydes are linked to the CD via imine bond, and a physicochemical (supramolecular) barrier, as we established that aldehydes formed inclusion complexes in aqueous solution with β-CD. We confirmed from the NMR kinetic study of the imine bond decomposition that Shiff base hydrolysis is very fast in acidic conditions and slows down when going to higher pH values. Multiple headspace extraction experiments revealed the role of pH and the presence of supramolecular interaction between aldehyde and β-CD on the rate of aldehyde release from the system. Sustained release of the aldehyde was demonstrated both in aqueous solutions and from a solid state upon humidity exposure.

Experimental

Instruments, general methods, and chemicals

^{1}H NMR, ^{13}C NMR, 2D NMR (H,H-COSY, HSQC, and HMBC) were measured on Bruker AVANCE III 600 MHz (600.17 MHz for ^{1}H, 150.04 MHz for ^{13}C) and Varian ^{UNITY}INOVA 400 (399,95 MHz for ^{1}H and 100,58 MHz for ^{13}C) spectrometers. For the kinetic studies, the ^{1}H NMR spectra were acquired on a Varian VNMRS 300 spectrometer (300 MHz for ^{1}H). DMSO-d_6 and D_2O were used as the solvents. The chemical shift values (δ) are given in ppm, and the values of the interaction constants (J) in Hz. Standard numbering for cyclodextrin's glucose units and numbering with apostrophes for substituents were used to assign NMR signals.

Static headspace-gas chromatography measurements were conducted with an Agilent headspace autosampler. Henry law constants (H_c) were determined as described previously [32,33]. Briefly, the same amount of aldehyde was added to vials containing different amounts of water. Using the phase ratio variation method as described by Kolb and Ettre [34], the values of H_c were determined by the relationship between the reciprocal chromatographic peak areas and the vapor–liquid volumetric ratio. The formation constant values were determined as described in previous works [28,35,36].

To study the release of aldehydes from aqueous buffered solutions, 10 mL of 0.1 M aqueous phosphate buffers were introduced into a 22 mL headspace vial, then 4 mg of compounds **3** were introduced in the vial, immediately sealed using silicone septa and aluminum foil, and analyzed by multiple headspace extraction at 30 °C. To evaluate the effect of humidity, 4 mg of compound **3** was put in a small (2 mL) vial, which was embedded into a 22 mL headspace vial containing 1 mL of saturated salt solution to obtain the given percentage of humidity at 60 °C and sealed using silicone septa and aluminum foil. Saturated K_2SO_4, KNO_3, and LiCl salt solutions were used to obtain 97, 47, and 11% of humidity, respectively. The samples were then immediately analyzed by MHE at 60 °C. 1 mL of vapor from the above solution was withdrawn from the vial using a gas-tight syringe and injected directly into the chromatographic column via a transfer line (250 °C). Each sample was then analyzed by gas chromatography (Perkin Elmer Autosystem XL equipped with a flame-ionization detector using a DB624 column). The GC settings were set as follows: detector temperature, 250 °C; column temperature: 160 °C for benzaldehyde and 5-methylfurfural and 120 °C for heptanal. The retention times under the given conditions were 2.1 min for benzaldehyde (**2d**) and 5-methylfurfural (**2j**) and 3.1 min for heptanal (**2h**).

The mass spectra were measured by the Bruker ESQUIRE 3000 ES-ion trap and the samples were ionized using an electrospray technique (ESI). The samples were dissolved in methanol.

Specific optical rotation was measured by the Rudolph Research AUTOPOL™ III Polarimeter at 25 °C and at the wavelength of the sodium doublet. Specific optical rotation values ($[\alpha]_D^{25}$) are given in 10^{-1} cm^2·g^{-1}.

For evaporation of the solvents, a rotary vacuum evaporator from Büchi was used at temperatures up to 50 °C and a Glass oven B-528 Kugelrohr from Büchi at temperatures up to 110 °C.

For thin-layer chromatography (TLC) DC-Alufolien Kieselgel 60 F265 (Merck, Darmstadt, Germany) silica gel plates were

used. Carbonization in 50% sulfuric acid was used to detect the substances. An eluent mixture propanol/water/25% aqueous ammonia/ethyl acetate 6:3:1:1 (EM1) was used for TLC.

Anhydrous DMF was prepared by distillation with P_2O_5 at reduced pressure and was stored over molecular sieves 3 Å under argon atmosphere. Organic solvents were distilled before use. β-CD was purchased from WAKO Chemicals (Germany). Other reagents were purchased from common commercial sources and used without further purification (Sigma-Aldrich, Penta).

6^I-*O*-*p*-Toluenesulfonyl-β-cyclodextrin, 6^I-azido-6^I-deoxy-β-cyclodextrin, and 6^I-amino-6^I-deoxy-β-cyclodextrin (**1**) were prepared according to the published procedures [25-27]. NMR spectra were in agreement with the literature.

Kinetic studies of the imine hydrolysis by NMR

For the kinetic studies of the hydrolysis of imino-CDs, 6^I-benzylideneamino-6^I-deoxy-β-cyclodextrin (**3d**) was chosen. The release of the benzaldehyde was studied by ^{1}H NMR spectroscopy. Aqueous 0.1 M phosphate buffer solutions of pH 1.08, 2.00, 3.00, 4.00, 5.00, 6.00, 7.00, 8.00, 9.00, 10.00 11.00, 12.00, and 12.80 were prepared by mixing 0.1 M solutions of H_3PO_4, KH_2PO_4, K_2HPO_4, and K_3PO_4 in ratios given in Table 2 using deuterium oxide instead of distilled water to facilitate NMR spectroscopy experiments. The exact pH value was tuned with titration with the help of a pH meter. Because of the poor solubility of the pro-fragrance in water, it had to be dissolved in 0.5 mL of deuterated dimethyl sulfoxide. Then, the buffer solutions (0.5 mL) were added and mixed just before starting the measurements. The samples were kept at ambient temperature (20–25 °C). Every measurement for every pH value was repeated three times with about 10 mg of pro-fragrance **3d**. The measurement intervals of the benzaldehyde release by ^{1}H NMR spectroscopy were 2 min to 24 h for several days for the buffers with pH values from 1.08 to 4.00. For the rest of the buffers, the intervals were 2 h to several days for up to 3 months (for basic pH). The integrals of the signal at 8.30 ppm, corresponding to the hydrogen of the imine group of the non-hydrolyzed Schiff base, were compared to the integral of the signal corresponding to the same proton of the pro-fragrance measured in DMSO-d_6 (without buffer) used as a blank.

Table 2: Ratios of 0.1 M aqueous phosphates solutions used to prepare buffers of the specified pH.

pH	H_3PO_4	KH_2PO_4	K_2HPO_4	K_3PO_4
1.08	1	–	–	–
2.00	1	–	1	–
3.00	dropwise	1	–	–
4.00	–	1	dropwise	–
5.00	–	1	dropwise	–
6.00	–	10	1	–
7.00	–	15	5	3
8.00	–	3	17	dropwise
9.00	–	dropwise	1	–
10.00	–	–	1	dropwise
11.00	–	10	3	10
12.00	–	–	dropwise	1
12.80	–	–	–	1

The common procedure for preparation of CD imines **3**

Amino-β-CD **1** (≈0.2 mmol) and aldehyde **2** (up to 30 equiv) were refluxed in 100 mL of MeOH under argon overnight. The reaction was monitored by MS, and after the full conversion to imine, the solvent was evaporated. The unreacted aldehyde was extracted ten times with hexane (10 mL), and the product was dried in a Kugelrohr at 110 °C.

Supporting Information

Supporting Information File 1

Synthesis and characterization data for compounds **3a–f**. Experimental data of time evolutions of integral of the imine group proton signal at 8.30 ppm in the acquired ^{1}H NMR spectrum of the compound **3d** for various pH.
[https://www.beilstein-journals.org/bjoc/content/supplementary/1860-5397-18-140-S1.pdf]

Funding

The authors thank Erasmus + mobility program for the financial support of AP traineeship that resulted into the bachelor thesis: Palágyi, A. Cyclodextrin derivatives containing covalently bound volatile substances and studies of their release. Bachelor Thesis, Charles University, Czech Republic 2018.

ORCID® iDs

Jindřich Jindřich - https://orcid.org/0000-0003-3770-0214
Juraj Dian - https://orcid.org/0000-0002-3461-5797
Sophie Fourmentin - https://orcid.org/0000-0002-4334-0051

References

1. Reis, D. R.; Ambrosi, A.; Di Luccio, M. *Future Foods* **2022,** *5,* 100126. doi:10.1016/j.fufo.2022.100126
2. Cid-Samamed, A.; Rakmai, J.; Mejuto, J. C.; Simal-Gandara, J.; Astray, G. *Food Chem.* **2022,** *384,* 132467. doi:10.1016/j.foodchem.2022.132467

3. Crini, G.; Fourmentin, S.; Fenyvesi, É.; Torri, G.; Fourmentin, M.; Morin-Crini, N. *Environ. Chem. Lett.* **2018,** *16,* 1361–1375. doi:10.1007/s10311-018-0763-2
4. Szejtli, J. *Chem. Rev.* **1998,** *98,* 1743–1754. doi:10.1021/cr970022c
5. Ogata, Y.; Inoue, Y.; Ikeda, N.; Murata, I.; Kanamoto, I. *J. Mol. Struct.* **2020,** *1215,* 128161. doi:10.1016/j.molstruc.2020.128161
6. Kfoury, M.; Auezova, L.; Greige-Gerges, H.; Ruellan, S.; Fourmentin, S. *Food Chem.* **2014,** *164,* 454–461. doi:10.1016/j.foodchem.2014.05.052
7. Fourmentin, S.; Ciobanu, A.; Landy, D.; Wenz, G. *Beilstein J. Org. Chem.* **2013,** *9,* 1185–1191. doi:10.3762/bjoc.9.133
8. Kfoury, M.; Landy, D.; Auezova, L.; Greige-Gerges, H.; Fourmentin, S. *Beilstein J. Org. Chem.* **2014,** *10,* 2322–2331. doi:10.3762/bjoc.10.241
9. Marques, H. M. C. *Flavour Fragrance J.* **2010,** *25,* 313–326. doi:10.1002/ffj.2019
10. Kfoury, M.; Auezova, L.; Greige-Gerges, H.; Fourmentin, S. *Environ. Chem. Lett.* **2019,** *17,* 129–143. doi:10.1007/s10311-018-0783-y
11. Kfoury, M.; Landy, D.; Fourmentin, S. *Molecules* **2018,** *23,* 1204. doi:10.3390/molecules23051204
12. Kfoury, M.; Auezova, L.; Ruellan, S.; Greige-Gerges, H.; Fourmentin, S. *Carbohydr. Polym.* **2015,** *118,* 156–164. doi:10.1016/j.carbpol.2014.10.073
13. Kfoury, M.; Auezova, L.; Greige-Gerges, H.; Fourmentin, S. *Carbohydr. Polym.* **2015,** *131,* 264–272. doi:10.1016/j.carbpol.2015.06.014
14. Kfoury, M.; Landy, D.; Ruellan, S.; Auezova, L.; Greige-Gerges, H.; Fourmentin, S. *Food Chem.* **2017,** *236,* 41–48. doi:10.1016/j.foodchem.2016.12.086
15. Abril-Sánchez, C.; Matencio, A.; Navarro-Orcajada, S.; García-Carmona, F.; López-Nicolás, J. M. *Chem. Phys. Lipids* **2019,** *219,* 72–78. doi:10.1016/j.chemphyslip.2019.02.001
16. Morin-Crini, N.; Fourmentin, S.; Fenyvesi, É.; Lichtfouse, E.; Torri, G.; Fourmentin, M.; Crini, G. *Environ. Chem. Lett.* **2021,** *19,* 2581–2617. doi:10.1007/s10311-020-01156-w
17. Herrmann, A. *Chimia* **2017,** *71,* 414. doi:10.2533/chimia.2017.414
18. Herrmann, A. *Angew. Chem., Int. Ed.* **2007,** *46,* 5836–5863. doi:10.1002/anie.200700264
19. Tree-udom, T.; Wanichwecharungruang, S. P.; Seemork, J.; Arayachukeat, S. *Carbohydr. Polym.* **2011,** *86,* 1602–1609. doi:10.1016/j.carbpol.2011.06.074
20. Berton, P.; Shamshina, J. L.; Bica, K.; Rogers, R. D. *Ind. Eng. Chem. Res.* **2018,** *57,* 16069–16076. doi:10.1021/acs.iecr.8b02903
21. Lopez-Sanchez, J.; Alajarin, M.; Pastor, A.; Berna, J. *J. Org. Chem.* **2021,** *86,* 15045–15054. doi:10.1021/acs.joc.1c01725
22. Kuhnt, T.; Herrmann, A.; Benczédi, D.; Weder, C.; Foster, E. J. *RSC Adv.* **2014,** *4,* 50882–50890. doi:10.1039/c4ra07728h
23. Del Valle, E. M. M. *Process Biochem. (Oxford, U. K.)* **2004,** *39,* 1033–1046. doi:10.1016/s0032-9592(03)00258-9
24. Ribeaucourt, D.; Bissaro, B.; Lambert, F.; Lafond, M.; Berrin, J.-G. *Biotechnol. Adv.* **2022,** *56,* 107787. doi:10.1016/j.biotechadv.2021.107787
25. Trotta, F.; Martina, K.; Robaldo, B.; Barge, A.; Cravotto, G. *J. Inclusion Phenom. Macrocyclic Chem.* **2007,** *57,* 3–7. doi:10.1007/s10847-006-9169-z
26. Bonnet, V.; Duval, R.; Tran, V.; Rabiller, C. *Eur. J. Org. Chem.* **2003,** 4810–4818. doi:10.1002/ejoc.200300449
27. Muderawan, I. W.; Ong, T. T.; Lee, T. C.; Young, D. J.; Ching, C. B.; Ng, S. C. *Tetrahedron Lett.* **2005,** *46,* 7905–7907. doi:10.1016/j.tetlet.2005.09.099
28. Decock, G.; Landy, D.; Surpateanu, G.; Fourmentin, S. *J. Inclusion Phenom. Macrocyclic Chem.* **2008,** *62,* 297–302. doi:10.1007/s10847-008-9471-z
29. Ciobanu, A.; Mallard, I.; Landy, D.; Brabie, G.; Nistor, D.; Fourmentin, S. *Food Chem.* **2013,** *138,* 291–297. doi:10.1016/j.foodchem.2012.10.106
30. El Achkar, T.; Moura, L.; Moufawad, T.; Ruellan, S.; Panda, S.; Longuemart, S.; Legrand, F.-X.; Costa Gomes, M.; Landy, D.; Greige-Gerges, H.; Fourmentin, S. *Int. J. Pharm.* **2020,** *584,* 119443. doi:10.1016/j.ijpharm.2020.119443
31. Ciobanu, A.; Mallard, I.; Landy, D.; Brabie, G.; Nistor, D.; Fourmentin, S. *Carbohydr. Polym.* **2012,** *87,* 1963–1970. doi:10.1016/j.carbpol.2011.10.005
32. Blach, P.; Fourmentin, S.; Landy, D.; Cazier, F.; Surpateanu, G. *Chemosphere* **2008,** *70,* 374–380. doi:10.1016/j.chemosphere.2007.07.018
33. Moura, L.; Moufawad, T.; Ferreira, M.; Bricout, H.; Tilloy, S.; Monflier, E.; Costa Gomes, M. F.; Landy, D.; Fourmentin, S. *Environ. Chem. Lett.* **2017,** *15,* 747–753. doi:10.1007/s10311-017-0654-y
34. Kolb, B.; Ettre, L. S. *Static Headspace-Gas Chromatography: Theory and Practice,* 2nd ed.; John Wiley & Sons: Hoboken, NJ, USA, 2006. doi:10.1002/0471914584
35. Kfoury, M.; Landy, D.; Fourmentin, S. *J. Inclusion Phenom. Macrocyclic Chem.* **2019,** *93,* 19–32. doi:10.1007/s10847-018-0818-9
36. Fourmentin, S.; Outirite, M.; Blach, P.; Landy, D.; Ponchel, A.; Monflier, E.; Surpateanu, G. *J. Hazard. Mater.* **2007,** *141,* 92–97. doi:10.1016/j.jhazmat.2006.06.090

License and Terms

This is an open access article licensed under the terms of the Beilstein-Institut Open Access License Agreement (https://www.beilstein-journals.org/bjoc/terms), which is identical to the Creative Commons Attribution 4.0 International License (https://creativecommons.org/licenses/by/4.0). The reuse of material under this license requires that the author(s), source and license are credited. Third-party material in this article could be subject to other licenses (typically indicated in the credit line), and in this case, users are required to obtain permission from the license holder to reuse the material.

The definitive version of this article is the electronic one which can be found at:
https://doi.org/10.3762/bjoc.18.140

BEILSTEIN JOURNAL OF ORGANIC CHEMISTRY

A study of the DIBAL-promoted selective debenzylation of α-cyclodextrin protected with two different benzyl groups

Naser-Abdul Yousefi, Morten L. Zimmermann and Mikael Bols*§

Full Research Paper

Open Access

Address:
Department of chemistry, University of Copenhagen, Universitetsparken 5, 2100, Copenhagen, Denmark

Email:
Mikael Bols* - bols@chem.ku.dk

* Corresponding author
§ @MikaelBols

Keywords:
aluminum hydrides; cyclodextrin; debenzylation; 2,4-dichlorobenzyl; selective

Beilstein J. Org. Chem. **2022,** *18,* 1553–1559.
https://doi.org/10.3762/bjoc.18.165

Received: 09 September 2022
Accepted: 09 November 2022
Published: 17 November 2022

This article is part of the thematic issue "Cyclodextrins as building blocks for new materials".

Guest Editor: S. Fourmentin

© 2022 Yousefi et al.; licensee Beilstein-Institut.
License and terms: see end of document.

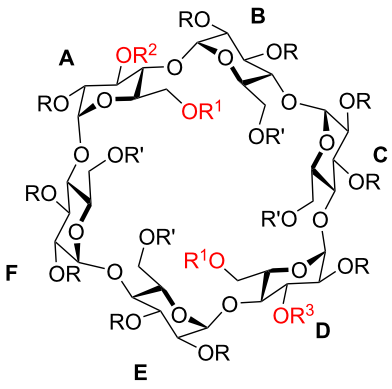
Abstract

An α-cyclodextrin protected with 2,4-dichlorobenzyl groups on the primary alcohols and ordinary benzyl groups on the secondary alcohols was prepared and subjected to DIBAL (diisobutylaluminum hydride)-promoted selective debenzylation. Debenzylation proceeded by first removing two dichlorobenzyl groups from the $6^{A,D}$ positions and then removing one or two benzyl groups from the $3^{A,D}$ positions.

Introduction

α-Cyclodextrin (**1**) is a cyclic carbohydrate consisting of six α-1,4-linked D-glucose molecules (Figure 1). It has a donut-like structure with the glucose residues all aligned with the α-side towards the center of the ring and the polar hydroxy groups pointing towards the sides [1]. This makes the 'hole' in the donut a lipophilic cavity that in water can form complexes with small hydrophobic molecules [2] driven by the entropy increase by expulsion of water [3]. Compound **1** has a wide range of applications where the complexation of substances such as pharmaceuticals or fragrances is exploited since it is cheap, harmless and biodegradable [4]. It is also a useful building block for sensors and/or capture devices, advanced materials, and even artificial enzymes.

Most such uses require that compound **1** can be chemically modified so that linkers, lids or catalytic groups can be installed which is no simple task due to the many similar functionalities in **1** [5-7]. A very useful way to access the hydroxy groups in a selective manner is the perbenzylation of **1** and the subsequent selective debenzylation of **2** using DIBAL [8-10]. This gives access to 6^{A}-mono- and $6^{A,D}$ diol (**3**) in high yields and purity, and by extension of this method further deprotection on the primary [10-12] and secondary rim can be made [13-15]. The reaction of **2** with DIBAL leads quite rapidly to diol **3** and then much slower to triol **4** and tetrol **5**. These methods are so useful because virtually any chemical modification at the deprotected sites can be made followed by



1 (α-CD, R = R' = $R^{1–3}$ = H)
2 (R = R' = $R^{1–3}$ = CH_2Ph)
3 (R = R' = $R^{2,3}$ = CH_2Ph, R^1 = H)
4 (R = R' = R^3 = CH_2Ph, $R^{1,2}$ = H)
5 (R = R' = CH_2Ph, $R^{1–3}$ = H)
6 (R = $R^{2,3}$ = CH_2Ph, R' = R^1 = H)
7 (R = $R^{2,3}$ = CH_2Ph, R' = R^1 = DCB)
8 (R = $R^{2,3}$ = CH_2Ph, R' = DCB, R^1 = H)
9 (R = R^3 = CH_2Ph, R' = DCB, $R^{1,2}$ = H)
10 (R = R^3 = CH_2Ph, R' = DCB, $R^{1–3}$ = H)

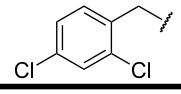
DCB= 

Figure 1: Structure of α-cyclodextrins **1**–**10**.

global deprotection of the *O*-benzyl groups with hydrogenolysis.

Recently, we observed a strong substituent effect when substituted benzyl groups were used in these reactions with electron-poor benzyl groups reacting much more sluggishly. Indeed the per-2,4-dichlorobenzyl (DCB) protected compound **1** was completely resistant to DIBAL even when treated for several days [15]. This led us to wonder if an α-cyclodextrin protected on the primary hydroxy groups with DCB groups and on the secondary hydroxy groups with ordinary benzyl groups would lead to selective debenzylation of one or more of the secondary hydroxy groups without the primary hydroxy groups being touched. In this work we have investigated this hypothesis and found that even when protected as DCB groups the primary alcohols are deprotected more readily than the secondary alcohols of **1**.

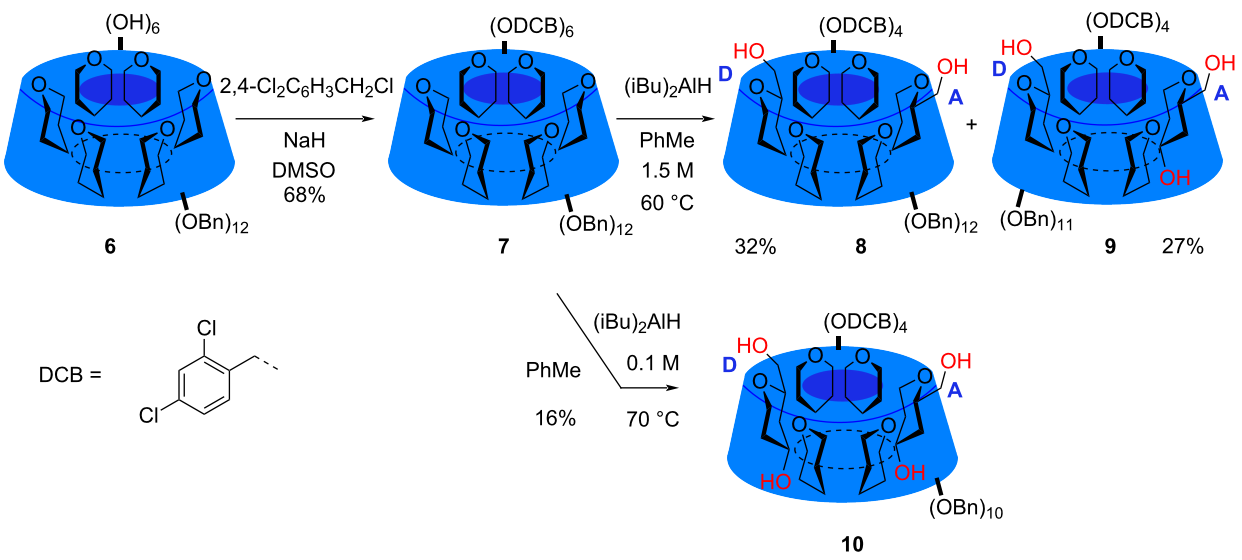
Results and Discussion

The starting point of the synthesis is the known partially benzylated derivative **6**, which according to the literature can be made either from **2** by selective acetolysis of all the primary benzyl groups and ester cleavage [16] or from **1** by selective protection of the primary OH groups with *tert*-butyldimethylsilyl groups, followed by benzylation and desilylation [17,18]. We used both methods to prepare **6**: The acetolysis method is convenient when perbenzyl α-cyclodextrin (**2**) is at hand but requires very strict temperature control during the acetolysis step. The silylation method requires careful drying of **1** before the silylation but is otherwise experimentally simple. Hexol **6** was then DCB-protected using 2,4-dichlorobenzyl chloride and sodium hydride in DMSO. As self-condensation of the alkylating agent is possible the reaction was carried out by mixing **6** and NaH in DMSO and then adding the 2,4-dichlorobenzyl chloride with a syringe pump over several hours. This gave the fully protected compound **7** in 68% yield (Scheme 1).

Reaction of **7** with DIBAL was carried out under a number of different conditions as listed in Table 1. Firstly, reaction with DIBAL in toluene at 0.3 M concentration and at 50 °C gave after 24 h almost complete conversion of the starting material to a symmetrical compound **8** that according to MALDI–TOF MS has lost two DCB groups and not any benzyl group.

The compound was analyzed with ^1H and ^{13}C NMR (800/201 MHz), COSY, HSQC, TOCSY, and ROESY (Supporting Information File 1) which gave the NMR assignments shown in Table 2 and identification of **8** as the $6^{A,D}$ diol. The most significant observations in this assignment were 1) the compound is symmetric with only 3 different sugar residues which combined with the knowledge from MS that two DCB groups have been lost means that only the structure **8** is possible. 2) The residues with the lowest anomeric proton (δ 4.71) could be seen to correlate to the OH proton at δ 3.15 in TOCSY identifying them as **A**/**D**. 3) The residues with the highest anomeric proton (δ 5.70) could be seen to correlate to H-4 (at δ 3.80) of the **A**/**D** residues in ROESY identifying them as **B**/**E**. 4) The anomeric proton of the final residue (δ 4.73) correlated to H-4 at δ 3.92 in ROESY confirming them to be **C**/**F**.

Remaining in the reaction mixture was some of the monool though this compound was not isolated and identified. Carrying out the same reaction with 1.5 M DIBAL gave complete conversion to **8** (Table 1, entry 2). The formation of **8** from **7** is surprising because it contrasts the complete lack of reaction of



Scheme 1: The reaction of perbenzylated α-cyclodextrin with iBu_2AlH.

Table 1: Reaction conditions for the partial debenzylation of **7**. The solvent was always toluene.

Entry	[Substrate]	[DIBAL]	*T* (°C)	Time (h)	Compounds[a]	Isolated (yield)
1	2.9 mM	0.3 M	50	24	**8** (93%) & monool 7%	–
2	14 mM	1.5 M	50	24	**8** (100%)	–
3	13 mM	1.5 M	60	24	**8** (51%) & **9** (49%)	**8** (32%) & **9** (27%)
4	1.3 mM	0.1 M	70	72	**8** (18%), **9** (55%) & **10** (27%)	–
5	1.3 mM	0.1 M	70	144	**8** (4%), **9** (32%) & **10** (64%)	**10** (16%)

[a]The ratio of compounds in the crude reaction product according to ^{1}H NMR.

Table 2: ^{1}H and ^{13}C NMR (800/201 MHz, $CDCl_3$) chemical shifts of diol **8**.

	A/D[a]	B/E[a]	C/F[a]
H-1	4.71 (d)	5.70 (d, *J* = 4.0 Hz)	4.73 (d)
H-2	3.42 (dd)	3.58 (dd, *J* = 9.7, 3.9 Hz)	3.41 (dd)
H-3	4.10	4.21 (dd, *J* = 9.6, 7.6 Hz)	4.03
H-4	3.80 (t)	3.92	3.73
H-5	4.02	3.96	3.97
H-6a	3.73	4.08	3.94
H-6b	3.73	3.74	3.84
OH	3.15 (s)	–	–
Bn	5.43 (d, *J* = 10.3 Hz, 2H), 5.16 (d, *J* = 10.7 Hz, 2H), 4.88 (d, 2H), 4.87 (d, 2H), 4.82–4.68 (m, 6H), 4.60 (d, *J* = 13.3 Hz, 2H), 4.56–4.43 (m, 12H), 4.36 (2d, 4H)		
Ar	7.21 (m, 72H)		
C-1	98.4	98.2	98.3
C-2	80.1	77.8	79.1
C-3	81.6	80.9	80.7
C-4	75.0	81.3	81.9
C-5	71.5	71.8	72.2

Table 2: ^{1}H and ^{13}C NMR (800/201 MHz, $CDCl_3$) chemical shifts of diol **8**. (continued)

C-6	62.4	70.3	70.9
Bn	76.6, 76.2, 74.1, 73.6, 73.2, 72.6, 70.00, 69.95		
Ar	139.31, 139.27, 139.26, 138.7, 138.3, 138.0 (ipsoC Ph), 134.5, 134.3, 134.1, 133.8, 133.6, 133.3 (ipsoC DCB), 130.0, 129.9, 129.2, 129.1, 128.5, 128.5, 128.3, 128.24, 128.21, 128.18, 128.18, 128.16, 128.0, 127.9, 127.8, 127.37, 127.35, 127.3, 127.24, 127.21, 127.17, 127.0, 126.5 (CH Ph & DCB)		

[a]The letters A to F refer to each of the monosaccharides using normal cyclodextrin nomenclature as of Figure 1.

fully DCB protected **1** with DIBAL [15]. It means that the identity of protective groups on the secondary rim influence the reaction at the primary rim significantly, most probably by a collective inductive effect.

When the reaction of **7** with DIBAL was carried out at higher temperature further debenzylation was observed with, according to MS, a triol **9** being formed from **8**. When **7** was reacted with 1.5 M DIBAL in toluene at 60 °C for 24 hours an almost equal amount of **8** and **9** was present (Table 1, entry 3) and 27% of triol **9** together with 32% of **8** was isolated. A tetrol **10** was obtained upon even longer reaction of **7**: If reacted with 0.1 M DIBAL in toluene for 3 days at 70 °C a mixture of 18% of **8**, 55% of **9**, and 27% of **10** was seen (Table 1, entry 4). When the time was extended to 6 days **10** was the predominant compound (Table 1, entry 5) and could be isolated in 16% yield. Triol **9** was identified using ^{1}H and ^{13}C NMR (800/201 MHz), COSY, HSQC, HMBC, TOCSY, and ROESY (Supporting Information File 1) leading to NMR assignments shown in Table 3 and identification as the $3^{A},6^{A,D}$ triol. The most significant observations in this assignment were 1) MS showed the compound had lost a benzyl group from the structure of **8**. 2) One of the residues (A) which have an anomeric proton at δ 4.80 is seen on TOCSY and COSY to correlate to a H-3 signal at δ 4.22 which has a corresponding carbon at δ 73.5. This carbon is 7–8 ppm lower than other C-3 signals revealing that it is not alkylated. 3) This same residue (A) has an outlying H-2 proton signal at δ 3.28 which correlates in TOCSY to an OH proton at δ 2.80. 4) A HMBC correlation connects the carbon signal at δ 62.3 to the unusual H-4 signal at δ 3.35 in residue A.

Table 3: ^{1}H and ^{13}C NMR (800/201 MHz, $CDCl_3$) chemical shifts of triol **9**.

	A[a]	B[a]	C[a]	D[a]	E[a]	F[a]
H-1	4.80	5.08	4.71	4.76	5.58	4.78
H-2	3.28	3.62	3.38	3.45	3.56	3.39
H-3	4.22	4.26	4.01	4.12	4.11	4.03
H-4	3.35	3.82	3.76	3.74	3.88	3.63
H-5	3.86	3.88	3.97[b]	4.15[b]	3.97	3.97[b]
H-6a	3.70	4.06	3.94[c]	3.73	4.12[c]	3.88[c]
H-6b	3.63	3.72	3.82[c]	3.73	3.71[c]	3.77[c]
OH	2.80 (bs, 1H)	–	–	2.98 (bs, 1H)	–	–
Bn	5.51 (d, *J* = 10.8 Hz, 1H), 5.28 (d, *J* = 10.6 Hz, 1H), 5.17 (d, *J* = 10.5 Hz, 1H), 5.13 (d, *J* = 11.2 Hz, 1H), 4.96 (d, *J* = 11.0 Hz, 1H), 4.90 (2d, 2H), 4.84 (d, *J* = 11.5 Hz, 1H), 4.82–4.68 (m, 4H), 4.62–4.38 (m, 18H)					
Ar	7.42 (m,2H), 7.35 (m, 4H), 7.32–7.08 (m, 61H)					
C-1	100.4	100.8	99.6	98.0	98.7	98.4
C-2	77.5	78.2	78.7	80.0	77.6	79.6
C-3	73.5	81.2	80.8	80.6[d]	81.5[d]	80.6
C-4	82.1	82.4	76.5[e]	81.5[e]	80.9	82.7
C-5	71.8	72.2	71.8[f]	71.5	71.8[f]	72.4[f]
C-6	62.3	70.2	71.1[g]	62.5	70.0[g]	71.2[g]
Bn	76.62, 76.47, 76.03, 76.01, 74.52, 74.31, 73.48, 73.01, 72.96, 72.78, 72.62, 71.99, 69.96, 69.88, 69.82					
Ar	139.7–137.6 (Ph ipso), 134.5–133.3 (Ar ipso), 129.9–126.6 (Ph & Ar CH)					

[a]The letters A to F refers to each of the monosaccharides using normal cyclodextrin nomenclature as of Figure 1. [b]Shifts may be interchanged. [c]Shifts may be interchanged. [d]Shifts may be interchanged. [e]Shifts may be interchanged. [f]Shifts may be interchanged. [g]Shifts may be interchanged.

This with the knowledge that **9** is formed from **8** gives the structure of **9**. Overall the spectrum of **9** resembles that of the benzylated triol [13] **4** and the assignment is not surprisingly very similar [15].

Similar NMR analysis of **10** gave the assignments shown in Table 4. The most significant observations in this structural assignment were 1) MS showed the compound had lost two benzyl groups from the structure of **8** and from NMR it was found to be symmetrical. 2) The residues (A/D) which have an anomeric proton at δ 4.79 is seen on TOCSY and COSY to correlate a H-3 signal at δ 4.28 which has a corresponding carbon signal at δ 73.0 revealing that C-3 is debenzylated. This with the symmetry of the compound and the knowledge it is formed from **9** gives the structure. 3) HMBC correlations between C-1 and H-4 in the former glucose (101.8 → 3.40, 101.2 → 3.65, 100.2 → 3.81) gave the order of residues. Overall the spectrum of **10** resembles that of the fully benzylated tetrol **5** [13].

As **9** and **10** are analogues to the products formed from **2** this means that **7** is debenzylated almost similarly other than the DCB removal at the primary rim is somewhat slower. Debenzylation on the secondary rim does not occur before DCB groups have been removed on the primary side supporting the hypothesis that the debenzylation on the secondary side is intramolecular or at least directed by alkoxy aluminate at O6.

Conclusion

It is clear that the O2,O3-DCB groups in fully DCB-protected **1** are affecting the DIBAL-promoted debenzylation tremendously: When present no reaction is observed and when exchanged with unsubstituted benzyl groups debenzylation occurs following the already known pattern. The reason for this behavior is probably due to the collective electron-withdrawing effect of the chlorine atoms making the glucose residues of the fully DCB-protected compound more electron deficient at the ring oxygen. This means that the Lewis acidic aluminum reagent has more difficulty binding to this oxygen which is important in the mechanism [9,15].

Experimental

General information: In a manner similar to [15] dry solvents were tapped from a PureSolv solvent purification system. Reactants were purchased from commercial sources and used without further purification. HRMS were recorded on a Bruker Solarix XR mass spectrometer analyzing TOF. Generally, NMR spectra were recorded on a 500 MHz Bruker instrument with a cryoprobe. The 800 MHz spectra were recorded at 25 °C on a Bruker Avance Neo spectrometer with 5 mm CPTXO Cryoprobe C/N-H-D optimized for direct ^{13}C detection. Chemical shifts (δ) are reported in ppm relative to the residue solvent signals or other solvent present. Flash chromatography was carried out on a Büchi Pure Chromatography Instrument C-805 using silica gel columns.

Table 4: ^{1}H and ^{13}C NMR (800/126 MHz, $CDCl_3$) chemical shifts of tetrol **10**.

	A/D[a]	B/E[a]	C/F[a]
H-1	4.79	4.92	4.70
H-2	3.29	3.60	3.33
H-3	4.28	4.17	3.96
H-4	3.40	3.81	3.65
H-5	3.89	3.88	3.88
H-6a	3.67	3.80	4.04
H-6b	3.67	3.79	3.67
Bn	5.42 (d, *J* = 11.0 Hz, 2H), 5.21 (d, *J* = 11.2 Hz, 2H), 4.95–4.16 (m, 24H)		
Ar	7.53–6.93 (m, 62H)		
C-1	101.2	101.8	100.2
C-2	77.5	78.8	79.1
C-3	73.0	81.4	80.8
C-4	83.7	82.4	82.7
C-5	72.0[b]	72.3[b]	71.4[b]
C-6	62.1	70.9	70.0
Bn	76.5, 76.0, 74.7, 72.7, 72.6, 69.9, 69.8		
Ar	139.6, 139.5, 138.6, 138.5, 137.3 (Ph ipso), 134.5, 134.4, 134.0, 133.8, 133.4, 133.2 (Ar ipso), 129.8, 129.8, 129.1, 129.05, 128.9, 128.73, 128.69, 128.5, 128.4, 128.36, 128.32, 128.28, 128.23, 128.15, 128.1, 127.8, 127.7, 127.5, 127.3, 127.24, 127.15, 127.1 (Ar & Ph CH)		

[a]The letters A to F refers to each of the monosaccharides using normal cyclodextrin nomenclature as of Figure 1. [b]Shifts may be interchanged.

$6^{A–F}$-Hexa-*O*-(2,4-dichlorobenzyl)-$2^{A–F}$,$3^{A–F}$-dodeca-*O*-benzyl-α-cyclodextrin (7): NaH (60% dispersion in mineral oil, 162 mg, 4.05 mmol) was added to a solution of hexol **6** (694 mg, 0.338 mmol) in anhydrous DMSO (20 mL) under a nitrogen atmosphere at room temperature. After bubbling had subsided, 2,4-dichlorobenzyl chloride (0.563 mL, 4.05 mmol) was added over four hours with a syringe pump. The mixture was left to stir overnight, and the reaction was quenched by addition of MeOH (10 mL). The mixture was diluted with toluene, and the organic phase washed with H_2SO_4 (1 M, 20 mL), then brine (3 × 20 mL), dried ($MgSO_4$), filtered, and concentrated. Column chromatography in a solvent gradient of heptane/EtOAc 1:0 to 0:1 gave product **7** (693 mg, 0.230 mmol, 68%). ^{1}H NMR ($CDCl_3$, 500 MHz) δ 7.21–7.07 (m, 78H, Ar), 5.17 (d, J = 10.9 Hz, 1H, ArCH, 6H), 5.08 (d, $J_{1,2}$ = 3.4 Hz, 1H, 6H, H-1) , 4.86 (d, J = 10.9 Hz, 6H, ArCH), 4.52–4.41 (m, 18H, 3 × ArCH), 4.37 (d, J = 13.4 Hz, 6H, ArCH), 4.16–4.08 (m, 12H, H-3, H-6a), 4.02–3.94 (m, 12H, H-4, H-5), 3.59 (d, J = 10.6 Hz, 6H, H-6b), 3.47 (dd, $J_{2,3}$ = 9.8 Hz, 6H, H-2) ppm; ^{13}C NMR (126 MHz, $CDCl_3$) δ 139.17, 138.23, 134.35, 133.79, 132.95, 129.46, 128.98, 128.20, 128.06, 127.73, 127.51, 127.29, 127.07 (Ar), 98.75 (C-1), 80.90 (C-3), 79.37 (C-4), 78.97 (C-2), 75.66 ($ArCH_2$), 72.93 ($ArCH_2$), 71.62 (C-5), 69.94 ($ArCH_2$) 69.91 (C-6) ppm; HRMS–MALDI$^+$ (m/z): $[M + Na]^+$ calcd for $C_{162}H_{156}Cl_{12}O_{30}Na^+$, 3030.6782; found, 3030.67364.

General procedure for the reactions of 7 with DIBAL: A sample of compound **7** (65 mg, 22 µmol) was dissolved in 0 to 6 mL anhydrous toluene in a dry round-bottomed flask fitted with a septum and a stirring bar under nitrogen. Then, 1.5 mL DIBAL as a 1.5 M solution in toluene were added with a syringe. The reaction mixture was stirred at fixed temperature (50–70 °C) controlled by an oil bath. At the end of the reaction, the flasks' contents were diluted with 20 mL toluene and was washed with 20 mL 1 M H_2SO_4 and water in a separating funnel. The organic layer was dried with sodium sulfate, filtered, concentrated, and analyzed by ^{1}H NMR in $CDCl_3$. The relative content of **7**, monool, **8**, **9**, and **10** in the sample was determined by comparing the integrals of peaks at δ 5.70 (d, 2H, H-1^{BE}, **8**), 5.58 (d, 1H, H-1^E, **9**), 5.50 (d, 1H, monool), 5.42 (d, 2H, Bn, **10**) and 5.08 (d, 6H, **7**) ppm.

$6^{B,C,E,F}$-Tetra-*O*-(2,4-dichlorobenzyl)-$2^{A–F}$,$3^{A–F}$-dodeca-*O*-benzyl-α-cyclodextrin (8) and $6^{B,C,E,F}$-tetra-*O*-(2,4-dichlorobenzyl)-$2^{A–F}$,$3^{B–F}$-undeca-*O*-benzyl-α-cyclodextrin (9): Compound **7** (200 mg, 66.5 µmol) was dissolved in DIBAL-H (1.5 M in toluene, 5 mL, 7.5 mmol) in a flask under nitrogen and stirred at 60 °C for 24 hours. Methanol (1 mL) was slowly added and the solution was poured into 20 mL H_2SO_4 (1 M) and toluene (20 mL). The layers were partitioned, and the organic layer washed with saturated aqueous $NaHCO_3$ (20 mL), dried with Na_2SO_4, filtered, and concentrated. Column chromatography in a solvent gradient of heptane/EtOAc 1:0 to 0:1 gave consecutively **8** (56 mg, 21 µmol, 32 %) and **9** (47 mg, 18 µmol, 27%). NMR data and assignments see Table 2 (**8**) and Table 3 (**9**). HRMS–MALDI (m/z): for **8** $[M + Na]^+$ calcd for $C_{141}H_{142}Cl_8O_{30}Na^+$, 2712.7431; found: 2712.74127. for **9** $[M + K]^+$ calcd for $C_{162}H_{156}Cl_{12}O_{30}K^+$, 2638.6701; found, 2638.71363.

$6^{B,C,E,F}$-Tetra-*O*-(2,4-dichlorobenzyl)-$2^{A–F}$,$3^{B,C,E,F}$-dodeca-*O*-benzyl-α-cyclodextrin (10): Compound **7** (59 mg, 20 µmol) was dissolved in anhydrous toluene (14 mL) and DIBAL (1.5 M in toluene, 1 mL, 1.5 mmol) was added. The reaction mixture was stirred at 70 °C under nitrogen atmosphere. After 6 days the reaction mixture was diluted with toluene (25 mL) and quenched by addition of H_2SO_4 (1 M, 25 mL), then the organic layer was washed with water (25 mL), dried (Na_2SO_4), and concentrated to a crude product (35 mg) that according to NMR contained 4% **8**, 32% **9**, and 64% **10**. Flash chromatography in a EtOAc/heptane going from 1:3 to 1:1 gave **10** (8 mg, 3 µmol, 16%). NMR data and assignment see Table 4. HRMS–MALDI$^+$ (m/z): $[M + H]^+$ calcd for $C_{134}H_{137}Cl_8O_{30}^+$, 2511.6706 (71.9%); found, 2511.69097.

Supporting Information

Supporting Information File 1

Copies of NMR spectra of compounds **7**–**10**.
[https://www.beilstein-journals.org/bjoc/content/supplementary/1860-5397-18-165-S1.pdf]

Funding

800 MHz NMR data was recorded at cOpenNMR an infrastructure facility funded by the Novo Nordisk Foundation (#NNF18OC0032996).

ORCID® iDs

Morten L. Zimmermann - https://orcid.org/0000-0002-8046-7211
Mikael Bols - https://orcid.org/0000-0002-6561-6952

References

1. Szejtli, J. *Chem. Rev.* **1998,** *98,* 1743–1754. doi:10.1021/cr970022c
2. Cramer, F.; Henglein, F. M. *Chem. Ber.* **1957,** *90,* 2561–2571. doi:10.1002/cber.19570901122
3. Rekharsky, M. V.; Inoue, Y. *Chem. Rev.* **1998,** *98,* 1875–1918. doi:10.1021/cr970015o
4. Ho, T. M.; Yoshii, Y.; Terao, K.; Bhandari, B. R., Eds. *Functionality of Cyclodextrins in Encapsulation for Food Applications;* Springer: Cham, Switzerland, 2021. doi:10.1007/978-3-030-80056-7

5. Khan, A. R.; Forgo, P.; Stine, K. J.; D'Souza, V. T. *Chem. Rev.* **1998,** *98,* 1977–1996. doi:10.1021/cr970012b
6. Tang, W.; Ng, S.-C. *Nat. Protoc.* **2008,** *3,* 691–697. doi:10.1038/nprot.2008.37
7. Řezanka, M. *Environ. Chem. Lett.* **2019,** *17,* 49–63. doi:10.1007/s10311-018-0779-7
8. Pearce, A. J.; Sinaÿ, P. *Angew. Chem., Int. Ed.* **2000,** *39,* 3610–3612. doi:10.1002/1521-3773(20001016)39:20<3610::aid-anie3610>3.0.co;2-v
9. Lecourt, T.; Herault, A.; Pearce, A. J.; Sollogoub, M.; Sinaÿ, P. *Chem. – Eur. J.* **2004,** *10,* 2960–2971. doi:10.1002/chem.200305683
10. Bistri, O.; Sinaÿ, P.; Jiménez Barbero, J.; Sollogoub, M. *Chem. – Eur. J.* **2007,** *13,* 9757–9774. doi:10.1002/chem.200700971
11. Liu, J.; Wang, B.; Przybylski, C.; Bistri-Aslanoff, O.; Ménand, M.; Zhang, Y.; Sollogoub, M. *Angew. Chem., Int. Ed.* **2021,** *60,* 12090–12096. doi:10.1002/anie.202102182
12. Wang, B.; Zaborova, E.; Guieu, S.; Petrillo, M.; Guitet, M.; Blériot, Y.; Ménand, M.; Zhang, Y.; Sollogoub, M. *Nat. Commun.* **2014,** *5,* 5354. doi:10.1038/ncomms6354
13. Rawal, G. K.; Rani, S.; Ling, C.-C. *Tetrahedron Lett.* **2009,** *50,* 4633–4636. doi:10.1016/j.tetlet.2009.05.108
14. Rawal, G. K.; Rani, S.; Ward, S.; Ling, C.-C. *Org. Biomol. Chem.* **2010,** *8,* 171–180. doi:10.1039/b915450g
15. Bols, M.; Friis, V. *Chem. – Eur. J.* **2022,** *28,* e202200564. doi:10.1002/chem.202200564
16. Angibeaud, P.; Utille, J.-P. *Synthesis* **1991,** 737–738. doi:10.1055/s-1991-26560
17. Meppen, M.; Wang, Y.; Cheon, H.-S.; Kishi, Y. *J. Org. Chem.* **2007,** *72,* 1941–1950. doi:10.1021/jo061990v
18. Uccello-Barretta, G.; Sicoli, G.; Balzano, F.; Salvadori, P. *Carbohydr. Res.* **2005,** *340,* 271–281. doi:10.1016/j.carres.2004.11.022

License and Terms

This is an open access article licensed under the terms of the Beilstein-Institut Open Access License Agreement (https://www.beilstein-journals.org/bjoc/terms), which is identical to the Creative Commons Attribution 4.0 International License (https://creativecommons.org/licenses/by/4.0). The reuse of material under this license requires that the author(s), source and license are credited. Third-party material in this article could be subject to other licenses (typically indicated in the credit line), and in this case, users are required to obtain permission from the license holder to reuse the material.

The definitive version of this article is the electronic one which can be found at:
https://doi.org/10.3762/bjoc.18.165

BEILSTEIN JOURNAL OF ORGANIC CHEMISTRY

Preparation of β-cyclodextrin-based dimers with selectively methylated rims and their use for solubilization of tetracene

Konstantin Lebedinskiy[1], Volodymyr Lobaz[2] and Jindřich Jindřich[*1]

Full Research Paper

Open Access

Address:
[1]Department of Organic Chemistry, Faculty of Science, Charles University, Hlavova 8, 128 43 Prague, Czech Republic and [2]Institute of Macromolecular Chemistry, Department of Supramolecular Systems and Self-Assembling Processes, Heyrovského nám. 2, 162 06 Prague, Czech Republic

Email:
Jindřich Jindřich[*] - jindrich.jindrich@natur.cuni.cz

* Corresponding author

Keywords:
cyclodextrin; dimer; methylation; solubilization; tetracene

Beilstein J. Org. Chem. **2022,** *18,* 1596–1606.
https://doi.org/10.3762/bjoc.18.170

Received: 05 September 2022
Accepted: 08 November 2022
Published: 25 November 2022

This article is part of the thematic issue "Cyclodextrins as building blocks for new materials".

Associate Editor: H. Ritter

© 2022 Lebedinskiy et al.; licensee Beilstein-Institut.
License and terms: see end of document.

Abstract

A series of β-cyclodextrin dimers selectively permethylated on the primary or secondary rim with two different types of spacers have been synthesized effectively utilizing conventional and newly developed methods. Their structure analyses by ^{1}H NMR and NOESY NMR imply the dependence of molecular symmetry on the type of spacer. The ability of synthesized dimers to increase the solubility of tetracene in DMSO was evaluated and compared to native cyclodextrins and their methylated derivatives. The newly synthesized compounds expressed better effectiveness than other tested supramolecular hosts.

Introduction

Cyclodextrins (CDs) are cyclic oligomers of glucose that play an important role in supramolecular chemistry [1]. The structure of any CD contains a hydrophobic cavity inside the molecule, while all hydrophilic hydroxy groups are arranged outside the cavity. This feature determines the main practical application of CDs as supramolecular hosts for host–guest interaction. Due to their low cost, low toxicity, and good complexation ability, they are frequently used in pharmaceutical, food, and chemical industries, agriculture, and environmental engineering [1]. They possess many hydroxy groups and are suitable for further chemical transformations that could alter their complexation ability [2]. Every glucose unit in CDs bears three hydroxy groups, i.e., the CD contains three types of hydroxy groups with different chemical reactivity. The difference in the reactivity and combination of synthetic procedures allow obtaining many molecules with selectively substituted positions [3]. Perhaps, the most investigated CD derivatives with selectively substituted rims are partially methylated CDs. Methylation reduces the formation of intramolecular hydrogen bonds, enhancing CDs water solubility, and also extends the hydrophobic cavity, thus improving its binding potential. A substantial increase of binding constant (K) for per-6-methylated CD compared to native CD was described, but an order of magnitude decrease of K was found for permethylated CD [2]. Also, methylation changes the solubility of CDs in organic solvents, expanding their potential field of application. CDs form the most stable

complexes with hydrophobic compounds in polar solvents such as water [4]. The complexation of organic molecules by CDs in nonpolar media has not been widely studied yet, but in several cases, such results have been achieved [5,6]. Another interesting type of CD transformation is a connection of two CD molecules by some spacer via covalent bonds. Many such "dimers" (not exactly the correct name, but widely used) have been reported in the literature [7-17]. The most crucial feature of such dimers is a sufficient increase in binding constants with several potential guests, particularly with ditopic or stick-shaped molecules. So it could be expected that the extension of the hydrophobic cavity by the combined methylation and “dimerization” may improve the binding potential towards such substrates even more.

Linear polycyclic aromatic hydrocarbons (acenes) and their derivatives are good organic semiconductors and show interesting light-absorbance properties. They found their application in material science, where they are used in developing organic photovoltaic prototypes as potential dichroic dyes and organic thin-film transistors. However, due to strong π-stacking interaction, these compounds are not readily soluble, and the solubility decreases with the increased number of aromatic rings in a molecule [18]. Pentacene with five conjugated aromatic rings has been extensively investigated; however, it is quite challenging to investigate the spectral and electrical properties of acenes with a number of rings higher than 6 because of poor solubility and mainly because of their low stability [18-20]. Moreover, a general method for the preparation of long acenes have been recently published [21]. According to the literature [22], the only reasonable solution to overcome the solubility and stability problems is functionalizing these molecules, for example, by inserting some protecting groups. Substituted heptacenes demonstrate remarkable stability and exceptional electric properties.

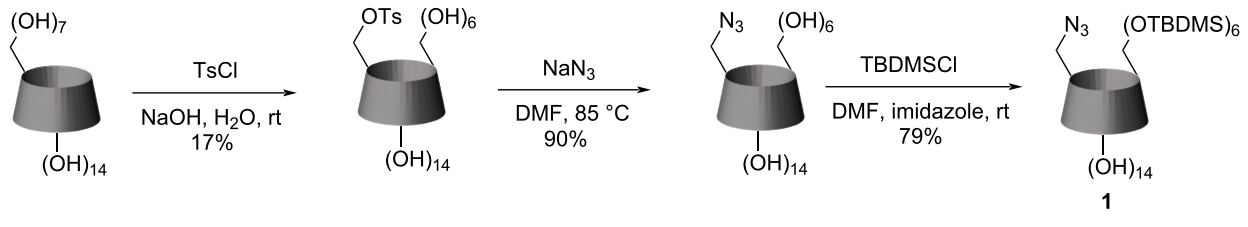
Nevertheless, studying the properties of unsubstituted acenes is also essential. We guessed that some increase in solubility of acene might be achieved by a supramolecular interaction with a suitable host. Our initial plan was to enhance the solubility of higher acenes by the complexation with CDs. However, linear acenes with more aromatic rings (such as pentacene or heptacene) are, in addition to their poor solubility, also quite unstable, for example, towards oxidation. So, we have chosen tetracene as the object of our research. This molecule is also known as an organic semiconductor and is poorly soluble, but it demonstrates some stability to oxidation, making it easier to work with. We assumed these results might be extended to pentacene and other larger linear acenes if we would achieve some success with it. In this work, we report on the efficient synthesis of new cyclodextrin supramolecular hosts based on selectively methylated β-CD derivatives and their dimers; moreover, we compare their effectiveness in the solubilization of tetracene in DMSO.

Results and Discussion

Synthesis of β-cyclodextrin dimers with selectively methylated rims

Selective methylation has been used in CD chemistry for at least 30 years [23,24], and since then, scientists have developed advanced and relatively cheap synthetic procedures [25]. Almost all of these methods are also applicable for the methylation of 6-mono-azido derivatives.

Compound **1** was used as the starting compound to prepare all dimers with partially methylated rims. It contains one azido group in position 6, and all remaining 6-OH are protected with TBDMS groups; it was prepared according to the published procedure (Scheme 1) [26] with some modifications to achieve better results. We started with silylation of 6-azido-β-CD, using imidazole/DMF base/solvent mixture instead of pyridine, which gave higher yields and lower reaction time. Also, we found the recrystallization from the mixture of methanol/acetonitrile to be more suitable for the purification of the compound rather than DCM/acetone [26]. However, we do not recommend recrystallization when the presence of oversilylated compounds in the reaction mixture is too high; here, the column chromatography with $CHCl_3$/MeOH elution mixture gives much better yields in a shorter time.



Scheme 1: The synthesis of 6^A-azido-6^A-deoxy-per-6-*O*-*tert*-butyldimethylsilyl-β-cyclodextrin.

The synthesis of dimers selectively permethylated on the secondary side is shown in Scheme 2. While methylating the secondary rim of the silylated cyclodextrin **1**, we met the obstacle that the reaction mixture contained a non-negligible amount of undermethylated products regardless of the reaction time or the amount of methyl iodide added. In the literature [25], this problem is solved by using methyltriphenylphosphine bromide as a phase-transfer catalyst, and it has also worked in our reaction. Refluxing in NH_4F methanol solution was chosen to cleave the silyl groups. Both other reagents used for the cleavage in CD chemistry (TBAF and $BF_3{\cdot}Et_2O$) yielded byproducts that unnecessarily complicated the purification.

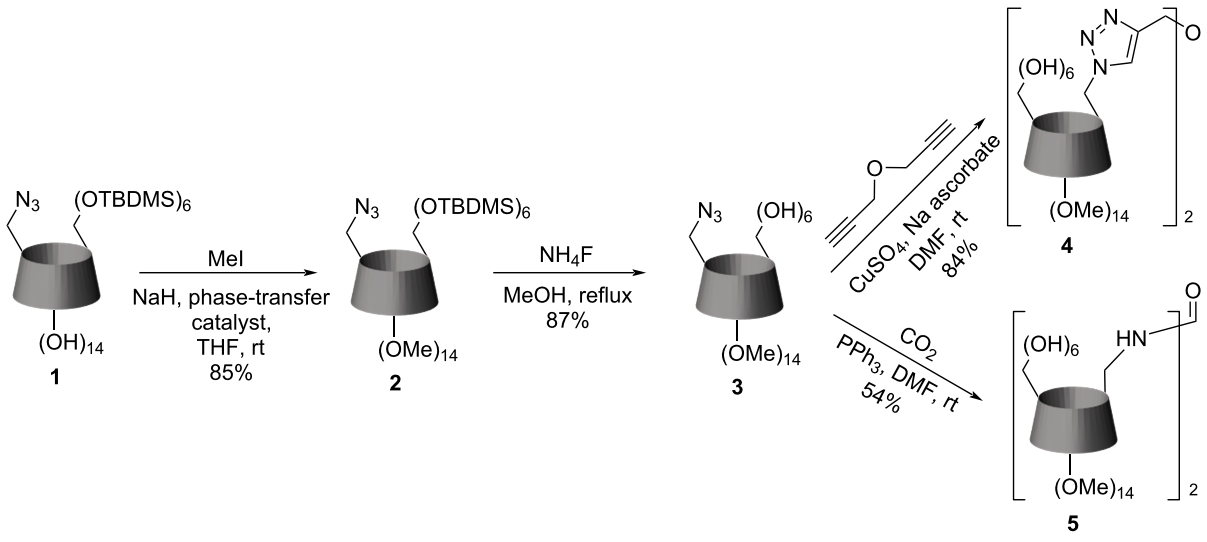
The CuAAC "click reaction" in CD chemistry is also a well-known approach, allowing coupling reactions of azido-containing CDs with different propargyl-containing compounds, including other CDs, to form a dimer [12]. Usually, such reactions proceed with a Cu(I) catalyst [27]; however, Cu(I) can be generated in situ by the reduction of Cu(II) [12,28] or by the dissolution of metal copper [29]. Moreover, the load of the catalyst varies from catalytical amounts (0.02 equiv) [27] to semi-equivalent [12]. Optimal conditions for a click reaction are a subject to discovery in every case, because temperature, microwave or ultrasonic irradiation, and type of catalyst strongly influence the reaction time and yields.

In the preparation of dimer **4**, the most crucial restriction in coupling two CD units by propargyl ether is the volatility of the latter compound. Thus, we discovered that performing the reaction at room temperature, prolonging the reaction time, and using an equivalent amount of the copper catalyst resulted in the best yields.

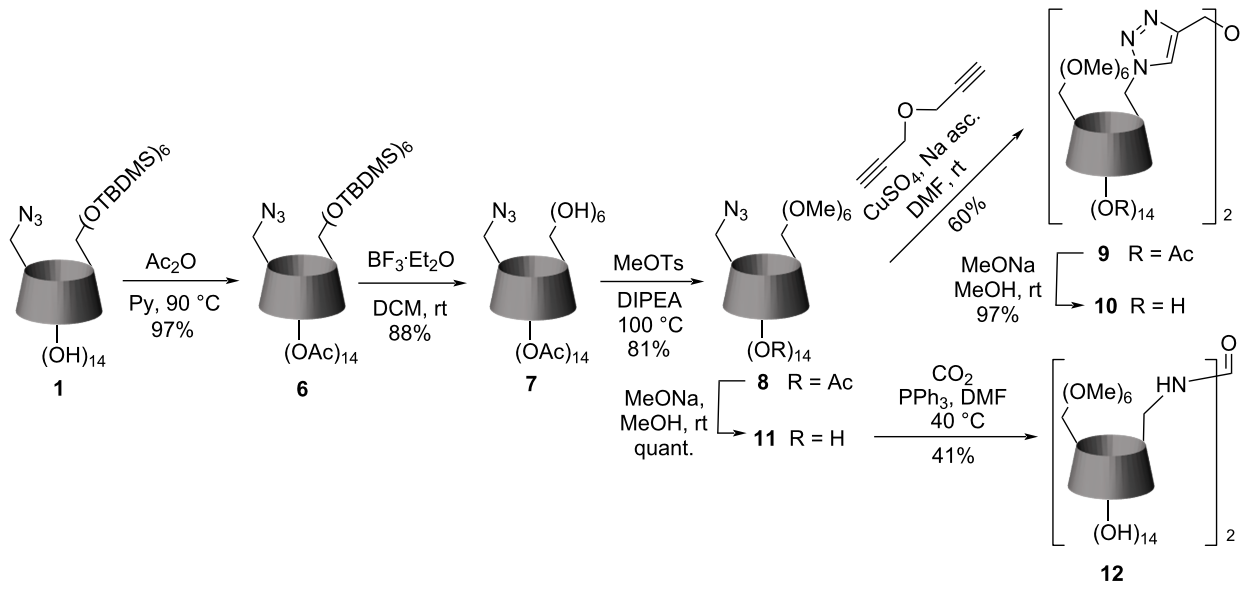
Another kind of reaction engaging the azido group in the CD chemistry is the phosphine imide reaction [30,31]. This transformation involves triphenylphosphine and carbon dioxide to convert azide into isocyanate [31], allowing coupling with amines or other nucleophile groups. It is interesting to note that the same conditions lead to a different product in CD chemistry [30]. In the absence of strong nucleophiles such as amines, the CD gives a dimer with a urea bridge instead of providing the isocyanate. The compound **5** was synthesized from **3** according to the standard procedure [30].

The synthesis of dimers selectively permethylated on the primary side is shown in Scheme 3. The method described by Varga [25] was not suitable for the preparation of **11** because of the strong reductive conditions required for the cleavage of benzyl protective groups. Other described procedures [23,24] also have disadvantages, such as the price of some reagents and relatively low yields.

In this work, we describe a method using low-cost reactants, such as methyl tosylate and DIPEA, which provides moderate to high yields and is a reasonable alternative to the existing methods. The acetylation of compound **1** using standard conditions gave the secondary side peracetylated **6** in a high yield. The selective deprotection of silyl groups, yielding compound **7**, was also performed standardly using $BF_3O{\cdot}Et_2O$. Our new procedure is based on the methylation of this acetyl-protected β-CD **7** using a DIPEA/methyl tosylate mixture without adding any solvent. The DIPEA can be effectively replaced by another relatively weak organic base, such as TEA, TBA, or 2,6-lutidine. The reaction proceeds at 100 °C and is usually finished in 10–12 hours, yielding compound **8**. However, it demands a



Scheme 2: The synthesis of β-cyclodextrin dimers with permethylated secondary rims.



Scheme 3: The synthesis of β-cyclodextrin dimers with permethylated primary rims.

steady pH control because the basicity of the reaction mixture decreases during the first several hours due to the quaternization of DIPEA. We found that adding small portions of the base over the reaction course allows us to avoid this problem and finish the process successfully. Purifying the reaction mixture requires the removal of excess methyl tosylate, which can be easily done by shaking the reaction mixture with NaI ethanol/water solution in a separation funnel.

The click reaction of compound **8** proceeds at a different rate than **3** under the same conditions. The coupling of **3** can be finished overnight with high yields, whereas the coupling of **8** is much slower and gives a lower conversion. Mourer and co-authors [12] also have reported varying reactivity of 6-azido permethylated CD over 6-azido CD in click reactions, claiming the presence of hydroxy groups on the secondary face reduces the catalytical activity of copper.

Compound **11**, prepared by standard deacetylation of **8**, proved to be not reactive enough to complete the reaction in 24 h under the conditions used to prepare the dimer **5**. The prolongation of the reaction time increased the yield slightly, but it was still too low (17%). To improve the yield, we used lithium iodide and increased the temperature somewhat, giving us a 41% yield after 12 h of the reaction. Testing the same conditions for dimer **5**, we also noticed a speed up in the reaction rate, but a presence of the trimer with an extra CD moiety connected by carbamate group ($M_r \approx 4000$) was spotted, giving us lower yields. We assume the Lewis acid activates isocyanates, affording reactions with alcohols. Since the hydroxy groups on the primary rim of CD express higher nucleophilicity than hydroxy groups on the secondary rim, this type of reaction is not observable with the permethylated primary ring.

NMR studies of β-cyclodextrin dimers with selectively methylated rims

The important part of this work was proving the structure of the synthesized compounds because we worked with non-symmetrical CDs; moreover, we used protection–deprotection methods for partial methylation, so we could expect a cleavage or even migration of protective groups. Despite this, we have found mass spectrometry and combined NMR analysis to be reliable methods to prove the structure of these compounds. On NMR spectra, we paid particular attention to the H^1-region, where most of our products have several doublets, which referred to the signals from each hydrogen-1 in every glucose moiety. Sometimes these signals overlap and merge; however, it is still possible to isolate at least one small doublet, whose intensity is 1/7 of the whole H^1-region. After dimerization, the H^1-region can be more complex, indicating the further loss of symmetry in the molecules.

The NMR spectra of the dimers possess several features, making them quite different from the spectra of their starting materials. The spectra of the dimers with the urea linker in water contain much fewer distortions in the hydrogen and carbon signals than the spectra of a corresponding azido-compound, so they look more like the symmetrical partially methyl-

ated compounds without azido group. This phenomenon could be attributed to the increased molecular symmetry after the dimerization with this type of spacer.

A methyltriazole ether linker connects the CD moieties in dimers **4**, **9**, and **10**. The aromatic part of the spacer is a less polar substituent than an oxygen atom. It justifies the magnetic anisotropy of the space surrounding the aromatic ring, leading to some specific signals becoming isolated and easily distinguishable. For example, a clearly defined H^6 signal from the glucose unit A bearing the triazole ring in **10** are at 2.6–3.0 ppm; the 5^A-hydrogen is also quite distinctive on the spectra (4.17–4.23 ppm). These observations agree with the reported data [13,32] and may help to confirm the structure. The other resonance signals from the CD skeleton are difficult to follow due to total overlapping and the whole asymmetry of the molecule; however, each methyl group in a molecule gives a singlet that is quite prominent on a spectrum, even if it represents only one group. The spectrum of compound **4** contains two sharp peaks at 3.41 (6H) and 3.43 (6H) ppm, which belong to the methyl groups attached to the carbon-3 positions. The other signals (36H) from Me–O–C^3 are concentrated in two overlapped singlets of different intensities. The single peak at 3.54 ppm represents all signals from Me–O–C^2, implying that the triazole ring interacts mainly with the hydrogens inside the cavity. Another solid proof of the partial self-inclusion of the triazole into the internal space of CD is the fragment of the NOESY spectrum (Figure 1a), where the interaction of the triazole hydrogen with H–C^{6A}, H–C^{5A}, and H–C^6 from the glucose unit next to the unit A is clearly seen indicating the interaction between the triazole proton and the internal cavity of the CD.

The spectra of **10** share several trends with **4**, including the scattering of hydrogen-6 signals, the interaction of triazole proton with several hydrogens inside the cavity (Figure 1b) on the NOESY spectrum, and the splitting of signals from methyl groups. However, the latter looks even more prominent on the spectrum since the methyls on the primary rim are near the aromatic system. Six separated singlets could be found in the 3.06–3.34 ppm range, where one peak represents one methyl group from one CD unit. Such observations may be explained by the desymmetrization of the molecule caused by a partial and reversible self-inclusion of the triazole moiety into the CD cavity, as was previously studied in detail for the CD dimers prepared by CuAAC reaction [15]. Although such self-inclusion was not prominent for dimers based on the short propargyl ether linker and unsubstituted CD, in our case, the Me–O–C^6 groups could have changed the situation due to the steric hindrance. The interaction of the triazole proton with the protons inside the cavity was not observed in the spectra of compound **9,** which is acetyl-protected **10** (Figure 1c). However, it shares with **10** the same pattern of methyl splitting, though a much weaker one (Figure 2). We suppose that the chloroform where the spectrum of **9** was measured prevents the self-inclusion of the triazole ring.

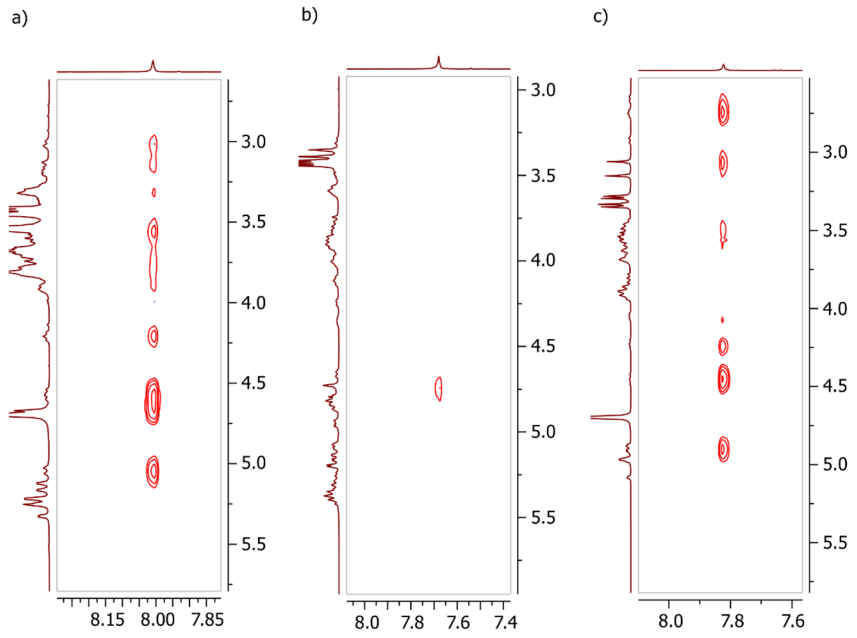


Figure 1: The fragments of ^{1}H NOESY NMR spectra of **4** (a), **10** (b), and **9** (c) indicating the interaction between the triazole proton and the internal cavity of the CD.

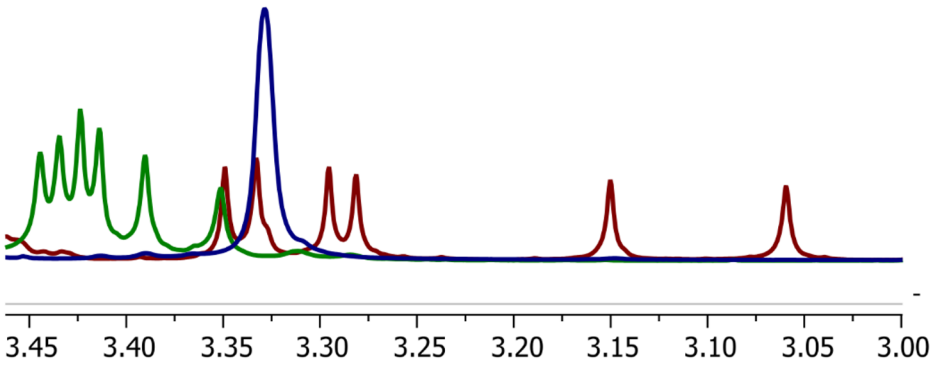


Figure 2: The fragment of the ^{1}H NMR spectrum of compounds **9** (green); **10** (red); **12** (blue) representing the signals from Me–O–C^6.

Concluding all the abovementioned, we may assume that a type of spacer between two CD parts in a dimer could affect molecular symmetry, altering its binding ability. The influence of the triazole ring and its potential inclusion into the cavity must also be considered. Nevertheless, a recent study proved that the tumbling of the CD cavity is reversible and a strongly binding quest is capable of filling all CD cavities; thus, reversing the CD tumbling [33].

The UV determination of tetracene solubility in solutions of supramolecular hosts

The obtained CD dimers with partially methylated rims, along with some other CD derivatives (Figure 3), were tested to increase the solubility of tetracene. Tetracene has limited solubility in several organic solvents such as chloroform, DMSO, THF, and chlorinated arenes [34-36]. Its solubility sufficiently increases with temperature, even more in a sealed vial where low boiling point solvents can be heated more. This way, we obtained concentrated hot solutions even in methanol and other solvents that almost do not dissolve tetracene at room temperature. DMSO demonstrated a moderate dissolving ability towards tetracene. Still, it does not have UV absorbance and dissolves all supramolecular hosts we prepared, making it the best choice for our study. Unfortunately, we did not succeed with solvents, such as water or methanol, where an increase in solubility is most desired. But some success we obtained with DMSO. For our experiments, we used the same mass of a host in every experiment, meaning the molar concentration of a CD in the samples was different. Especially it concerned the dimers whose solutions were approximately two times less concentrated than others. However, we decided from the practical point of view that the effectiveness of the solubilization effect should be calculated to the host's mass rather than its molar concentration.

The UV absorbance spectrum of tetracene in DMSO consists of several regions gradually rising with the concentration. The absorption band at 476 nm is the best choice for building a calibration plot with a sufficient linear region (Figure 4). Exceeding the concentration above 1 mmol/L slowly decreases the linearity of the plot. Concentrated tetracene solutions with supramolecular hosts have UV absorbances out of the linear region. So we had to dilute them 5 and 10 times for the measurements.

The relative concentration of tetracene in the presence of supramolecular hosts, relative to the concentration of tetracene in the saturated solution is shown in Figure 5. This chart implies an actual increase in solubility of tetracene for the majority of the tested samples. Since the size and shape of the cavities of α-CD

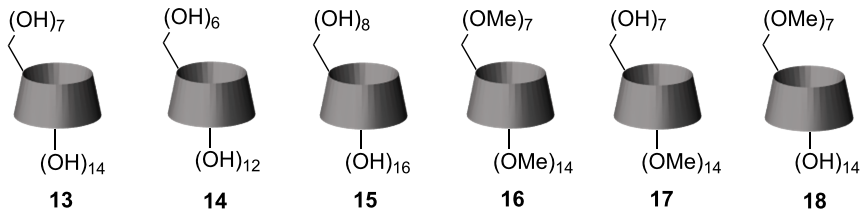


Figure 3: Other cyclodextrins that were used in the solubilization experiments with tetracene.

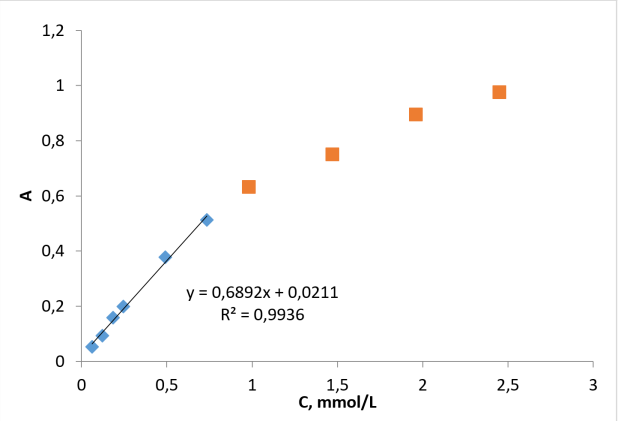


Figure 4: The tetracene UV absorbance dependence on concentration at 476 nm.

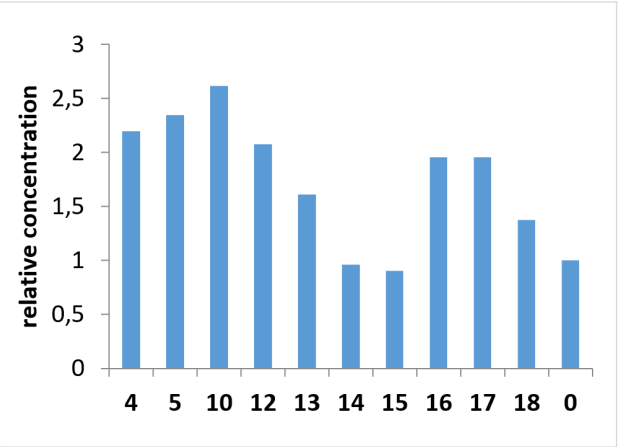


Figure 5: The relative concentrations of tetracene in DMSO solutions with hosts **4**, **5**, **10**, **12**, **13–18** referred to its concentrated solution without any hosts (**0**).

and γ-CD are not comparable with tetracene's geometry, they do not provide any changes from the blank solution. The other compounds more or less enhanced the solubility. Ranging all β-CD derivatives from worst one to best one, we got the row:

18 < **13** < **16** ≈ **17** < **12** < **4** < **5** < **10**

The same results recalculated to the molar concentration of hosts in the solutions (Table 1) do not change the order in this row. However, it highlights the difference between the "dimeric" and "monomeric" compounds, suggesting that both the dimers' CD parts are effectively involved in the complexation with tetracene. On the other hand, the recalculation equalizes the effectiveness of compounds **4**, **5,** and **10**, whereas compound **12** is still behind them.

Comparing the dimers with the corresponding "monomers", one could find a notable difference in the performances of the compounds with methylated primary rims. The dimer **10** facilitates the dissolution of approximately 2 times more tetracene than **18**. Along with **18**, compound **13** (β-CD) has also shown poor solubilizing activity. We suggest that the presence of hydroxy groups on the secondary rim of CD allows the hydrogen bond formation between two molecules, creating a capsule (tail-to-tail interaction, Figure 6a). It seems the generation of such capsules in solution disfavors the complexation with tetracene. The compounds with occupied secondary rims, such as **16** and **17,** have shown better effectiveness, losing only to the dimers. A spacer connecting two primary rims in a dimer promotes the interaction between them, forming a capsule with the inverted orientation of CD moieties (head-to-head interaction, Figure 6b). We suppose this type of interaction results in better complexation with the guest.

Table 1: The calculated concentrations of tetracene in DMSO solutions with various hosts and the relative concentrations of tetracene in these solutions related to the concentrations of the corresponding hosts.

Host	The concentration of tetracene in the solution *c*, mM	The relative concentration of tetracene relative to the host concentration in the solution c/c_h
–	3.11	–
4	6.85	0.38
5	7.3	0.39
10	8.14	0.42
12	6.47	0.32
13	5.01	0.11
14	3	0.08
15	2.81	0.05
16	6.09	0.17
17	6.08	0.16
18	4.28	0.11

The synthesized dimers have given us the best results in the experiment. However, it is quite difficult to highlight a trend in this small group because the dimers with methylated primary rims have shown the worst and best result, with a significant gap between their performances. In contrast, the dimers with methylated secondary rims have average solubilizing abilities. The phenomena we described above might be a reason for such behavior. The ^{1}H NMR spectrum of compound **10** (Figure 2) indicates a significant degree of distortion in the molecule's symmetry. We suppose that the "tail-to-tail" interaction, which is unfavorable for the complexation with tetracene, does not take part in this case because the distorted secondary rims fail to build a system with strong hydrogen bonds. The spectrum of **12** clearly belongs to a compound with high symmetry, favoring this interaction and reducing the solubilization efficiency; also,

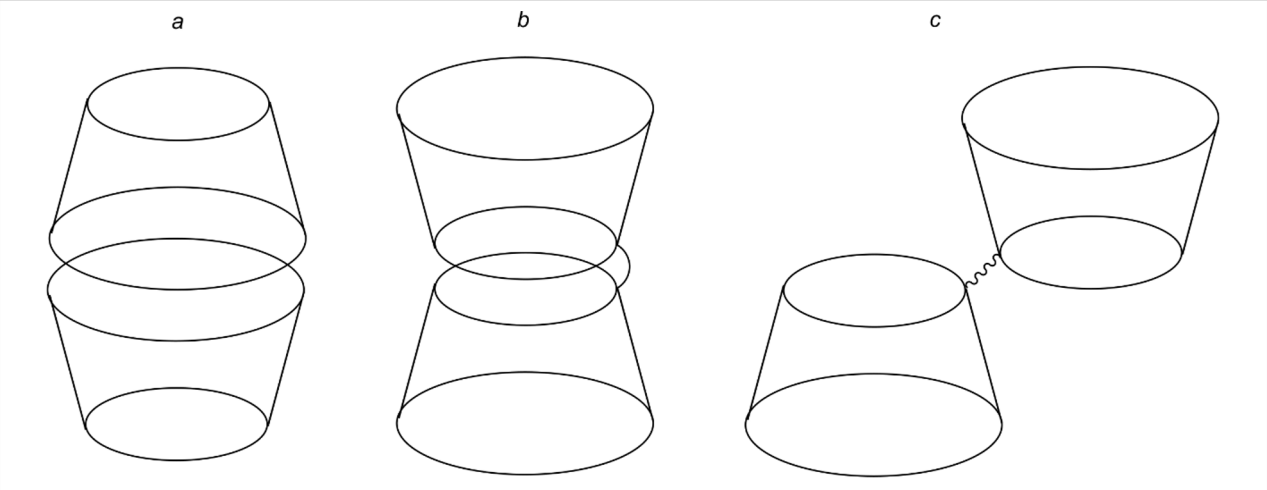


Figure 6: "Tail-to-tail" (a) and "head-to-head" (b) orientation of two cyclodextrin moieties and primary-rim connected CDs with non-interacting rims (c).

the spacer length might be too short for the "head-to-head" orientation (Figure 6c).

Determination of the binding parameters

Despite achieving some success in the increase of tetracene solubility, we struggled to evaluate the supramolecular interaction. Unfortunately, it seems that the complexation does not change the position of the chemical shifts on the NMR spectra and the shape or intensity of the UV–vis spectrum. The decrease in the guest's diffusion coefficient by binding with a high-molecular-weight host serves as a reliable indicator for the determination of binding parameters in a case if, for example, no alternation of chemical shifts is observed on the NMR spectrum. The diffusion coefficient can be estimated by a DOSY experiment [37]. In our case, a gradual, steady decline of tetracene's diffusion coefficient was detected by titration with **4**, but it exceeded the measurement error only at the maximum concentration of the CD. Thus, this method discovers a poor supramolecular interaction where a reliable determination of the binding parameters is impossible.

ITC (isothermal titration calorimetry) is a popular technique for evaluating supramolecular interaction with CDs [38], mainly in the aqueous medium. We performed the titrations of tetracene DMSO solution by the series of CDs used in the solubility experiments (Figure 7, Figure 8). The titrations were accompanied by measurable heat, different from the heat of dilution of both tetracene and CDs with pure solvent (see Supporting Information File 1). Therefore, the measured heat was attributed to the interactions of CDs with tetracene and the titration isotherms, which were successfully fitted to the 1:1 binding model.

The thermodynamic parameters for the interaction of CDs with tetracene are given in Table 2. The dilution of CDs to DMSO

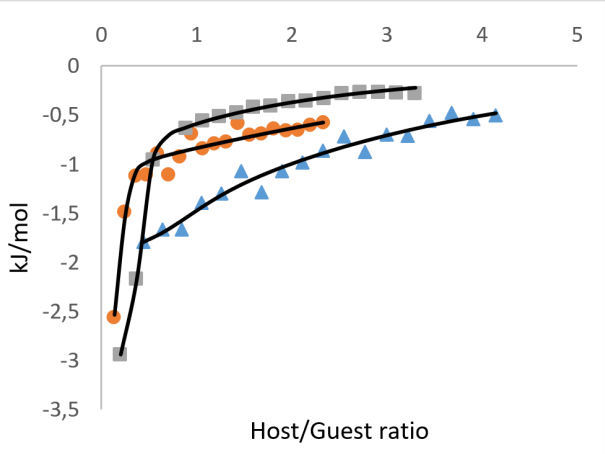


Figure 7: Isotherms of the titration of tetracene with "dimeric" CD solutions in DMSO at 298 K (circles – **10**; squares – **4**; triangles – **5**).

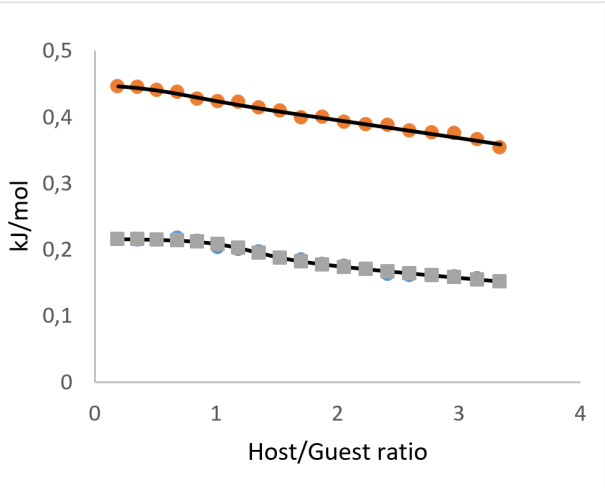


Figure 8: Isotherms of the titration of tetracene with "monomeric" CD solutions in DMSO at 298 K (circles – **16**; squares – **13**).

Table 2: The thermodynamic parameters of the binding calculated from ITC experiments.

CD	Stoichiometry *n*	Affinity constant, $K_a \cdot 10^{-4}$, M^{-1}	Gibbs free energy Δ*G*, kJ/mol	Enthalpy Δ*H*, kJ/mol	Entropy Δ*S*, J/mol·K
13	1.22	2.6	–25.2	0.2	85.3
16	0.72	1.3	–23.5	0.5	79.9
10	0.15	10.9	–28.7	–2.9	86.6
4	0.32	8.6	–28.2	–3.1	84.1
5	0.83	0.7	–21.9	–2.0	66.5

was exothermic for all five samples, with the lowest heat recorded for permethylated **16**. The dilution of CDs in an aqueous system, published elsewhere, is always endothermic [39]. The DMSO with 0.02% of water (roughly 11 mM, given by the manufacturer) was used. The dilution experiments demonstrated that DMSO does not absorb additional water in the timescale of the ITC experiment, which may produce measurement artifacts. Additionally, the titration of a DMSO to a DMSO with 5 vol % of water was carried out to manifest the contamination with water (see Supporting Information File 1). Therefore, the exothermic signal from the dilution of CDs in DMSO was attributed to the hydration of hydroxy and, to a lesser extent, methoxy groups from partially methylated CDs with the admixture of water in DMSO.

All CDs interactions with tetracene were accompanied by sufficient entropy gain, which points to the desolvation of interacting molecules. The interaction of CD "monomers" **13** and **16** with tetracene is weakly endothermic and, therefore, understood as an entropy-driven process with the potential formation of a complex in 1:1 stoichiometry. All CD dimers interacted with tetracene exothermically. Since the overall amount of water in the system is one order lower than the amount of hydroxy groups in CDs, they preserve the capacity for hydrogen bonding. The presence of tetracene in the solution enhances inter- or intramolecular associations of CD rings in dimers. The CD dimer **5**, linked with urea, demonstrated stoichiometry close to unity. Still, dimers **4** and **10**, linked with triazole-based spacer, exhibited strong exothermic interaction at an unusual stoichiometry range of 0.15–0.32 (3 to 7 tetracene molecules to one CD dimer). These two CD dimers, according to NMR, have the triazole linker partially included in CD rings. We assume that their interaction with tetracene is a multistep process, and the obtained thermodynamic parameters are the effective values for the sum of all interaction steps.

Although from the sole ITC experiment, the formation of tetracene inclusion complex with CDs can't be affirmed, the observed stoichiometry favors this hypothesis. Additionally, the binding strength in terms of K_a (M^{-1}) well matches the solubility experiments' results and emphasizes the exceptional performance of the synthesized dimers.

Conclusion

In conclusion, we have prepared four new CD dimers from 6-azido partially methylated β-CD derivatives with two types of spacers between CD moieties. A new method for preparing β-CDs with selectively methylated primary rim based on the remarkable methylation ability of methyl tosylate with relatively mild bases at solvent-free conditions has been developed. It has been proved that using Lewis acid in the phosphine imide reactions with CDs can increase the reactivity of some low-reactive compounds, giving better yields and reducing the reaction time. The UV measurements have confirmed an increase in solubility of tetracene in DMSO in the presence of some CD derivatives. The partially methylated CD dimers are more than twice effective in solubilization than the compounds with one CD unit in the molecule in the molar ratio, implying that both CD fragments are engaged in complexation with tetracene. The compounds possessing hydroxy groups on the secondary rim generally perform worse than those with a methylated secondary rim. ITC studies and tetracene's increased solubility prove the host–guest interaction's existence. The obtained results give hope for a successful continuation of the study with higher acenes.

Experimental

Materials. α- (**14**), β- (**13**), and γ-cyclodextrin (**15**) were purchased from Wacker Chemie AG; methyl tosylate was purchased from Acros Organics; the remaining chemicals were bought from Merck. The methyl tosylate contained traces of *p*-toluenesulfonic acid, so, before use, we washed it with saturated $NaHCO_3$ solution in a dropping funnel and dried it over anhydrous $MgSO_4$. The other chemicals for synthesis were used without further purification. SiliaFlash P60 40–63 μm from SiliCycle was used for column chromatography. The solvents were supplied by Penta and were distilled before use. The course of the reactions was followed on TLC Silica gel 60 F_{254} bought

from Merck company. For the UV measurements, α-, β-, and γ-cyclodextrin were recrystallized from hot water or a water/methanol mixture. The purity of the prepared products was considered enough for use in UV experiments without additional purification.

Methods. Low-resolution mass spectra were measured with a Shimadzu LCMS-2020 spectrometer. Samples were ionized by electrospray technique (ESI) and detected by quadrupole or TOF. The drying and nebulizer gas was nitrogen. High-resolution mass spectra were measured with an Agilent Technologies 6530 Accurate-Mass Q-TOF LC/MS spectrometer. Samples were ionized by electrospray technique (ESI) and detected by quadrupole or TOF. UV–vis spectroscopy spectra were measured with Thermo Scientific Helios γ with wolfram and deuterium lamp. The wavelength range is 190–800 nm. ^{1}H, ^{13}C, and 2D NMR spectra were measured on Bruker Avance III HD 400 spectrometer. For TLC detection of CDs, we charred a TLC plate with 50% sulfuric acid water solution at 250 °C.

UV measurements

The determination of tetracene's solubility in DMSO

To determine the solubility of tetracene in DMSO, we put a small amount of tetracene (2.0–2.5 mg) in a vial, added 2 mL of DMSO, and heated the vial until the whole compound had been dissolved. Then we cooled down the vial in a dark place, and after 1 hour, we filtered off the formed crystals, took 50 and 100 μL of the solution, diluted them to 1 mL, and measured the UV spectra. A comparison with the calibration plot determined the concentration of the tetracene. Thus, we estimated tetracene's solubility in DMSO to be 0.71 mg/mL at room temperature.

The calibration of tetracene UV absorption dependence

To determine the UV absorbance dependence of tetracene on its concentration, we prepared a stock solution containing 2.8 mg of tetracene in 5 mL of DMSO. The stock solution was then used to prepare a series of solutions with different concentrations (see the Supporting Information File 1). The solutions' light absorbance at 476 nm was used to build the calibration plot.

The determination of tetracene's solubility in DMSO in the presence of the supramolecular hosts

To determine how a supramolecular host affects the guest's solubility, we used the same procedure for preparing the concentrated tetracene solution. We used 3 mg of tetracene and 50 mg of a host for every sample, dissolved in 1 mL of DMSO. The samples were heated until the compounds were fully dissolved and let cool down. The undissolved tetracene was filtered off, and the samples were diluted 5 and 10 times to get the absorbance of the solution into the linear range of the tetracene concentration/UV absorption calibration plot.

ITC measurements

The saturated solution of tetracene (0.71 mg/mL, 3.1 mM) was titrated at 298 K with the solutions of cyclodextrins: **13** (57 mg/mL; 50 mM), **16** (71 mg/mL, 50 mM), **10** (27 mM; 70 mg/mL), **4** (41 mM, 114 mg/mL), **5** (48 mM, 129 mg/mL) in DMSO on MicroCal ITC200 (Malvern Panalytical Ltd, UK) isothermal titration calorimeter. The titrations were performed in 20 consecutive injections, where the first injection of 0.4 μL was followed by 19 injections of 2 μL of CD solution. The blank titrations of CDs to the solvent were performed similarly, and the heat of dilution was subtracted from the corresponding isotherms. The isotherms were fitted with ITC 200 1.25.5 (Malvern Panalytical Ltd, UK) software, based on Origin 7SR4 v 7.0552 (OriginLab Corporation, MA, USA), to the two independent binding sites model. From the fit, the stoichiometry (n), binding enthalpy change (ΔH, kJ·mol^{-1}), affinity constant (K_a, M^{-1}), binding free energy change (ΔG, kJ·mol^{-1}), and binding entropy change (ΔS, J·mol^{-1}·K^{-1}) for the first binding site were calculated. The thermodynamic parameters for the second binding site were not discussed but used to subtract the non-linear residual heat at high molar ratios. Separate titration experiments of pure DMSO to the solution of tetracene in DMSO and DMSO to the solution of water in DMSO were carried out to account for potential measurement artifacts originating from water concentration mismatch in highly hygroscopic DMSO.

Supporting Information

Supporting Information File 1

Synthetic procedures, characterization, ^{1}H, ^{13}C DEPT, 2D NMR, IR, UV–vis spectra of synthesized compounds; UV–vis spectra of tetracene solutions in DMSO; ITC thermograms.
[https://www.beilstein-journals.org/bjoc/content/supplementary/1860-5397-18-170-S1.pdf]

Funding

This work has been supported by Charles University Research Centre program No. UNCE/SCI/014 and Ministry of Education, Youth and Sports (grant # LM2018133 ERIC EATRIS-CZ).

ORCID® iDs

Konstantin Lebedinskiy - https://orcid.org/0000-0002-9559-4029
Volodymyr Lobaz - https://orcid.org/0000-0003-0479-2837
Jindřich Jindřich - https://orcid.org/0000-0003-3770-0214

References

1. Del Valle, E. M. M. *Process Biochem. (Oxford, U. K.)* **2004,** *39,* 1033–1046. doi:10.1016/s0032-9592(03)00258-9
2. Wenz, G. *Beilstein J. Org. Chem.* **2012,** *8,* 1890–1895. doi:10.3762/bjoc.8.218
3. Řezanka, M. *Environ. Chem. Lett.* **2019,** *17,* 49–63. doi:10.1007/s10311-018-0779-7
4. Connors, K. A. *Chem. Rev.* **1997,** *97,* 1325–1358. doi:10.1021/cr960371r
5. Kida, T.; Fujino, Y.; Miyawaki, K.; Kato, E.; Akashi, M. *Org. Lett.* **2009,** *11,* 5282–5285. doi:10.1021/ol902239e
6. Kida, T.; Iwamoto, T.; Fujino, Y.; Tohnai, N.; Miyata, M.; Akashi, M. *Org. Lett.* **2011,** *13,* 4570–4573. doi:10.1021/ol2017627
7. Breslow, R.; Greenspoon, N.; Guo, T.; Zarzycki, R. *J. Am. Chem. Soc.* **1989,** *111,* 8296–8297. doi:10.1021/ja00203a050
8. Breslow, R.; Chung, S. *J. Am. Chem. Soc.* **1990,** *112,* 9659–9660. doi:10.1021/ja00182a046
9. Breslow, R.; Zhang, B. *J. Am. Chem. Soc.* **1994,** *116,* 7893–7894. doi:10.1021/ja00096a055
10. Breslow, R.; Zhang, B. *J. Am. Chem. Soc.* **1996,** *118,* 8495–8496. doi:10.1021/ja961567b
11. Liu, Y.; Chen, Y. *Acc. Chem. Res.* **2006,** *39,* 681–691. doi:10.1021/ar0502275
12. Mourer, M.; Hapiot, F.; Monflier, E.; Menuel, S. *Tetrahedron* **2008,** *64,* 7159–7163. doi:10.1016/j.tet.2008.05.095
13. Mourer, M.; Hapiot, F.; Tilloy, S.; Monflier, E.; Menuel, S. *Eur. J. Org. Chem.* **2008,** 5723–5730. doi:10.1002/ejoc.200800728
14. Blaszkiewicz, C.; Bricout, H.; Léonard, E.; Len, C.; Landy, D.; Cézard, C.; Djedaïni-Pilard, F.; Monflier, E.; Tilloy, S. *Chem. Commun.* **2013,** *49,* 6989. doi:10.1039/c3cc43647k
15. Potier, J.; Menuel, S.; Azaroual, N.; Monflier, E.; Hapiot, F. *Eur. J. Org. Chem.* **2014,** 1547–1556. doi:10.1002/ejoc.201301681
16. Hamon, F.; Blaszkiewicz, C.; Buchotte, M.; Banaszak-Léonard, E.; Bricout, H.; Tilloy, S.; Monflier, E.; Cézard, C.; Bouteiller, L.; Len, C.; Djedaini-Pilard, F. *Beilstein J. Org. Chem.* **2014,** *10,* 2874–2885. doi:10.3762/bjoc.10.304
17. Chaudhuri, S.; Verderame, M.; Mako, T. L.; Bandara, Y. M. N. D. Y.; Fernando, A. I.; Levine, M. *Eur. J. Org. Chem.* **2018,** 1964–1974. doi:10.1002/ejoc.201800283
18. Anthony, J. E. *Angew. Chem., Int. Ed.* **2008,** *47,* 452–483. doi:10.1002/anie.200604045
19. Zade, S. S.; Bendikov, M. *Angew. Chem., Int. Ed.* **2010,** *49,* 4012–4015. doi:10.1002/anie.200906002
20. Nagano, M.; Hasegawa, T.; Myoujin, N.; Yamaguchi, J.; Itaka, K.; Fukumoto, H.; Yamamoto, T.; Koinuma, H. *Jpn. J. Appl. Phys., Part 1* **2004,** *43,* L315–L316. doi:10.1143/jjap.43.l315
21. Jancarik, A.; Levet, G.; Gourdon, A. *Chem. – Eur. J.* **2019,** *25,* 2366–2374. doi:10.1002/chem.201805975
22. Payne, M. M.; Parkin, S. R.; Anthony, J. E. *J. Am. Chem. Soc.* **2005,** *127,* 8028–8029. doi:10.1021/ja051798v
23. Takeo, K.; Ueraura, K.; Mitoh, H. *J. Carbohydr. Chem.* **1988,** *7,* 293–308. doi:10.1080/07328308808058926
24. Takeo, K.; Mitoh, H.; Uemura, K. *Carbohydr. Res.* **1989,** *187,* 203–221. doi:10.1016/0008-6215(89)80004-7
25. Varga, E.; Benkovics, G.; Darcsi, A.; Várnai, B.; Sohajda, T.; Malanga, M.; Béni, S. *Electrophoresis* **2019,** *40,* 2789–2798. doi:10.1002/elps.201900134
26. Carofiglio, T.; Cordioli, M.; Fornasier, R.; Jicsinszky, L.; Tonellato, U. *Carbohydr. Res.* **2004,** *339,* 1361–1366. doi:10.1016/j.carres.2004.03.007
27. Tungala, K.; Adhikary, P.; Krishnamoorthi, S. *Carbohydr. Polym.* **2013,** *95,* 295–298. doi:10.1016/j.carbpol.2013.02.074
28. Munteanu, M.; Choi, S.; Ritter, H. *Macromolecules* **2009,** *42,* 3887–3891. doi:10.1021/ma900397m
29. Cintas, P.; Barge, A.; Tagliapietra, S.; Boffa, L.; Cravotto, G. *Nat. Protoc.* **2010,** *5,* 607–616. doi:10.1038/nprot.2010.1
30. Sallas, F.; Marsura, A.; Petot, V.; Pintér, I.; Kovács, J.; Jicsinszky, L. *Helv. Chim. Acta* **1998,** *81,* 632–645. doi:10.1002/hlca.19980810314
31. Menuel, S.; Porwanski, S.; Marsura, A. *New J. Chem.* **2006,** *30,* 603–608. doi:10.1039/b600023a
32. Cravotto, G.; Fokin, V. V.; Garella, D.; Binello, A.; Boffa, L.; Barge, A. *J. Comb. Chem.* **2010,** *12,* 13–15. doi:10.1021/cc900150d
33. González-Méndez, I.; Hameau, A.; Laurent, R.; Bijani, C.; Bourdon, V.; Caminade, A.-M.; Rivera, E.; Moineau-Chane Ching, K. I. *Eur. J. Org. Chem.* **2020,** 1114–1121. doi:10.1002/ejoc.201901823
34. Liang, Z.; Zhao, W.; Wang, S.; Tang, Q.; Lam, S.-C.; Miao, Q. *Org. Lett.* **2008,** *10,* 2007–2010. doi:10.1021/ol800620s
35. Kim, H. Y.; Bjorklund, T. G.; Lim, S.-H.; Bardeen, C. J. *Langmuir* **2003,** *19,* 3941–3946. doi:10.1021/la026851x
36. Griffini, G.; Brambilla, L.; Levi, M.; Castiglioni, C.; Del Zoppo, M.; Turri, S. *RSC Adv.* **2014,** *4,* 9893. doi:10.1039/c3ra46810k
37. Ferrazza, R.; Rossi, B.; Guella, G. *J. Phys. Chem. B* **2014,** *118,* 7147–7155. doi:10.1021/jp504406j
38. Mura, P. *J. Pharm. Biomed. Anal.* **2014,** *101,* 238–250. doi:10.1016/j.jpba.2014.02.022
39. Zheng, P. J.; Wang, C.; Hu, X.; Tam, K. C.; Li, L. *Macromolecules* **2005,** *38,* 2859–2864. doi:10.1021/ma048324l

License and Terms

This is an open access article licensed under the terms of the Beilstein-Institut Open Access License Agreement (https://www.beilstein-journals.org/bjoc/terms), which is identical to the Creative Commons Attribution 4.0 International License (https://creativecommons.org/licenses/by/4.0). The reuse of material under this license requires that the author(s), source and license are credited. Third-party material in this article could be subject to other licenses (typically indicated in the credit line), and in this case, users are required to obtain permission from the license holder to reuse the material.

The definitive version of this article is the electronic one which can be found at:
https://doi.org/10.3762/bjoc.18.170

BEILSTEIN JOURNAL OF ORGANIC CHEMISTRY

Inclusion complexes of the steroid hormones 17β-estradiol and progesterone with β- and γ-cyclodextrin hosts: syntheses, X-ray structures, thermal analyses and API solubility enhancements

Alexios I. Vicatos, Zakiena Hoossen and Mino R. Caira*

Full Research Paper

Open Access

Address:
Centre for Supramolecular Chemistry Research (CSCR), Department of Chemistry, University of Cape Town, Rondebosch 7701, South Africa

Email:
Mino R. Caira* - Mino.Caira@uct.ac.za

* Corresponding author

Keywords:
cyclodextrin; complexation; 17β-estradiol; progesterone; solubility; X-ray diffraction

Beilstein J. Org. Chem. **2022,** *18,* 1749–1762.
https://doi.org/10.3762/bjoc.18.184

Received: 27 October 2022
Accepted: 09 December 2022
Published: 22 December 2022

This article is part of the thematic issue "Cyclodextrins as building blocks for new materials".

Guest Editor: S. Fourmentin

© 2022 Vicatos et al.; licensee Beilstein-Institut.
License and terms: see end of document.

Abstract

Overcoming the challenges of poor aqueous solubility of active pharmaceutical ingredients (APIs) is necessary to render them bioavailable. This study addresses the poor solubility of two potent steroid hormones, 17β-estradiol (BES) and progesterone (PRO), via their complexation with two water-soluble native cyclodextrins (CDs) namely β-CD and γ-CD. The hydrated inclusion complexes β-CD·BES, β-CD·PRO, γ-CD·BES and γ-CD·PRO were prepared via kneading and co-precipitation, and ^{1}H NMR spectroscopic analysis of solutions of their pure complex crystals yielded the host–guest stoichiometries 2:1, 2:1, 1:1 and 3:2, respectively. Both powder X-ray diffraction (PXRD) and single-crystal X-ray diffraction (SCXRD) were employed for focused studies of the isostructurality of the CD complexes with known complexes and structural elucidation of the new complexes, respectively. SCXRD analyses of β-CD·BES, β-CD·PRO and γ-CD·PRO at 100(2) K yielded the first crystal structures of CD complexes containing the hormones BES and PRO, while the complex γ-CD·BES was readily shown to be isostructural with γ-CD·PRO by PXRD. Severe disorder of the encapsulated steroid molecules in the respective channels of the CD molecular assemblies was evident, however, preventing their modelling, but combination of the host–guest stoichiometries and water contents of the four hydrated inclusion complexes enabled accurate assignment of the chemical formulae of these ternary systems. Predicted electron counts for the complexed molecules BES and PRO correlated reasonably well with the complex compositions indicated by ^{1}H NMR spectroscopy. Subsequent measurements of the aqueous solubilities of the four complexes confirmed significant solubility improvements effected by encapsulation of the steroids within the CDs, yielding solubility enhancement factors for BES and PRO in the approximate range 5–20.

Introduction

The insolubility of active pharmaceutical ingredients (APIs) and other bioactive compounds in aqueous media and the associated challenges for effective drug delivery are well known to have beleaguered the pharmaceutical industry for many decades. However, the complexation of APIs with cyclodextrins (cyclic oligosaccharides) resulting in the formation of inclusion complexes, has proven to be a versatile technology for overcoming not only the poor aqueous solubility of APIs, but also unfavourable properties such as their chemical instability, adverse side effects such as gastrointestinal irritation, and unpleasant tastes and odours [1-5]. Here we report an investigation of the cyclodextrin (CD) inclusion of two notable bioactive compounds (Figure 1), namely the most potent human estrogen, 17β-estradiol (BES) and progesterone (PRO), the steroid hormone associated with female fertility and pregnancy. Both compounds have very low aqueous solubility values (3.6×10^{-3} mg·cm^{-3} at 27 °C, and 8.81×10^{-3} mg·cm^{-3} at 25 °C, respectively) [6-8]. This drawback hinders their use as medications in hormone replacement therapy and other treatments, and one aim of this study is to enhance their solubilities via their inclusion in selected native (natural) CDs. A commercially available synthetic derivative of BES, ethinylestradiol, which is used as (inter alia) a contraceptive, has an aqueous solubility of 11.3×10^{-3} mg·cm^{-3} at 27 °C [6,9], and a significantly higher oral bioavailability relative to that of BES. The steroid hormone PRO is commercially available either in its natural form or as micronized natural progesterone [10].

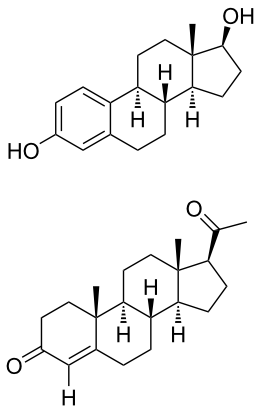


Figure 1: Chemical structures of 17β-estradiol (top) and progesterone (bottom).

A substantial volume of research on the topic of CD inclusion of BES and PRO has already been published, the majority of the publications being focused on medicinal applications, for example, using formulations of these drugs with CDs for ophthalmic and nasal delivery [11-21]. The scientific literature abounds with reports featuring the use of a wide variety of analytical and confirmatory techniques [22-28] as well as solubility analyses [29-38] to investigate the physicochemical properties of CD inclusion complexes and multicomponent CD inclusion systems based on numerous derivatised CDs containing BES and PRO, thus confirming the sustained interest in this approach and its significance in drug delivery. Previous studies of the complexation of BES, PRO and related compounds by CDs in the solution phase have typically reported the use of NMR spectroscopy to investigate complex formation, complex structure, stoichiometry and association constants via the detection and measurement of small deviations in the ^{1}H NMR chemical shifts for both host and guest molecules upon complexation. PXRD studies were generally used to detect the formation of new crystalline phases following attempts to prepare complexes by spray-drying, freeze-drying, co-grinding, kneading and solution-based crystallization; however, this modest type of 'fingerprinting' has not generally been pursued further to deduce important features of CD complexes such as the crystal packing of the CD host molecules. Furthermore, no previous structure determinations via SCXRD analysis of CD complexes of BES and PRO have been reported. Many studies involved phase solubility analyses to determine CD complex formation and association constants. Our previous study of the complexation of the steroidal anticancer agent 2-methoxyestradiol (2ME) by selected CDs [39] yielded two significant positive outcomes, namely a considerable increase in the aqueous solubility and dissolution rate of 2ME derived from its β-CD complex, and for the first time, the determination of the modes of inclusion of a steroidal molecule within the cavities of CD host molecules (dimethylated and permethylated β-CD) by SCXRD. Motivated by these favourable results, we recently prepared the four crystalline inclusion complexes β-CD·BES, β-CD·PRO, γ-CD·BES and γ-CD·PRO with a view to using PXRD, not simply as a routine fingerprint technique, but in a more innovative study of their crystal isostructurality within the series and with published complexes. SCXRD was employed to deduce structural features of the complexes at the molecular level, while the occurrence of severe guest disorder prompted the non-routine application of a method for yielding complex composition from the residual electron density peaks in the respective crystal structures. We carried out analogous studies on the four CD complexes to establish whether they might also display enhanced aqueous solubilities of the included steroids relative to those of the pure drugs. We also present here results of comprehensive thermal characterization of these complexes, with emphasis on the determination of their water contents.

While it is widely known that the solubility of poorly water-soluble steroidal compounds such as BES and PRO may be very

significantly enhanced by various derivatised CDs, it was of interest to us to establish to what extent the native host compounds β-CD and γ-CD could improve the aqueous solubilities of BES and PRO, specifically upon dissolution of their solid hydrated inclusion complexes whose accurately derived ternary formulae were established in this study. The relatively low cost of these CDs and in particular the low toxicity of γ-CD are advantageous for potential drug delivery. Furthermore, the amorphous nature of highly water-soluble CD derivatives (e.g., hydroxypropyl-CD and sulfobutyl ether CD) precludes their formation of crystalline inclusion complexes, which is a distinct disadvantage for solid-state structural investigation and complex characterization by X-ray diffraction methods.

Results and Discussion

Complex screening

The isolation of solid inclusion complexes of BES and PRO with the native cyclodextrins β-CD and γ-CD was successfully achieved by kneading experiments (co-grinding of the respective hosts and guests with water as a medium), the complex identities being subsequently determined unequivocally by powder X-ray diffraction (PXRD). Authentic CD complex formation was deduced from close correlation between the angular peak positions of the products and those of known isostructural CD inclusion complexes retrieved from the Cambridge Structural Database (CSD) [40]. Figure 2 and Figure 3 show representative examples of peak-matching for isostructural complexes [41] and the respective PXRD patterns of β-CD·BES and γ-CD·BES are also available (Figures S1 and S2 in Supporting Information File 1). This method enabled initial assignment of the space group for each new complex and estimation of its unit cell parameters, these data being subsequently confirmed by single crystal X-ray diffraction for those complexes that formed crystals of adequate size and quality.

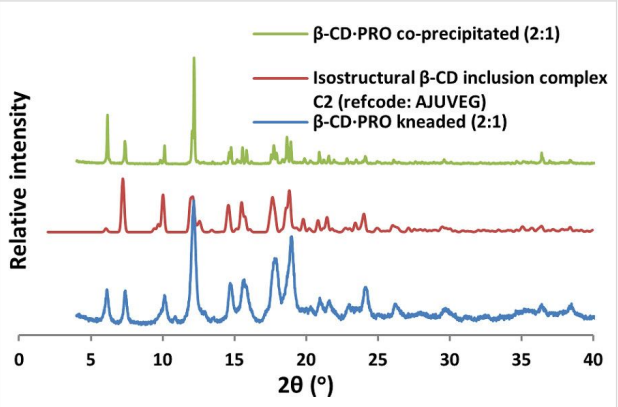


Figure 2: The PXRD patterns of the β-CD·PRO complex produced via kneading (2:1), an isostructural β-CD complex crystallizing in the space group *C*2 (refcode: AJUVEG), and the β-CD·PRO complex produced via co-precipitation (2:1).

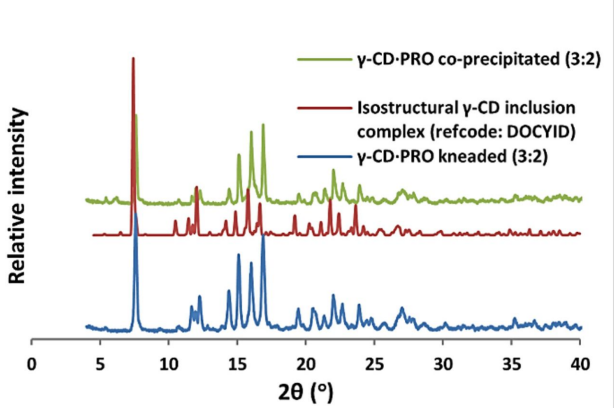


Figure 3: The PXRD patterns of the γ-CD·PRO complex produced via kneading (3:2), an isostructural γ-CD complex crystallizing in the space group $P42_12$ (refcode: DOCYID), and the γ-CD·PRO complex produced via co-precipitation (3:2).

Co-precipitation experiments yielded single crystals of all four CD inclusion complexes with distinctive transparent monoclinic morphologies for β-CD·BES and β-CD·PRO, and transparent rods with a square cross-section for γ-CD·BES and γ-CD·PRO (Figure 4). PXRD analysis also confirmed that pure crystalline phases were obtained for each complex product via co-precipitation experiments and that each of these was the same crystalline phase as the respective complex product produced via kneading. These single crystals were of adequate quality for SCXRD except for the single crystals of γ-CD·BES, which diffracted very weakly.

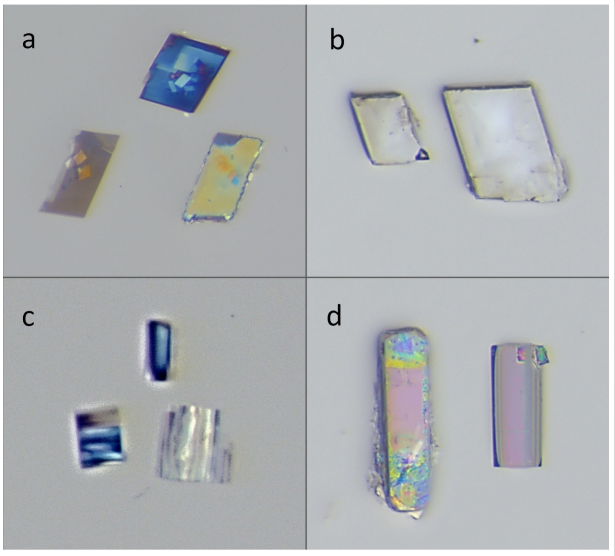


Figure 4: (a) The crystal morphology of β-CD·BES recorded with polarised light. (b) The crystal morphology of β-CD·PRO. (c) The highly magnified crystal morphology of γ-CD·BES. (d) The crystal morphology of γ-CD·PRO.

Host–guest stoichiometric determination by ^{1}H NMR spectroscopy

The host–guest stoichiometries for these complexes were unambiguously determined via solution-state ^{1}H NMR spectroscopy, the samples for the analyses being the complex product materials produced via co-precipitation. The results for the host–guest ratios were as follows: β-CD·BES (2:1), β-CD·PRO (2:1), γ-CD·BES (1:1), γ-CD·PRO (3:2). Fully assigned spectral analyses are also available (Figures S3–S8 and Tables S1–S4 in Supporting Information File 1).

Thermal analysis

The highly reproducible thermogravimetric analyses (TGA) and differential scanning calorimetry (DSC) analyses for the four CD inclusion complexes (Figure 5a–d) primarily indicated their water content and thermal stability, the data for their thermal events being summarised in Table 1. These results were further accompanied by hot stage microscopy (HSM) analyses for all four complexes (Figures S9–S12 in Supporting Information File 1) and variable temperature powder X-ray diffraction (VTPXRD) analyses for β-CD·BES and β-CD·PRO (Figures S13 and S14 in Supporting Information File 1). The precise temperature onset values did not always correlate when comparing the results obtained from the TGA and DSC instruments, but the two methods did involve different sample configurations (samples in open pans vs crimped, vented pans).

For all four complexes dehydration was initially observed, either as a multi- or single-step process, as confirmed by the respective DSC curves (Figures S15–S18 in Supporting Information File 1) and dTGA curves (Figures S19–S22 in Supporting Information File 1). Other thermal events such as minor phase transitions were observed for β-CD·BES and β-CD·PRO as well as premature decomposition, displayed by β-CD·BES in particular (Table 1). Thus, all CD complexes displayed thermal integrity until relatively high temperatures of at least 100 °C, prior to phase transitions and decomposition, indicating acceptable thermal stability for commercial pharmaceutical applications. Further analytical details regarding the TGA, dTGA and DSC results for each sample are available (Section 5, pp. S15 and S16 in Supporting Information File 1).

Single crystal X-ray structural analysis

The crystal structures of β-CD·BES, β-CD·PRO and γ-CD·PRO were solved by isomorphous replacement using as trial models the rigid host atom frameworks of the complexes with CSD refcodes AJUVEG, NUFTUE and MUXBIT, respectively. (Single crystal intensity data could not be collected for

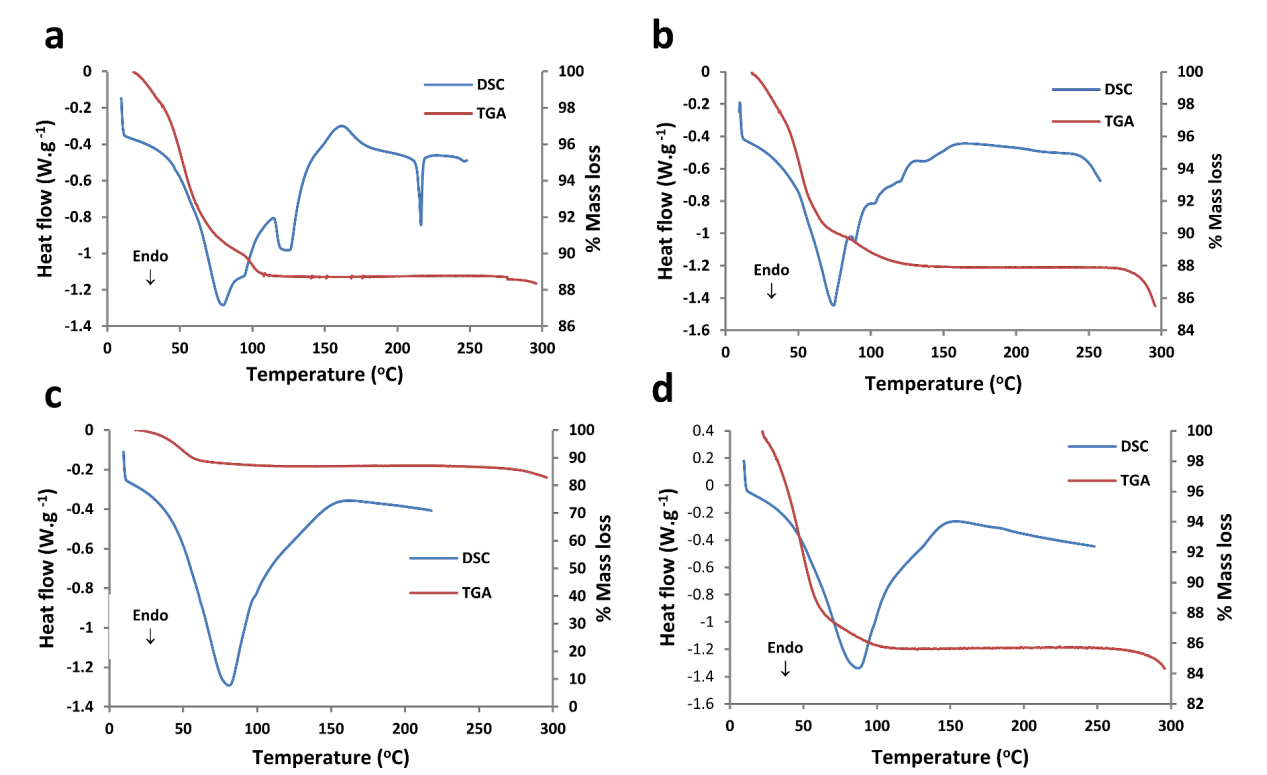


Figure 5: (a) A representative DSC curve (n = 2) of β-CD·BES, with the respective TGA curve (n = 3); (b) a representative DSC curve (n = 2) of β-CD·PRO, with the respective TGA curve (n = 2); (c) a representative DSC curve of γ-CD·BES (n = 2), with the respective TGA curve as a reference (n = 2); (d) a representative DSC curve of γ-CD·PRO (n = 3), with the respective TGA curve as a reference (n = 3).

Table 1: Data for the TGA and DSC thermal events for β-CD·BES, β-CD·PRO, γ-CD·BES, γ-CD·PRO.

CD inclusion complex	TGA	DSC
β-CD·BES	dehydration: temperature range of event: 18.7 ± 1.1 and 120.4 ± 1.3 °C associated mass loss: 11.1 ± 0.2%, corresponding to 8.8 ± 0.2 water molecules per host molecule. decomposition onset: 266.4 ± 5.5 °C	onset temp. (dehydration): 53.2 ± 1.0 °C peak temp. (dehydration): 83.0 ± 4.7 °C onset of shoulder endotherm (dehydration): 91.8 ± 5.1 °C peak shoulder temp. (dehydration): 99.9 ± 5.3 °C onset temp. (dehydration): 119.0 ± 3.4 °C peak temp. (dehydration): 128.9 ± 3.5 °C onset temp. (exotherm): 154.7 ± 2.5 °C peak temp. (exotherm): 158.7 ± 2.0 °C onset temp. (decomp.): 213.4 ± 0.1 °C peak temp. (decomp.): 216.4 ± 0.1 °C
β-CD·PRO	dehydration: temperature range of event: 20.2 ± 2.1 °C and 148.4 ± 0.9 °C associated mass loss: 12.3 ± 0.2% corresponding to 10.0 ± 0.2 water molecules per host molecule. decomposition onset: 267.8 ± 3.1 °C	onset temp. (dehydration): 46.5 ± 0.4 °C peak temp. (dehydration): 74.1 ± 0.2 °C shoulder temp. (dehydration): 89.6 ± 0.5 °C shoulder temp. (dehydration): 103.3 ± 0.2 °C shoulder temp. (dehydration): 121.2 ± 0.6 °C shoulder temp. (dehydration): 138.5 ±0.9 °C onset temp. (phase transition exotherm): 157.1 ± 0.1 °C peak temp. (phase transition exotherm): 162.0 ± 0.2 °C
γ-CD·BES	temperature range of dehydration: 17.8 ± 0.3 to 144.9 ± 0.1 °C associated mass loss for dehydration: 12.7 ± 0.4% corresponding to 12.7 ± 0.4 water molecules per host molecule. onset of decreased dehydration rate (shoulder peak in dTGA): 64.5 ± 0.6 °C decomposition onset: 219.5 ± 2.4	onset temp. (dehydration): 46.7 ± 2.5 °C peak temp. (dehydration): 83.5 ± 2.9 °C
γ-CD·PRO	temperature range of dehydration: 20.6 ± 1.8 °C and 119.6 ± 5.0 °C associated mass for dehydration loss: 14.7 ± 0.3% corresponding to 14.4 ± 0.3 water molecules per host molecule. onset of decreased dehydration rate (shoulder in dTGA): 77.5 ± 4.5 °C decomposition onset: 246.8 ± 2.5 °C	onset temp. (dehydration): 49.3 ± 0.5 °C peak temp. (dehydration): 87.9 ± 0.1 °C shoulder temp. (dehydration): 131.1 ± 0.6 °C

γ-CD·PRO owing to the poor quality of diffraction from selected crystal specimens). Following least-squares refinements of the respective host atoms in β-CD·BES, β-CD·PRO and γ-CD·PRO and location and refinement of water oxygen atoms, difference electron density (Δρ) peaks with very low magnitudes (generally ≤ 1 e·Å^{-3}) appeared within the respective host cavities, indicating severe disorder of the included steroidal guest molecules. This is a common situation for β-CD complexes crystallizing in the space groups *C*2 and $P42_12$, in which the host molecules stack with successive host cavities in alignment, generating infinite channels occupied by guest molecules. In the case of β-CD inclusion complexes, guest molecules can assume multiple orientations and positions within the channels having twofold rotational symmetry, rendering them impossible to model. Analogously, regarding γ-CD inclusion complexes, in addition to the possibility of guest molecules assuming random orientations and locations within the infinite channels, the latter possess four-fold rotational symmetry and thus, unless the guest molecule also possesses this symmetry, it will be severely disordered and hence not able to be modelled. In many instances, the pursuance of the crystal structure of an inclusion compound that suffers from such severe guest disorder is eventually abandoned owing to the uninterpretable, unassigned electron density that results in unacceptable values for X-ray refinement parameters.

However, to circumvent this problem we used a well-known method that enables integration of multiple unassigned Δρ peaks located in crystal voids, namely the SQUEEZE routine [42] implemented in the program PLATON [43]. Following

automatic location of prominent voids in the unit cell of each crystal structure, this procedure provides an estimate of the total number of residual electrons they contain, which in these complexes would correspond to those of the included steroidal molecules. From these respective electron counts, it was thus possible to estimate the host–guest stoichiometric ratios in each complex for comparison with the accurate stoichiometry determinations using ^{1}H NMR spectroscopy. In addition, final X-ray refinement parameters improved following application of the SQUEEZE routine. Although this procedure is most commonly used for dealing with disordered solvent molecules for which an atomistic model is not achievable from the observed residual Δρ peaks, we found that its extension to the treatment of significantly larger molecules (viz. disordered steroidal guests BES and PRO) yielded quite reasonable electron count values for their contributions. Details of the estimations of the host–guest stoichiometries for the β-CD·BES, β-CD·PRO and γ-CD·PRO complexes based on these values are provided (Section 6, p. S21 in Supporting Information File 1). The host–guest stoichiometric estimates obtained consequently correlated with the results from the ^{1}H NMR analyses to varying degrees from very good to fair.

PXRD patterns generated from the final single crystal X-ray structures were in good agreement with the respective PXRD patterns of the CD complexes formed via co-precipitation (Figure S23 in Supporting Information File 1) indicating that the single crystal specimens selected for X-ray analysis are representative of their corresponding bulk materials. The crystallographic data for these complexes are summarised in Table 2. The hydrated CD inclusion complexes of 17β-estradiol and progesterone are ternary systems and their accurate chemical formulae listed in Table 2 were established by combining ^{1}H NMR data (for host–guest ratios) and TGA (for crystal

Table 2: The crystal data and refinement parameters for the β-CD·BES, β-CD·PRO and γ-CD•PRO inclusion complexes.

Parameter	β-CD·BES	β-CD·PRO	γ-CD·PRO
complex formula	$2(C_{42}H_{70}O_{35})\cdot(C_{18}H_{24}O_2)\cdot 17.7H_2O$	$2(C_{42}H_{70}O_{35})\cdot(C_{21}H_{30}O_2)\cdot 20H_2O$	$C_{48}H_{80}O_{40}\cdot(C_{21}H_{30}O_2)_{0.67}\cdot 14.4H_2O$
formula weight (g·mol^{-1})	2859.40	2944.72	1765.64
temperature (K)	100(2)	100(2)	100(2)
wavelength (Å)	0.71073	0.71073	0.71073
crystal system	monoclinic	monoclinic	tetragonal
space group	*C*2	*C*2	$P42_12$
a (Å)	19.087(2)	18.9408(8)	23.6991(9)
b (Å)	24.427(2)	24.540(1)	23.6991(9)
c (Å)	15.581(1)	15.6585(8)	22.896(1)
α (°)	90	90	90
β (°)	109.555(2)	109.161(1)	90
γ (°)	90	90	90
volume (Å^3)	6845.4(10)	6875.1(6)	12860(1)
Z	2	2	6
calculated density (g·cm^{-3})	1.387	1.422	1.368
μ (mm^{-1})	0.123	0.126	0.121
F (000)	3056	3152	5678
crystal size (mm)	0.48 × 0.44 × 0.10	0.34 × 0.24 × 0.16	0.20 × 0.21 × 0.36
θ-range scanned (°)	1.39–26.87	2.74–28.34	1.24–26.41
index range	*h*: –24, 24; *k*: –30, 30; *l*: –19, 19	*h*: –25, 25; *k*: –32, 32; *l*: –20, 20	*h*: –29, 29; *k*: –29, 29; *l*: –27, 28
no. of reflections collected	75496	150313	118399
no. of unique reflections	14663	17104	13196
data completeness (%)	99.5	99.6	99.7
data/restraints/parameters	14663/19/756	17104/28/750	13196/12/365
S (goodness-of-fit on F^2)	1.038	1.021	1.099
final R indices R_1, wR_2, [I > 2σ(I)]	0.0829, 0.2352	0.0782, 0.2174	0.0969, 0.2319
R indices, all data (R_1, wR_2)	0.1043, 0.2593	0.0903, 0.2306	0.0996, 0.2337
largest diff. peak and hole (e.Å^{-3})	0.72, –1.30	0.83, –0.43	0.85, –0.46
CCDC deposition numbers	2213533	2213538	2213558

water contents). The same method was employed to determine the chemical formula for γ-CD·BES (namely $C_{48}H_{80}O_{40}·C_{21}H_{30}O_2·12.7H_2O$) for which no single crystals of adequate diffraction quality were isolated.

The asymmetric units (ASUs) of β-CD·BES and β-CD·PRO (Figure 6) each consist of a single β-CD molecule, one severely disordered guest molecule (either 17β-estradiol for β-CD·BES, or progesterone for β-CD·PRO), and water molecules distributed over 15 sites for β-CD·BES, and 17 sites for β-CD·PRO. The water contents for β-CD·BES and β-CD·PRO based on their X-ray analyses were 9.1 and 9.9 water molecules per β-CD molecule, which correlated well with the TGA results (Table 1). Minor disorder was observed for the host molecules of both complexes, while in contrast, severe disorder for their respective guest molecules was evident, despite the intensity data being collected at 100(2) K. Lastly, reasonable hydrogen bonding distances were observed between the assigned oxygen atoms of the water molecules and neighbouring water oxygen atoms, or the host molecules.

Isostructurality of the host molecules in the two β-CD complexes is evident from the figures below, but it is also notable that isostructurality extends beyond these molecules to include numerous water oxygen atoms as well. The stacking arrangements of the dimeric host molecule units of β-CD inclusion complexes crystallizing in the space group *C*2 are well-known [44], these arrangements resulting in endless channel formation occurring in the crystal structures of β-CD·BES and β-CD·PRO (Figure 7 and Figure 8, depicting stereoscopic views observed down the *c*-axis). Furthermore, it is evident that the water molecules which occupy the interstitial spaces between the columns

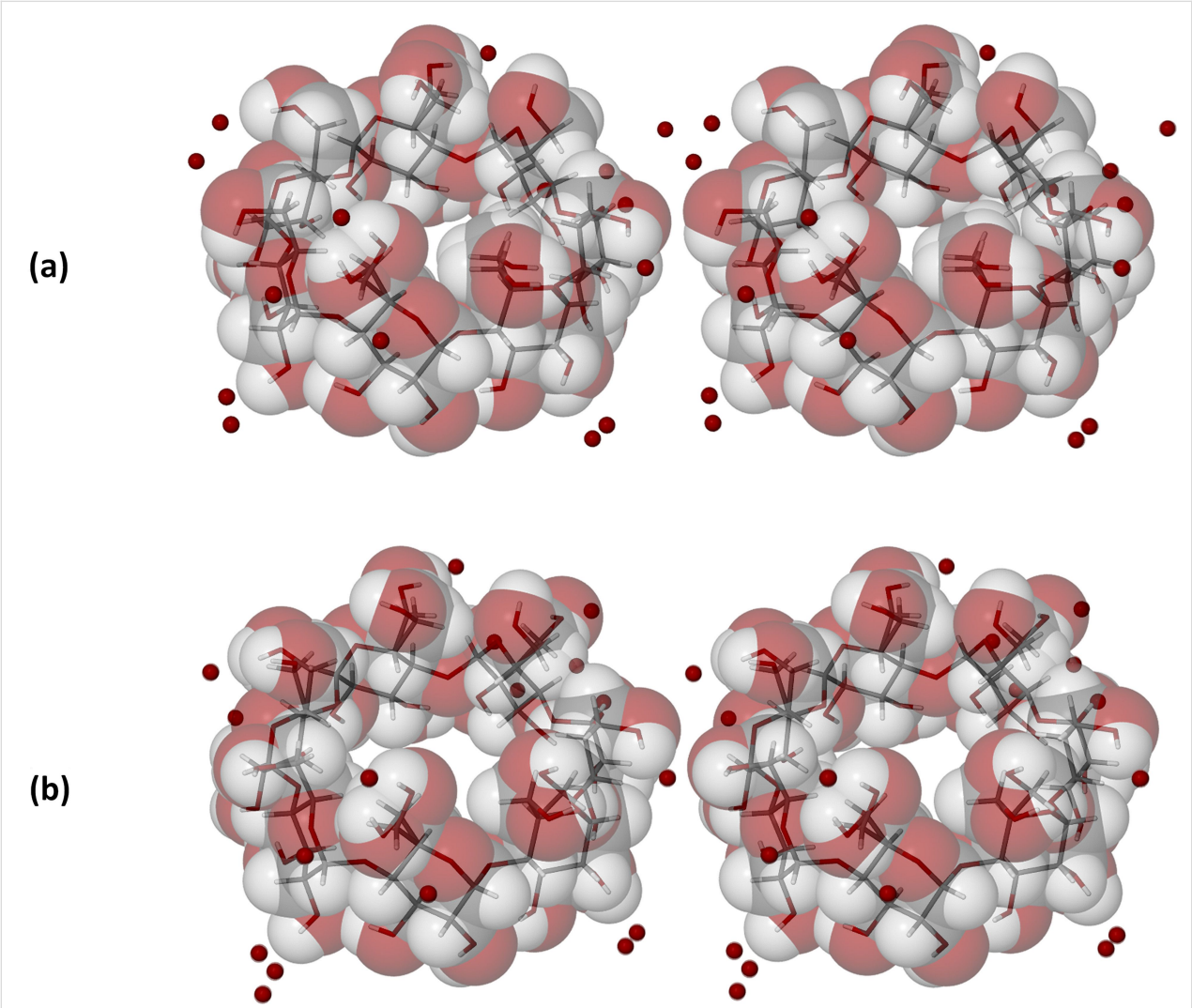


Figure 6: Stereoscopic views of the host molecule and water oxygen atoms in the ASUs of (a) β-CD·BES and (b) β-CD·PRO displaying their 'empty' host cavities.

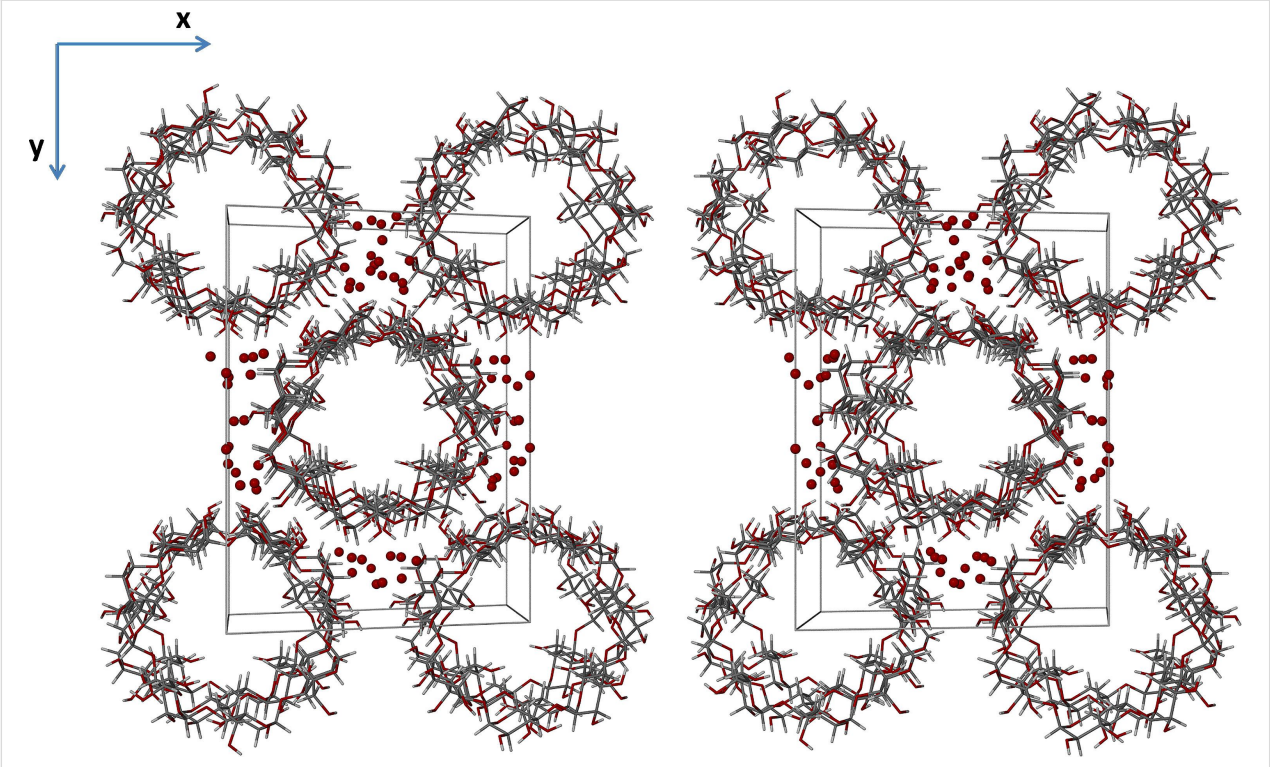


Figure 7: A stereoscopic view down the *c*-axis displaying the packing arrangement for β-CD·BES.

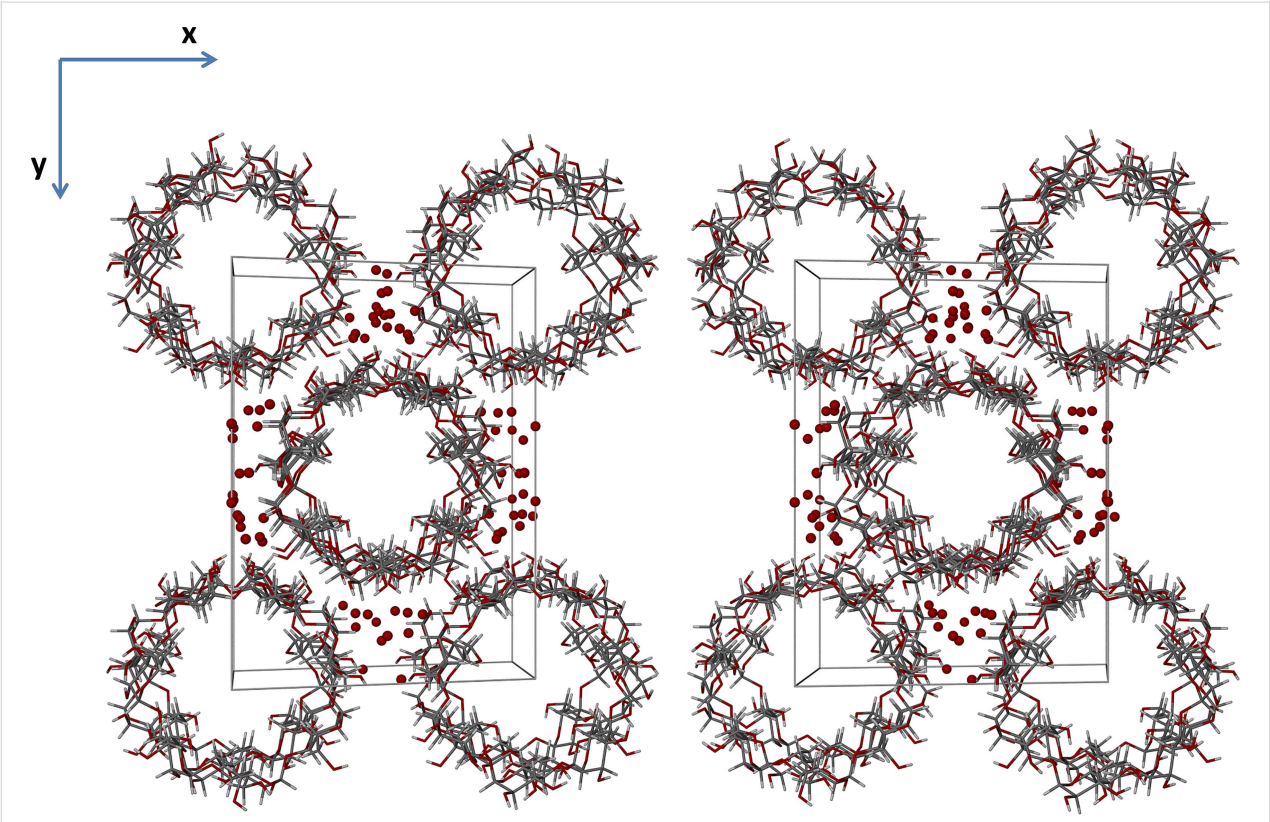


Figure 8: A stereoscopic view down the c-axis displaying the packing arrangement for β-CD·PRO.

reinforce this assembly of complex units via multiple O–H···O hydrogen bonds. These depictions also indicate that there are four β-CD molecules in the unit cell, corresponding to two dimeric complex units per cell and again reveal the similarity in the conservation of water molecule sites in the two isostructural complexes.

The detailed host conformations are defined by numerous, relevant geometrical parameters that include measures of the angular tilts of the individual glucose rings relative to the seven-fold axes of the β-CD molecules (Figures S24–S25 and Tables S5–S6 in Supporting Information File 1). The narrower ranges of the tilt angles for β-CD·BES and β-CD·PRO relative to the tilt angle range for uncomplexed hydrated β-CD (4.5°–27.0°) [45] indicate that additional distortion took place with host–guest complexation, as a consequence of a mutual-induced fit of host and guest molecules [39].

With reference to γ-CD·PRO, the asymmetric unit (ASU) comprises three pairs of glucose rings that generate three complete γ-CD molecules when rotation of these units around the four-fold axis parallel to the *c*-axis is applied (Figure 9). The level of disorder in the host molecules was found to be minimal, only two of the hydroxymethyl groups being disordered over two positions. This is in contrast to the guest molecules which are instead severely disordered and consequently not observable. Water oxygen atoms were identified over 20 sites (as previously mentioned) and it is evident that these sites are all external to the γ-CD molecule cavities (Figure 10). Hydrogen atoms were not placed on the water oxygen atoms, as there was no evidence for them in the difference Fourier map.

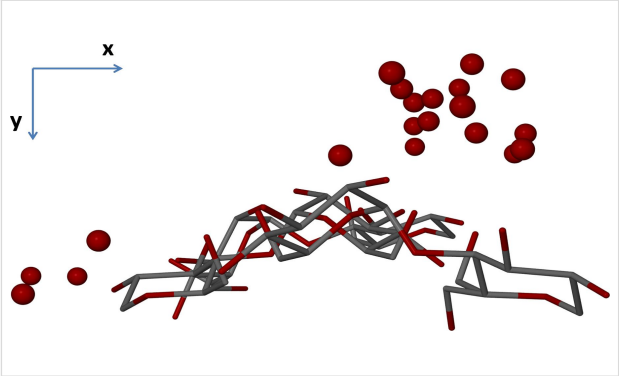


Figure 10: The host atoms and water oxygen atoms of the ASU viewed down the *c*-axis, showing that the water molecule sites are all external to the cavities of the γ-CD molecules.

Three independent γ-CD molecules (A, B, C) comprise the major structural motif in the γ-CD·PRO crystal, and they stack to form infinite columns, arranging themselves in a head-to-tail motif between molecules C and A, a tail-to-tail motif between molecules B and C, and a head-to-head motif between molecules A and B (Figure 11) [46]. At each of the C–A, B–C and A–B interfaces extensive O–H···O hydrogen bonding takes place. This is a characteristic structural arrangement that has been observed in all γ-CD inclusion complexes crystallizing in the space group $P42_12$ [41].

Water molecules similarly occupy the interstitial spaces between the columns (Figure 12, viewed down the c-axis) and are thus also responsible for reinforcing the assembly of γ-CD complex columnar units via water–water and water–host hydrogen bonds. It should be noted that, since PXRD analyses indicated

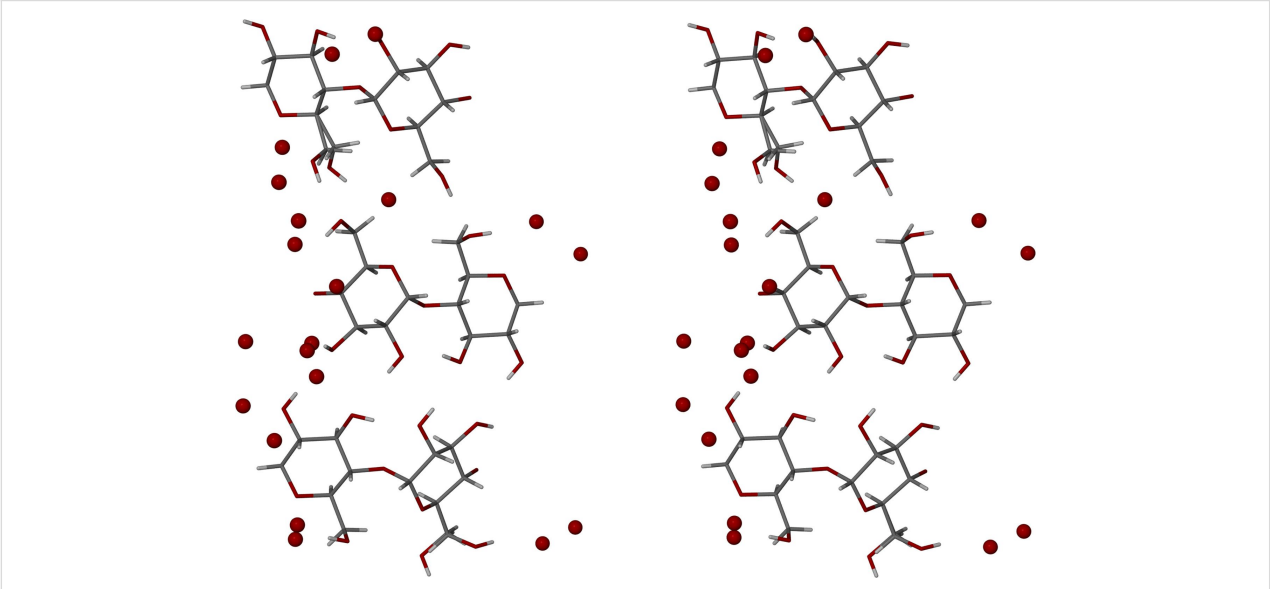


Figure 9: A stereoscopic view of the host atoms and water oxygen atoms in the ASU of γ-CD·PRO.

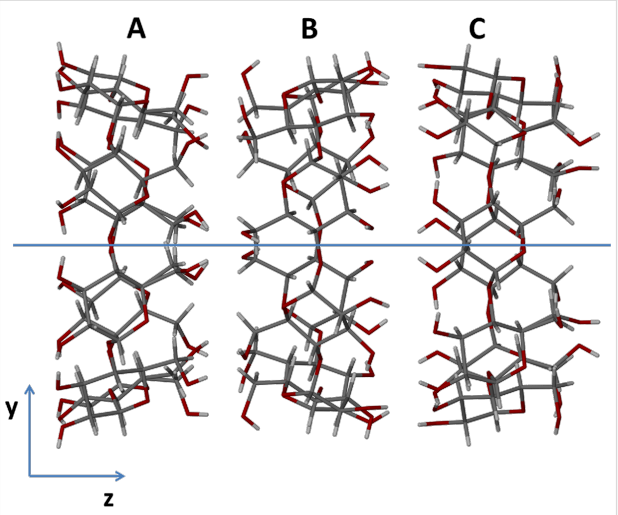


Figure 11: The distinct packing arrangement of the repeat unit of the host molecules in γ-CD·PRO. The four-fold axis (blue line) runs through the centre of the channel, parallel to the *c*-axis. The water molecules are omitted for clarity.

that the γ-CD·PRO and γ-CD·BES crystal structures are isostructural, all of the salient structural features illustrated above and below for the γ-CD·PRO crystal are common to the γ-CD·BES crystal, which was not amenable to single crystal X-ray analysis.

Solubility analysis

Solubility determinations for the four native CD inclusion complexes (β-CD·BES, β-CD·PRO, γ-CD·BES and γ-CD·PRO) were performed in duplicate simultaneously. The intrinsic aqueous solubilities of 17β-estradiol and progesterone are 3.6×10^{-3} mg·cm^{-3} (at 27 °C) and 8.81×10^{-3} mg·cm^{-3} (at 25 °C), respectively [6,8], and the results obtained (Table 3) indicated that the CD inclusion of 17β-estradiol and progesterone did indeed enhance the aqueous solubility of both APIs significantly, most prominently in the cases of β-CD·BES and γ-CD·PRO. Improvement in the aqueous solubilities of PRO through its complexation with β-CD and γ-CD reported earlier [33] is consistent with the data for these complexes in Table 3.

Conclusion

The reported crystal structures of β-CD·BES, β-CD·PRO and γ-CD·PRO represent the first single crystal X-ray structural determinations of CD inclusion complexes of 17β-estradiol and progesterone. Comprehensive PXRD analyses of the complexes prepared by kneading enabled prediction of their space groups based on their isostructurality with known reference complexes. Comparison of these experimental patterns with simulated PXRD patterns based on SCXRD data revealed that the single crystals obtained by co-precipitation were isostructural with their counterparts prepared by kneading. The occur-

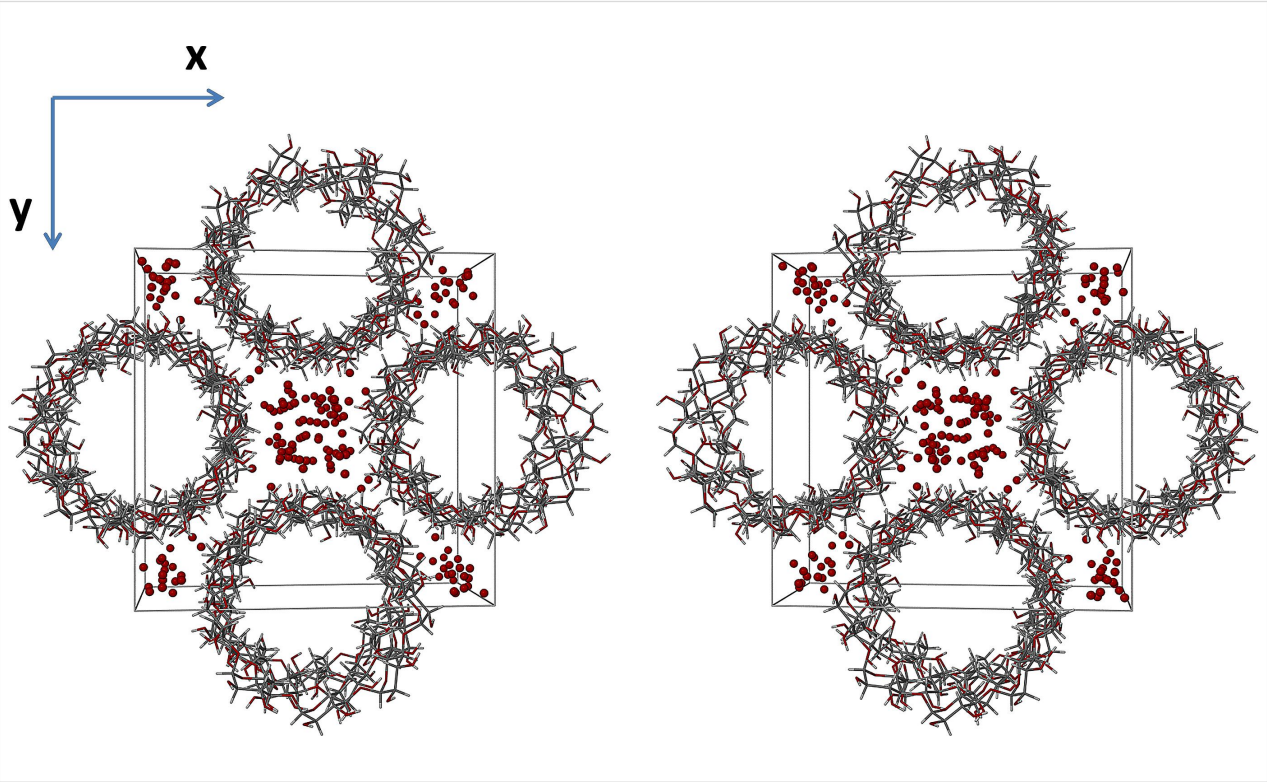


Figure 12: A stereoscopic view of γ-CD·PRO viewed down the *c*-axis, which displays the infinite channel packing arrangement. The water molecules (red spheres) occupy the interstitial spaces between the columns of stacked complex units.

Table 3: Aqueous solubility data for the β-CD·BES, β-CD·PRO, γ-CD·BES, and γ-CD·PRO inclusion complexes at 27 °C.

Number	CD complex	Solubility range of API ($mg \cdot cm^{-3}$)	Approximate solubility enhancement ratio ($S_{API(CD)}/S_{API}$)[a]	Average $S_{API(CD)}/S_{API}$ ratio
1	β-CD·BES produced via kneading (experiment 1)	0.0743–0.0784	21.8	21.9 ± 0.1
2	β-CD·BES produced via kneading (experiment 2)	0.0731–0.0790	21.9	
3	β-CD·PRO produced via kneading (experiment 1)	0.0380–0.0511	5.8	5.6 ± 0.2
4	β-CD·PRO produced via kneading (experiment 2)	0.0366–0.0474	5.4	
5	γ-CD·BES produced via kneading (experiment 1)	0.0193–0.0288	8.0	8.0 ± 0.1
6	γ-CD·BES produced via kneading (experiment 2)	0.0206–0.0283	7.9	
7	γ-CD·PRO produced via kneading (experiment 1)	0.162–0.174	19.8	19.9 ± 0.1
8	γ-CD·PRO produced via kneading (experiment 2)	0.161–0.175	19.9	

[a]$S_{API(CD)}$ is the aqueous solubility of the API in the form of a CD inclusion complex, and S_{API} is the aqueous solubility of the API.

rence of severe guest disorder in all three cases precluded detailed determination of the host–guest interactions. Despite this limitation, complete chemical formulae were determined for the ternary complexes listed above, as well as that of γ-CD·BES, by combining accurate host–guest stoichiometric ratios obtained from ^{1}H NMR analyses with the respective crystal water contents derived from thermogravimetric analyses. The aqueous solubilities of the two APIs, 17β-estradiol and progesterone, were found to be significantly enhanced via their encapsulation by β-CD and γ-CD. It is notable that these measured solubilities are also superior to those of the commercially utilized formulations containing ethinylestradiol and micronized progesterone. Further investigation should include in vivo experimentation to assess the efficacy of the four CD inclusion complexes as the active components of alternative commercial solid formulations for potential therapeutic treatment. Such CD-based formulations could be administered orally, as the absorption of cyclodextrins in the gastrointestinal tract is negligible (usually less than 4%) and the CDs are thus considered practically non-toxic [1,2]. Another advantageous feature of the four CD inclusion complexes investigated in this study is their ability to be synthesised rapidly via an efficient mechanochemical process, namely kneading of their respective host–guest mixtures, with water as the liquid medium. Furthermore, the proven significant API solubility enhancements reported here should result in less of the active ingredient being required in each dosage, thus rendering these CD inclusion complexes potentially financially attractive for pharmaceutical applications.

Experimental

Materials

17β-Estradiol ($C_{18}H_{24}O_2$,) with purity >98% and progesterone ($C_{21}H_{30}O_2$) with purity >98% were purchased from Sigma-Aldrich Chemie GmbH (Steinheim, Germany). β-Cyclodextrin (β-CD; $C_{42}H_{70}O_{35}$) with purity >98% and water content 13.7(1)% (n = 2) was purchased from Cyclolab (Budapest, Hungary), while γ-cyclodextrin (γ-CD; $C_{48}H_{80}O_{40}$) with purity >98% and water content 7.6(1)% (n = 2) was purchased from Wacker Biosolutions (Halle, Germany).

CD complex preparation

Kneading experiments: Specific stoichiometric amounts of CD and API were utilized in the following host–guest ratios: β-CD·BES (2:1), β-CD·PRO (2:1), γ-CD·BES (1:1), γ-CD·PRO (3:2). The two components were placed in a mortar with a small amount of Milli-Q® water [47], and the mixture was kneaded into a paste with a pestle for 40 minutes. Small increments (0.3 cm^3) of water were added where necessary. These samples were used for the solubility determinations.

Single-crystal preparation: Initially, 35.24 mg (0.0310 mmol) of pure β-CD was dissolved in 3 cm^3 water for the β-CD·BES system, and 30.53 mg (0.0269 mmol) of pure β-CD was dis-

solved in 15 cm^3 water for the β-CD·PRO system. These CD solutions were stirred at 70 °C and the APIs were added in small increments over a 10 minute period to the respective CD solutions. 4.9 mg (0.0180 mmol) of pure BES and 4.9 mg (0.0156 mmol) of pure PRO were added, respectively. These amounts correspond to host–guest ratios of 1.72:1 and 1.72:1, respectively. Almost complete dissolution was attained after 15 minutes of stirring at 70 °C, but a very slight turbidity was still observed in the β-CD·BES solution. The solutions were left to stir for an additional 3 hours (to allow for the complex equilibrium to be achieved), after which they were filtered and prepared for slow cooling in a Dewar flask. Crystals appeared after 3 days and were shown to have 2:1 host/guest stoichiometry by ^{1}H NMR spectroscopy.

Single-crystal preparation for both γ-CD·BES and γ-CD·PRO utilized a large excess of γ-CD in order to obtain crystalline inclusion complexes with 1:1 and 3:2 stoichiometric ratios, respectively. Approximately 100 mg (0.0771 mmol) of pure γ-CD was used for both systems, and the masses of the pure APIs were both 4.9 mg (0.0180 mmol for 17β-estradiol and 0.0156 mmol for progesterone). This corresponded to host–guest ratios of 4.28:1 and 4.94:1, respectively. The two weighed samples of γ-CD were dissolved in water in separate vials (3 cm^3 for the γ-CD·PRO system and 2.5 cm^3 for the γ-CD·BES system) and stirred vigorously at 70 °C. The APIs were added fairly slowly to their respective vials over a period of about 5 minutes and the solutions were left to stir for a further 3 hours and were subsequently filtered and prepared for slow cooling. Crystals appeared after 3 days, and it should be noted that complete evaporation of the mother liquors must be avoided in order to prevent the excess γ-CD subsequently precipitating. Subsequently, ^{1}H NMR spectroscopy revealed host/guest stoichiometries of 1:1 for γ-CD·BES and 3:2 for γ-CD·PRO.

Powder X-ray diffraction (PXRD)

PXRD patterns were recorded at 23 °C for each reagent as well as the products formed from kneading and co-precipitation. PXRD analyses were performed on a Bruker D2 Phaser desktop powder diffractometer (Billerica, Massachusetts, U.S.A.) with Cu $K\alpha_1$ radiation (λ = 1.5406 Å) with the X-ray generator set at 30 kV and 10 mA. All samples were lightly ground (to minimise the effects of preferred orientation) and placed on a silicon zero-background sample holder. The scanning range was 4° – 40° 2θ with a step size of 0.0164° and a primary beam path slit of 0.6 mm.

^{1}H NMR spectroscopy

Solution-state ^{1}H NMR analyses were performed to quantify the stoichiometric ratios of the CD inclusion complexes, and all of the crystalline samples obtained by co-precipitation were dissolved in deuterated dimethyl sulfoxide (DMSO-d_6) at 23 °C. These analyses were performed on a Bruker Ultrashield 400 Plus Spectrometer (Billerica, Massachusetts, U.S.A.) and the program MestReNova was used to analyse the resulting data [48].

Thermal analysis

Hot stage microscopy (HSM): The crystals were immersed in a small amount of silicone oil and heated at a constant rate of 10 $K \cdot min^{-1}$ until decomposition. The HSM experiment was viewed through a Nikon SMZ-10 stereoscopic microscope fitted with a Linkam THM600 hot stage and a Linkam TP92 temperature control unit. The images were captured by a real-time Sony Digital Hyper HAD colour video at selected temperatures. The captured images were viewed with the Soft Imaging Program AnalySIS [49].

Thermogravimetric analysis (TGA): TGA analyses were performed on the TA-Q500 (Texas Instruments) with Universal Analysis 2000 software. Sample preparation involved rapidly removing the crystals from their mother liquor and subsequently lightly pressing them between a filter paper to dry their surfaces, and the TGA experiment commenced immediately after the mother liquor was removed. Masses between 0.7 mg and 2.0 mg were used for the analyses, which were performed either in duplicate or triplicate. The analyses took place in open pans under dry nitrogen gas with a constant flow rate of 60 $cm^3 \cdot min^{-1}$ and the samples were heated to a maximum temperature of 400 °C at a constant rate of 10 $K \cdot min^{-1}$.

Differential scanning calorimetry (DSC): DSC analyses were performed on a DSC XP-10 instrument (Surface Solutions GmbH), and the data analysed with TRIOS software [50]. Sample preparation entailed drying the crystal surfaces from the mother liquor and placing the crystals in a crimped aluminium pan with two venting holes. A constant rate of 10 $K \cdot min^{-1}$ was used to heat the samples (mass range 1–2 mg) under dry N_2 purge gas with a flux of 60 $cm^3 \cdot min^{-1}$. All DSC experiments were terminated prior to the decomposition of each sample.

Solubility analysis by gravimetric increments

A gravimetric solubility approach was used involving the addition of small, accurately pre-weighed incremental amounts of a given CD inclusion complex (total mass approximately 30 mg each) into a vial containing 3 cm^3 of water. A visual estimation of the solubility was established after the final suspension was stirred for 72 hours at 27 °C. This procedure ensured that a very narrow solubility range was spanned by the penultimate and final incremental CD inclusion complex additions, the final amount resulting in saturation of the solution. The apparatus

involved a Radleys Standard stirring hotplate with a 2.5 cm high vial supporting stand attached to it. The vials were placed on the stand in a circle at a radius of 4 cm from the centre, and the solutions were stirred at a rate of 250 rpm for 72 hours.

Single crystal X-ray diffraction (SCXRD) analysis

Unit cell determinations and data-collections were performed on a Bruker KAPPA APEX II DUO single-crystal X-ray diffractometer (Madison Wisconsin, U.S.A.) and a Bruker D8 VENTURE SCXRD single-crystal X-ray diffractometer (Madison Wisconsin, U.S.A.). The crystals were coated in Paratone N oil [51]. The unit cell determinations were initially performed at room temperature and thereafter reconfirmed following cooling to 100(2) K in a nitrogen vapour stream using an Oxford Cryostream cooler (Oxford Cryosystems Ltd, Oxford, U.K.). The data-collection was then performed and the collected intensity datasets were read into the program XPREP [52]. The structures were solved using isomorphous replacement, and the water oxygen atoms were refined anisotropically if they possessed full site-occupancy. No water hydrogen atoms were included in the models. Thereafter, the structures were refined by full-matrix least-squares techniques with SHELXL-97 [53], implemented in the X-SEED [54] interface.

Supporting Information

Supporting Information File 1

PXRD patterns, ^{1}H NMR data, thermal data for hot stage microscopy (HSM), variable temperature powder X-ray diffraction (VTPXRD) patterns, TGA, dTGA and DSC analytical data, details of electron counts derived from the Squeeze procedure, and geometrical parameters of the β-CD host molecules.
[https://www.beilstein-journals.org/bjoc/content/supplementary/1860-5397-18-184-S1.pdf]

Acknowledgements

The authors acknowledge the University of Cape Town for access to research facilities.

Funding

ZH thanks the National Research Foundation (Pretoria) for support.

ORCID® iDs

Alexios I. Vicatos - https://orcid.org/0000-0002-5427-0773
Zakiena Hoossen - https://orcid.org/0000-0002-3984-859X
Mino R. Caira - https://orcid.org/0000-0002-7802-2600

References

1. Loftsson, T.; Brewster, M. E. *J. Pharm. Pharmacol.* **2010,** *62,* 1607–1621. doi:10.1111/j.2042-7158.2010.01030.x
2. Del Valle, E. M. M. *Process Biochem. (Oxford, U. K.)* **2004,** *39,* 1033–1046. doi:10.1016/s0032-9592(03)00258-9
3. Szejtli, J. *Chem. Rev.* **1998,** *98,* 1743–1754. doi:10.1021/cr970022c
4. Zhang, J.; Ma, P. X. *Adv. Drug Delivery Rev.* **2013,** *65,* 1215–1233. doi:10.1016/j.addr.2013.05.001
5. Hirayama, F.; Uekama, K. *Adv. Drug Delivery Rev.* **1999,** *36,* 125–141. doi:10.1016/s0169-409x(98)00058-1
6. National Center for Biotechnology Information. PubChem Compound Summary for CID 5757, Estradiol. 2020; https://pubchem.ncbi.nlm.nih.gov/compound/Estradiol (accessed Jan 3, 2022).
7. National Center for Biotechnology Information. PubChem Compound Summary for CID 5994, Progesterone. 2020; https://pubchem.ncbi.nlm.nih.gov/compound/Progesterone (accessed Aug 9, 2020).
8. Yalkowsky, S. H.; He, Y. *Handbook of Aqueous Solubility Data: An Extensive Compilation of Aqueous Solubility Data for Organic Compounds Extracted from the AQUASOL DATAbASE;* CRC Press LLC: Boca Raton, FL, 2003.
9. National Center for Biotechnology Information. PubChem Compound Summary for CID 5991, Ethinyl estradiol.. 2020; https://pubchem.ncbi.nlm.nih.gov/compound/Ethinyl-estradiol (accessed Aug 9, 2020).
10. Goletiani, N. V.; Keith, D. R.; Gorsky, S. J. *Exp. Clin. Psychopharmacol.* **2007,** *15,* 427–444. doi:10.1037/1064-1297.15.5.427
11. Okamoto, S. Eye Drops and Kits for Treatment of Eye Disease. WO2006040839 A1, April 20, 2006.
12. Okamoto, S. Ophthalmic Preparations Containing Steroids. WO2004093882 A1, Nov 4, 2004.
13. Pharmatech GmbH. Water-Soluble Inclusion Complexes of Drugs with Methyl-β-Cyclodextrin. DE4207922 A1, Sept 23, 1993.
14. Wang, X.; He, H.; Leng, W.; Tang, X. *Int. J. Pharm.* **2006,** *317,* 40–46. doi:10.1016/j.ijpharm.2006.02.055
15. Lee, B. J. Site-Specific Release Preparation Containing Inclusion Complex. KR211222 B1, July 15, 1999.
16. Hansen, J.; Mollgaard, B. Transdermal System. Pharmaceutical Composition Containing Cyclodextrin Inclusion Compounds. US-5120546-A, June 9, 1992.
17. Hesler, M.; Schwarz, D. H.; Dähnhardt-Pfeiffer, S.; Wagner, S.; von Briesen, H.; Wenz, G.; Kohl, Y. *Eur. J. Pharm. Sci.* **2020,** *143,* 105181. doi:10.1016/j.ejps.2019.105181
18. Caliceti, P.; Salmaso, S.; Semenzato, A.; Carofiglio, T.; Fornasier, R.; Fermeglia, M.; Ferrone, M.; Pricl, S. *Bioconjugate Chem.* **2003,** *14,* 899–908. doi:10.1021/bc034080i
19. Shangraw, R. F.; Pande, G. S.; Gala, P. *Drug Dev. Ind. Pharm.* **1992,** *18,* 1831–1851. doi:10.3109/03639049209046334
20. Schipper, N. G. M.; Hermens, W. A. J. J.; Romeyn, S. G.; Verhoef, J.; Merkus, F. W. H. M. *Int. J. Pharm.* **1990,** *64,* 61–66. doi:10.1016/0378-5173(90)90179-8
21. Pitha, J. Verifiable Absorption Drug Delivery Form Based on Cyclodextrins. US20040048831 A1, March 11, 2004.
22. Yañez, C.; Basquinzay, R. *J. Electroanal. Chem.* **2008,** *622,* 242–245. doi:10.1016/j.jelechem.2008.06.005
23. Yañez, C.; Basualdo, J.; Jara-Ulloa, P.; Squella, J. A. *J. Phys. Org. Chem.* **2007,** *20,* 499–505. doi:10.1002/poc.1186

24. Pérez, R. L.; Escandar, G. M. *Analyst* **2013,** *138,* 1239. doi:10.1039/c2an36395j
25. Arafa, R. M.; Yehia, A. M.; Abbas, S. S.; Amer, S. M. *Spectrochim. Acta, Part A* **2019,** *222,* 117237. doi:10.1016/j.saa.2019.117237
26. Takahashi, K.; Kaburagi, W.; Narusawa, T. *Tokyo Kogei Daigaku Kogakubu Kiyo* **2012,** *35,* 87–94.
27. Caballero, J.; Zamora, C.; Aguayo, D.; Yañez, C.; González-Nilo, F. D. *J. Phys. Chem. B* **2008,** *112,* 10194–10201. doi:10.1021/jp8006766
28. Wang, X.; Xuan, Z. *Zhongguo Yiyuan Yaoxue Zazhi* **2003,** *23,* 719–721.
29. Rodriguez-Tenreiro, C.; Alvarez-Lorenzo, C.; Rodriguez-Perez, A.; Concheiro, A.; Torres-Labandeira, J. J. *Eur. J. Pharm. Biopharm.* **2007,** *66,* 55–62. doi:10.1016/j.ejpb.2006.09.003
30. Zoppetti, G.; Puppini, N.; Pizzutti, M.; Fini, A.; Giovani, T.; Comini, S. *J. Inclusion Phenom. Macrocyclic Chem.* **2007,** *57,* 283–288. doi:10.1007/s10847-006-9174-2
31. Másson, M.; Karlsson, F. J.; Valdimarsdóttir, M.; Magnúsdóttir, K.; Loftsson, T. *J. Inclusion Phenom. Macrocyclic Chem.* **2007,** *57,* 481–487. doi:10.1007/s10847-006-9238-3
32. Liu, F.-y.; Kildsig, D. O.; Mitra, A. K. *Pharm. Res.* **1990,** *07,* 869–873. doi:10.1023/a:1015973218303
33. Lin, S.-Z.; Skiba, M.; Wouessidjewe, D.; Agnus, B.; Duchene, D. Inclusion Complexes of Progesterone and Its Analog X with Cyclodextrins. Proceedings of the Minutes of the 6th International Symposium on Cyclodextrins; Hedges, A. R., Ed.; Editions de Sante: Paris, 1992; pp 460–465.
34. Lahiani-Skiba, M.; Barbot, C.; Bounoure, F.; Joudieh, S.; Skiba, M. *Drug Dev. Ind. Pharm.* **2006,** *32,* 1043–1058. doi:10.1080/03639040600897093
35. Cerchiara, T.; Luppi, B.; Bigucci, F.; Zecchi, V. *Int. J. Pharm.* **2003,** *258,* 209–215. doi:10.1016/s0378-5173(03)00202-3
36. Zoppetti, G.; Puppini, N.; Ospitali, F.; Fini, A. *J. Pharm. Sci.* **2007,** *96,* 1729–1736. doi:10.1002/jps.20671
37. Gedeon, R.; Hung, V. G. R. Inclusion Complexes of Steroids with γ-Cyclodextrin and Pharmaceutical Compositions Containing Them. BE894825 A1, Feb 14, 1983.
38. Kanehito, K.; Kazuo, Y. Solubilization of Pharmaceuticals by Maltosyl-β-Cyclodextrin. JP63135402 A, June 7, 1988.
39. Caira, M. R.; Bourne, S. A.; Samsodien, H.; Smith, V. J. *Beilstein J. Org. Chem.* **2015,** *11,* 2616–2630. doi:10.3762/bjoc.11.281
40. Groom, C. R.; Bruno, I. J.; Lightfoot, M. P.; Ward, S. C. *Acta Crystallogr., Sect. B: Struct. Sci., Cryst. Eng. Mater.* **2016,** *72,* 171–179. doi:10.1107/s2052520616003954
41. Caira, M. R. *Rev. Roum. Chim.* **2001,** *46,* 371–386.
42. Spek, A. L. *Acta Crystallogr., Sect. C: Struct. Chem.* **2015,** *71,* 9–18. doi:10.1107/s2053229614024929
43. Spek, A. L. *Acta Crystallogr., Sect. D: Biol. Crystallogr.* **2009,** *D65,* 148–155. doi:10.1107/s090744490804362x
44. Mentzafos, D.; Mavridis, I. M.; Le Bas, G.; Tsoucaris, G. *Acta Crystallogr., Sect. B: Struct. Sci.* **1991,** *47,* 746–757. doi:10.1107/s010876819100366x
45. Steiner, T.; Koellner, G. *J. Am. Chem. Soc.* **1994,** *116,* 5122–5128. doi:10.1021/ja00091a014
46. Steiner, T.; Saenger, W. *Acta Crystallogr., Sect. B: Struct. Sci.* **1998,** *54,* 450–455. doi:10.1107/s0108768197014547
47. Milli-Q Water, Millipore Corporation, Billerica, Massachusetts, USA.
48. *MestReNova,* Version 6.0.2-5475; Chemistry Software Solutions, Mestrelab Research, S.L., 2009.
49. *Digital Solutions for Imaging and Microscopy,* Version 3.1 for Windows; Soft Imaging System GmbH. 1987–2000.
50. TA Instruments-Waters LLC. 159 Lukens Drive, New Castle, DE19720 2020.
51. Paratone N Oil, Exxon Chemical Co., Texas, USA.
52. *XPREP, Data Preparation and Reciprocal Space Exploration,* Version 2008/2; Bruker Analytical X-Ray Systems, 2008.
53. Sheldrick, G. M. *Acta Crystallogr., Sect. A: Found. Crystallogr.* **2008,** *64,* 112–122. doi:10.1107/s0108767307043930
54. Barbour, L. J. *J. Supramol. Chem.* **2001,** *1,* 189–191. doi:10.1016/s1472-7862(02)00030-8

License and Terms

This is an open access article licensed under the terms of the Beilstein-Institut Open Access License Agreement (https://www.beilstein-journals.org/bjoc/terms), which is identical to the Creative Commons Attribution 4.0 International License (https://creativecommons.org/licenses/by/4.0). The reuse of material under this license requires that the author(s), source and license are credited. Third-party material in this article could be subject to other licenses (typically indicated in the credit line), and in this case, users are required to obtain permission from the license holder to reuse the material.

The definitive version of this article is the electronic one which can be found at:
https://doi.org/10.3762/bjoc.18.184

BEILSTEIN JOURNAL OF ORGANIC CHEMISTRY

Preparation of β-cyclodextrin/polysaccharide foams using saponin

Max Petitjean and José Ramón Isasi*§

Full Research Paper

Open Access

Address:
Department of Chemistry. University of Navarra. 31080 Pamplona, Spain

Email:
José Ramón Isasi* - jrisasi@unav.es

* Corresponding author
§ Tel.: +34 948 425 600; fax: +34 948 425 740

Keywords:
chitosan; cyclodextrin polymers; green synthesis; locust bean gum; saponin; sorption; xanthan gum

Beilstein J. Org. Chem. **2023,** *19,* 78–88.
https://doi.org/10.3762/bjoc.19.7

Received: 31 October 2022
Accepted: 10 January 2023
Published: 24 January 2023

This article is part of the thematic issue "Cyclodextrins as building blocks for new materials".

Guest Editor: S. Fourmentin

© 2023 Petitjean and Isasi; licensee Beilstein-Institut.
License and terms: see end of document.

Abstract

Cyclodextrins, cyclic oligosaccharides with a hydrophobic cavity that form inclusion complexes with nonpolar molecules, can be used to functionalize other polysaccharides. Xanthan gum, locust bean gum or chitosan can be crosslinked using citric acid in the presence of β-cyclodextrin to produce insoluble matrices. In this work, polymeric foams based on those polysaccharides and saponin have been prepared using a green synthesis method to increase the porosity of the matrices. The saponin of soapbark (*Quillaja saponaria*) has been used to obtain foams using different procedures. The influence of the synthesis path on the porosity of the materials and their corresponding sorption capacities in the aqueous phase were evaluated.

Introduction

Saponins are a family of natural molecules consisting of a hydrophobic aglycone backbone grafted with hydrophilic sugar molecules, allowing the plant to be protected from illnesses [1] and from herbivores endangerment [2]. The aglycone part is composed of steroid and triterpene molecules [3]. Not only present in plants [4,5], saponins have also been discovered in marine animals, such as sea cucumbers [6] or starfish [7]. Chemical structures of this family are varied [1], so they will show different properties [8]. Saponins, because of their amphiphilic nature, are known as natural surfactants [9]. They have been used as natural detergents, foaming agents, stabilizers, emulsifiers and wetting agents, for example [10]. The micelles produced will be different in size and shape as a function of the type of saponin, their aglycone forms but also the number of sugar molecules involved [11]. They can be found in beverage emulsions [12], and as food surfactants [13], because they are useful also to prevent the development of virus or bacteria in food or beverages [14,15]. As for medical purposes, it has been reported that saponins possess anticancer properties, by limiting proliferation and metastasis. This has been tested on different

cancers such as leukemia [16], breast cancer [17] or prostate cancer to cite only a few of them [18]. They also present antimicrobial, antioxidant, anti-inflammatory, antidiabetic and cholesterol lowering properties, for example [10]. As reported by Liu et al. [19], saponins can show interesting interactions with hydrophobic organic compounds (HOC) and more precisely with polycyclic aromatic hydrocarbons (PAHs). For example, phenanthrene can be removed by saponins [20], by complexing with the PAH and having repulsive interactions with soil [21]. A large quantity of HOCs have been studied, such as naphthalene or fluoranthene [19]. The authors reported also the possibility of remediation of heavy metals by saponins [22]. Therefore, saponins are useful in soil washing technologies [23] or phytoremediation [24].

When chitosan and saponins are mixed, their foamability properties change, leading to a longer foam stability due to the higher viscosity achieved [25]. The use of chitosan to absorb saponins have been studied for different purposes. A high specific area activated carbon has been developed by Ma et al. [26], by the production of chitosan–saponin gels thanks to glutaraldehyde crosslinking. After adding potassium hydroxide, they freeze-dried the material and pyrolyzed the product. The resulting material possess a high absorption capacity of methylene blue, thanks to the presence of porosity and some chemical functions after pyrolysis. Chitosan–saponin–bentonite composite films can also be produced to absorb methyl orange and Cr(VI) [27]. Native [28] or derivatized [29] chitosans allow also a good sorption of *Quillaja* saponins useful to liberate them from wound dressings. This saponin possesses two large hydrophilic parts, surrounding the aglycone [30]. The association chitosan–saponin can show other functions for medicinal purposes, and anticancer nanoparticles made of chitosan loaded with saponins have been prepared by Nair and Jayakumar [31], and even coronavirus vaccine chitosan–saponin coatings have been developed to study its immunogenic potential [32].

A complexation between saponin and cyclodextrins (native or derivative) is possible [33], and the resulting release kinetics is appropriate for the creation of new saponin-based drugs [34]. Their potential uses can be either for oral delivery targeting intestine [33] or for an anti-skin cancer treatment [35], for example. This complexation step is also interesting for the synthesis of molecular imprinted polymers containing cyclodextrin [36].

In previous works, we have produced crosslinked polysaccharide networks using cyclodextrin to prepare green adsorbents [37]. The use of saponins added into the reactive mixture in order to produce a foam allows us to prepare porous materials, in order to enhance their sorption capabilities when a low amount of the sorbate is present in the solution. The specific area of the matrix is intended to be increased, permitting a greater accessibility to β-cyclodextrin sites.

Results and Discussion

Production of saponin foams

As a first step, the determination of the foamability of saponin aqueous solutions allows us to find the surfactant concentration for which a maximum of foam volume will be produced. This value will correspond to the minimum amount of this ingredient required to produce the cyclodextrin/polysaccharide foams. As can be seen in Figure 1 (left), two linear fittings were applied in the foam volume vs concentration plot, where the junction of both lines gives us an approximate optimal foamability for a saponin concentration value of ca. 0.3%. These mea-

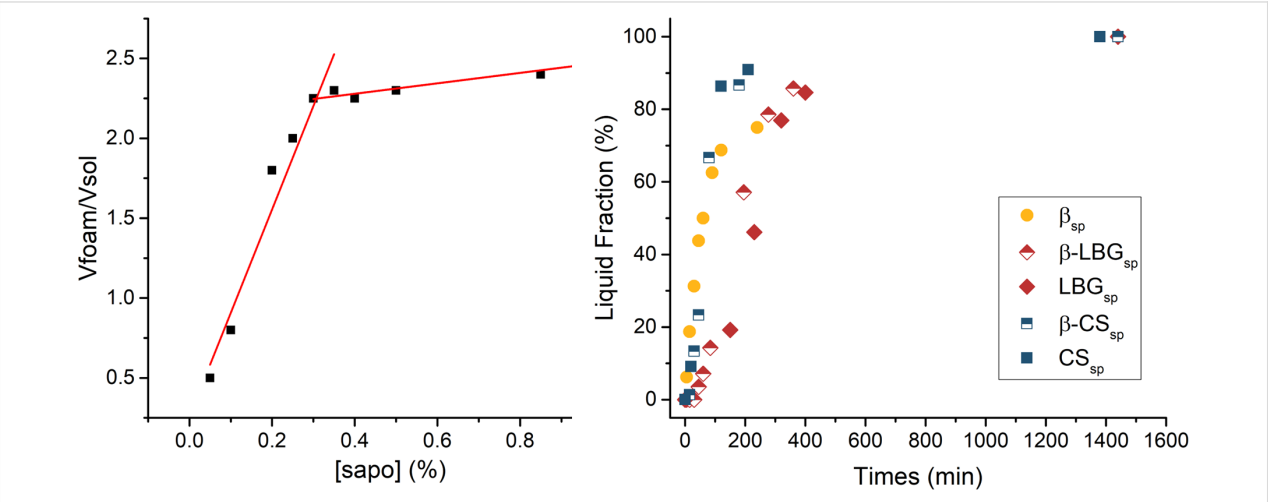


Figure 1: *Quillaja* saponin foamability (left) and foam stability over time for the β-cyclodextrin/polysaccharide (CS: chitosan, LBG: locust bean gum) mixtures (right).

surements correspond to solutions prepared using deionized water. Other factors such as the viscosity due to the polysaccharides or the ionic strength contributed by the catalyst can affect this value. Nevertheless, a concentration of 0.5% of saponin was selected as an initial value to prepare the polysaccharide foams.

In order to study their stability, the foams were introduced into a graduated cylinder after stirring each mixture solution (Figure 1, right). Samples with three different polysaccharides (chitosan (CS), locust bean gum (LBG) and xanthan gum (XG)) were tested either by themselves or mixed in a 50:50 ratio with β-cyclodextrin. A fast emergence of the liquid fraction occurred with the solution containing cyclodextrin with no polysaccharides. These results show that the emulsion production needs to be followed quickly by the freezing of the foam, otherwise a continuous liquid phase could be formed prior to the lyophilization process. The two chitosan solutions, with or without cyclodextrin, produce foams with similar stabilities. On the other hand, the presence of LBG impacts the stability of the foam in a remarkable way. Finally, the solutions of xanthan are not shown in Figure 1, because their foams are very stable due to the much higher viscosity of those solutions. In fact, the liquid fraction was not even falling down, and liquid agglomeration began to be observable at different heights in the graduated cylinder. Several interaction processes can influence the viscosity behaviour of these mixtures and have an impact on their stability. For instance, when considering mixtures of chitosan with saponin, the possibility of solubilization of chitosan molecules into the cavity of the glycoside micelles should be taken into account. Our main goal in this part of the study is to guarantee that the prepared foams remain stable at least until the crosslinking reaction takes place.

Once the six experimental synthetic paths were set (see Experimental section and Table 1), three types of matrices produced using saponin (*45spPow*, *45spLiq**, *45spFoam**) were compared to three with no saponin (*20Pow*, *45Pow*, *45Liq**). First of all, the synthesis procedure influences the yield achieved for each polysaccharide (Supporting Information File 1, Figure S1). In the absence of saponin, by increasing the reaction time from 20 to 45 min (samples *20Pow* and *45Pow*, respectively), the yield will increase due to a higher crosslinking efficiency of the solventless procedure [38]. A mixture dissolved in water and then freeze-dried (sample *45Liq**) shows a better yield, certainly because of a higher homogenization of the pre-crosslinked matrix. When prepared in powder (solid-state) form (*45spPow*), adding saponin will decrease the percent yield from 70% to 50%. Interestingly, the yield is not affected in that way when adding saponin into the liquid mixture (*45spLiq**). However, crosslinking the foam (*45spFoam**) will reduce considerably the yield for the chitosan matrix while the two other polysaccharides show no important modifications, which can be explained by the different stabilities of the foams produced.

Table 1: Methods of preparation of the thermally crosslinked cyclodextrin/polysaccharide matrices (*lyophilized).

Name	Crosslinking time (min)	Physical form	Saponin added
*45spFoam**	45	foam	yes
*45spLiq**	45	liquid	yes
*45Liq**	45	liquid	no
45spPow	45	powder	yes
45Pow	45	powder	no
20Pow	20	powder	no

On the second set of yield results (Supporting Information File 1, Figure S1, bottom), the crosslinking of cyclodextrin with or without the polysaccharides using saponin show a slightly higher yield when prepared by lyophilization from the homogeneous liquid state (*45spLiq**) than when lyophilized from the foam-like state (*45spFoam**). These differences can be correlated to the foam stability.

Morphology of the matrices studied by scanning electron microscopy (SEM)

The different microstructures of the samples have been analysed for the three polysaccharide combinations. Those of β-cyclodextrin/LBG matrices will be shown here, since all the polysaccharides originated similar morphologies. In addition, the differences found for the three matrices prepared using the solventless procedures (*20Pow*, *45Pow*, *45spPow*) are not significant either. Figure 2 shows a powder-like material with the same average size (≈15 μm); some dispersity is detected in the *20 Pow* micrograph. In contrast, the use of the freeze-drying method produces some thinner and longer sheet-like particles. These sheets look also the same with or without the presence of saponin. The foaming process (*spFoam**) creates thinner sheets than the liquid processes, and we can observe also some tubes for the latter, looking like sheets being rolled around themselves. These images correspond to the lyophilized, crushed, washed, and subsequently dried matrices. The washing process of the crosslinked matrices produces a swelling phenomenon because of the hydrophilicity of the polysaccharides and the citrate crosslinker, changing the morphology of the internal structures. As can be seen in Figure 3 for sample β-c_{sp} (cyclodextrin/saponin without polysaccharides), the washing process causes a swelling of the walls, transforming an ordered porous structure into a random structure, composed of a mixture of tubes and sheets. For these particular samples, the freeze-dried

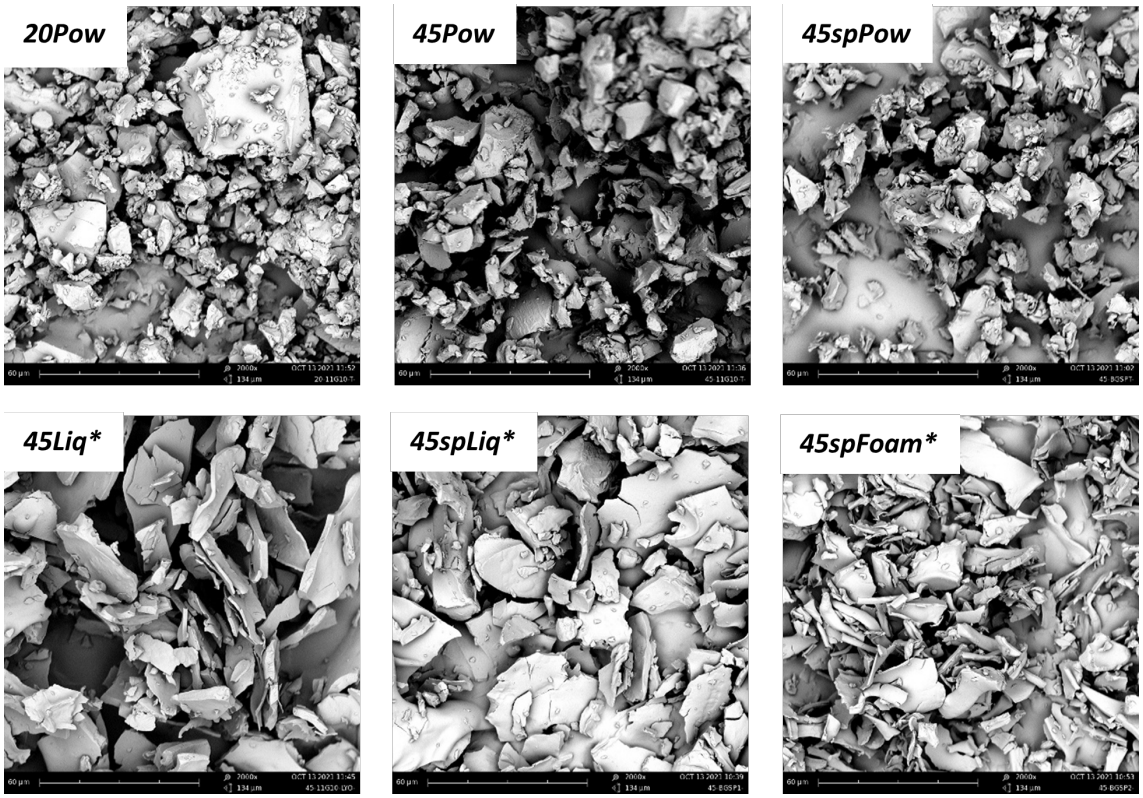


Figure 2: SEM images of crushed β-c-LBG as a function of the synthesis pathways (see below, Experimental section). Part "45Pow" of Figure 2 was reprinted from [39], Carbohydrate Polymers, vol. 288, by M. Petitjean; N. Lamberto; A. Zornoza; J. R. Isasi, "Green synthesis and chemometric characterization of hydrophobic xanthan matrices: Interactions with phenolic compounds", article no. 119387, Copyright 2022 The Authors, with permission from Elsevier. Published by Elsevier Ltd, distributed under the terms of the Creative Commons Attribution-NonCommercial-NoDerivatives 4.0 International License, https://creativecommons.org/licenses/by-nc-nd/4.0/. This content is not subject to CC BY 4.0.

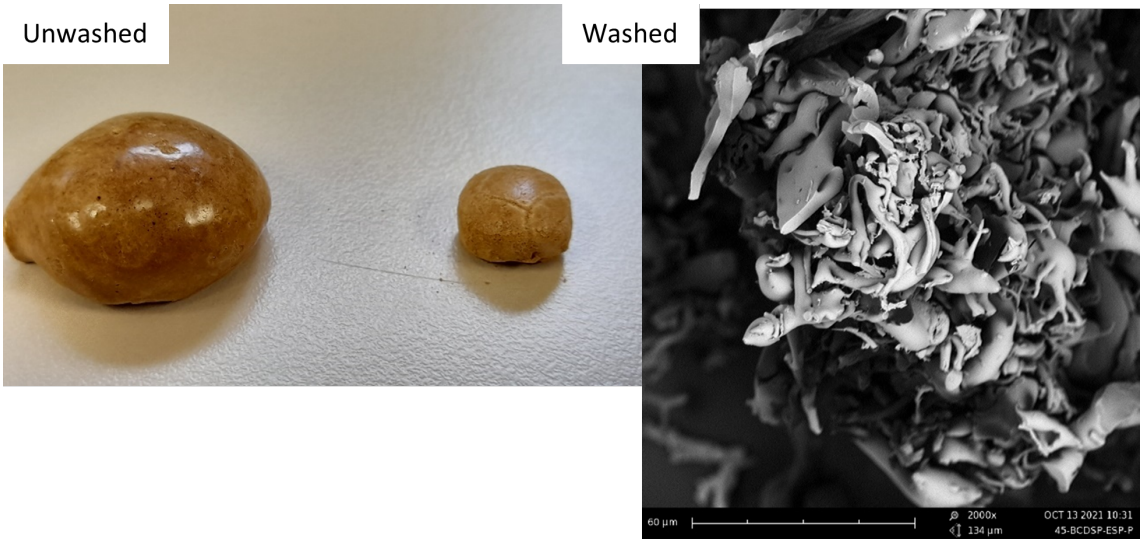


Figure 3: SEM of β-c_{sp} after crosslinking with or without washing the sample.

mixtures produce a spherical material in the heating step, covered by a fragile and brilliant layer but possessing a highly porous inner structure. This thin layer is more evident for the β-c_{sp} sample produced using the liquid path than for the one obtained by the foam path. The latter possesses also a higher specific area (Supporting Information File 1, Figure S2). On the

other hand, the polysaccharide matrices (see Figure 4 for chitosan matrices) do no create the same type of pores; the successful emulsion process keeps its structure as shown by the spherical bubble pores. Chitosan produces fragile matrices once they are dried. However, looking at the structures produced by the xanthan gum and locust bean gum matrices, the presence of a sphere-like porous scaffold is also evident when the material is not washed.

Chemical characterization of the β-cyclodextrin/saponin foams

The infrared spectra for the three crosslinked polysaccharides produced following different paths have been compared (Supporting Information File 1, Figure S3). In the fingerprint region, the main differences between the powder and liquid/foam matrices correspond to the ca. 1200 cm^{-1} region. The latter show a better resolution for the 1200 and 1150 cm^{-1} bands. In addition, a larger band at 1600 cm^{-1} is also observed for the saponin matrices; unfortunately, it is overlapped by other bands present in the polysaccharide spectra, so the amount of saponin incorporated into the matrices is difficult to quantify by this method. The infrared study of this region for similar samples (in the absence of saponin) has been reported in our previous works [37-39]. In addition to those, a small band can be detected also around 1500 cm^{-1} only for saponin matrices. This one might be useful for quantification purposes, provided some validation can be obtained using other appropriate methodologies.

A shift of the 1000 cm^{-1} C–O band towards higher wavenumbers (Supporting Information File 1, Figure S4) occurs for each matrix when going from 100:0 to 0:100 ratio of cyclodextrin/polysaccharide. The 1200 cm^{-1} band is also more intense when changing that ratio. This difference is also correlated to the C=O band found at 1700 cm^{-1}. In the case of the chitosan matrices, for a high concentration of chitosan, the crosslinking reactions include esterification links, amide formation and the Maillard reaction [39]. This behaviour can be analysed by the intensities of the 1600–1500 cm^{-1} regions.

An interesting method of comparison from the molecular point of view is the use of phenolphthalein as a probe to analyse the amount of 'free cyclodextrin' moieties present in the matrices, i.e., those available for inclusional interactions [38]. The first and most important difference is between both liquid and foam saponin samples and the rest (Figure 5). The amount of 'free cyclodextrin' found for the solventless (powder) synthesis, with or without saponin, is always low, around 15 mg/g of matrix. Similar results are found for the liquid path in the absence of saponin. The favourable influence of saponin to produce a more efficient matrix is confirmed. The freeze drying of solutions permits to produce microporous materials, as seen in the SEM images of Figure 2, where the sheet-like structures observed being those macrostructures modified by water swelling and crushing after drying. Saponins, at a molecular level, probably confer an additional microporosity to the matrix, permitting the cyclodextrin moieties to be more available for complexation with phenolphthalein or other molecules.

In addition, the foam and liquid saponin/cyclodextrin/polysaccharide samples are compared to the corresponding cyclodextrin/saponin (no polysaccharide) and saponin/polysaccharide (no cyclodextrin) matrices (Figure 5, bottom). All the cyclodextrin/polysaccharide samples show a higher amount of 'free cyclodextrin' per gram than that of pure cyclodextrin. This may be due to a possible saponin/β-CD complexation, yielding the cyclodextrin unavailable, or because the polysaccharides en-

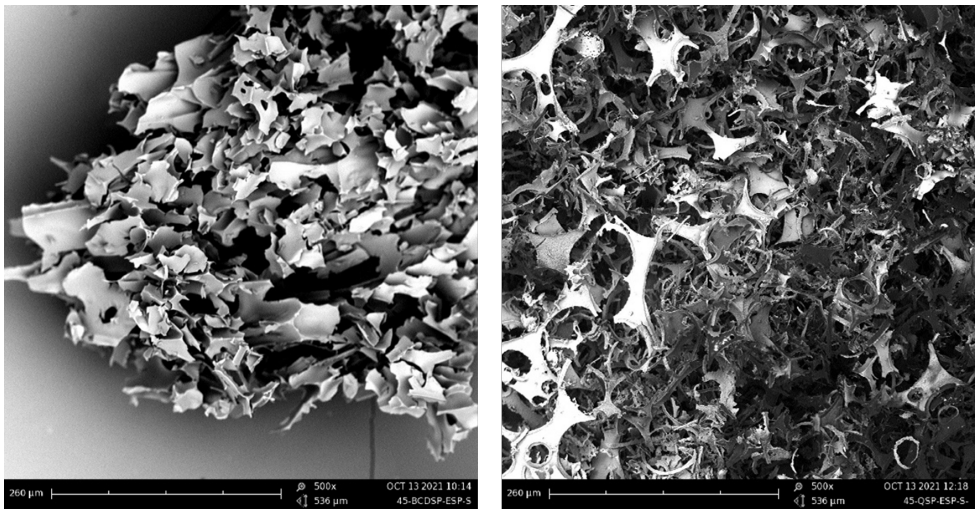


Figure 4: β-c_{sp} (left) and c-CS_{sp} (right) matrices unwashed showing the "foam-like" morphologies.

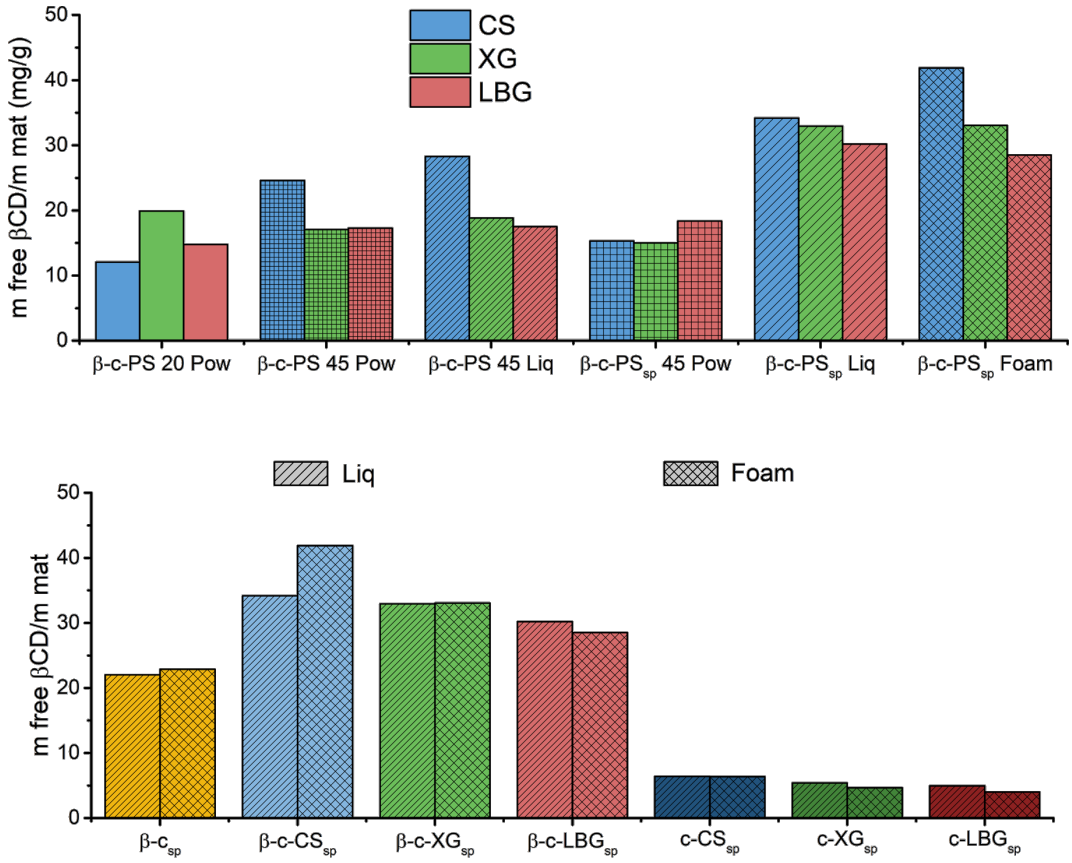


Figure 5: Values (in mg/g) of equivalent 'free β-cyclodextrin' in the polysaccharide (PS) matrices, as a function of the synthesis path (top), and comparisons between the liquid and foam saponin matrices with (bottom left) or without cyclodextrin (bottom right).

hance the grafting of cyclodextrin into their chains. It needs to be added that pure polysaccharide matrices (last columns in Figure 5, bottom) show also an affinity with phenolphthalein. Because these samples do not possess any cyclodextrin modifications, this non-zero values should be explained as an 'equivalent free cyclodextrin'. In our previous work [38], we checked that those crosslinked polysaccharide matrices without cyclodextrin did not show any affinities towards phenolphthalein, so, in this case, we can attribute this effect to certain favourable interactions between phenolphthalein and the saponin moieties.

Sorption capabilities of the matrices

This 'free cyclodextrin' impact on the sorption capabilities of the matrices has been studied with the corresponding 1-naphthol (1-N) isotherms (Figure 6). When comparing the isotherms of *20Pow*, *45spLiq* and *45spFoam* of single component matrices, a better sorption from the saponin matrices for low 1-naphthol concentrations is detected. Thus, β-c$_{sp}$ (with no polysaccharide) absorbed more 1-N when saponin is present between 2 ppm and 200 ppm, which is the largest range of higher efficiency for all matrices. For the others, there seems to be no effect in the low 1-N concentration range. Nevertheless, we need to look at the graph insets, which show the sorption isotherms at low solute concentrations. The c-LBG *20Pow* matrix sorption behaviour was fitted following the Hill function, but this model does not represent well the absorption process in the low concentration region. For c-XG and c-CS, a wider 1-N concentration range where saponins impact on sorption is observable: between 2 and 50 ppm for c-XG, and between 2 and 150 ppm for c-CS. As a possible explanation for this anomalous behaviour, it is known that 1-N can self-associate from a certain concentration level. Before this, the 1-N molecules are easily complexed within cyclodextrin matrices, or, in this case, associated to the new hydrophobic regions provided by saponin. When this concentration is higher, the association of 1-N appears to create aggregates, saturating the cyclodextrin sites but allowing the polysaccharide networks affect the sorption. When saponin is introduced, this last impact can be assumed by the saponin moieties. The difference between *45spLiq* and *45spFoam* is quite small; it is not observable for β-c$_{sp}$, and the biggest difference is seen for c-LBG$_{sp}$ produced by a "liquid

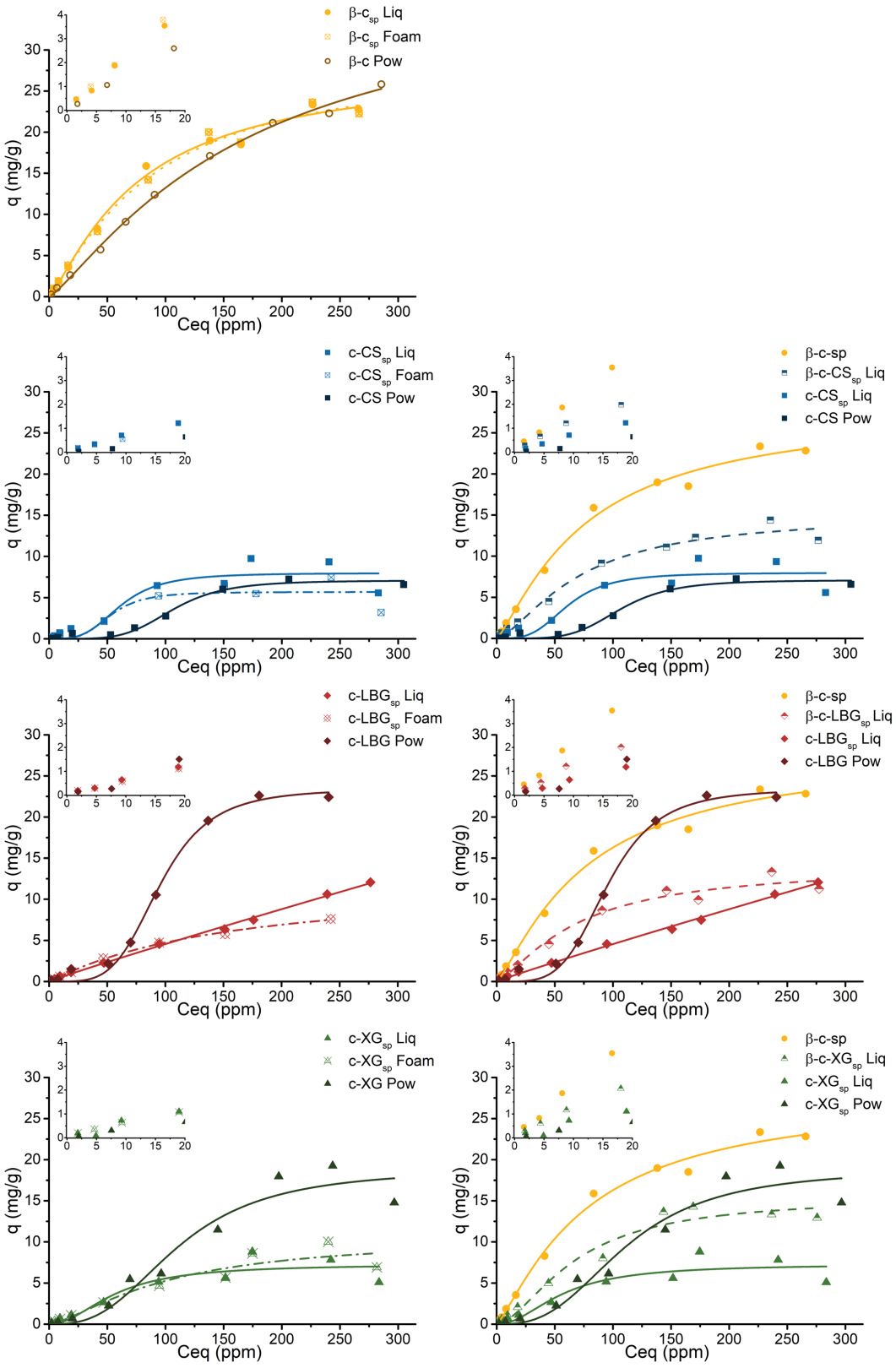


Figure 6: 1-Naphthol isotherms of crosslinked β-cyclodextrin/polysaccharides (blue curves for chitosan, red for locust bean gum, green for xanthan gum) with saponin (yellow curves correspond to cyclodextrin matrices, without polysaccharide).

path" synthesis. This variation reflects the sorption mechanism, as the curve follows the Freundlich model, while the Hill model represent the others better. As seen for the isotherms in previous works, the higher the cyclodextrin/polysaccharide ratio, the better the sorption. The effects of LBG or XG on the sorption is absent when saponin is in the matrix, letting these polysaccharides being a simple hydrogel scaffold for the sorption of 1-naphthol.

An aqueous sorbate mixture of five phenolic compounds has been also tested to assess the differences in the sorption behaviours of the different matrices. The absorbed amount changes as a function of the cyclodextrin/polysaccharide ratio, and the same trends are observed for all the polysaccharide types (Figure 7). Those matrices with cyclodextrin (yellow bars in Figure 7) absorbed better all the phenolic compounds tested. In addition, the incorporation of saponin does not produce a higher sorption capacity except for the XG matrices. In these matrices, the sorption of 4-ethylphenol and eugenol are the most favourable, followed by that of vanillin. Finally, the synthesis pathway (either liquid or foam) is not a determinant factor for the sorption capacity either. This fact can be explained by the similar microstructures produced in each case, though their macroporosities are remarkably different.

Experimental

Materials

β-cyclodextrin (Wacker, 12.5% H_2O), xanthan gum (Sigma-Aldrich), locust bean gum (Sigma-Aldrich), chitosan (deacetylation degree of 90%), citric acid (Panreac AppliChem) and dibasic sodium phosphate (Na_2HPO_4 ≥ 98%), soapbark (*Quillaja saponaria*; Sp. 'quillay', from Mapuche 'küllay') saponin (Sigma-Aldrich, sapogenin content ≥ 10%, India), phenol (99.5%; Panreac, Spain), *m*-cresol (99%; Sigma, Germany), 4-ethylphenol (99%, Sigma, China), vanillin (99%; Panreac, Spain) and eugenol (99%; Sigma, Germany) were used as received. Phenolphthalein and 1-naphthol (≥99%) were obtained from Merck (Germany).

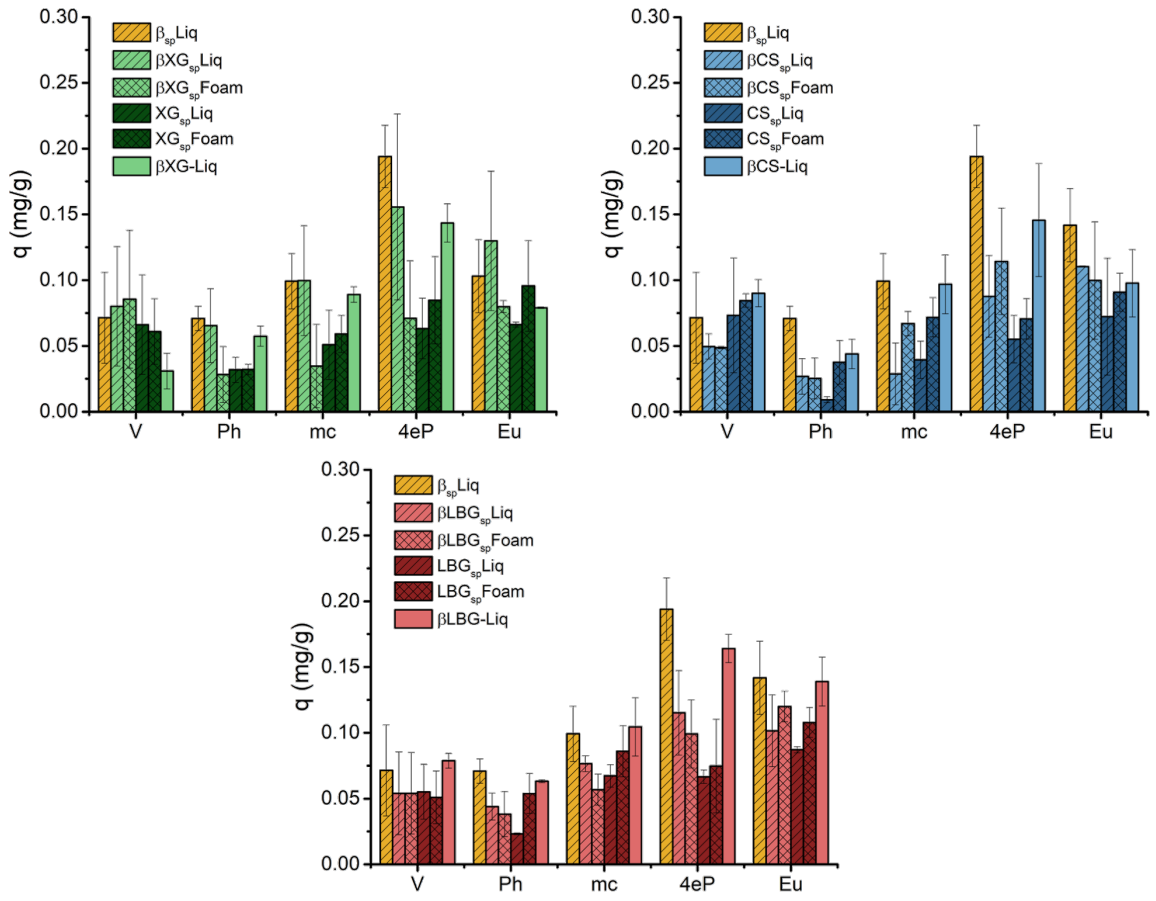


Figure 7: Sorption of phenols (V, vanillin; Ph, phenol; m-c, *m*-cresol; 4eP, 4-ethylphenol; Eu, eugenol) in β-cyclodextrin/polysaccharides (xanthan, XG; chitosan, CS; and locust bean gum, LBG) with saponin (sp) produced by different pathways (liquid and foam).

Methods

Synthesis procedures: Firstly, citric acid (1.3 g) is dissolved into 100 mL of deionized water (acidic pH is required for chitosan) with 1.5 g of polysaccharide (either xanthan, or locust bean gum, or chitosan) and/or β-cyclodextrin, plus 0.5 g of *Quillaja saponaria* saponin. After that, sodium phosphate dibasic (Na_2HPO_4, 0.28 g) is added to catalyse the reaction (see Supporting Information File 1, Table S1).

Two main types of materials are prepared from these stock solutions. The first one (*45spLiq**) is directly lyophilized until a perfectly dried sample is obtained (two freeze drying steps of 24 h can be necessary with an additional freezing at −40 °C between the two). The resulting material is then thermally crosslinked at 170 °C during 45 min. Then, it is washed twice in 100 mL of deionized water, filtered and freeze dried again. The second process (*45spFoam**) consists of introducing 20 mL of the stock solution into a large crystallizer, where the liquid height reaches around 1 cm. The liquid is stirred during 5 min at high speed to make an air/water emulsion. The resulting foam is quickly frozen at −40 °C, lyophilized, thermally crosslinked, washed and dried using the same conditions as for the previous path.

In order to understand the effect of saponins and the influence of the synthesis procedures, the crosslinked matrices have been prepared by four other routes, with or without saponin, starting either from solutions or in the solid state, as shown in Figure 8. Thus, the solid mixtures were homogenized using a mortar as in previous works [38,39], and crosslinked at 170 °C during 20 or 45 min (samples *20Pow* and *45Pow*). A solid-state mixture with the addition of 0.5 g of saponin and a thermal crosslinking at 170 °C during 45 min was prepared also, for comparison purposes (sample *45spPow*).

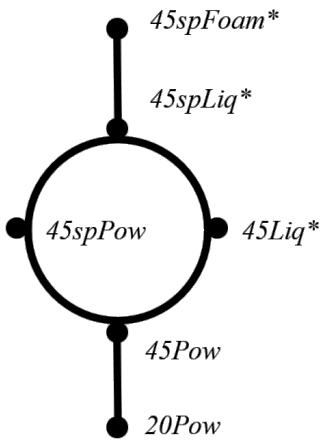


Figure 8: Six synthesis routes (*lyophilized matrices) used to prepare samples β-c-XG_{sp}; β-c-LBG_{sp}; β-c-CS_{sp} using β-cyclodextrin (β), citric acid (c), xanthan gum (XG), locust bean gum (LBG) and chitosan (CS) with saponin (sp) in different physical forms (see also Table 1).

Finally, the three reagents (cyclodextrin, polysaccharide and citric acid) plus the catalyst, without saponin, were dissolved into 100 mL of deionized water, freeze dried, crosslinked, washed and dried as for the first path explained in this section (sample *45Liq**). The matrices formed were then crushed during 30 seconds in a Retsch MM300 ball mill.

Saponin solutions: The foamability of *Quillaja* saponin was measured by dissolving different concentrations of saponin into deionized water (from 0.05 to 1%). Then, 20 mL of the solutions were vigorously agitated with a mechanical stirrer. The maximal foam volume is then measured and plotted against the saponin concentration (see Figure 1, above). To measure the foam stability, the foam was recovered and introduced into a graduated cylinder. The liquid volume was measured at different times and the percent emergence of the liquid fraction was plotted vs time (see also Figure 1).

Characterization of matrices: Scanning electron microscopy (SEM) of gold-sputter-coated samples was carried out using a Phenom Pro 739 microscope. Infrared analysis was carried out for the crushed samples using a Shimadzu IRAffinity-1S instrument coupled with a Golden Gate™ attenuated total reflectance (ATR) accessory device (Specac).

Sorption experiments: The absorption of phenolphthalein and 1-naphthol was analysed using an Agilent Technologies Cary 8454 UV–vis device, equipped with an Agilent ChemStation software. In the case of the phenolic mixtures, an Agilent 110 series HPLC system with a Phenomenex Luna C18 column and a gradient mobile phase were used (H_2O 65% to 50%, acetonitrile 25% to 40%, plus 10% methanol).

Supporting Information

Supporting Information File 1

Percent yields reached following different synthetic paths, additional SEM micrographs, infrared spectra of the samples in the fingerprint region, table with compositions of the reacting mixtures.
[https://www.beilstein-journals.org/bjoc/content/supplementary/1860-5397-19-7-S1.pdf]

Acknowledgements

The authors wish to thank M. Domeño for his help with UV–vis and HPLC measurements.

Funding

The authors also thank the University of Navarra (PIUNA 2018-15) for financial aid. MP thanks the Asociación de Amigos (University of Navarra) for a doctoral grant.

ORCID® iDs

José Ramón Isasi - https://orcid.org/0000-0002-0481-5800

References

1. Bach, T. J.; Rohmer, M., Eds. *Isoprenoid Synthesis in Plants and Microorganisms. New Concepts and Experimental Approaches;* Springer: New York, NY, USA, 2013. doi:10.1007/978-1-4614-4063-5
2. Francis, G.; Kerem, Z.; Makkar, H. P. S.; Becker, K. *Br. J. Nutr.* **2002,** *88,* 587–605. doi:10.1079/bjn2002725
3. Hostettmann, K.; Marston, A. *Saponins;* Cambridge University Press: Cambridge, UK, 1995. doi:10.1017/cbo9780511565113
4. Shi, J.; Arunasalam, K.; Yeung, D.; Kakuda, Y.; Mittal, G.; Jiang, Y. *J. Med. Food* **2004,** *7,* 67–78. doi:10.1089/109662004322984734
5. Dawid, C.; Hofmann, T. *J. Agric. Food Chem.* **2012,** *60,* 11889–11900. doi:10.1021/jf304085j
6. Van Dyck, S.; Flammang, P.; Meriaux, C.; Bonnel, D.; Salzet, M.; Fournier, I.; Wisztorski, M. *PLoS One* **2010,** *5,* e13923. doi:10.1371/journal.pone.0013923
7. Liu, H.-W.; Li, J.-K.; Zhang, D.-W.; Zhang, J.-C.; Wang, N.-L.; Cai, G.-P.; Yao, X.-S. *J. Asian Nat. Prod. Res.* **2008,** *10,* 521–529. doi:10.1080/10286020801966674
8. Sharma, P.; Tyagi, A.; Bhansali, P.; Pareek, S.; Singh, V.; Ilyas, A.; Mishra, R.; Poddar, N. K. *Food Chem. Toxicol.* **2021,** *150,* 112075. doi:10.1016/j.fct.2021.112075
9. Wisetkomolmat, J.; Suksathan, R.; Puangpradab, R.; Kunasakdakul, K.; Jantanasakulwong, K.; Rachtanapun, P.; Sommano, S. R. *Plants* **2020,** *9,* 1521. doi:10.3390/plants9111521
10. Rai, S.; Acharya-Siwakoti, E.; Kafle, A.; Devkota, H. P.; Bhattarai, A. *Sci* **2021,** *3,* 44. doi:10.3390/sci3040044
11. Oleszek, W.; Hamed, A. Saponin-Based Surfactants. In *Surfactants from Renewable Resources;* Kjellin, M.; Johansson, I., Eds.; John Wiley & Sons: Chichester, UK, 2010; pp 239–249. doi:10.1002/9780470686607.ch12
12. Piorkowski, D. T.; McClements, D. J. *Food Hydrocolloids* **2014,** *42,* 5–41. doi:10.1016/j.foodhyd.2013.07.009
13. Zhang, J.; Bing, L.; Reineccius, G. A. *Food Chem.* **2016,** *192,* 53–59. doi:10.1016/j.foodchem.2015.06.078
14. Li, D.; Baert, L.; Uyttendaele, M. *Food Microbiol.* **2013,** *35,* 1–9. doi:10.1016/j.fm.2013.02.009
15. Alberice, J. V.; Funes-Huacca, M. E.; Guterres, S. B.; Carrilho, E. *Int. J. Food Microbiol.* **2012,** *159,* 130–135. doi:10.1016/j.ijfoodmicro.2012.08.004
16. Huang, J.; Peng, K.; Wang, L.; Wen, B.; Zhou, L.; Luo, T.; Su, M.; Li, J.; Luo, Z. *Acta Biochim. Biophys. Sin.* **2016,** *48,* 750–755. doi:10.1093/abbs/gmw049
17. Choi, S.; Kim, T. W.; Singh, S. V. *Pharm. Res.* **2009,** *26,* 2280–2288. doi:10.1007/s11095-009-9944-9
18. Kim, H.-S.; Lee, E.-H.; Ko, S.-R.; Choi, K.-J.; Park, J.-H.; Im, D.-S. *Arch. Pharmacal Res.* **2004,** *27,* 429–435. doi:10.1007/bf02980085
19. Liu, Z.; Li, Z.; Zhong, H.; Zeng, G.; Liang, Y.; Chen, M.; Wu, Z.; Zhou, Y.; Yu, M.; Shao, B. *J. Environ. Chem. Eng.* **2017,** *5,* 6030–6038. doi:10.1016/j.jece.2017.11.021
20. Wu, M.; Xu, Y.; Ding, W.; Li, Y.; Xu, H. *Appl. Microbiol. Biotechnol.* **2016,** *100,* 7249–7261. doi:10.1007/s00253-016-7551-3
21. Zhou, W.; Yang, J.; Lou, L.; Zhu, L. *Environ. Pollut.* **2011,** *159,* 1198–1204. doi:10.1016/j.envpol.2011.02.001
22. Gusiatin, Z. M.; Klimiuk, E. *Chemosphere* **2012,** *86,* 383–391. doi:10.1016/j.chemosphere.2011.10.027
23. Hong, K.-J.; Tokunaga, S.; Kajiuchi, T. *Chemosphere* **2002,** *49,* 379–387. doi:10.1016/s0045-6535(02)00321-1
24. Zhu, T.; Fu, D.; Yang, F. *Bull. Environ. Contam. Toxicol.* **2015,** *94,* 129–133. doi:10.1007/s00128-014-1412-5
25. Santini, E.; Jarek, E.; Ravera, F.; Liggieri, L.; Warszynski, P.; Krzan, M. *Colloids Surf., B* **2019,** *181,* 198–206. doi:10.1016/j.colsurfb.2019.05.035
26. Ma, Z.-W.; Zhang, K.-N.; Zou, Z.-J.; Lü, Q.-F. *J. Environ. Chem. Eng.* **2021,** *9,* 105251. doi:10.1016/j.jece.2021.105251
27. Laysandra, L.; Ondang, I. J.; Ju, Y.-H.; Ariandini, B. H.; Mariska, A.; Soetaredjo, F. E.; Putro, J. N.; Santoso, S. P.; Darsono, F. L.; Ismadji, S. *Environ. Sci. Pollut. Res.* **2019,** *26,* 5020–5037. doi:10.1007/s11356-018-4035-2
28. Mironenko, N. V.; Smuseva, S. O.; Brezhneva, T. A.; Selemenev, V. F. *Russ. J. Phys. Chem. A* **2016,** *90,* 2459–2464. doi:10.1134/s0036024416120219
29. Zhao, Y.; Lu, W.; Shen, S.; Wei, L. *Cellulose* **2021,** *28,* 11429–11450. doi:10.1007/s10570-021-04258-y
30. Mironenko, N. V.; Smuseva, S. O.; Brezhneva, T. A.; Selemenev, V. F.; Nechaeva, L. S.; Butyrskaya, E. V. *Colloid J.* **2017,** *79,* 219–225. doi:10.1134/s1061933x17020077
31. Rejinold, N. S.; Muthunarayanan, M.; Muthuchelian, K.; Chennazhi, K. P.; Nair, S. V.; Jayakumar, R. *Carbohydr. Polym.* **2011,** *84,* 407–416. doi:10.1016/j.carbpol.2010.11.056
32. Bande, F.; Arshad, S. S.; Bejo, M. H.; Omar, A. R.; Moeini, H.; Khadkodaei, S.; Wei, T. S.; Keong, Y. S.; Abba, Y.; Anka, I. A. *Microb. Pathog.* **2020,** *149,* 104560. doi:10.1016/j.micpath.2020.104560
33. Lee, P. S.; Han, J.-Y.; Song, T. W.; Sung, J. H.; Kwon, O.-S.; Song, S.; Chung, Y. B. *Int. J. Pharm.* **2006,** *316,* 29–36. doi:10.1016/j.ijpharm.2006.02.035
34. Huang, J.; Liu, Y.; Li, X.; Song, Y.; Li, W.; Liu, K.; Su, D.; Feng, Y.; Yang, S. *Biomed. Chromatogr.* **2015,** *29,* 1885–1892. doi:10.1002/bmc.3511
35. Hu, S. C.-S.; Lai, Y.-C.; Lin, C.-L.; Tzeng, W.-S.; Yen, F.-L. *Phytomedicine* **2019,** *57,* 174–182. doi:10.1016/j.phymed.2018.11.012
36. Guo, H.; Xiong, J.; Ma, W.; Wu, M.; Yan, L.; Li, K.; Liu, Y. *J. Sep. Sci.* **2016,** *39,* 4439–4448. doi:10.1002/jssc.201600834
37. Petitjean, M.; Isasi, J. R. *Int. J. Biol. Macromol.* **2021,** *180,* 570–577. doi:10.1016/j.ijbiomac.2021.03.098
38. Petitjean, M.; Aussant, F.; Vergara, A.; Isasi, J. R. *Gels* **2020,** *6,* 51. doi:10.3390/gels6040051
39. Petitjean, M.; Lamberto, N.; Zornoza, A.; Isasi, J. R. *Carbohydr. Polym.* **2022,** *288,* 119387. doi:10.1016/j.carbpol.2022.119387

License and Terms

This is an open access article licensed under the terms of the Beilstein-Institut Open Access License Agreement (https://www.beilstein-journals.org/bjoc/terms), which is identical to the Creative Commons Attribution 4.0 International License (https://creativecommons.org/licenses/by/4.0). The reuse of material under this license requires that the author(s), source and license are credited. Third-party material in this article could be subject to other licenses (typically indicated in the credit line), and in this case, users are required to obtain permission from the license holder to reuse the material.

The definitive version of this article is the electronic one which can be found at:
https://doi.org/10.3762/bjoc.19.7

BEILSTEIN JOURNAL OF ORGANIC CHEMISTRY

Insight into oral amphiphilic cyclodextrin nanoparticles for colorectal cancer: comprehensive mathematical model of drug release kinetic studies and antitumoral efficacy in 3D spheroid colon tumors

Sedat Ünal[1], Gamze Varan‡[2], Juan M. Benito‡[3], Yeşim Aktaş‡[1] and Erem Bilensoy*[4,§]

Full Research Paper

Open Access

Address:
[1]Department of Pharmaceutical Technology, Faculty of Pharmacy, Erciyes University, 38280, Kayseri, Turkey, [2]Department of Vaccine Technology, Vaccine Institute, Hacettepe University, 06100, Ankara, Turkey, [3]Institute for Chemical Research, CSIC - University of Sevilla, Av. Americo Vespucio 49, 41092, Sevilla, Spain and [4]Department of Pharmaceutical Technology, Faculty of Pharmacy, Hacettepe University, 06100, Ankara, Turkey

Email:
Erem Bilensoy* - eremino@hacettepe.edu.tr

* Corresponding author ‡ Equal contributors
§ Mobile phone: +90 (532) 273 25 65

Keywords:
colorectal cancer; camptothecin; 3D spheroid; cyclodextrin; oral nanoparticle; release kinetics

Beilstein J. Org. Chem. **2023,** *19,* 139–157.
https://doi.org/10.3762/bjoc.19.14

Received: 31 October 2022
Accepted: 30 January 2023
Published: 13 February 2023

This article is part of the thematic issue "Cyclodextrins as building blocks for new materials".

Guest Editor: S. Fourmentin

© 2023 Ünal et al.; licensee Beilstein-Institut.
License and terms: see end of document.

Abstract

Colorectal cancer (CRC) is the third most diagnosed cancer type globally and ranks second in cancer-related deaths. With the current treatment possibilities, a definitive, safe, and effective treatment approach for CRC has not been presented yet. However, new drug delivery systems show promise in this field. Amphiphilic cyclodextrin-based nanocarriers are innovative and interesting formulation approaches for targeting the colon through oral administration. In our previous studies, oral chemotherapy for colon tumors was aimed and promising results were obtained with formulation development studies, mucin interaction, mucus penetration, cytotoxicity, and permeability in 2D cell culture, and furthermore in vivo antitumoral and antimetastatic efficacy in early and late-stage colon cancer models and biodistribution after single dose oral administration. This study was carried out to further elucidate oral camptothecin (CPT)-loaded amphiphilic cyclodextrin nanoparticles for the local treatment of colorectal tumors in terms of their drug release behavior and efficacy in 3-dimensional tumor models to predict the in vivo efficacy of different nanocarriers. The main objective was to build a bridge between formulation development and in vitro phase and animal studies. In this context, CPT-loaded polycationic-β-cyclodextrin nanoparticles caused reduced cell viability in CT26 and HT29 colon carcinoma spheroid tumors of mice and human origin, respectively. In addition, the release profile, which is one of the critical quality parameters in new drug delivery systems, was investigated mathematically by release kinetic modeling for the first time. The overall findings indicated that the strategy of orally targeting anticancer drugs such as CPT with positively charged poly-β-CD-C6 nanoparticles to colon tumors for local and/or systemic efficacy is a promising approach.

Introduction

Cancer is still one of the most common, highly variable and fatal diseases worldwide. Therefore, studies are continuing to develop effective/innovative and more flexible treatments for various types of cancer [1]. Colorectal cancers (CRC) are characterized by the presence of tumors that begin as polyps in the inner wall of the colon and rectum with uncontrolled growth. CRC is a common and metastatically aggressive disease ranking second in terms of cancer-related deaths [2]. Although surgical resection is possible, chemotherapeutic treatment is still one of the most researched approaches in terms of tumor recurrence and the progression of the disease. In CRC chemotherapy, the most common approach is mainly an intravenous administration of anticancer drugs such as camptothecin (CPT) analogs (irinotecan, topotecan), 5-fluorouracil (5-FU), oxaliplatin (OXA) or the combination of these drugs. However, current treatment approaches frequently result in major adverse effects, non-specific biodistribution, poor patient compliance, and clinically inadequate results in terms of efficacy [3-5]. Today, there is an intense focus on oral drug delivery, especially in the treatment of chronic diseases such as cancers. Even though there have been many developments in the field of chemotherapy in recent years, both in terms of diagnosis and treatment, oral chemotherapy has not yet been fully achieved due to the physicochemical properties and poor bioavailability of many widely used anticancer drugs.

Specifically in the treatment of CRC, since the colon is the most distant part of the gastrointestinal (GI) tract, the ability of oral delivery of anticancer drugs to reach the colon in a stable and effective structure is one of the biggest problems for researchers [6-9]. In the gastrointestinal environment, self-assembled nanoparticles are envisioned to protect the active ingredient from pH, enzymatic degradation, and efflux pumps in the intestines. Furthermore, the release profiles of the drug molecules from the dosage system may be controlled by altering the physicochemical parameters (particle size, zeta potential, hydrophobicity) of the self-assembling units utilized to design nanoparticles [9-12]. However, oral nano drug delivery systems capable of providing all the necessary features using polymeric nanoparticles for anticancer drug delivery have not been developed yet. Previous data showed encapsulation in non-ionic uncoated or coated cyclodextrin (CD) nanoparticles enhanced the CPT stability and GI absorption [9,11], and compared to PCL and PLGA nanoparticles, CD nanoparticles also had better release, physical stability, and cytotoxicity [13].

CPT is an anticancer small molecule drug that inhibits the topoisomerase I enzyme, which has a critical role in cellular DNA functions [14], and is effective in a wide spectrum of cancers such as metastatic colon cancer, breast cancer, and small cell lung cancer. It still has not been used clinically for CRC treatment due to its physiological instability and clinical inefficacy due to its physicochemical structure and hydrolytic degradation potential [9,13,15]. While the active lactone form of CPT is present at acidic pH, it is hydrolyzed to the ineffective carboxylate form at basic pH, resulting in decreased clinical efficacy and increased drug-related toxicity. As only the lactone structure of CPT can be transferred through cellular membranes and inhibit topoisomerase I, it is the functional component of CPT lactone form that is primarily responsible for the anticancer action [8,14,16-18]. To avoid CPT inactivation at alkaline medium, the concept that the lactone form can be kept stable by being encapsulated in an acidic microenvironment is also fascinating. Custom synthesized polycationic cyclodextrin amphiphiles have shown the ability to self-assemble into NPs amenable for encapsulation of an array of therapeutics (from small molecule drugs to nucleic acids) [19]. Moreover, their dense ammonium functional display furnishes their NPs with an overall positive charge and large buffering capabilities [19] at physiological pH. Preliminary studies have evidenced pK_a values in the 8.3 range for non-amphiphilic surrogates of these cationic CDs, supporting the cationic character of the resulting NPs [20]. We hypothesized that these polycationic CD NPs, which we designed in our previous studies, could protect the active and stable lactone form of encapsulated CPT due to their acidic chemical structure [8,9,11,13].

CDs are biocompatible cyclic polysaccharides formed by (1→4)-bound α-glucopyranose subunits obtained as a result of enzymatic degradation of starch by glucosyltransferase [21]. With their troncoconic structures having hydrophobic cavities and hydrophilic exterior surfaces, CDs are widely used in the pharmaceutical field to form inclusion complexes mostly with nonpolar molecules in their cavities [22]. In addition, CDs also offer several advantages for colonic drug delivery, because CDs are broken down by the intestinal microflora and dextrans are broken down by the endodextranases in the colon. Since they can predominantly be degraded by colonic microflora, CDs have been investigated in terms of drug delivery systems targeting the colon for many years [9,23,24]. Amphiphilic CD nanocarriers have been extensively investigated in new drug and gene delivery studies, particularly in cancer therapy, for targeted drug delivery, extended/controlled release, and improving cellular interaction [25-29].

Within the scope of this study, advanced studies were carried out for the oral polycationic nanodrug delivery system, developed in our previous research for the treatment of CRC to build a bridge between in vitro characterization and in vivo animal efficacy studies and to establish a screening tool for

nanoparticulate formulations for poorly bioavailable anticancer drugs administered through a non-parenteral route.

In this context, release kinetic modeling studies and 3D cell culture studies of colon carcinoma cells of mice and human origin were carried out for the first time for CPT-loaded positively charged β-CD nanoparticles with different formulations. A positive surface charge was achieved through either (i) the cationic nature of the CD such as poly-β-CD-C6 or (ii) coating of non-ionic 6-O-capro-β-CD with the cationic polymer chitosan (CS). Uncoated 6-O-capro-β-CD negatively charged NPs were used as control formulation.

Results and Discussion

Fabrication and in vitro characterization of CPT-loaded amphiphilic CD NPs

CPT-loaded amphiphilic CD nanoparticles have been previously optimized in our laboratories [9], as reported, NPs using two different amphiphilic CDs were prepared and 6-O-capro-β-CD nanoparticles coated with chitosan (CS) to obtain a positively charged surface. In vitro characterization and cell culture studies for 6-O-capro-β-CD, CS-(6-O-capro-β-CD), and poly-β-CD-C6 formulations have been comprehensively evaluated previously [9]. According to the pre-formulation studies, an optimal formulation with desired characteristics was determined as CPT/poly-β-CD-C6 NPs with a 135 nm particle size, very low polydispersity index, and a zeta potential of + 40 mV. In vitro release experiments showed that amphiphilic CD NPs have properties suitable for colon targeting, but the most promising were poly-β-CD-C6 NPs with 52% of encapsulated CPT successfully delivered all the way to the simulated colon. When compared to the equivalent CPT dose in solution, CPT-loaded poly-β-CD-C6 nanoparticles exhibited higher cytotoxicity in HT-29 cells. Permeability studies performed with the Caco-2 cell line revealed a 276% increase in drug permeability and significantly higher intestinal penetration with the cationic CD formulation. In our further research [8], it was also reported that the oral CPT-loaded poly-β-CD-C6 NPs showed antitumoral and antimetastatic effects in a colorectal tumor-bearing animal model.

Drug release from amphiphilic CD nanoparticles

In vitro release studies were performed over 48 hours in order to clearly elucidate the release kinetics (Figure 1). An in vitro release study was carried out at 0–2 hours in simulated gastric fluid (SGF), 2–5 hours in simulated intestinal fluid (SIF), then in simulated colonic fluid (SCoF) settings till the completion of the experiment in order to imitate GIT circumstances in terms of pH and transit duration. The purpose of the release study was to elucidate the ability of the formulation to retain the encapsulated drug in the stomach and small intestine and preferably release it when it reaches the colon. The optimum nanoparticle formulation was considered to deliver most of the effective lactone-form CPT to the colon.

It is known that it takes approximately 5 hours for oral drug delivery systems to reach the colon; the first 2 hours in the stomach and the last 3 hours in the small intestine [30]. At the end of the 5th hour, 6-O-capro-β-CD and CS-(6-O-capro-β-CD) formulations revealed faster release profiles ($p > 0.05$) than

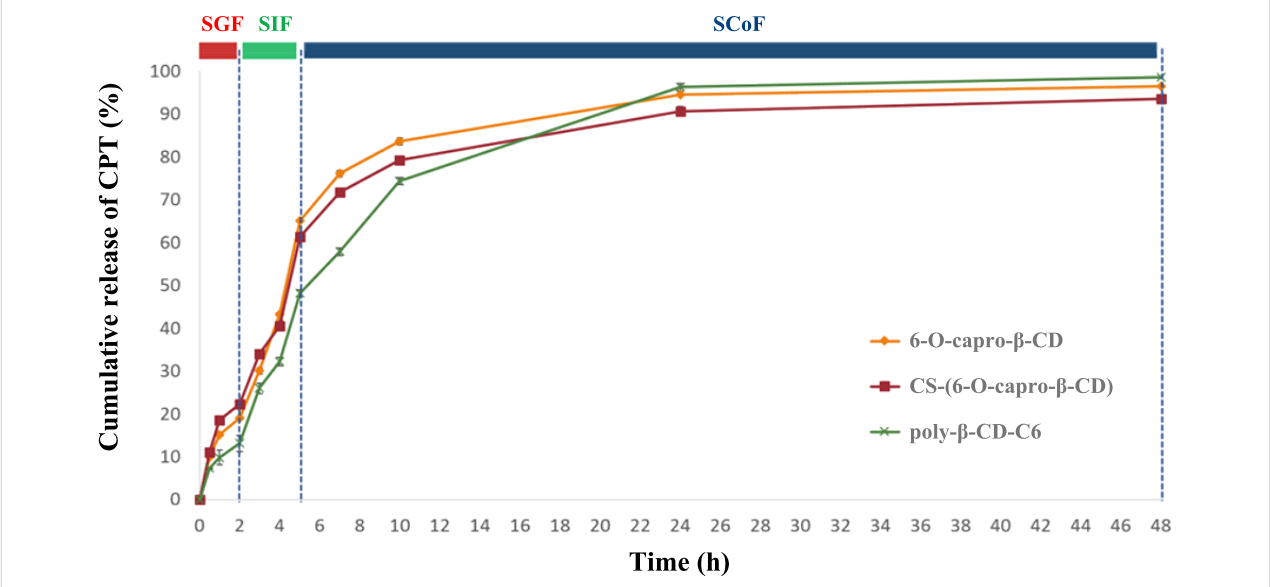


Figure 1: In vitro release profile of CPT from nanoparticle formulations (n = 3, ± SD).

poly-β-CD-C6 nanoparticles. Poly-β-CD-C6 nanoparticles showed a slower release of CPT (48%) until the colonic area as compared to the other formulations ($p < 0.05$). Previous research has looked into detailed assessments of this topic [9].

Release kinetics study

The in vitro release profiles of CPT-loaded amphiphilic cyclodextrin nanoparticles were fitted with a variety of kinetic models, and the release mechanisms, which are illuminating markers for novel drug delivery systems, were mathematically investigated. In this context, 6 models (first order, Hopfenberg, Korsmeyer–Peppas, Higuchi, Peppas–Sahlin, and Weibull models) and 3 criteria (coefficient of determination (R^2), Akaike information criterion (AIC) and model selection criterion (MSC)) were evaluated for the in vitro release profiles. Much of the research in this field generally evaluates the kinetic data of the total release profiles of the nanoparticles, although it is useful to look at potential alterations in the release kinetics at different release mediums (SGF, SIF, SCoF) as well, especially in orally administered drug delivery systems. To achieve this, a thorough and in-depth release kinetic study was conducted, and the parameters were compared for the GIT conditions. Table 1 displays the findings of the release kinetic modeling studies and graphical reports are presented in Figure 2, Figure 3, and Figure 4. Figures 2–4 show that the kinetic models' predicted and observed CPT releases appear to be consistent with formulations for the best correlated models. Thus, the mathematical compatibility of the kinetic models' graphics with good correlation was also proven. Furthermore, as seen in Table 2, the release profiles of CPT from different formulations were compared in terms of similarity (*f*2) and difference (*f*1) factors, and the results revealed that the release profiles of nanoparticles, which we obtained using the same formulation parameters with structurally similar amphiphilic cyclodextrin derivatives, showed similar release profiles. Formulation parameters affected the release kinetics of the drug-loaded nanoparticles [31,32].

According to the release kinetic parameters in SGF medium, as seen in Table 1, the highest R^2, MSC and lowest AIC values were observed in the Weibull model for 6-O-capro-β-CD and CS-(6-O-capro-β-CD) formulations, and in the

Table 1: Release kinetic modelling and results of NP formulations.

	SGF				SIF				SCoF			
	0–2 hours kinetics				2–5 hours kinetics				5–48 hours kinetics			
Model and equation	R^2	AIC	MSC	*n*/*m**	R^2	AIC	MSC	*n*/*m**	R^2	AIC	MSC	*n*/*m**
6-O-Capro-β-CD												
First-order F = 100·[1−Exp(−k1·t)]	0.823	16.307	0.328	–	0.765	24.496	0.947	–	0.929	21.434	2.243	–
Higuchi F = kH·t^0.5	0.991	4.366	3.313	–	0.606	26.554	0.432	–	−3.300	41.940	−1.859	–
Korsmeyer–Peppas F = kKP·t^n	0.993	5.205	3.103	0.471	**0.982**	**16.301**	**2.996**	**1.319**	0.861	26.790	1.171	0.163
Peppas–Sahlin F = k1·t^m + k2·t^(2·m)	0.994	6.564	2.764	0.450	0.976	19.342	2.235	0.450	0.975	20.277	2.474	0.450
Hopfenberg F = 100·[1−(1−kHB·t)^n]	0.809	18.610	−0.248	3.000	0.915	22.416	1.467	1.000	−2.188	42.443	−1.959	3.000
Weibull F = 100·{1−Exp[−((t−Ti)^β)/α]}	**0.997**	**3.640**	**3.495**	**–**	0.946	22.605	1.420	–	**0.987**	**17.087**	**3.112**	**–**
CS-(6-O-Capro-β-CD)												
First-order F = 100·[1−Exp(−k1·t)]	0.830	17.597	0.406	–	0.846	21.276	1.368	–	−0.370	36.415	−0.715	–
Higuchi F = kH·t^0.5	0.981	11.809	2.603	–	0.685	24.130	0.654	–	−2.498	41.103	−1.652	–
Korsmeyer–Peppas F = kKP·t^n	0.980	10.967	2.064	0.507	**0.949**	**18.874**	**1.968**	**1.039**	0.886	25.998	1.369	0.176
Peppas–Sahlin F = k1·t^m + k2·t^(2·m)	0.983	12.359	1.716	0.450	**0.950**	**20.802**	**1.486**	**0.450**	0.983	18.406	2.887	0.422
Hopfenberg F = 100·[1−(1−kHB·t)^n]	0.814	19.964	−0.185	3.000	0.944	19.206	1.885	1.000	−2.105	42.508	−1.933	3.000

Table 1: Release kinetic modelling and results of NP formulations. (continued)

Poly-β-CD-C6												
First-order F = 100·[1−Exp(−k1·t)]	0.805	13.614	0.192	–	0.847	20.320	1.377	–	**0.992**	**16.096**	**4.389**	–
Higuchi F = kH·t^0.5	0.995	−1.199	3.895	–	0.627	23.886	0.485	–	0.404	37.459	0.117	–
Korsmeyer–Peppas F = kKP·t^n	**0.999**	**−18.653**	**8.259**	**0.429**	**0.978**	**14.572**	**2.814**	**1.362**	0.862	32.156	1.177	0.318
Peppas–Sahlin F = k1·t^m + k2·t^(2·m)	**0.999**	**−20.534**	**8.729**	**0.450**	0.975	17.011	2.204	0.450	0.935	30.393	1.530	0.450
Hopfenberg F = 100·[1−(1−kHB·t)^n]	0.795	15.806	−0.356		0.927	19.383	0.952	1.000	0.985	21.122	3.384	3.188
Weibull F = 100·{1−Exp[−((t−Ti)^β)/α]}	0.996	−7.005	5.346	–	0.967	18.149	1.920	–	**0.991**	**20.463**	**3.516**	–

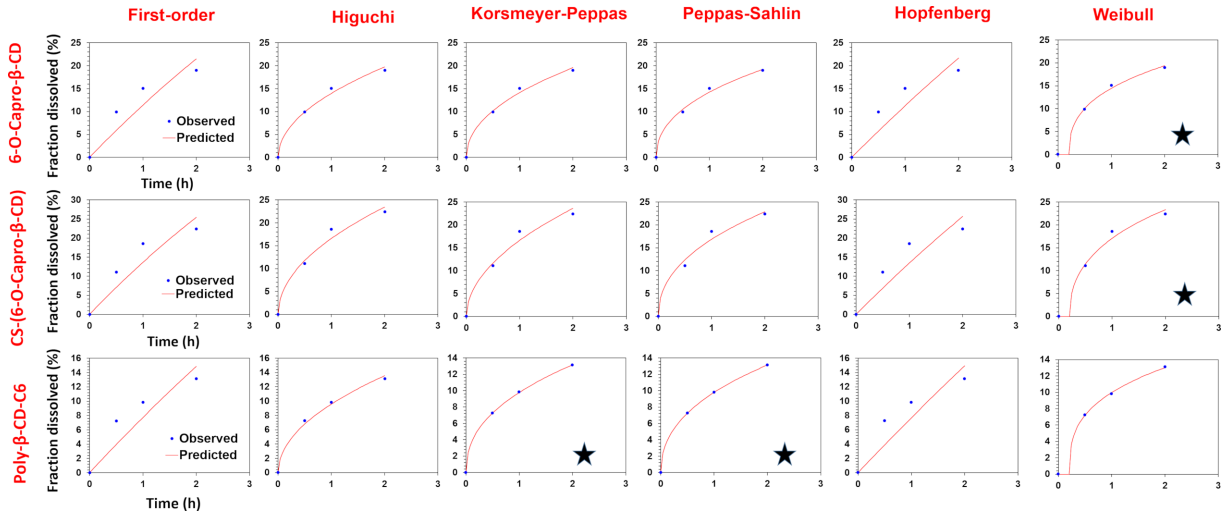


Figure 2: Results for release kinetics obtained automatically by the DDSolver software for SGF release medium (*represents best fit models).

Korsmeyer–Peppas and Peppas–Sahlin models for the poly-β-CD-C6 formulation. For the poly-β-CD-C6 NPs, two models were found to be compatible with high correlation. There are also studies in the literature indicating that the release kinetic model of nanoparticles can fit to more than one model [33,34]. Since it is the first study to evaluate the release kinetics of amphiphilic cyclodextrin nanoparticles, we have reported that a drug release profile that fits more than one model can be observed for amphiphilic cyclodextrin nanoparticles. In the Weibull model, the "β" (shape parameter of the release curve) value is a criterion used to illuminate the release from a polymeric matrix. "β" ≤ 0.75 indicates Fickian diffusion, while 0.75 < "β" < 1 indicates Fickian diffusion and controlled release combination [35]. The "β" value for the Weibull model was calculated as 0.396 and 0.434 for the 6-O-capro-β-CD and CS-(6-O-capro-β-CD) nanoparticle formulations, respectively. According to the Weibull model, CPT release kinetics from nanoparticles were found to be compatible with Fickian diffusion in SGF medium [36]. In the model-independent principal evaluation of in vitro release profiles, this was considered as the rapid/burst and initial release of the drug adsorbed on the nanoparticle surface or encapsulated in the nanoparticle material matrix. It has been confirmed by mathematical modeling that the release is based on diffusion. This indicates the release of the CPT, which is weakly bound in the nanoparticle matrix and adsorbed on the surface, for the 6-O-capro-β-CD and CS-(6-O-capro-β-CD) formulations. These results we obtained confirm each other with the data we interpreted in our previous studies [9]. The release kinetics, however, also appeared to be consistent with the Korsmeyer–Peppas and Peppas–Sahlin models for poly-β-CD-C6 NPs. While the Korsmeyer–Peppas model expresses diffusion-controlled release from matrix-type nano-

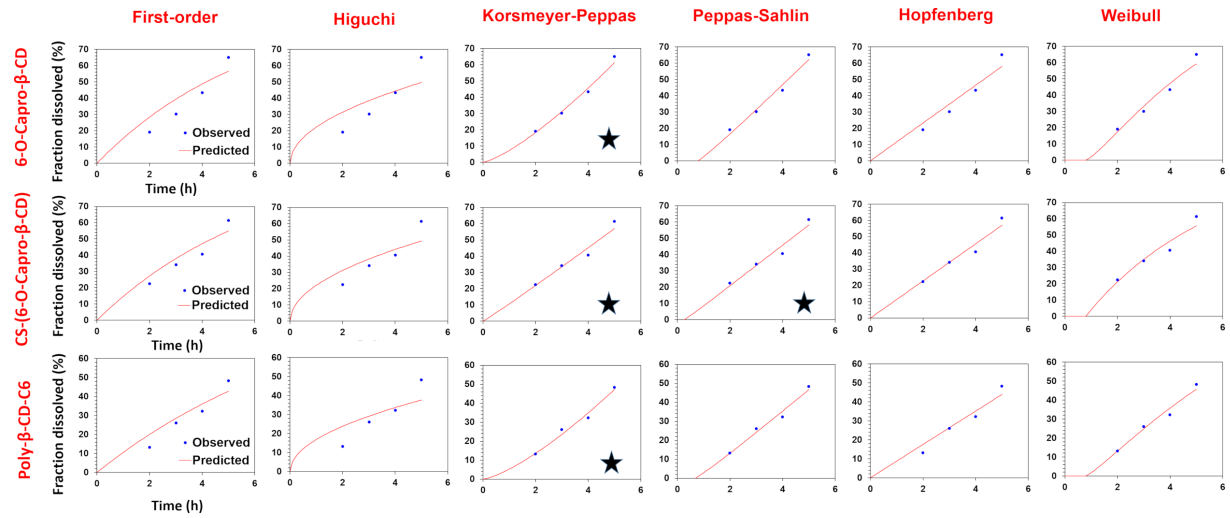


Figure 3: Results for release kinetics obtained automatically by the DDSolver software for SIF release medium (*represents best fit models).

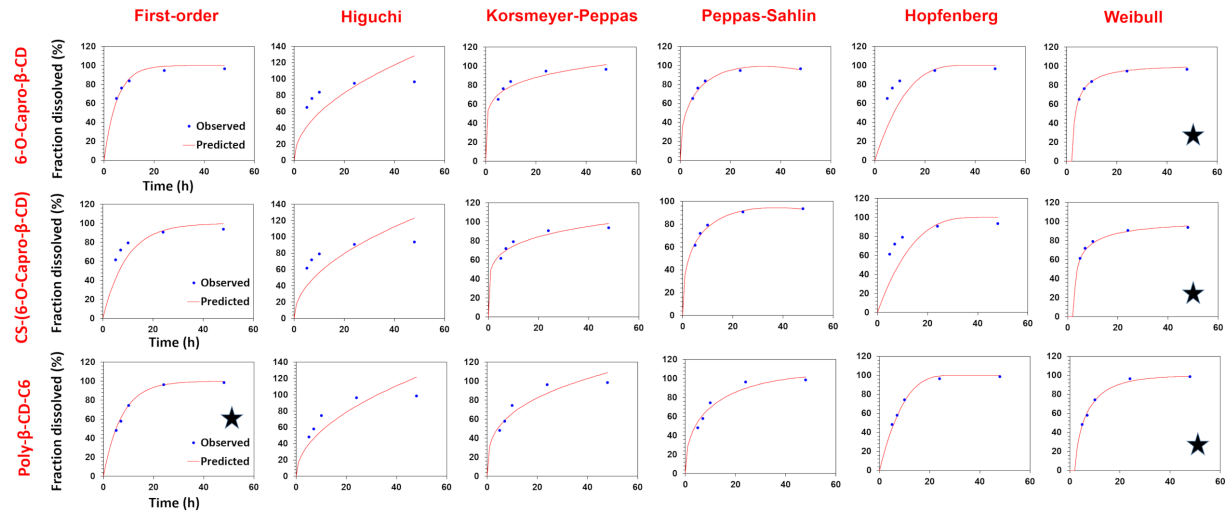


Figure 4: Results for release kinetics obtained automatically by the DDSolver software for SCoF release medium (*represents best fit models).

Table 2: Difference and similarity factors between formulations.

CPT-loaded amphiphilic CD nanoparticles		difference factor (*f*1)	similarity factor (*f*2)
6-O-capro-β-CD	CS-(6-O-capro-β-CD)	6.63	73.82
CS-(6-O-capro-β-CD)	poly-β-CD-C6	13.73	58.86
poly-β-CD-C6	6-O-capro-β-CD	11.72	61.57

systems, the Peppas–Sahlin model is based on the combination of diffusion and erosion of the nanoparticle matrix. In order to further elucidate the kinetics of these models, the diffusional exponent values (n or m) regarding the release kinetics from the nanoparticles were computed [37]. In the Korsmeyer–Peppas model, "n" represents the diffusional exponent illustrating the drug release mechanism, but in the Peppas–Sahlin model, "m" represents the same parameter [38]. In this context, "m" and "n"

diffusional exponent values were computed as 0.450 and 0.429, respectively. A diffusional exponent (m/n) ≤ 0.45 indicates that Fickian diffusion is a factor in drug release [39]. For $0.45 < m/n < 0.85$, the drug release occurs through a non-Fickian diffusion mechanism, for $m/n = 0.85$ the release occurs by case II transport and $m/n > 0.85$ indicates super case II transport [38-42]. It has been determined that there is Fickian diffusion in the release kinetics based on the diffusional exponent values of the Korsmeyer–Peppas and Peppas–Sahlin models [39]. When all the data were analyzed together, it was determined that a single kinetic model was not dominant in the SGF release kinetics, and compliance with different models was observed. However, although the models were different in all formulations, it was observed that the dominant mechanism was diffusion-based release. In our previous studies, it was evaluated that the drug release observed in SGF might be related to the diffusional release of the surface-adsorbed drug and the poorly bound surface drug to the matrix. In the mathematical modeling data, it has been confirmed that the first release seen in the SGF medium is dominantly diffusion-related.

According to the release kinetic parameters in SIF medium, as seen in Table 1, the highest R^2, MSC and lowest AIC values were observed in the Korsmeyer–Peppas model for 6-O-capro-β-CD and poly-β-CD-C6 NPs, and in Korsmeyer–Peppas and Peppas–Sahlin models for CS-(6-O-capro-β-CD) formulation. Two models were found to be compatible with high correlation for the CS-(6-O-capro-β-CD) formulation for SIF medium. Similarly, studies showing that nanoparticles can fit more than one model in the literature were also mentioned for SGF data [43]. The Korsmeyer–Peppas model difussional exponent values (n) for 6-O-capro-β-CD and poly-β-CD-C6 NPs were computed as 1.319 and 1.362, respectively. Considering the difussional exponent data over 0.85 indicates that the release mechanism is compatible with super case II transport. Case II transport refers to the release that occurs as a result of relaxation of the polymeric structure [40,42]. These results were interpreted as supporting our idea that the release of the drug adsorbed to the surface is completed by diffusion in the SGF medium, and that the erosion of the nanoparticle material and the relaxation of the polymer chain begins and accelerates the release in SIF. When a further evaluation was made for the CS-(6-O-capro-β-CD), which showed a high correlation between the two models, the diffusional exponent values of the Korsmeyer–Peppas and Peppas–Sahlin models were calculated as 1.039 and 0.450, respectively. Similarly, the n value of Korsmeyer–Peppas above 0.85 indicates that the release mechanism is realized by super case II [44]. This value was interpreted as indicative of the release seen with the erosion of the nanoparticle material and the initiation of polymer relaxation [45]. On the other hand, the "m" value calculated as 0.45 in the Peppas–Sahlin model indicates Fickian diffusion. This situation was evaluated as a very significant and meaningful data when compared with other formulations. Unlike the other two formulations, CS-(6-O-capro-β-CD) is coated on its surface with chitosan, a cationic coating material. The theoretical interpretations so far have been that the drug can be adsorbed in the coating material or weakly bound to the coating polymer structure, and it will be released first. The data obtained from the kinetic modeling provided results that support this interpretation. For the 6-O-capro-β-CD and poly-β-CD-C6 NPs (uncoated formulations), it was confirmed that the release occurred as a result of the relaxation of the nanoparticle material in SIF, while the Fickian diffusion continued for the CS-(6-O-capro-β-CD) formulation, that is, the release of the weakly bound drug adsorbed on the coating material. The diffusional exponent values in SIF for CS-(6-O-capro-β-CD) showed that the release continues as a combination of both the diffusion release of the drug adsorbed to the coating material, chitosan, and the case II release, which occurs as a result of the relaxation of the nanoparticle polymer structure [46].

According to the release kinetic parameters in the targeted main release medium, SCof, the highest R^2, MSC, and lowest AIC values were observed in the Weibull model for 6-O-capro-β-CD and CS-(6-O-capro-β-CD) formulations, and in the first order release and Weibull models for the poly-β-CD-C6 NPs, as seen in Table 1. In the Weibull model, the "β" (shape parameter of the release curve) exponent is a parameter used to elucidate the release from a nanoparticle matrix. "β" ≤ 0.75 indicates Fickian diffusion, while 0.75 < "β" < 1 indicates a complex mechanism (Fickian diffusion and controlled release). For values of "β" higher than 1, it was demonstrated that the drug transport follows a complex release mechanism [35,47,48]. The "β" value for the Weibull model was calculated as 0.493 and 0.401 for the 6-O-capro-β-CD and CS-(6-O-capro-β-CD) NPs, respectively. When evaluated within the framework of the literature, it was determined that the release mechanism of encapsulated CPT in SCof medium is by Fickian diffusion [36]. In addition, this situation has also been interpreted as further relaxation of the nanoparticle matrix structure in the SCoF medium, making diffusion easier and coming to the fore as a primary release mechanism [49]. On the other hand, the other formulation, the poly-β-CD-C6 NPs, was found in accordance with both Weibull and first order kinetics. According to the Weibull model, the "β" value was calculated as 0.762. Within the framework of the information explained above, it was evaluated as a complex (Fickian diffusion and controlled release) release mechanism according to the Weibull model for the poly-β-CD-C6 NPs. As stated in the literature, values of "β" in the range of 0.75–1.0 indicate a combined mechanism which is frequently encountered in release studies. When the power law can adequately represent

the whole collection of data in these situations, further confirmation can be gained. The special case of "β" = 1 is compatible with first order release, whereas the concentration gradient in the dissolution medium drives the rate of release [35]. In our calculations, results compatible with first order kinetics were found for the poly-β-CD-C6 and it was considered to fit both models. The partially high "β" value for the Weibull model also confirmed the tendency towards first order kinetics, which is also evaluated in the previous sentence in line with the literature. In this context, it has been evaluated that the first order kinetics associated with diffusion in the SCoF medium for the poly-β-CD-C6 formulation also occurs as a release mechanism. It was observed that the Weibull and first order models were compatible, supported and confirmed each other, providing an explanatory idea about CPT release from the formulation.

Cell culture studies

Determination of IC_{50} values of camptothecin

CT26 and HT29 cells were incubated with increasing concentrations of CPT and different CD nanoparticle formulations containing equal amounts of camptothecin for 48 or 72 hours. When the incubation period was over (48 or 72 h), cell viability was determined with the WST-1 assay. IC_{50} values are shown in Table 3.

It was observed that the IC_{50} values of the drug solution and nanoparticle formulations in each cell line were different and the IC_{50} values of CPT-loaded nanoparticles was lower than the CPT solution in both cell lines. For CT26 cells, the IC_{50} values of the drug solution was calculated as 1.86 ± 0.28 μM and 1.27 ± 0.42 μM for 48 h and 72 h, respectively. Among different formulations, the CS-(6-O-capro-β-CD) nanoparticle formulation had the highest efficiency for both time points against the CT26 cell line. After 48 hours of incubation, the IC_{50} values of anionic CPT-loaded 6-O-capro-β-CD and CPT-loaded poly-β-CD-C nanoparticles were calculated as 1.23 ± 0.02 μM and 1.35 ± 0.46 μM, respectively, and the difference between the two groups was not statistically significant ($p > 0.05$). However, after 72 hours of incubation, the IC_{50} value of the anionic nanoparticles was found to be two folds of the cationic nanoparticles. Considering these findings, it is thought that the difference between the IC_{50} values of three different nanoparticle formulations containing equal amounts of drug may be related to the surface charges of the nanoparticles. For CT26 cells, when 6-O-capro-β-CD and CS-(6-O-capro-β-CD) nanoparticle formulations are compared, it can be interpreted that the switch of NP charge upon chitosan coating enhances this membrane binding ability. However, there was no significant difference in IC_{50} values against HT29 cells between 6-O-capro-β-CD and CS-(6-O-capro-β-CD) groups. Due to the increased biological membrane interaction, the amount of drug transported into the cell may also have increased. The 6-O-capro-β-CD and poly-β-CD-C6 derivatives used in the study are cyclodextrin derivatives with the same core structure. Heptakis(6-*O*-hexanoyl)-β-CD (6-O-capro-β-CD) is a primary face-modified amphiphilic CD derivative with a 6C fatty acid chain attached via an ester bond to the primary hydroxy groups of the macrocyclic ring. On the contrary, poly-β-CD-C6 is furnished with a set of primary aminoethyl segments on the primary rim of the β-CD core and a cluster of 14 hexanoyl chains on the secondary face. The effect of the change in surface modifications on cell viability has been demonstrated by cell culture studies performed within the scope of this paper. The anionic 6-O-capro-β-CD nanoparticle formulation has a lower IC_{50} value after 48 hours than the polycationic poly-β-CD-C6 nanoparticle formulation. However, it was observed that the IC_{50} value of the poly-β-CD-C6 nanoparticle formulation decreased upon incubation. Based on previous studies with breast cancer cell lines, it is comprehensible that anionic nanoparticles induce cell proliferation inhibition earlier than polycationic nanoparticles. The impact of anionic nanoparticles on free cholesterol level was shown to decrease after 24 hours in a cholesterol extraction assay from MCF-7 cells. Poly-β-CD-C6 nanoparticles, on the other hand, removed three times more cholesterol from cells in 48 hours than anionic CD nanoparticles. In addition to surface charges, the molecular weight, and number of aliphatic groups on the surfaces of CD derivatives play a direct role in the interaction time with the cell and cell membrane components [50]. It is well established that positively charged nanoparticles interact with the cell membrane more favorably than negatively charged ones. However,

Table 3: IC_{50} (μM) values of CPT solution and CPT-loaded CD nanoparticle formulations for CT26 murine and HT29 human colon cancer cell lines at 48 h and 72 h (n = 6, mean ± SD).

	CT26		HT29	
Formulation	48 h	72 h	48 h	72 h
CPT/6-O-capro-β-CD	1.23 ± 0.02	1.19 ± 0.06	0.76 ± 0.09	0.58 ± 0.14
CPT/CS-(6-O-capro-β-CD)	0.72 ± 0.26	0.59 ± 0.12	0.89 ± 0.07	0.59 ± 0.16
CPT/poly-β-CD-C6	1.35 ± 0.46	0.61 ± 0.14	0.30 ± 0.03	0.25 ± 0.04
CPT solution in DMSO	1.86 ± 0.28	1.27 ± 0.42	1.47 ± 0.06	1.31 ± 0.06

their passing through the cell membrane is challenging because of the agglomeration of positive charge on the cell membrane [51]. This knowledge might explain why the 6-O-capro-β-CD nanoparticle IC_{50} values are lower at 48 hours than those of the poly-β-CD-C6 nanoparticles. Besides, chitosan coating on nanoparticles reduced the IC_{50} value. It is believed that chitosan's antiproliferative properties also are involved in this situation.

When cell viability in HT29 cells was evaluated, it was observed that the polycationic derivative had the lowest IC_{50} value. It can be said that the chitosan coating did not cause a positive change in 6-O-capro-β-CD nanoparticles. It is known that the same nanoparticles may have different effects on cancer cells of different species. In addition to the surface charges, particle size and distribution also play a very important role in the cellular interactions of nanoparticles. For this reason, while evaluating the effects of nanoparticles, the selection of particles with the most ideal parameters for the target disease or organ is very important in terms of the effectiveness of the treatment. Due to the differences between colorectal cancer cells of different species, it is possible that the same formulations have different effects on these cells, and this result supports the publications in the literature [52-54].

Determination of doubling time

After 48 hours, 42.410 cells/mL for CT26 and 37.112 cells/mL for HT29 were counted. According to Equation 4, doubling times were calculated as 23.03 h and 25.37 h, respectively.

The factors affecting cells in 2D and 3D cell culture media are quite different from each other. In addition to physiological differences, cell culture protocols are also different. In conventional 2D cell culture studies, cells proliferate and then are detached with trypsin and inoculated on appropriate plates followed by overnight incubation for attachment. In the 3D cell culture method, cells are plated after detachment and allowed to form a spheroid for more than 24 hours (i.e., 3 days for this study). Due to the differences in the initial incubation time between the two methods, the number of cells treated with nanoparticles at the beginning of the experiment is quite different. Therefore, to equalize the number of cells between the two methods, the doubling times of the cells were calculated as detailed in the methods section.

Evaluation of anticancer efficiency of CPT-loaded nanoparticles on 2D cell cultures

According to the results of the conventional 2D cell culture study, the CPT-loaded poly-β-CD-C6 nanoparticle treatment group in CT26 cells had the highest antiproliferative effect after 48 h (Figure 5a). When compared to CPT solution-treated cells, cell viability was considerably reduced in the CPT-loaded poly-β-CD-C6 nanoparticle formulation and the CPT solution + blank poly-β-CD-C6 nanoparticle formulation groups at the conclusion of the 48-hour incubation period. For 6-O-capro-β-CD and CS-(6-O-capro-β-CD) nanoparticles, the co-administration of blank nanoparticles and drug solution was shown to be more efficient in terms of cell survival than the drug solution alone at the end of the 72-hour incubation. The efficiency of drug-loaded nanoparticles is higher than that of co-administered formulations in all three nanoparticle dispersions (Figure 5a). Considering that the amount of drug and carrier is equal, it is thought that loading the drug into the nanoparticles may have increased cellular uptake and the amount of accumulated drug.

When data from a 48-hour anticancer efficiency on HT29 cells was evaluated, it was observed that the drug-loaded nanoparticle formulations had better anticancer activity than the drug solution (Figure 5b). Moreover, the group treated with blank CS-(6-O-capro-β-CD) nanoparticles + CPT solution showed a substantial reduction in cell viability. Cell viability in HT29 cells cultured with CPT solution alone was calculated to be 40% after 72 hours of incubation (Figure 5b). Cell viability of drug-loaded nanoparticles was determined as 20.6%, 26.5%, and 31.2% for 6-O-capro-β-CD, CS-(6-O-capro-β-CD), and poly-β-CD-C6 nanoparticles, respectively. In addition to the chitosan-coated nanoparticles, it was determined that the blank poly-β-CD-C6 nanoparticles plus CPT solution treated group had higher anticancer activity than the only drug solution treated group at the end of 72 hours. Furthermore, the anticancer activity of blank poly-β-CD-C6 nanoparticles was shown to be greater than that of the drug solution. It was established that both drug-loaded nanoparticles and drug + nanoparticles demonstrated better effectiveness than the drug solution in 72-hour incubation results in CT26 cells. The CPT-loaded CS-coated nanoparticle and poly-β-CD-C6 nanoparticle formulations, on the other hand, had the lowest cell viability.

According to the results of the study performed with colon cancer cell lines of two different origin (murine and human), it was observed that the blank nanoparticles caused a decrease in cell viability (to <70%). Similar results were obtained in cell culture studies performed on different cancer cells by our group, and detailed studies were carried out to elucidate the mechanism. Both the results of our studies and the literature emphasize that cyclodextrins show high affinity for lipid-based molecules such as cholesterol and phospholipids in biological membranes [50,55,56]. Furthermore, it was reported that depletion of cholesterol by methyl-β-cyclodextrin could inhibit EGFR signals, induce apoptosis, and suppress tumor growth in colon tumor-induced mice [57]. Shimolina et al. evaluated membrane

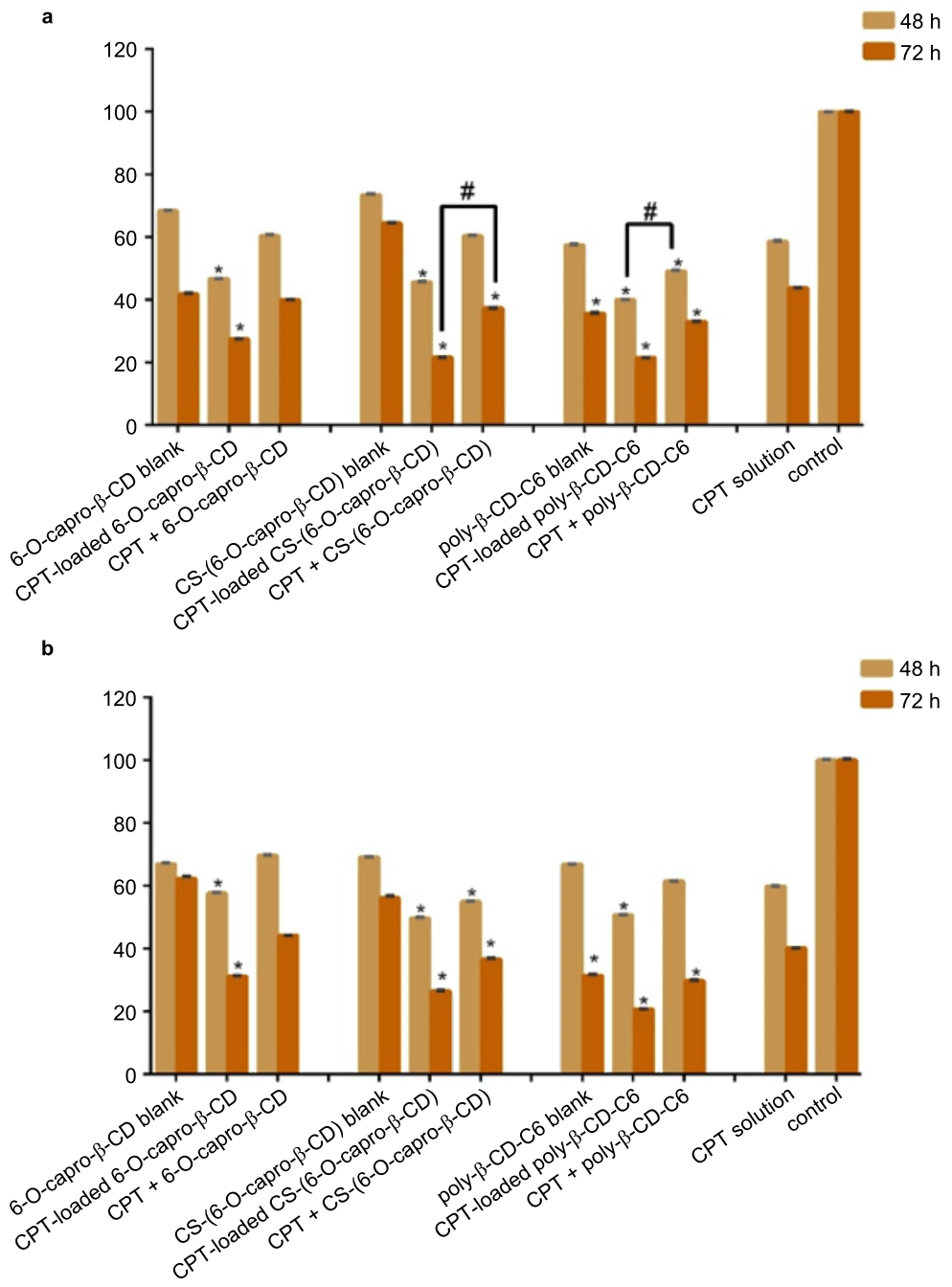


Figure 5: Anticancer effect of blank or CPT-loaded CD nanoparticles and camptothecin solution against 2D CT26 murine (a) and HT29 human (b) colon cancer cell lines at 48 h and 72 h. Cell viability was evaluated by WST-1 assay. (n = 6, mean ± SD), ($^{\#}p < 0.05$ and $^{*}p < 0.05$ compared with CPT solution in DMSO).

fluidity in CT26 and HeLa Kyoto cells treated with cisplatin in a monolayer conventional cell culture. It was emphasized that the increased plasma membrane fluidity due to the decrease of lipid rafts and, moreover, cholesterol in the biological membrane plays a role in inducing apoptosis [58]. When the literature information and the findings are evaluated, it can be said that the use of CD nanoparticles in the treatment of colon cancer can make it possible to reduce the amount of anticancer drugs required for treatment by taking advantage of the synergistic effect. The morphological change in CT26 and HT29 cells treated with different nanoparticle formulations was also examined microscopically. As seen in Figure 6, cells were double-stained with calcein AM and ethidium homodimer-1 (EthD-1). The control group consisted of cells incubated only

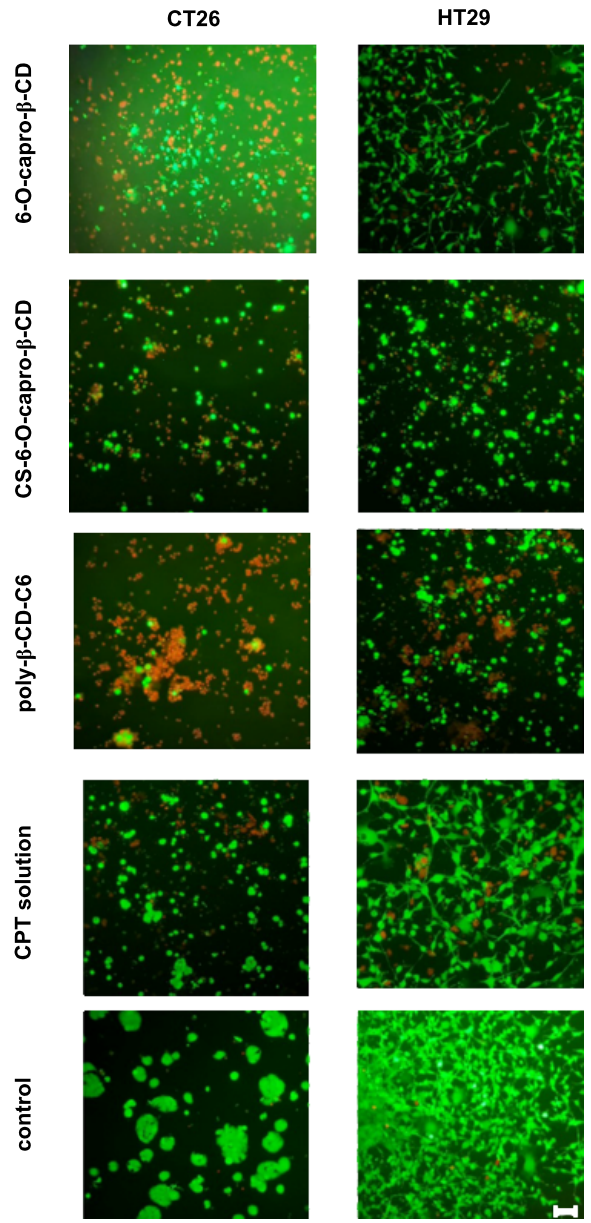


Figure 6: Live/dead analysis of CT26 and HT29 cells using double staining with calcein AM and ethidium homodimer-1 (EthD-1) after treatment with different formulations at 48 h. Control group is treated with only complete Dulbecco's modified Eagle medium (DMEM). Live cells stained with calcein AM fluoresce green while dead cells stained with EthD-1 fluoresce red. Scale bar: 100 µm.

with the medium. Living cells were stained green with the membrane dye calcein AM, while dead cells were stained red with the nuclear dye EthD-1. Both the decrease in cell number and the change in cell morphology draw attention in the microscopic images. In particular, in the CT26 cell line incubated with poly-β-CD-C6 nanoparticles the presence of red-labeled dead cells was observed. Especially in HT29 cells, it is noteworthy that the cellular interaction in the control group was not observed in the groups treated with nanoparticles. Similarly, it was determined that incubation with nanoparticles caused a change in the colonization of CT26 cells. Based on the results of both mitochondrial functional activity and microscopic imaging analyses following staining, CT26 cells are more sensitive to formulations than HT29 cells. The underlying processes must be elucidated in order to explain this variation. In fact, this is an expected result considering the origins of the cells. The primary factor causing the effects of nanoparticle formulations on two different colon tumors to differ from each other is the origin of the cells. The genome-transcriptome mapping investigation revealed that despite having two separate origins, the CT26 cell has characteristics similar to human primary colorectal cancers in terms of drug resistance mechanisms, gene expression and mutation patterns, and pathways in onco-related genes [59,60]. Nevertheless, because of their different origins, these cell lines exhibit various genetic and epigenetic changes as well as mutations due to their diverse origins. Efficacy/cytotoxicity studies on both cell lines indicate that cells respond differently to the treated groups [61-63].

Evaluation of antitumoral efficiency of CPT-loaded CD nanoparticles on 3D cell cultures

Anticancer activity of nanoparticles prepared from different CD derivatives was also investigated in a 3D cell culture method. Matrigel® was used as the extracellular matrix in 3D cultures of colorectal cancer cell lines prepared using polymer-based scaffolds.

Murine or human colon cancer cells were seeded on poly-HEMA-coated cell plates prepared as described in the methods section, and the plates were centrifuged. The cells were found to be collected in the middle of the wells after centrifugation. Within 3 days, cells that interacted maximally with each other formed highly spherical tumors measuring about 200 µm in diameter (Figure 7).

According to the results of the anticancer activity analysis performed in the 3D cell culture studies, at the end of the 48-hour incubation period, the effect of drug-loaded CD nanoparticles on cell death was found to be greater than that of the CPT solution on the CT26 cell line (Figure 8a). However, when the 3D spherical tumor results were compared with the 2D conventional cell culture results, significant differences were observed in the efficacy of all drug-loaded CD nanoparticle formulations and each formulation caused more cell death in the 2D cell culture. It was determined that 6-O-capro-β-CD and poly-β-CD-C6 derivatives showed higher anticancer efficacy than drug solution in both drug-loaded nanoparticle formulations and drug + blank nanoparticle formulations that were co-administered. Cell viability was the same for both drug solution and in the group

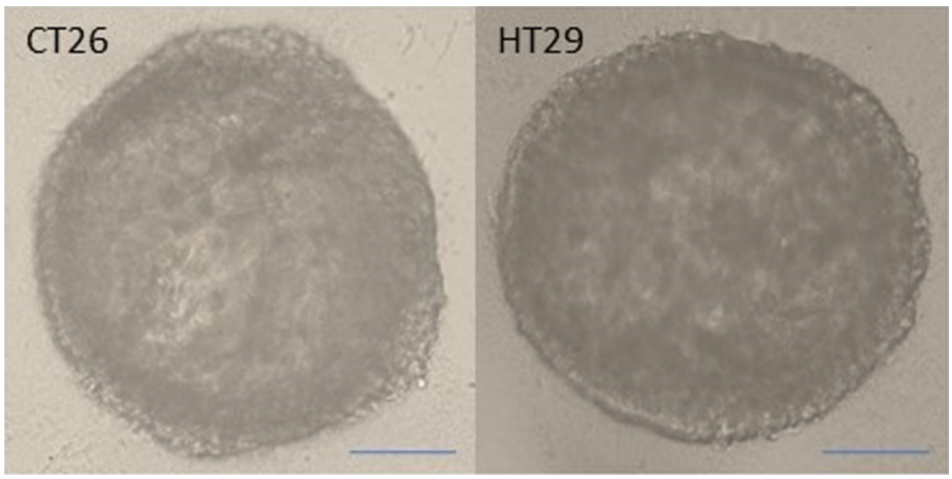


Figure 7: Murine (CT26) and human (HT29) colon cancer spheroid was formed by scaffold-based method, and the morphological structure was observed under a light microscope. Scale bar: 50 µm.

treated with the drug + blank CS-(6-O-capro-β-CD) nanoparticle formulation treated groups at 72 h. In addition, the lowest cell viability was observed in the CPT-loaded poly-β-CD-C6 nanoparticle formulation (Figure 8a). Moreover, cell viability was calculated as 43.5% after 72 hours in the group incubated with blank poly-β-CD-C6 nanoparticle formulations.

Similar results were obtained in the antitumoral efficacy analysis against 3D HT29 spheroids. The most effective formulation were CPT-loaded poly-β-CD-C6 nanoparticles (Figure 8b).

At the end of 72 hours of incubation, there was a significant decrease in cell viability for CS-(6-O-capro-β-CD) and poly-β-CD-C6 derivatives in the drug solution + blank nanoparticle formulation groups compared to the drug solution in 3D HT29 spheroids. Again, it was observed that blank nanoparticles caused a significant decrease in cell viability in 3D cell studies compared to the control group [55,64]. The reduction in cell viability for the blank poly-β-CD-C6 derivative was even higher than for the group that was treated with the drug solution.

As in 2D cell culture results, it was observed that CT26 cells were more sensitive than HT29 cells in cell culture studies with 3D spheroids. It is known that cells in 3D multicellular tumor spheroids typically have lower sensitivity to cytotoxic drugs compared to 2D cultured cells. It is suggested that this difference is due to various reasons, such as decreased drug penetration, development of hypoxic nuclei, and decreased growth [65]. The findings are explained by the differences between conventional cell culture and 3D tumor spheroids. The predicted toxicity/efficacy is enhanced as a result of the formulation's exposure to cells arranged in a monolayer. However, in a 3D cell culture, the disparity in cell proliferation values in mouse and human cell lines is smaller (Figure 8). In terms of formulations, only the 6-O-capro-β-CD nanoparticles have more significant effect on CT26 cells, whilst no other nanoparticle groups show this variation between cell lines.

In 2D conventional cell culture, the cells form a monolayer on the plate and all cells interact equally and directly with the added drug or nanoparticle formulation. Furthermore, it is well recognized that increased intercellular communication by increasing cell–cell contact in 3D cell culture influences drug sensitivity in spherical tumors [66]. In a study, HT29 human colorectal adenocarcinoma cells were treated with an E-cadherin inhibiting antibody before being tested for sensitivity to several anticancer drugs. It was discovered that inhibiting E-cadherins, which are adhesion molecules that provide intracellular connection, increases the sensitivity of 3D colon cancer tumors to 5-fluorouracil, paclitaxel, vinblastine, and etoposide [67]. In the literature, uptake mechanisms of nanoparticles and free drugs in 2D and 3D cell culture methods have been investigated comparatively. The findings showed that nanoparticles and free drugs less effectively reach the underlying cells in 3D spherical tumors due to multilayered cells, and the concentration of 3D tumor-penetrating drugs is lower than in conventional cell culture.

In this paper, cell culture studies were used to evaluate the efficacy of co-administration of drug solution and empty nanoparticles as well as drug-loaded nanoparticles. According to the results of 2D cell culture, the co-administration of CS-(6-O-capro-β-CD) and poly-β-CD-C6 nanoparticles resulted in a significant decrease in cell viability in both cell lines as compared to the drug solution. While there was a significant decrease in CT26 cells in the groups treated with 6-O-capro-β-CD and

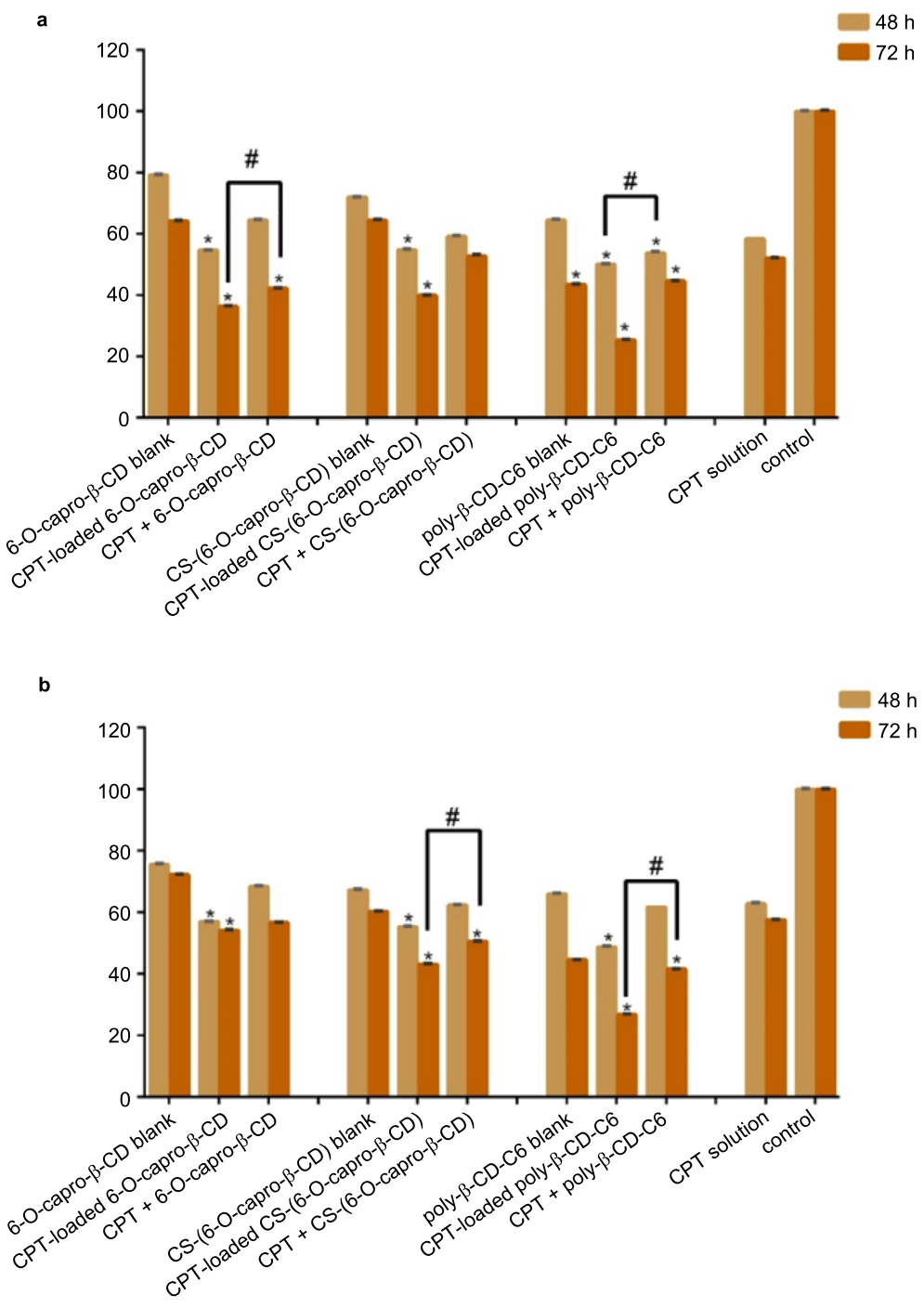


Figure 8: Anticancer effect of blank or drug-loaded cyclodextrin nanoparticles and CPT solution against 3D CT26 murine (a) and HT29 human (b) colon cancer cell line at 48 h and 72 h. Cell viability was evaluated by WST-1 assay. (n = 6, mean ± SD), (# $p < 0.05$ and * $p < 0.05$ compared with CPT solution).

poly-β-CD-C6 in 3D cell culture, the results for HT29 cells were similar to the conventional 2D cell culture study. As previously noted, CDs have a known affinity for cell membrane structures and components, and they are used for this purpose in the literature. The cholesterol affinity of CD derivatives has been used in the literature for a variety of applications in cancer treatment. Cholesterol concentration has been related to cell membrane fluidity and rigidity, treatment resistance in cancer cells, and drug uptake through the cell membrane. Excipients such as methyl-β-CD are widely used to extract cholesterol

from cancer cells such as melanoma and MCF7 cells in order to promote cellular uptake of anticancer medicines [68-70]. It was reported that cholesterol content is related to metastasis and tumor growth in oral squamous cell carcinoma, and cholesterol depletion using methyl-β-cyclodextrin caused an increase in the expression of stem cell markers in cancer cell lines [71]. According to a recent study, cellular cholesterol is directly involved in T cell-mediated cytotoxicity. Cancer cells with cholesterol-rich plasma membranes can evade the immune system by blocking toxicity caused by T cells, but as the amount of cholesterol in the tumor decreases, T cell-mediated cytotoxicity rises [72]. In both traditional and 3D cell culture investigations, incubating cells with empty CD nanoparticles and drug solutions has a synergistic impact due to the antiproliferative activity of the CD nanoparticles themselves. Co-administration of pharmaceuticals with empty nanoparticles, as well as encapsulation into nanoparticles, is an approach worth investigating.

Conclusion

Oral cancer therapy is still a milestone, attracting researchers' efforts, especially in cancers with high mortality such as CRC. Any progress in this area would be very promising. In this context, oral chemotherapy formulations in the treatment of CRC should be examined comprehensively and in detail, and each past study should shed light on possible future studies. In this study, 3D spheroid tumor models were studied to further elucidate the information we obtained in previous studies, and also mathematical release kinetic modeling was performed for the first time for CPT-loaded amphiphilic cyclodextrin nanoparticles prepared by our team. As a result, when all our publications are evaluated together, it is seen that we have completed comprehensive studies focused on oral CRC treatment with amphiphilic CD nanoparticles. With the increasing progress of studies in this field, it is considered that oral chemotherapy with innovative drug delivery systems in chemotherapy is possible. In this context, especially oral polycationic CD nanoparticles are considered as a promising drug delivery system.

Experimental

Materials

6-O-capro-β-CD (MW = 1813 g/mol) and poly-β-CD-C6 (MW = 3178 g/mol) seen in Figure 9 were synthetized, purified, and characterized in the Institute for Chemical Research (CSIC-University of Sevilla, Spain) as previously reported [9,25,50].

(*S*)-(+)-Camptothecin (95% HPLC powder, MW: 348.35 g/mol) was purchased from Sigma-Aldrich, USA. Chitosan (Protasan UP G-113; MW < 200 kDa) was purchased from Novamatrix, Norway. Dialysis cellulose tubing membrane for in vitro release studies (average flat width 25 mm, MWCO: 14,000 Da) was obtained from Sigma-Aldrich, USA. Cell culture studies were performed on CT26 mouse (ATCC® CRL-2638™) and HT29

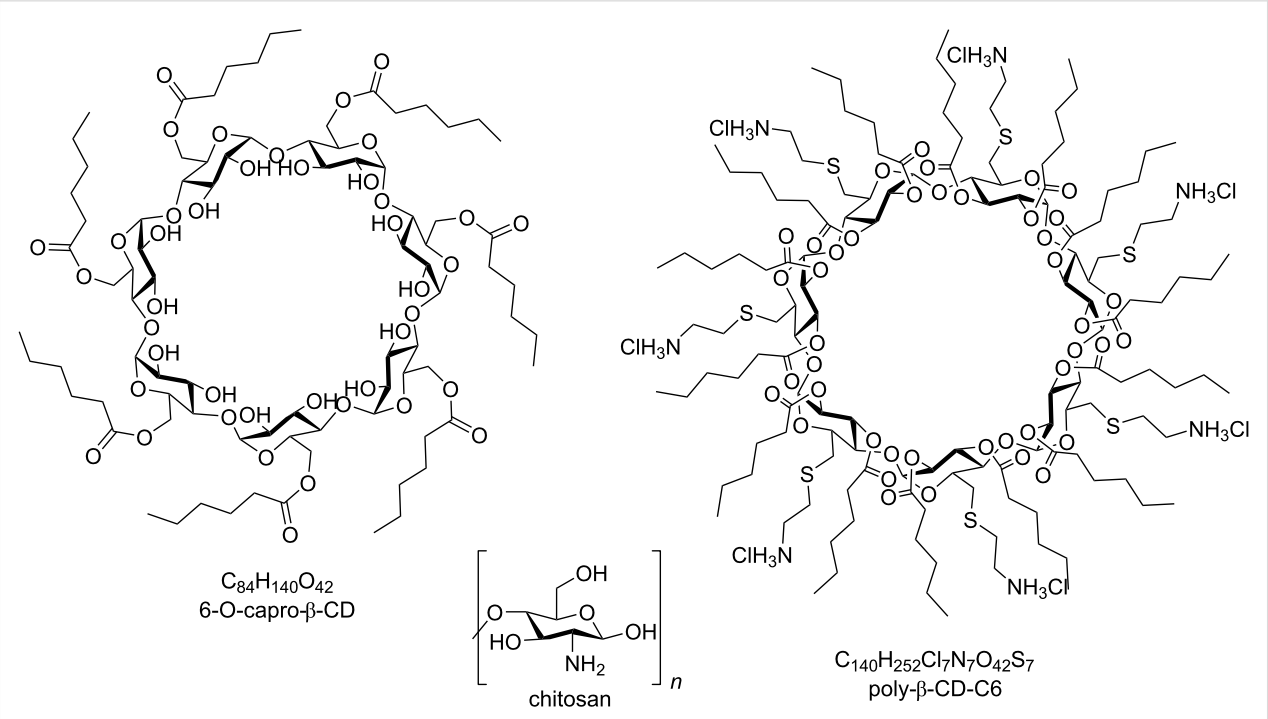


Figure 9: Chemical structures of 6-O-capro-β-CD, poly-β-CD-C6, and chitosan.

human colon carcinoma cell line (ATCC® HTB-38™) both purchased from American Type Culture Collection (ATCC, USA). Dulbecco's modified Eagle medium (DMEM, D5796, Sigma-Aldrich, USA), supplemented with 10% (v/v) fetal bovine serum (FBS, F7524, Sigma-Aldrich, USA) and 1% penicillin/streptomycin (P4333, Sigma-Aldrich, USA) was used for 2D and 3D cell culture studies. Ultrapure water was obtained from a Millipore Simplicity 185 Ultrapure Water System (Millipore, France). All other chemicals were purchased from Sigma-Aldrich and were of analytical purity. Release kinetic analyses were performed using an add-in program, DDSolver 1.0 [73].

Fabrication and in vitro characterization of CPT-loaded amphiphilic CD NPs

The nanoprecipitation process was used to prepare blank and CPT-loaded nanoparticles, as described previously for amphiphilic CD nanoparticles [9,74]. In earlier investigations, the ideal formulation parameters and component ratios were identified [9,11,74]. Thus, organic solvent (acetone), polycationic CD derivate (0.1% w/v), organic phase:aqueous phase ratio 1:2 (v/v), and 600 rpm stirring rate were applied [9]. In brief, a determined quantity of amphiphilic CD was dissolved in 1 mL of acetone to achieve an organic phase concentration of 0.1% (w/v). This organic phase was added drop-by-drop into 2 mL of the aqueous phase with magnetic stirring at room temperature for 30 min. The organic solvent was evaporated under vacuum at 45 °C to a final dispersion volume of 2 mL. The same technique was used to prepare chitosan (CS)-coated 6-O-capro-β-CD nanoparticles in the presence of CS (0.025% (w/v)) in the aqueous phase. CPT (10% of CD weight) was dissolved in the organic phase to develop drug-loaded nanoparticles. All the details regarding the preparation and characterization of the formulations have been covered extensively in our previous publication [9].

Drug release from amphiphilic CD nanoparticles

In vitro release experiments were designed to evaluate the release profiles of colon-targeted nanoparticles in the environments encountered along the GIT and the actual transit time. For this purpose, continuous release studies were performed first in pH 1.2 simulated gastric fluid (SGF) within the range of 0–2 hours, then in pH 4.5 simulated intestinal fluid (SIF) during 2–5 hours, and in pH 7.4 simulated colon fluid (SCoF) for the rest of the release period as 5–48 hours, respectively. In this context, the dialysis bag was transferred to the previously prepared release media, respectively [9].

The dialysis membrane method at 37 °C in a shaking water bath (100 rpm) was used. The closed dialysis membrane bag (average flat width 25 mm, MWCO: 14,000 Da) containing the nanoparticle dispersion (3 mL) was then put in release medium (20 mL) that ensured external sink conditions. At predefined time intervals (0.5, 1, 2, 3, 5, 7, 10, and 24 h), 500 µL of sample were taken from the dialysis membrane and replaced with an equal volume of fresh release medium at the same temperature. HPLC was used to quantify the cumulative percentage of CPT released for each time point [9].

Release kinetics study

In vitro release profiles of CD nanoparticles were analyzed using DDSolver 1.0 [73], designed to reduce computation time and minimize computational errors, and the data were fitted to different kinetic models and analyzed for the appropriate release mechanism (zero order, first order, Higuchi, Korsmeyer–Peppas, Hixson–Crowell, Peppas–Sahlin, Hopfenberg, and Weibull model) [73]. Following the elucidation of the in vitro release profiles of nanoparticles, inputs were computed with the DDSolver software to define the three most important criteria; coefficient of determination (R^2), Akaike information criterion (AIC), and model selection criterion (MSC). The highest R^2 and MSC values and the lowest AIC values were used for evaluating different kinetic models [73,75]. Furthermore, release differences or similarities of CPT-loaded amphiphilic cylodextrin nanoparticles were computed according to "difference ($f1$)" and "similarity ($f2$)" factors [73,76] for evaluating through model-independent method. In order to evaluate the release patterns of nanoparticles, the difference factor ($f1$) and similarity factor ($f2$) were computed using a method outlined in the Guidance for Industry from the FDA's Center for Drug Evaluation and Research (CDER) [77]. These two factors can be calculated mathematically by the following equations [78]. R and T are the percentage dissolved of the reference and test profile, respectively, t is the time point, n is the number of sampling points. It is noted that $f1$ values for 0–15 and $f2$ values 50–100 indicate that the these release profiles are similar [79].

$$f1 = \left\{\left(\sum_{t=1}^{n}\left|R-T\right|\right)\Big/\left(\sum_{t=1}^{n}R\right)\right\}\times 100 \quad (1)$$

$$f2 = 50\cdot\log\left[\frac{100}{\sqrt{1+\frac{\sum_{t=1}^{n}\left(Rt-Tt\right)^2}{n}}}\right] \quad (2)$$

Cell culture studies

Determination of IC_{50} values of camptothecin

IC_{50} values of camptothecin (CPT)-loaded cyclodextrin (CD) nanoparticles and CPT solution in DMSO were determined

against CT26 mouse and HT29 human colon carcinoma cell lines at 48 h and 72 h. For this purpose, CT26 and HT29 cells were grown in cell flasks separately. Then, cells were seeded in a 96-well cell culture plate with an initial seeding density of 1×10^4 cells per well in DMEM (100 µL) and allowed to attach overnight. The formulations were diluted with serum-free DMEM to obtain the appropriate CPT concentration according to their loading efficiency, and the medium on the cells was replaced with medium containing the formulation and incubated for 48 and 72 hours. Our previous research demonstrated that HT29 cells treated with 1.44 µM CPT after 48 hours of incubation had almost 50% viability [9]. Therefore, the lower and upper concentrations of CPT (0.4, 0.8, 1.6, 3.2, 6.4, and 12.8 µM) were examined in this study. Equal DMSO concentrations were applied to the cells as a separate group, and cell viability was normalized relative to the DMSO group. After 48 h and 72 h of incubation time, cell viability was determined by the WST-1 assay with a microplate reader at a wavelength of 450 nm. Cells that were incubated with the medium were used as control group with 100% cell viability. The following equation was used to calculate cell viability percentage

$$\text{Cell viability (\%)} = \frac{\text{optical density (OD) of treated cells}}{\text{optical density (OD) of untreaded cells}} \times 100 \quad (3)$$

IC_{50} values were calculated with the GraphPad Prism version 6 (San Diego, CA, USA) using the data of cell viability against increasing drug concentration.

Determination of doubling time

The initial cell number concentration was calculated to use the same number of cells in 2D and 3D cell culture studies. For this purpose, first the doubling times of the cells were determined. Separately, CT26 and HT29 cells were seeded into 96-well plates (10,000 cells/well). After 48 hours of incubation, the medium was removed from the plates, cells were trypsinized and counted. Based on the formula below, the doubling time was calculated.

$$\text{Doubling time} = \frac{\text{duration} * \log(2)}{\log(\text{final concentration}) - \log(\text{initial concentration})} \quad (4)$$

Evaluation of anticancer efficiency of CPT-loaded CD nanoparticles on 2D cell cultures

The anticancer activities of CPT-loaded amphiphilic CD nanoparticles were determined against CT26 and HT29 cell lines. Cells were seeded at a density of 1×10^4 cells/well in full DMEM (100 µL) into each well of 96-well plates. The cells were then cultured at 37 °C for 24 h in a 5% CO_2 incubator. The medium was replaced after 24 h with new serum-free medium containing drug solution, blank nanoparticle formulations, drug-loaded nanoparticles (CPT-loaded 6-O-capro-β-CD, CPT-loaded CS-(6-O-capro-β-CD), and CPT-loaded poly-β-CD-C6), or free drug solution + blank nanoparticle formulations (CPT + 6-O-capro-β-CD, CPT + CS-(6-O-capro-β-CD), and CPT + poly-β-CD-C6). After 48 h and 72 h of incubation, WST-1 (10 µL) was added to the cells. After a 3-hour incubation period, the absorbance at 450 nm was measured using a microplate reader, and cell viability was estimated. A viability/cytotoxicity assay kit was also used to test cell viability microscopically (30002, Biotium, Fremont, CA, USA). CT26 and HT29 cells were incubated with nanoparticle formulations or free drug solution for 48 h. Then, the medium was removed, and 200 µL of dye mixture were added to each well and incubated for 45 minutes further. Fluorescence microscopy was used to see groups of cells after the incubation.

Evaluation of antitumoral efficiency of CPT-loaded CD nanoparticles on 3D cell cultures

The scaffold-based approach for in vitro 3D cell culture studies, which was previously reported by Varan et al. [80], was adopted for this paper. Poly(2-hydroxyethyl methacrylate) (poly-HEMA, P3932, Sigma, St. Louis, MO, USA) was used to achieve a low attachment surface in round-bottomed wells. Under sterile conditions, 1.2 g of poly-HEMA was dissolved in 40 mL of 95% ethanol, and 50 µL of this solution were distributed into each well. For at least 24 hours, plates were maintained under laminar flow to evaporate the organic solvent. Following this evaporation, CT26 or HT29 cells (1,250 cells/200 µL medium per well) were added into each well in DMEM containing 3% Matrigel® Basement Membrane Matrix, and the plate was agitated at 1,000 rpm for 10 minutes. 100 µL of fresh medium was replaced every 2 days. Microscopical analysis of the spheroid development was performed. After 3 days, DMEM was exchanged with nanoparticle formulations, and cell viability was measured at 48 h and 72 h using the WST-1 assay.

Funding

This research has been supported by Erciyes University Scientific Research Projects Coordination Unit (Project Number: ERU BAP TOA-2019-8956).

Declaration of Interest

No potential conflict of interest was reported by the authors. The authors declare that they have no known competing financial interests or personal relationships that could have appeared to influence the work reported in this paper.

ORCID® iDs

Sedat Ünal - https://orcid.org/0000-0002-1518-010X
Gamze Varan - https://orcid.org/0000-0002-1291-9503
Juan M. Benito - https://orcid.org/0000-0002-9788-1507
Yeşim Aktaş - https://orcid.org/0000-0002-3427-6078
Erem Bilensoy - https://orcid.org/0000-0003-3911-6388

References

1. Darroudi, M.; Gholami, M.; Rezayi, M.; Khazaei, M. *J. Nanobiotechnol.* **2021,** *19,* 399. doi:10.1186/s12951-021-01150-6
2. Cabeza, L.; Perazzoli, G.; Mesas, C.; Jiménez-Luna, C.; Prados, J.; Rama, A. R.; Melguizo, C. *AAPS PharmSciTech* **2020,** *21,* 178. doi:10.1208/s12249-020-01731-y
3. Cisterna, B. A.; Kamaly, N.; Choi, W. I.; Tavakkoli, A.; Farokhzad, O. C.; Vilos, C. *Nanomedicine (London, U. K.)* **2016,** *11,* 2443–2456. doi:10.2217/nnm-2016-0194
4. Iranpour, S.; Bahrami, A. R.; Saljooghi, A. S.; Matin, M. M. *Coord. Chem. Rev.* **2021,** *442,* 213949. doi:10.1016/j.ccr.2021.213949
5. Wathoni, N.; Nguyen, A. N.; Rusdin, A.; Umar, A. K.; Mohammed, A. F. A.; Motoyama, K.; Joni, I. M.; Muchtaridi, M. *Drug Des., Dev. Ther.* **2020,** *14,* 4387–4405. doi:10.2147/dddt.s273612
6. Zhang, X.; Song, H.; Canup, B. S. B.; Xiao, B. *Expert Opin. Drug Delivery* **2020,** *17,* 781–790. doi:10.1080/17425247.2020.1748005
7. Ying, K.; Bai, B.; Gao, X.; Xu, Y.; Wang, H.; Xie, B. *Front. Bioeng. Biotechnol.* **2021,** *9,* 670124. doi:10.3389/fbioe.2021.670124
8. Ünal, S.; Can Öztürk, S.; Bilgiç, E.; Yanık, H.; Korkusuz, P.; Aktaş, Y.; Benito, J. M.; Esendağlı, G.; Bilensoy, E. *Eur. J. Pharm. Biopharm.* **2021,** *169,* 168–177. doi:10.1016/j.ejpb.2021.10.010
9. Ünal, S.; Aktaş, Y.; Benito, J. M.; Bilensoy, E. *Int. J. Pharm.* **2020,** *584,* 119468. doi:10.1016/j.ijpharm.2020.119468
10. Wang, Y.; Pi, C.; Feng, X.; Hou, Y.; Zhao, L.; Wei, Y. *Int. J. Nanomed.* **2020,** *15,* 6295–6310. doi:10.2147/ijn.s257269
11. Ünal, H.; Öztürk, N.; Bilensoy, E. *Beilstein J. Org. Chem.* **2015,** *11,* 204–212. doi:10.3762/bjoc.11.22
12. Alexis, F.; Pridgen, E.; Molnar, L. K.; Farokhzad, O. C. *Mol. Pharmaceutics* **2008,** *5,* 505–515. doi:10.1021/mp800051m
13. Çirpanli, Y.; Bilensoy, E.; Lale Doğan, A.; Çaliş, S. *Eur. J. Pharm. Biopharm.* **2009,** *73,* 82–89. doi:10.1016/j.ejpb.2009.04.013
14. Bao, H.; Zhang, Q.; Yan, Z. *Int. J. Nanomed.* **2019,** *14,* 383–391. doi:10.2147/ijn.s188984
15. Wen, Y.; Wang, Y.; Liu, X.; Zhang, W.; Xiong, X.; Han, Z.; Liang, X. *Cancer Biol. Med.* **2017,** *14,* 363–370. doi:10.20892/j.issn.2095-3941.2017.0099
16. Xiao, B.; Si, X.; Han, M. K.; Viennois, E.; Zhang, M.; Merlin, D. *J. Mater. Chem. B* **2015,** *3,* 7724–7733. doi:10.1039/c5tb01245g
17. Huarte, J.; Espuelas, S.; Lai, Y.; He, B.; Tang, J.; Irache, J. M. *Int. J. Pharm.* **2016,** *506,* 116–128. doi:10.1016/j.ijpharm.2016.04.045
18. Zhan, H.; Zhou, X.; Cao, Y.; Jagtiani, T.; Chang, T.-L.; Liang, J. F. *J. Mater. Chem. B* **2017,** *5,* 2692–2701. doi:10.1039/c7tb00134g
19. Pflueger, I.; Charrat, C.; Mellet, C. O.; García Fernández, J. M.; Di Giorgio, C.; Benito, J. M. *Org. Biomol. Chem.* **2016,** *14,* 10037–10049. doi:10.1039/c6ob01882c
20. Gallego-Yerga, L.; Blanco-Fernández, L.; Urbiola, K.; Carmona, T.; Marcelo, G.; Benito, J. M.; Mendicuti, F.; Tros de Ilarduya, C.; Ortiz Mellet, C.; García Fernández, J. M. *Chem. – Eur. J.* **2015,** *21,* 12093–12104. doi:10.1002/chem.201501678
21. Haimhoffer, Á.; Rusznyák, Á.; Réti-Nagy, K.; Vasvári, G.; Váradi, J.; Vecsernyés, M.; Bácskay, I.; Fehér, P.; Ujhelyi, Z.; Fenyvesi, F. *Sci. Pharm.* **2019,** *87,* 33. doi:10.3390/scipharm87040033
22. Szente, L.; Singhal, A.; Domokos, A.; Song, B. *Molecules* **2018,** *23,* 1228. doi:10.3390/molecules23051228
23. Chourasia, M.; Jain, S. *J. Pharm. Pharm. Sci.* **2003,** *6,* 33–66.
24. Vieira, A. C. F.; Serra, A. C.; Veiga, F. J.; Gonsalves, A. M. d. R.; Basit, A. W.; Murdan, S. *Int. J. Pharm.* **2016,** *500,* 366–370. doi:10.1016/j.ijpharm.2016.01.024
25. Díaz-Moscoso, A.; Balbuena, P.; Gómez-García, M.; Ortiz Mellet, C.; Benito, J. M.; Le Gourriérec, L.; Di Giorgio, C.; Vierling, P.; Mazzaglia, A.; Micali, N.; Defaye, J.; García Fernández, J. M. *Chem. Commun.* **2008,** 2001–2003. doi:10.1039/b718672j
26. Bilensoy, E.; Hincal, A. A. *Expert Opin. Drug Delivery* **2009,** *6,* 1161–1173. doi:10.1517/17425240903222218
27. Bilensoy, E.; Gürkaynak, O.; Doğan, A. L.; Hıncal, A. A. *Int. J. Pharm.* **2008,** *347,* 163–170. doi:10.1016/j.ijpharm.2007.06.051
28. Erdoğar, N.; Esendağlı, G.; Nielsen, T. T.; Şen, M.; Öner, L.; Bilensoy, E. *Int. J. Pharm.* **2016,** *509,* 375–390. doi:10.1016/j.ijpharm.2016.05.040
29. Rivero-Barbarroja, G.; Benito, J. M.; Ortiz Mellet, C.; García Fernández, J. M. *Nanomaterials* **2020,** *10,* 2517. doi:10.3390/nano10122517
30. Belali, N.; Wathoni, N.; Muchtaridi, M. *J. Adv. Pharm. Technol. Res.* **2019,** *10,* 100. doi:10.4103/japtr.japtr_26_19
31. Weng, J.; Tong, H. H. Y.; Chow, S. F. *Pharmaceutics* **2020,** *12,* 732. doi:10.3390/pharmaceutics12080732
32. Sethi, M.; Sukumar, R.; Karve, S.; Werner, M. E.; Wang, E. C.; Moore, D. T.; Kowalczyk, S. R.; Zhang, L.; Wang, A. Z. *Nanoscale* **2014,** *6,* 2321–2327. doi:10.1039/c3nr05961h
33. Mircioiu, C.; Voicu, V.; Anuta, V.; Tudose, A.; Celia, C.; Paolino, D.; Fresta, M.; Sandulovici, R.; Mircioiu, I. *Pharmaceutics* **2019,** *11,* 140. doi:10.3390/pharmaceutics11030140
34. Pourtalebi Jahromi, L.; Ghazali, M.; Ashrafi, H.; Azadi, A. *Heliyon* **2020,** *6,* e03451. doi:10.1016/j.heliyon.2020.e03451
35. Papadopoulou, V.; Kosmidis, K.; Vlachou, M.; Macheras, P. *Int. J. Pharm.* **2006,** *309,* 44–50. doi:10.1016/j.ijpharm.2005.10.044
36. Sorasitthiyanukarn, F. N.; Muangnoi, C.; Ratnatilaka Na Bhuket, P.; Rojsitthisak, P.; Rojsitthisak, P. *Mater. Sci. Eng., C* **2018,** *93,* 178–190. doi:10.1016/j.msec.2018.07.069
37. Sanchez, L. T.; Pinzon, M. I.; Villa, C. C. *Food Chem.* **2022,** *371,* 131121. doi:10.1016/j.foodchem.2021.131121
38. Ainurofiq, A.; Choiri, S. *Trop. J. Pharm. Res.* **2015,** *14,* 1129–1135. doi:10.4314/tjpr.v14i7.2
39. Ünal, S.; Aktaş, Y. *Int. J. Polym. Mater. Polym. Biomater.* **2023,** *72,* 89–100. doi:10.1080/00914037.2022.2082425
40. Prajapati, S. K.; Richhaiya, R.; Singh, V. K.; Singh, A. K.; Kumar, S.; Chaudhary, R. K. *J. Drug Delivery Ther.* **2012,** *2,* 16–24. doi:10.22270/jddt.v2i1.57
41. Cellet, T. S. P.; Pereira, G. M.; Muniz, E. C.; Silva, R.; Rubira, A. F. *J. Mater. Chem. B* **2015,** *3,* 6837–6846. doi:10.1039/c5tb00856e
42. Basak, S. C.; Jayakumar Reddy, B. M.; Lucas Mani, K. P. *Indian J. Pharm. Sci.* **2006,** *68,* 594–598. doi:10.4103/0250-474x.29626

43. Öztürk, A. A.; Yenilmez, E.; Şenel, B.; Kıyan, H. T.; Güven, U. M. *Drug Dev. Ind. Pharm.* **2020,** *46,* 682–695. doi:10.1080/03639045.2020.1755304
44. Permanadewi, I.; Kumoro, A. C.; Wardhani, D. H.; Aryanti, N. *J. Phys.: Conf. Ser.* **2019,** *1295,* 012063. doi:10.1088/1742-6596/1295/1/012063
45. Lisik, A.; Musiał, W. *Materials* **2019,** *12,* 730. doi:10.3390/ma12050730
46. Chime, S.; Onunkwo, G.; Onyishi, I. *Res. J. Pharm., Biol. Chem. Sci.* **2013,** *4,* 97–103.
47. Paolino, D.; Tudose, A.; Celia, C.; Di Marzio, L.; Cilurzo, F.; Mircioiu, C. *Materials* **2019,** *12,* 693. doi:10.3390/ma12050693
48. Azadi, S.; Ashrafi, H.; Azadi, A. *J. Appl. Pharm. Sci.* **2017,** *7,* 125–133. doi:10.7324/japs.2017.70418
49. Corsaro, C.; Neri, G.; Mezzasalma, A. M.; Fazio, E. *Polymers (Basel, Switz.)* **2021,** *13,* 2897. doi:10.3390/polym13172897
50. Varan, G.; Öncül, S.; Ercan, A.; Benito, J. M.; Ortiz Mellet, C.; Bilensoy, E. *J. Pharm. Sci.* **2016,** *105,* 3172–3182. doi:10.1016/j.xphs.2016.06.021
51. Usman, M.; Zaheer, Y.; Younis, M. R.; Demirdogen, R. E.; Hussain, S. Z.; Sarwar, Y.; Rehman, M.; Khan, W. S.; Ihsan, A. *Colloid Interface Sci. Commun.* **2020,** *35,* 100243. doi:10.1016/j.colcom.2020.100243
52. Park, S. M.; Jeon, S. K.; Kim, O. H.; Ahn, J. Y.; Kim, C.-H.; Park, S.-D.; Lee, J.-H. *Chin. Med. (London, U. K.)* **2019,** *14,* 43. doi:10.1186/s13020-019-0263-8
53. Orlova, A.; Sirotkina, M.; Smolina, E.; Elagin, V.; Kovalchuk, A.; Turchin, I.; Subochev, P. *Photoacoustics* **2019,** *13,* 25–32. doi:10.1016/j.pacs.2018.11.005
54. Ye, T.-H.; Yang, F.-F.; Zhu, Y.-X.; Li, Y.-L.; Lei, Q.; Song, X.-J.; Xia, Y.; Xiong, Y.; Zhang, L.-D.; Wang, N.-Y.; Zhao, L.-F.; Gou, H.-F.; Xie, Y.-M.; Yang, S.-Y.; Yu, L.-T.; Yang, L.; Wei, Y.-Q. *Cell Death Dis.* **2018,** *8,* e2534. doi:10.1038/cddis.2016.452
55. Varan, G.; Akkın, S.; Demirtürk, N.; Benito, J. M.; Bilensoy, E. *J. Drug Targeting* **2021,** *29,* 439–453. doi:10.1080/1061186x.2020.1853743
56. Ercan, A.; Çelebier, M.; Varan, G.; Öncül, S.; Nenni, M.; Kaplan, O.; Bilensoy, E. *Eur. J. Pharm. Sci.* **2018,** *123,* 377–386. doi:10.1016/j.ejps.2018.07.060
57. Kishi, S.; Fujiwara-Tani, R.; Luo, Y.; Kawahara, I.; Goto, K.; Fujii, K.; Ohmori, H.; Nakashima, C.; Sasaki, T.; Kuniyasu, H. *Oncol. Lett.* **2018,** *15,* 4423–4426. doi:10.3892/ol.2018.7817
58. Shimolina, L. E.; Gulin, A. A.; Paez-Perez, M.; López-Duarte, I.; Druzhkova, I. N.; Lukina, M. M.; Gubina, M. V.; Brooks, N. J.; Zagaynova, E. V.; Kuimova, M. K.; Shirmanova, M. V. *J. Biomed. Opt.* **2020,** *25,* 126004. doi:10.1117/1.jbo.25.12.126004
59. Castle, J. C.; Loewer, M.; Boegel, S.; de Graaf, J.; Bender, C.; Tadmor, A. D.; Boisguerin, V.; Bukur, T.; Sorn, P.; Paret, C.; Diken, M.; Kreiter, S.; Türeci, Ö.; Sahin, U. *BMC Genomics* **2014,** *15,* 190. doi:10.1186/1471-2164-15-190
60. Xie, Y.; Ding, M.; Zhang, B.; Yang, J.; Pei, T.; Ma, P.; Dong, J. *BMC Genomics* **2020,** *21,* 630. doi:10.1186/s12864-020-07023-w
61. Spyridopoulou, K.; Tryfonopoulou, E.; Aindelis, G.; Ypsilantis, P.; Sarafidis, C.; Kalogirou, O.; Chlichlia, K. *Nanoscale Adv.* **2021,** *3,* 2516–2528. doi:10.1039/d0na00984a
62. Yaghoubi, A.; Asgharzadeh, F.; Movaqar, A.; Ghazvini, K.; Hassanian, S. M.; Avan, A.; Khazaei, M.; Soleimanpour, S. *J. Cancer Res. Clin. Oncol.* **2021,** *147,* 2851–2865. doi:10.1007/s00432-021-03683-7
63. Rashidi, M.; Ziai, S. A.; Moini Zanjani, T.; Khalilnezhad, A.; Jamshidi, H.; Amani, D. *Iran. Red. Crescent Med. J.* **2016,** *18,* e35167. doi:10.5812/ircmj.35167
64. Varan, G.; Varan, C.; Öztürk, S. C.; Benito, J. M.; Esendağlı, G.; Bilensoy, E. *Nanomaterials* **2021,** *11,* 515. doi:10.3390/nano11020515
65. Pinto, B.; Henriques, A. C.; Silva, P. M. A.; Bousbaa, H. *Pharmaceutics* **2020,** *12,* 1186. doi:10.3390/pharmaceutics12121186
66. Lv, D.; Hu, Z.; Lu, L.; Lu, H.; Xu, X. *Oncol. Lett.* **2017,** *14,* 6999–7010. doi:10.3892/ol.2017.7134
67. Green, S. K.; Francia, G.; Isidoro, C.; Kerbel, R. S. *Mol. Cancer Ther.* **2004,** *3,* 149–159. doi:10.1158/1535-7163.149.3.2
68. Mohammad, N.; Malvi, P.; Meena, A. S.; Singh, S. V.; Chaube, B.; Vannuruswamy, G.; Kulkarni, M. J.; Bhat, M. K. *Mol. Cancer* **2014,** *13,* 204. doi:10.1186/1476-4598-13-204
69. Maja, M.; Mohammed, D.; Dumitru, A. C.; Verstraeten, S.; Lingurski, M.; Mingeot-Leclercq, M.-P.; Alsteens, D.; Tyteca, D. *Cell. Mol. Life Sci.* **2022,** *79,* 417. doi:10.1007/s00018-022-04426-8
70. Weber, P.; Wagner, M.; Schneckenburger, H. *Int. J. Mol. Sci.* **2013,** *14,* 8358–8366. doi:10.3390/ijms14048358
71. De Lima Marinho Costa, M.; Silva, J. C.; Nascimento, R. B.; Rodrigues, F.; Da Silva Paiva, K. B.; De Aquino Xavier, F. C. *Oral Surg., Oral Med., Oral Pathol., Oral Radiol.* **2022,** *134,* e212. doi:10.1016/j.oooo.2022.01.663
72. Lei, K.; Kurum, A.; Kaynak, M.; Bonati, L.; Han, Y.; Cencen, V.; Gao, M.; Xie, Y.-Q.; Guo, Y.; Hannebelle, M. T. M.; Wu, Y.; Zhou, G.; Guo, M.; Fantner, G. E.; Sakar, M. S.; Tang, L. *Nat. Biomed. Eng.* **2021,** *5,* 1411–1425. doi:10.1038/s41551-021-00826-6
73. Zhang, Y.; Huo, M.; Zhou, J.; Zou, A.; Li, W.; Yao, C.; Xie, S. *AAPS J.* **2010,** *12,* 263–271. doi:10.1208/s12248-010-9185-1
74. Varan, G.; Benito, J. M.; Mellet, C. O.; Bilensoy, E. *Beilstein J. Nanotechnol.* **2017,** *8,* 1457–1468. doi:10.3762/bjnano.8.145
75. Gamal, A.; Saeed, H.; El-Ela, F. I. A.; Salem, H. F. *Pharmaceutics* **2021,** *13,* 1560. doi:10.3390/pharmaceutics13101560
76. Murtaza, G.; Ahmad, M.; Khan, S. A.; Hussain, I. *Dissolution Technol.* **2012,** *19,* 13–19. doi:10.14227/dt190212p13
77. Kassaye, L.; Genete, G. *Afr. Health Sci.* **2013,** *13,* 369–375. doi:10.4314/ahs.v13i2.25
78. Aldeek, F.; McCutcheon, N.; Smith, C.; Miller, J. H.; Danielson, T. L. *Separations* **2021,** *8,* 7. doi:10.3390/separations8010007
79. Puthli, S.; Vavia, P. R. *AAPS PharmSciTech* **2009,** *10,* 872. doi:10.1208/s12249-009-9280-8
80. Varan, G.; Patrulea, V.; Borchard, G.; Bilensoy, E. *Nanomaterials* **2018,** *8,* 67. doi:10.3390/nano8020067

License and Terms

This is an open access article licensed under the terms of the Beilstein-Institut Open Access License Agreement (https://www.beilstein-journals.org/bjoc/terms), which is identical to the Creative Commons Attribution 4.0 International License (https://creativecommons.org/licenses/by/4.0). The reuse of material under this license requires that the author(s), source and license are credited. Third-party material in this article could be subject to other licenses (typically indicated in the credit line), and in this case, users are required to obtain permission from the license holder to reuse the material.

The definitive version of this article is the electronic one which can be found at:
https://doi.org/10.3762/bjoc.19.14

BEILSTEIN JOURNAL OF ORGANIC CHEMISTRY

Continuous flow synthesis of 6-monoamino-6-monodeoxy-β-cyclodextrin

János Máté Orosz[1], Dóra Ujj[1], Petr Kasal[2], Gábor Benkovics[1] and Erika Bálint[*1]

Full Research Paper

Open Access

Address:
[1]Department of Organic Chemistry and Technology, Faculty of Chemical Technology and Biotechnology, Budapest University of Technology and Economics, Műegyetem rkp. 3., H-1111 Budapest, Hungary and [2]Department of Organic Chemistry, Faculty of Science, Charles University, 128 43 Prague 2, Czech Republic

Email:
Erika Bálint[*] - balint.erika@vbk.bme.hu

* Corresponding author

Keywords:
azidation; continuous flow; β-cyclodextrin; H-cube; 6-monoamino-6-monodeoxy-β-cyclodextrin; monosubstitution; reduction

Beilstein J. Org. Chem. **2023,** *19,* 294–302.
https://doi.org/10.3762/bjoc.19.25

Received: 02 January 2023
Accepted: 21 February 2023
Published: 09 March 2023

This article is part of the thematic issue "Cyclodextrins as building blocks for new materials".

Guest Editor: S. Fourmentin

© 2023 Orosz et al.; licensee Beilstein-Institut.
License and terms: see end of document.

Abstract

The first continuous flow method was developed for the synthesis of 6-monoamino-6-monodeoxy-β-cyclodextrin starting from native β-cyclodextrin through three reaction steps, such as monotosylation, azidation and reduction. All reaction steps were studied separately and optimized under continuous flow conditions. After the optimization, the reaction steps were coupled in a semi-continuous flow system, since a solvent exchange had to be performed after the tosylation. However, the azidation and the reduction steps were compatible to be coupled in one flow system obtaining 6-monoamino-6-monodeoxy-β-cyclodextrin in a high yield. Our flow method developed is safer and faster than the batch approaches.

Introduction

Cyclodextrins (CDs), as cyclic oligosaccharides, consist of a macrocyclic ring of glucose subunits linked by α-1,4-glycosidic bonds [1]. They are widely used in pharmaceutical, food and chemical industries, as well as in agriculture. It has been known for decades, that CD complexation can lead to a significant solubility enhancement of poorly water-soluble molecules, and therefore it can enable the biological testing of drugs, which would otherwise not be possible by any other means [2,3].

Monosubstituted CDs contain only one hydroxy group modified with a functional group. In most cases, the preparation of these compounds is based on the use of a limited amount of the reagent. However, due to the very similar reactivity of hydroxy groups, oversubstitution cannot be avoided during the reaction, thus chromatography or crystallization steps are essential for the preparation of pure monofunctionalized CDs. Alternative approaches use sterically hindered reagents, preventing the approach of the second molecule of the reagent to provide higher

yields for the monosubstituted compounds [4]. The three different hydroxy groups on the glucose subunits offer three different sites on the CD molecule where the monofunctionalization can occur. Consequently, monosubstituted CDs can be mixtures of three regioisomers.

The number of known monosubstituted CD derivatives is enormous, since monosubstitution was the almost exclusive reaction for the practical production of selectively modified CDs for a long time. From the synthetic point of view, the most important derivatives are those versatile intermediates that can be effectively transformed according to the requirements of the specific application. The modification of a monosubstituted CD with a suitable functional group is an easier process than the optimization of a new monosubstitution reaction on a native CD [5].

Monotosylation of the primary rim of CDs is the most widely used method to obtain C-6 monofunctionalized CDs. Tosyl chloride (TsCl) reacts with α-, β-, and γ-CD in pyridine to give the C-6-monosubstituted product in about 30% yield (for β-CD) [6,7]. The C-6 regioselectivity can be attributed to the inclusion of pyridine into the CD cavity in such a way that it activates only the hydroxy groups on the primary side. Several alternative methods have been developed with the aim of further improving the yield of monotosylation or replacing pyridine with a more user-friendly solvent [8]. Regardless of which strategy is used, the complete conversion of the starting material into the monosubstituted product does not occur, and a mixture of overtosylated products and unreacted starting CD is formed. The target monosulfonated compound is separated by recrystallization from hot water in the case of the β-CD derivative, and by chromatography in the case of α- and γ-CDs.

The larger cavity size of γ-CD is the reason of polysubstitution when TsCl is used [9]. To ensure a better yield of the monosubstituted product, bulkier sulfonyl chloride reagents are used. 2-Naphthalenesulfonyl chloride in pyridine is one common method. However, the concentration of γ-CD must be lower than 20 mM to favor monosubstitution and to ensure the optimal yield (around 30%) after recrystallization from hot water [9]. Sometimes purification using ion exchange column [10] or reversed-phase chromatography has been reported [11]. An even bulkier sulfonyl chloride reagent, specifically 2,4,6-triisopropylbenzenesulfonyl chloride, can also be used [12]. Again, the reaction is performed in pyridine and the desired monosubstituted product is obtained in 69% yield and 98% purity according to the authors.

Many nucleophiles can react with tosylated CDs to give the corresponding C-6-monofunctionalized CDs. However, alkaline bases cannot be used as nucleophiles due to the intramolecular substitution, resulting in a mono-3,6-anhydro product [13]. On the other hand, sodium azide in *N,N*-dimethylformamide (DMF) reacts with mono-6-*O*-tosyl-CDs to give CD monoazides in high yields. The obtained mono(6-azido-6-deoxy)-CDs (N_3-CDs) are valuable precursors that can be used as starting materials in azide–alkyne click reactions; furthermore, they can be readily reduced to mono(6-amino-6-deoxy)-CDs (NH_2-CDs) opening the way for the preparation of amine, thioureido or amide-linked CD scaffolds [14]. Several other nucleophiles can react with mono-6-*O*-tosyl-CDs, such as iodide, dithiol, hydroxylamine, alkylamine or polyalkylamine to give iodo- [15], thio- [16], hydroxylamino- [17], or alkylamino-CDs [18], monosubstituted at position C-6. In addition, the tosyl functional group can be oxidized to an aldehyde using a non-nucleophilic base in dimethyl sulfoxide (DMSO) [19]. The monoaldehyde CDs can be further oxidized selectively to afford the corresponding carboxylic acid derivatives [20].

An alternative strategy to overcome the difficulties associated with the preparation of mono-6-*O*-tosyl-CD intermediates is the direct preparation of 6-monoaldehyde-CD with Dess–Martin periodinane in a fairly good yield of 85%, which can be considered the most efficient reaction used so far for the selective monofunctionalization of CDs [1].

Besides traditional synthetic methods, alternative techniques, such as ultrasound and microwave irradiation [21], as well as mechanosynthesis [22,23] for the functionalizations, such as tosylation or azidation of CDs have been also described [24,25].

Continuous flow approaches have already attracted much attention in the oil, plastic, and fine chemical industries [26]. The vision of faster, safer, cheaper, more flexible and robust production also initiated the paradigm shift from batch reactions to continuous flow processes in the pharmaceutical industry [1,27]. During continuous flow reactions, the target molecules can be produced with better purity, selectivity and in higher yields, as well as in consistent quality due to the precise parameter control, low volume ratio and small quantities. The temperature control is simple and toxic or unstable intermediates are easier to handle, making the overall process safer.

To the best of our knowledge, there is no publication on the continuous flow monosubstitution of CD derivatives. In this paper, first we wished to summarize the batch synthesis of 6^A-*O*-(*p*-toluenesulfonyl)-β-CD, 6^A-azido-6^A-deoxy-β-CD, and 6^A-amino-6^A-deoxy-β-CD to see how compatible batch methods are with flow synthesis, and then our main aim was to develop continuous flow approaches for the preparation of the mentioned CD derivatives.

Results and Discussion

Batch synthesis of 6^A-*O*-(*p*-toluenesulfonyl)-β-CD (Ts-β-CD, **2**)

There are three standard methods for the preparation of this general and functional CD derivative. Two of them take advantage of the lower aqueous solubility of β-CD (**1**) and Ts-β-CD (**2**) compared to α- and γ-CD analogs. The third method is mainly used for Ts-α-CD and Ts-γ-CD synthesis, but Ts-β-CD (**2**) can also be prepared by this route. However, before discussing these methods in more detail, some issues related to tosylation reagents should be considered.

There are three tosylating agents utilized for the synthesis of Ts-β-CD, *p*-toluenesulfonyl chloride (TsCl) [14,28,29], (*p*-toluenesulfonyl)imidazole (TsIm) [30,31], and *p*-toluenesulfonic anhydride (Ts_2O) [32]. TsCl is the first choice due to its low price and availability, being a byproduct of saccharin production. The two other reagents are more expensive or can be prepared in the laboratory from TsCl. No significant differences are observed in the product yields concerning the types of the tosylating agents.

As already mentioned above, there are three standard methods for the preparation of Ts-β-CD (**2**). The first and most common method can be called *heterogeneous* approach [28,33,34]. Here, solid TsCl (sufficiently crushed) is added to a β-CD (**1**) aqueous solution and this heterogeneous mixture is stirred for several hours. Then, aqueous NaOH solution is added and the mixture is stirred for another 10–20 minutes. Unreacted TsCl is filtered off and Ts-β-CD, overreacted byproducts, and β-CD are precipitated after neutralization.

The second method could bear the name *homogeneous* approach [8,14,35]. It is very similar to the previous method, however, TsCl dissolved in MeCN is added to the basic β-CD aqueous solution. Turbidity or even slight precipitation is observed during the process. After a few hours, the reaction mixture is filtered and neutralized to induce precipitation.

The third method works with pyridine as a solvent [29,36,37]. In this method, β-CD is dissolved in pyridine and a pyridine solution of TsCl is added dropwise. After a few hours, the solvent is distilled off and the residue is precipitated in acetone in order to obtain solid β-CD compounds.

Two important things need to be mentioned before closing this part. First, the amounts of TsCl range from 0.5 to 9 equiv in the literature and there is no direct correlation between the yield and the amount of TsCl. Usually 1 to 1.3 equiv are sufficient to ensure good yields. However, the yields bring us to the second important point. As already mentioned, the yield of this reaction is not strongly influenced by the amount of TsCl, but by the purification method. If only the precipitation is carried out, then the crude product is always a mixture of Ts-β-CD (**2**), overreacted byproducts, and starting β-CD (**1**). However, in previous studies this has been reported as a clean product with a yield of almost 50% [31,33]. Recrystallization is mandatory to obtain pure Ts-β-CD (**2**) [38,39]. The best results are obtained by crystallization of the crude product from 50% MeOH/water [18], which we adopted for our batch synthesis of Ts-β-CD (**2**). After proper purification, the yield of the desired product **2** was around 25%. Readers can also find more information on problematic *p*-toluenesulfonylation, subsequent azidation and reduction, in a recently published review [5].

It is clear from the already mentioned facts about the synthesis of Ts-β-CD (**2**), that neither of these methods is suitable for the flow chemistry process. Heterogeneous mixtures should be strictly avoided and pyridine is a toxic compound and should not be used in large-scale syntheses or industrial processes.

Batch synthesis of 6^A-azido-6^A-deoxy-β-CD (N_3-β-CD) (**3**)

Substitution of the *p*-toluenesulfonyl group of Ts-β-CD (**2**) by azide can be carried out in water [40,41], DMF [14,42], or in their combination [43,44] at elevated temperatures. Water is preferred over DMF due to its lower cost and non-toxicity. However, partial hydrolysis of the *p*-toluenesulfonyl group takes place, so the final product is always contaminated with native β-CD (**1**). Despite this, the product mixture after precipitation from acetone was used in the next reaction step and a proper purification of the targeted monosubsituted compound was performed after this last modification. After precipitation, an apparent yield of more than 90% was noted; however, this value did not take into account native β-CD (**1**) as byproduct. On the other hand, if purification by column chromatography or crystallization is also used, yields of 60–80% can be achieved.

Partial hydrolysis can be avoided by using anhydrous DMF and purifying the starting Ts-β-CD (**2**) by crystallization. In this case, a lower amount of NaN_3 (1–2 equiv) is required and only purification by precipitation from acetone is necessary. In order to prepare N_3-β-CD (**3**) in batch, we decided to follow the protocol developed by Jicsinszky and Iványi [14], who performed this reaction in anhydrous DMF using 1.1 equiv of NaN_3 at 110 °C. The product **3** was purified by repeated precipitation from acetone and isolated in a yield of 81%.

Batch synthesis of 6^A-amino-6^A-deoxy-β-CD (NH_2-β-CD) (**4**)

Again, there are several common methods for the preparation of NH_2-β-CD (**4**). The most straightforward route is the reaction of Ts-β-CD (**2**) with condensed NH_3 in dry DMF [45]. However, this reaction leads to a complex mixture and the yield is around 50% after proper purification.

The Staudinger reduction using triphenylphosphine (PPh_3) and N_3-β-CD (**3**) in DMF has been the most popular method for the synthesis of NH_2-β-CD (**4**) since its first publication by Bonnet et al. [46]. This is despite the fact, that PPh_3 and its oxidized product (triphenylphosphine oxide) form complexes with β-CD derivatives. This complexation creates difficulties in the purification process, which consists mostly of precipitation from acetone or ion-exchange column chromatography. The price of the reagent needs to be also considered in the case of an attempted large-scale synthesis.

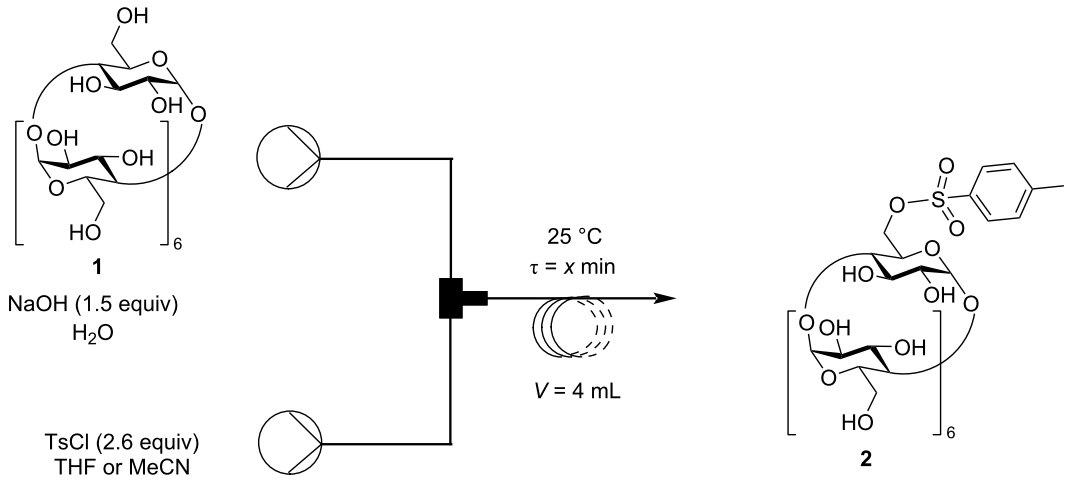
The second most used method is the hydrogenation of N_3-β-CD (**3**) in the presence of Pd/C under a H_2 atmosphere. In CD chemistry, this method was first described by Petter et al. [8] in the early 1990s. This method is very popular with small-scale syntheses because only gaseous N_2 is formed as a byproduct and no purification is required when pure N_3-β-CD (**3**) is used as substrate. However, for large-scale syntheses, mixing hydrogen with the Pd/C catalyst can be dangerous if an inert atmosphere is not properly maintained. In addition, Pd/C is pyrophoric and tends to ignite when it is separated from the reaction mixture by filtration. However, these two drawbacks are not a problem for large-scale flow synthesis when using an H-Cube system with an incorporated electrolytic cell producing H_2 in situ from ultrapure water [47]. The Pd/C catalyst is placed in a stainless steel cartridge, so it is not necessary to separate it from the solution after the reaction is complete.

Hydrazine hydrate can also be used as a hydrogen source instead of gaseous H_2, as described by Jicsinszky and Iványi [14], although this method is not so widespread and has limited potential for a large-scale synthesis. As a special feature, the protocol published by Reddy et al. [48] is worth mentioning, who used metallic indium and ammonium chloride for the reduction of N_3-β-CD.

Continuous flow synthesis of 6^A-*O*-(*p*-toluenesulfonyl)-β-CD (**2**)

According to the literature, most of the tosylations of CDs took place under heterogeneous conditions. However, small solid particles can easily cause clogging in the narrow tubing of a flow system, therefore homogenous solutions were tried to introduce into the flow systems in all experiments. Regarding the tosylation, β-CD (**1**) and the required base (NaOH) are soluble in water, however, TsCl needs to be dissolved in organic solvents. Alcohols were excluded as possible solvents, as they precipitate β-CD (**1**) and may cause side reactions, but aprotic solvents such as tetrahydrofuran (THF) or acetonitrile (MeCN) were found to be suitable for homogenous conditions, especially a H_2O/THF 2:1 mixture. This solvent mixture was prepared in situ in the flow tube reactor, as the aqueous solution containing β-CD (**1**) and NaOH (1.5 equiv) was introduced into the reactor at twice the flow rate as the solution of TsCl in THF (Scheme 1).

In this way, twice as many equivalents of TsCl were required compared to the general 1.3 equivalents used in the batch process. The reaction residence time (τ) was varied between 2.2



Scheme 1: Tosylation of β-CD under continuous flow conditions.

and 5.3 minutes (Table 1, entries 1–4). The 3 minute residence time was found to be the optimal one and led to a conversion of 24% (Table 1, entry 2). This is a significant advantage compared to batch methods, where similar conversions were achieved in over 2 hours. The flow tosylation was also investigated using acetonitrile instead of THF, however, a much lower conversion was observed (Table 1, entry 4).

Continuous flow synthesis of 6^A-azido-6^A-deoxy-β-CD (**3**)

After the tosylation step was successful in flow, next the tosyl–azide substitution was optimized (Scheme 2).

First, the best solvent was sought. Unfortunately, practically no reaction took place when the same solvent was used as for the tosylation reaction (Table 2, entries 1–4), so we had to evaporate the solution exiting the first flow reaction, and change the solvent. According to the literature, DMF proved to be a suitable solvent to conduct this reaction under homogenous conditions. By prolonging the residence time, the conversion greatly increased (Table 2, entries 5–7). However, with longer residence times, increasing hydrolysis of Ts-β-CD (**2**) was observed. To solve this issue, water was excluded from the azidation, which resulted in a total conversion to the corresponding N_3-β-CD (**3**) (Table 2, entries 8–10). In order allow comparison of the results with those from the batch synthesis, the amount of NaN_3 was decreased to 1.1 equivalents (Table 2, entries 13–16). Ultimately, the reactor was heated to its limit at 125 °C, by which a satisfying conversion could be achieved. Thus, it can be concluded, that a similar conversion in flow as compared to the batch azidation could be obtained and, in addition as a major advantage, the reaction time was greatly reduced to only 10 minutes.

Continuous flow synthesis of 6^A-amino-6^A-deoxy-β-CD (**4**)

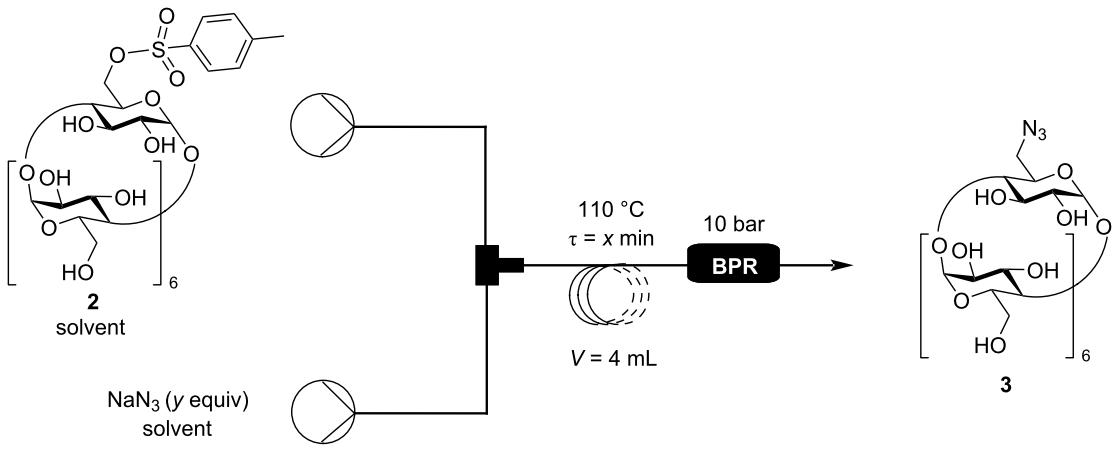
In the last step of the flow synthesis, the reduction of the N_3-β-CD (**3**) was investigated in an H-Cube Pro® flow hydrogenating reactor containing a 10% Pd/C pre-packed cartridge (Scheme 3). Generally, a 1 mL/min input flow was used while conducting the hydrogenations during the optimization, which resulted in approximately a 20 second residence time in all cases.

A complete conversion was observed using even the mildest conditions possible (25 °C, 1 bar H_2 pressure) in aqueous solution (Table 3, entry 1). In spite of this excellent result, the previous azidation reaction proceeded well in DMF, so in order

Table 1: Optimization of the tosylation of β-CD (**1**) under continuous flow conditions.

Entry	Flow rate of TsCl solution [mL/min]	Flow rate of β-CD solution [mL/min]	τ [min]	Solvent	Conversion[a] [%]
1	0.60	1.20	2.2	H_2O/THF 2:1	22
2	0.45	0.90	3.0	H_2O/THF 2:1	24
3	0.25	0.50	5.3	H_2O/THF 2:1	17
4	0.25	0.50	5.3	H_2O/MeCN 2:1	11

[a]On the basis of HPLC (214 nm).

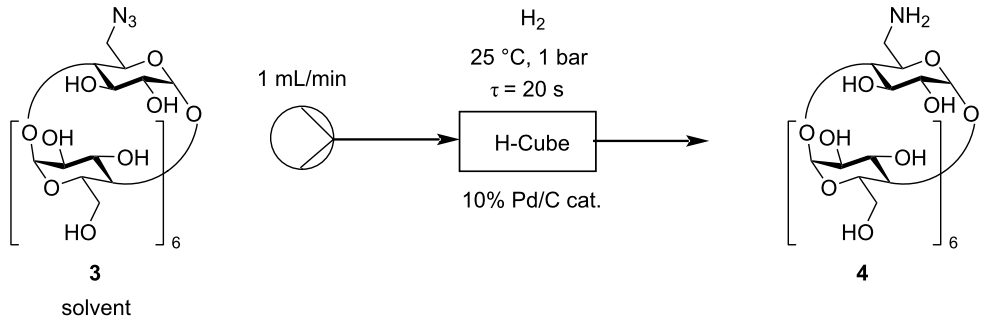


Scheme 2: Continuous flow azidation of Ts-β-CD (**2**).

Table 2: Optimization of the continuous flow azidation of Ts-β-CD (**2**).

Entry	NaN_3 [equiv]	Solvent	*T* [°C]	Total flow rate [mL/min]	τ [min]	Conversion[a] [%]
1[b]	2	H_2O/THF 2:1	25	1.5	2.7	0
2[c]	2	H_2O/THF 2:1	25	1.5	2.7	0
3	2	H_2O/THF 2:1	110	1.5	2.7	0
4	8	H_2O/THF 2:1	110	1.5	2.7	11
5	8	H_2O/DMF 1:1	110	0.75	5.3	39
6	8	H_2O/DMF 1:1	110	0.40	10	45
7	8	H_2O/DMF 1:1	110	0.20	20	60
8	8	DMF	110	0.40	10	100
9	6	DMF	110	0.40	10	100
10	4	DMF	110	0.40	10	100
11	3	DMF	110	0.40	10	96
12	2	DMF	110	0.40	10	83
13	1.1	DMF	110	0.40	10	45
14	1.1	DMF	125	0.40	10	86
15	1.1	DMF	125	0.20	20	85
16	1.1	DMF	125	0.13	30	78

[a]Based on HPLC (214 nm). [b]The reaction was carried out using the reaction mixture obtained by the flow tosylation. [c]Pure starting material was used, which was obtained from batch tosylation.



Scheme 3: Continuous flow hydrogenation of N_3-β-CD (**3**).

to connect the single flow steps together, the effect of DMF and water/DMF mixtures as solvents had to be studied as well. In DMF, the reaction was not complete and only 30% of NH_2-β-CD (**4**) were obtained (Table 3, entry 2). However, increasing the ratio of water in the solvent mixture afforded better results (Table 3, entries 3–6). The appropriate ratio of DMF/H_2O was determined as 1:4, which gave NH_2-β-CD (**4**) in a yield of 93% (Table 3, entry 5).

Table 3: Optimization of the continuous flow hydrogenation of N_3-β-CD (**3**).

Entry	Solvent	Yield[a] [%]
1	H_2O	94
2	DMF	30
3	DMF/H_2O 1:1	51
4	DMF/H_2O 1:3	85
5	DMF/H_2O 1:4	93
6	DMF/H_2O 1:9	94

[a]Isolated yield.

Semi-continuous flow system for the synthesis of 6^A-amino-6^A-deoxy-β-CD (**4**)

The main goal of this part of the work was to establish a continuous flow method for the synthesis of NH_2-β-CD (**4**) from β-CD (**1**). Thus, after the optimization of the single reaction steps, the connection of these steps was remaining. First of all, it was concluded, that the initial tosylation step could not be connected to the azidation step since in the tosylation's optimal solvent, the azidation did not proceed and vice versa (Table 4).

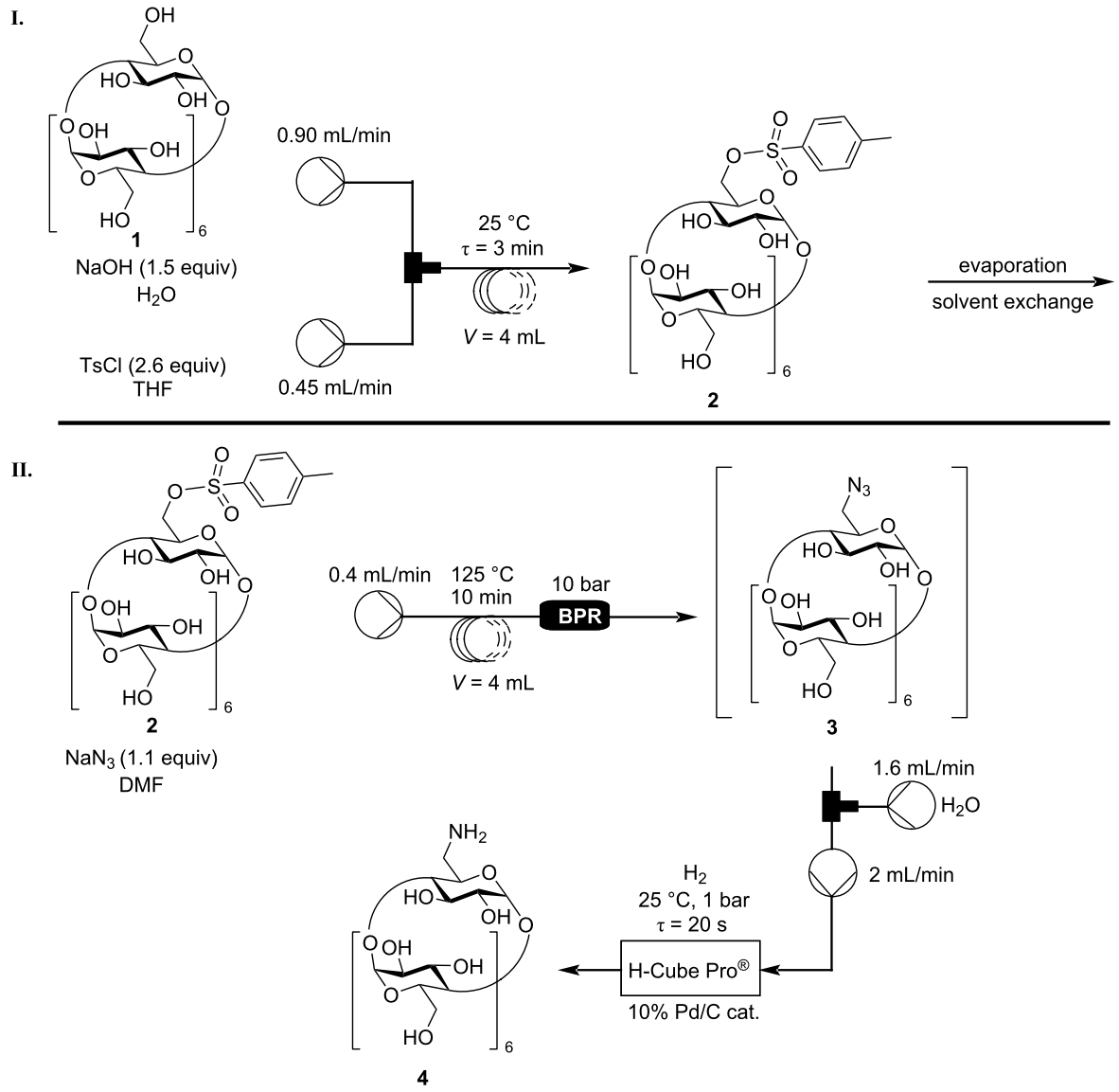
Table 4: Optimal reaction conditions for each flow reaction step.

Synthesis step	Reagent	Solvent	*T* [°C]	τ [min]	Conversion[a] [%]
tosylation	2.6 equiv TsCl	H_2O/THF 2:1	25	3	20
azidation	1.1 equiv NaN_3	DMF	125	10	81
hydrogenation[b]	H_2	H_2O/DMF 1:4	25	0.3	93

[a]Isolated yield. [b]1 bar H_2 pressure and 10 mol % Pd/C catalyst were used.

The only solution was to conduct the tosylation under flow conditions separately from the other two steps (Scheme 4I), evaporate the water/THF solvent, and introduce the Ts-β-CD (**2**) dissolved in DMF to the second part of the flow system. In order to simplify the azidation and subsequent reduction, Ts-β-CD (**2**) prepared from batch and properly purified was utilized.

The azidation and the hydrogenation were compatible with each other, however, after the azidation took place, water needed to



Scheme 4: Semi-continuous flow system for the synthesis of NH_2-β-CD **4**.

be introduced to the system before the hydrogenation to ensure full conversion during the reduction. According to our previous results, the reduction of N_3-β-CD (**3**) went to completion in a DMF/H_2O 1:4 mixture, so this solvent was chosen for the hydrogenation step in order to avoid re-optimization. This way, the exiting solution of 0.4 mL/min from the azidation reaction was joined with a 1.6 mL/min flow of water, and this new solution was gathered in a buffer container, from where the reaction mixture was immediately forwarded to the H-Cube Pro® (Scheme 4II). Although the hydrogenation was optimized for a 1 mL/min input flow rate, the catalyst cartridge was changed to another one, which doubled the reaction volume. In conclusion, a 2 mL/min input flow rate required no re-optimization, as the residence time remained the same. Under these conditions, the connected azidation and reduction steps led to an almost complete conversion of Ts-β-CD (**2**). The output of the H-Cube Pro® was partially evaporated, the product **4** precipitated with acetone and isolated in a yield of 91%.

Conclusion

In conclusion, we have developed continuous flow methods for the monotosylation of β-CD (**1**), for the azidation of 6^A-*O*-(*p*-toluenesulfonyl)-β-CD (**2**), and for the reduction of 6^A-azido-6^A-deoxy-β-CD (**3**). The flow methods are novel approaches for the preparation of the target compounds and were optimized for each case. Comparing the flow processes with batch methods, it can be concluded that similar yields were obtained in both cases, however, under continuous flow conditions, the reaction time could be reduced from hours to minutes. Finally, we made an attempt to connect the three reaction steps with each other in a continuous flow system. It was found that a solvent exchange step was required after the tosylation, however, the azidation and the reduction steps were compatible to be coupled in one flow system. Using our semi-flow method developed, the production of 6^A-amino-6^A-deoxy-β-CD (**4**) could be carried out in a safer way due to the easier handling of toxic derivatives and with more precise parameter control. Moreover, the reactions can be performed within a much shorter reaction time than under batch conditions.

Supporting Information

Experimental procedures, characterization data, details of the NMR structural determination of the products and copies of ^{1}H NMR spectra for the compounds synthesized.

Supporting Information File 1

Experimental section and copies of NMR spectra.
[https://www.beilstein-journals.org/bjoc/content/supplementary/1860-5397-19-25-S1.pdf]

Acknowledgements

The authors thank GB and PK for their contribution to the work with their Ph.D. dissertations.

Funding

This research was funded by the Hungarian Research Development and Innovation Office (FK142712) and by the Cylolab Grant. This work was performed in the frame of the Pharmaceutical Research and Development Laboratory project (PharmaLab, RRF-2.3.1-21-2022-00015), implemented with the support provided from the Széchenyi Plan Plus, financed under the National Laboratory Program funding scheme.

ORCID® iDs

Petr Kasal - https://orcid.org/0000-0001-7489-2898
Gábor Benkovics - https://orcid.org/0000-0001-6804-231X
Erika Bálint - https://orcid.org/0000-0002-5107-7089

References

1. Szejtli, J. *Chem. Rev.* **1998,** *98,* 1743–1754. doi:10.1021/cr970022c
2. Freudenberg, K.; Cramer, F.; Plieninger, H. Process for the preparation of inclusion compounds of physiologically active organic compounds. Ger. Patent DE895769C, May 11, 1953.
3. Crini, G. *Chem. Rev.* **2014,** *114,* 10940–10975. doi:10.1021/cr500081p
4. Cornwell, M. J.; Huff, J. B.; Bieniarz, C. *Tetrahedron Lett.* **1995,** *36,* 8371–8374. doi:10.1016/0040-4039(95)01808-u
5. Kasal, P.; Jindřich, J. *Molecules* **2021,** *26,* 5065. doi:10.3390/molecules26165065
6. Melton, L. D.; Slessor, K. N. *Carbohydr. Res.* **1971,** *18,* 29–37. doi:10.1016/s0008-6215(00)80256-6
7. Matsui, Y.; Yokoi, T.; Mochida, K. *Chem. Lett.* **1976,** *5,* 1037–1040. doi:10.1246/cl.1976.1037
8. Petter, R. C.; Salek, J. S.; Sikorski, C. T.; Kumaravel, G.; Lin, F.-T. *J. Am. Chem. Soc.* **1990,** *112,* 3860–3868. doi:10.1021/ja00166a021
9. Djedaïni-Pilard, F.; Azaroual-Bellanger, N.; Gosnat, M.; Vernet, D.; Perly, B. *J. Chem. Soc., Perkin Trans. 2* **1995,** 723–730. doi:10.1039/p29950000723
10. Uekama, K.; Minami, K.; Hirayama, F. *J. Med. Chem.* **1997,** *40,* 2755–2761. doi:10.1021/jm970130r
11. Kahee, F.; Tsutomu, T.; Taiji, I.; Toshitaka, K. *Chem. Lett.* **1988,** *17,* 1329–1332. doi:10.1246/cl.1988.1329
12. Palin, R.; Grove, S. J. A.; Prosser, A. B.; Zhang, M.-Q. *Tetrahedron Lett.* **2001,** *42,* 8897–8899. doi:10.1016/s0040-4039(01)01934-7
13. Fujita, K.; Yamamura, H.; Imoto, T.; Tabushi, I. *Chem. Lett.* **1988,** *17,* 543–546. doi:10.1246/cl.1988.543
14. Jicsinszky, L.; Iványi, R. *Carbohydr. Polym.* **2001,** *45,* 139–145. doi:10.1016/s0144-8617(00)00319-2
15. Ueno, A.; Moriwaki, F.; Osa, T.; Hamada, F.; Murai, K. *Tetrahedron* **1987,** *43,* 1571–1578. doi:10.1016/s0040-4020(01)90271-6
16. Bednářová, E.; Hybelbauerová, S.; Jindřich, J. *Beilstein J. Org. Chem.* **2016,** *12,* 349–352. doi:10.3762/bjoc.12.38
17. Fikes, L. E.; Winn, D. T.; Sweger, R. W.; Johnson, M. P.; Czarnik, A. W. *J. Am. Chem. Soc.* **1992,** *114,* 1493–1495. doi:10.1021/ja00030a062

18. Popr, M.; Hybelbauerová, S.; Jindřich, J. *Beilstein J. Org. Chem.* **2014,** *10,* 1390–1396. doi:10.3762/bjoc.10.142
19. Martin, K. A.; Czarnik, A. W. *Tetrahedron Lett.* **1994,** *35,* 6781–6782. doi:10.1016/0040-4039(94)85003-8
20. Yoon, J.; Hong, S.; Martin, K. A.; Czarnik, A. W. *J. Org. Chem.* **1995,** *60,* 2792–2795. doi:10.1021/jo00114a030
21. Martina, K.; Trotta, F.; Robaldo, B.; Belliardi, N.; Jicsinszky, L.; Cravotto, G. *Tetrahedron Lett.* **2007,** *48,* 9185–9189. doi:10.1016/j.tetlet.2007.10.104
22. Menuel, S.; Saitzek, S.; Monflier, E.; Hapiot, F. *Beilstein J. Org. Chem.* **2020,** *16,* 2598–2606. doi:10.3762/bjoc.16.211
23. Menuel, S.; Doumert, B.; Saitzek, S.; Ponchel, A.; Delevoye, L.; Monflier, E.; Hapiot, F. *J. Org. Chem.* **2015,** *80,* 6259–6266. doi:10.1021/acs.joc.5b00697
24. Cravotto, G.; Caporaso, M.; Jicsinszky, L.; Martina, K. *Beilstein J. Org. Chem.* **2016,** *12,* 278–294. doi:10.3762/bjoc.12.30
25. Jicsinszky, L.; Rossi, F.; Solarino, R.; Cravotto, G. *Molecules* **2023,** *28,* 467. doi:10.3390/molecules28020467
26. *Ullmann's Encyclopedia of Industrial Chemistry,* 7th ed.; Wiley-VCH: Weinheim, Germany, 2000.
27. Plutschack, M. B.; Pieber, B.; Gilmore, K.; Seeberger, P. H. *Chem. Rev.* **2017,** *117,* 11796–11893. doi:10.1021/acs.chemrev.7b00183
28. Hacket, F.; Simova, S.; Schneider, H.-J. *J. Phys. Org. Chem.* **2001,** *14,* 159–170. doi:10.1002/poc.348
29. Defaye, J.; Gadelle, A.; Guiller, A.; Darcy, R.; O'Sullivan, T. *Carbohydr. Res.* **1989,** *192,* 251–258. doi:10.1016/0008-6215(89)85184-5
30. Byun, H.-S.; Zhong, N.; Bittman, R. *Org. Synth.* **2000,** *77,* 225. doi:10.15227/orgsyn.077.0225
31. Trotta, F.; Martina, K.; Robaldo, B.; Barge, A.; Cravotto, G. *J. Inclusion Phenom. Macrocyclic Chem.* **2007,** *57,* 3–7. doi:10.1007/s10847-006-9169-z
32. Zhong, N.; Byun, H.-S.; Bittman, R. *Tetrahedron Lett.* **1998,** *39,* 2919–2920. doi:10.1016/s0040-4039(98)00417-1
33. McNaughton, M.; Engman, L.; Birmingham, A.; Powis, G.; Cotgreave, I. A. *J. Med. Chem.* **2004,** *47,* 233–239. doi:10.1021/jm030916r
34. Tripodo, G.; Wischke, C.; Neffe, A. T.; Lendlein, A. *Carbohydr. Res.* **2013,** *381,* 59–63. doi:10.1016/j.carres.2013.08.018
35. Vizitiu, D.; Walkinshaw, C. S.; Gorin, B. I.; Thatcher, G. R. J. *J. Org. Chem.* **1997,** *62,* 8760–8766. doi:10.1021/jo9711549
36. Ekberg, B.; Andersson, L. I.; Mosbach, K. *Carbohydr. Res.* **1989,** *192,* 111–117. doi:10.1016/0008-6215(89)85171-7
37. Sforza, S.; Galaverna, G.; Corradini, R.; Dossena, A.; Marchelli, R. *J. Am. Soc. Mass Spectrom.* **2003,** *14,* 124–135. doi:10.1016/s1044-0305(02)00853-x
38. Brady, B.; Lynam, N.; O'Sullivan, T.; Ahern, C.; Darcy, R. *Org. Synth.* **2000,** *77,* 220. doi:10.15227/orgsyn.077.0220
39. Xu, M.; Wu, S.; Zeng, F.; Yu, C. *Langmuir* **2010,** *26,* 4529–4534. doi:10.1021/la9033244
40. Uchida, W.; Yoshikawa, M.; Seki, T.; Miki, R.; Seki, T.; Fujihara, T.; Ishimaru, Y.; Egawa, Y. *J. Inclusion Phenom. Macrocyclic Chem.* **2017,** *89,* 281–288. doi:10.1007/s10847-017-0755-z
41. Quan, C.-Y.; Chen, J.-X.; Wang, H.-Y.; Li, C.; Chang, C.; Zhang, X.-Z.; Zhuo, R.-X. *ACS Nano* **2010,** *4,* 4211–4219. doi:10.1021/nn100534q
42. Chwalek, M.; Auzély, R.; Fort, S. *Org. Biomol. Chem.* **2009,** *7,* 1680–1688. doi:10.1039/b822976g
43. Yang, F.; Zhang, Y.; Guo, H. *New J. Chem.* **2013,** *37,* 2275–2279. doi:10.1039/c3nj00474k
44. Xu, W.; Liang, W.; Wu, W.; Fan, C.; Rao, M.; Su, D.; Zhong, Z.; Yang, C. *Chem. – Eur. J.* **2018,** *24,* 16677–16685. doi:10.1002/chem.201804001
45. Brown, S. E.; Coates, J. H.; Coghlan, D. R.; Easton, C. J.; Vaneyk, S. J.; Janowski, W.; Lepore, A.; Lincoln, S. F.; Luo, Y.; May, B. L.; Schiesser, D. S.; Wang, P.; Williams, M. L. *Aust. J. Chem.* **1993,** *46,* 953–958. doi:10.1071/ch9930953
46. Bonnet, V.; Duval, R.; Tran, V.; Rabiller, C. *Eur. J. Org. Chem.* **2003,** 4810–4818. doi:10.1002/ejoc.200300449
47. Jones, R. V.; Godorhazy, L.; Varga, N.; Szalay, D.; Urge, L.; Darvas, F. *J. Comb. Chem.* **2006,** *8,* 110–116. doi:10.1021/cc050107o
48. Reddy, L. R.; Reddy, M. A.; Bhanumathi, N.; Rao, K. R. *Indian J. Chem., Sect. B* **2002,** *41B,* 645–646.

License and Terms

This is an open access article licensed under the terms of the Beilstein-Institut Open Access License Agreement (https://www.beilstein-journals.org/bjoc/terms), which is identical to the Creative Commons Attribution 4.0 International License (https://creativecommons.org/licenses/by/4.0). The reuse of material under this license requires that the author(s), source and license are credited. Third-party material in this article could be subject to other licenses (typically indicated in the credit line), and in this case, users are required to obtain permission from the license holder to reuse the material.

The definitive version of this article is the electronic one which can be found at:
https://doi.org/10.3762/bjoc.19.25

BEILSTEIN JOURNAL OF ORGANIC CHEMISTRY

Discrimination of β-cyclodextrin/hazelnut (*Corylus avellana* L.) oil/flavonoid glycoside and flavonolignan ternary complexes by Fourier-transform infrared spectroscopy coupled with principal component analysis

Nicoleta G. Hădărugă[1,2,3], Gabriela Popescu[4], Dina Gligor (Pane)[1], Cristina L. Mitroi[3], Sorin M. Stanciu[5] and Daniel Ioan Hădărugă[*1,6]

Full Research Paper

Open Access

Address:
[1]Doctoral School "Engineering of Vegetable and Animal Resources", University of Life Sciences "King Mihai I" from Timişoara, Calea Aradului 119, 300645 Timişoara, Romania, [2]Research Institute for Biosecurity and Bioengineering, Calea Aradului 119, 300645 Timişoara, Romania, [3]Department of Food Science, University of Life Sciences "King Mihai I" from Timişoara, Calea Aradului 119, 300645 Timişoara, Romania, [4]Department of Rural Management and Development, University of Life Sciences "King Mihai I" from Timişoara, Calea Aradului 119, 300645 Timişoara, Romania, [5]Department of Economy and Company Financing, University of Life Sciences "King Mihai I" from Timişoara, Calea Aradului 119, 300645 Timişoara, Romania and [6]Department of Applied Chemistry, Organic and Natural Compounds Engineering, Polytechnic University of Timişoara, Carol Telbisz 6, 30001 Timişoara, Romania

Email:
Daniel Ioan Hădărugă[*] - daniel.hadaruga@upt.ro

* Corresponding author

Keywords:
antioxidant; cyclodextrin; flavonoid; hazelnut vegetable oil; ternary supramolecular inclusion complex

Beilstein J. Org. Chem. **2023,** *19,* 380–398.
https://doi.org/10.3762/bjoc.19.30

Received: 02 January 2023
Accepted: 20 March 2023
Published: 28 March 2023

This article is part of the thematic issue "Cyclodextrins as building blocks for new materials".

Guest Editor: S. Fourmentin

© 2023 Hădărugă et al.; licensee Beilstein-Institut.
License and terms: see end of document.

Abstract

The goal of the study was the discrimination of β-cyclodextrin (β-CD)/hazelnut (*Corylus avellana* L.) oil/antioxidant ternary complexes through Fourier-transform infrared spectroscopy coupled with principal component analysis (FTIR–PCA). These innovative complexes combine the characteristics of the three components and improve the properties of the resulting material such as the onsite protection against oxidative degradation of hazelnut oil unsaturated fatty acid glycerides. Also, the apparent water solubility and bioaccessibility of the hazelnut oil components and antioxidants can be increased, as well as the controlled release of bioactive compounds (fatty acid glycerides and antioxidant flavonoids, namely hesperidin, naringin, rutin, and silymarin). The appropriate method for obtaining the ternary complexes was kneading the components at various molar ratios (1:1:1 and 3:1:1 for β-CD hydrate:hazelnut oil (average molar mass of 900 g/mol):flavonoid). The recovering yields of the ternary complexes were in the range of 51.5–85.3% and were generally higher for the 3:1:1 samples. The thermal stability was evaluated by thermogravimetry and

differential scanning calorimetry. Discrimination of the ternary complexes was easily performed through the FTIR–PCA coupled method, especially based on the stretching vibrations of CO groups in flavonoids and/or CO/CC groups in the ternary complexes at 1014.6 (± 3.8) and 1023.2 (± 1.1) cm^{-1} along the second PCA component (PC_2), respectively. The wavenumbers were more appropriate for discrimination than the corresponding intensities of the specific FTIR bands. On the other hand, ternary complexes were clearly distinguishable from the starting β-CD hydrate along the first component (PC_1) by all FTIR band intensities and along PC_2 by the wavenumber of the asymmetric stretching vibrations of the CH groups at 2922.9 (± 0.4) cm^{-1} for ternary complexes and 2924.8 (± 1.4) cm^{-1} for β-CD hydrate. The first two PCA components explain 70.38% from the variance of the FTIR data (from a total number of 26 variables). Other valuable classifications were obtained for the antioxidant flavonoids, with a high similarity for hesperidin and naringin, according to FTIR–PCA, as well as for ternary complexes depending on molar ratios. The FTIR–PCA coupled technique is a fast, nondestructive and cheap method for the evaluation of quality and similarity/characteristics of these new types of cyclodextrin-based ternary complexes having enhanced properties and stability.

Introduction

Cyclodextrins (CDs) are studied for more than one hundred years due to their unique properties related to their spatial macrocyclic structure that comprises six to eight α-D-glucopyranose (Glc*p*) units for the natural α-, β-, and γ-CD [1-3]. All hydroxy groups are oriented to the exterior of the macrocycle, leading to high water solubility. On the other hand, the tetrahydropyran moieties of the Glc*p* units provide the hydrophobic property of the CD cavity [4]. As a consequence of their unique structure, CDs can encapsulate hydrophobic molecules or hydrophobic moieties of geometrically compatible bioactive compounds [5]. The resulting supramolecular inclusion complexes provide enhanced water solubility and bioavailability/bioaccessibility of the nanoencapsulated bioactive compounds, higher oxidative and thermal stability or photostability of labile compounds, and their controlled release [6,7].

Vegetable oil and animal fat components that especially consist of fatty acid (FA) triglycerides are appropriate guest molecules for obtaining CD-based complexes. The hydrophobic long-chain moieties of the FA glycerides allow obtaining CD:FA glyceride complexes at various molar ratios [8,9], with increased apparent water solubility and bioaccessibility of the oil and fat components. The oxidative stability of the polyunsaturated FA glycerides or free FAs is significantly increased by CD nanoencapsulation. Thus, a high thermal stability was obtained for linoleic acid encapsulated into α-CD by co-crystallization [10]. Omega-3 FA glycerides such as eicosapentaenoic and docosahexaenoic acid glycerides (EPA and DHA glycerides) from fish oil are less stable against oxidation. Their thermal and oxidative stabilities were significantly increased by CD nanoencapsulation as was shown for fish oil from common barbel (*Barbus barbus* L.), Pontic shad (*Alosa immaculata* Bennett), European wels catfish (*Silurus glanis* L.), common bleak (*Alburnus alburnus* L.), common nase (*Chondrostoma nasus* L.), Atlantic salmon (*Salmo salar* L.), and European anchovy (*Engraulis encrasicolus* L.) [11-14]. The stability and the level of degradation compounds were determined by thermal methods (thermogravimetry-differential thermogravimetry, TG–DTG, and differential scanning calorimetry, DSC) and gas chromatography–mass spectrometry (GC–MS), respectively. The addition of sodium caseinate during the CD complexation of fish oils was reported to further increase the oxidation stability and retardation of odor [15]. Poultry lipids have high contents of mono- and polyunsaturated FA glycerides, especially oleic and linoleic acid glycerides. The stability of chicken lipids was significantly increased by β-CD complexation which was demonstrated by both thermal (TG–DTG and DSC) and chromatographic (GC–MS for the degradation compounds, i.e., aldehydes, formylated carboxylic acids, or dicarboxylic acids) methods [16]. Also, vegetable oils containing unsaturated FA moieties were stabilized by CD complexation. Common bean (*Phaseolus vulgaris* L.) oil contains 55.7–58.8% of polyunsaturated FAs (relative content as methyl esters), with an important fraction of omega-3 α-linolenic acid (ALA) of 14.1–18.9%. It was stabilized by β-CD complexation, with an increased content of the omega-3 FAs into the nanoencapsulated oil of >14% [17]. Other complexes between CDs and various vegetable oils have been obtained and characterized. Soybean oil was combined with α-CD for obtaining a stable dry emulsion, which implied the partial molecular encapsulation of the soybean oil triglycerides. This emulsion was prepared in order to modulate the release of indomethacin in rats. Similar α-CD-based emulsions were obtained using wheat germ, sweet almond, borage, and virgin coconut oils [9,18,19]. The stability and bioavailability of peony (*Paeonia suffruticosa* Andr.) seed oil were significantly enhanced by complexation with β-CD through the co-precipitation from a saturated solution. The peony oil content in the complex was almost 26%, with a high ratio of unsaturated FA glycerides of ≈90% [20]. In a very recent study, perilla (*Perilla frutescens* (L.) Britton) seed oil was complexed by γ-CD and the inclusion complex was used for improving the bioavailability of ALA. This omega-3 FA was found in significantly higher concentrations in the plasma of rats fed with this complex [21]. Some vegetable oils were also encapsulated

using combined matrices or polymers containing CDs as was demonstrated for example for kenaf (*Hibiscus cannabinus* L.) seed oil or "Persian lilac" (*Melia azedarach* L.) seed oil. The oils were complexed by spray drying using β-CD/gum arabic/sodium caseinate or a β-CD polymer, respectively [22,23]. However, there are less studies on the CD encapsulation of non-volatile vegetable oils in comparison with essential oils. Essential oil components are also compatible guests for CD nanoencapsulation. They were studied as "pure" compounds or as essential oil mixtures (e.g., linalool, nerolidol, nootkatone, or sweet basil – *Ocimum basilicum* L., caraway – *Carum carvi* L., coriander – *Coriandrum sativum* L., fennel – *Foeniculum vulgare* Mill., dill – *Anethum graveolens* L., garlic – *Allium sativum* L., juniper – *Juniperus communis* L., clove – *Syzygium aromaticum* (L.) Merr. & L.M., and perilla – *Perilla frutescens* (L.) Britton essential oils, respectively) [24-30].

Among vegetable oils, hazelnut (*Corylus avellana* L.) oil is a valuable source of oleic acid bound in various triglyceride combinations. The highest content was observed for triolein, OOO (61–77.5% relative concentration), but also OOL (glyceryl 1,2-dioleate 3-linoleate) and OOP (glyceryl 1,2-dioleate 3-palmitate) were found in high relative contents of 10.5–22.8% and 6.4–11.0%, respectively [31]. The fatty acid profile of hazelnut oil revealed a significantly high content of oleic acid (as methyl ester, determined by GC–MS) of 74.2–82.8%, among linoleic acid and even ALA (9.8–18.7% and ≈0.1%, respectively) [32,33]. The very high content of unsaturated fatty acid glycerides significantly decreases the stability of hazelnut oil. Only one study was performed on the γ-CD nanoencapsulation of hazelnut oil by a co-precipitation method and the thermal decomposition of the complex was evaluated by TG [34].

One way of enhancing the oxidative stability of oils and fats is the addition of antioxidants. Among food grade antioxidants, natural polyphenols such as flavonoids and flavonoid-based extracts are widely used [35-41]. Generally, flavonoids have a high number of phenolic hydroxy groups that provide the antioxidant activity. On the contrary, the presence of highly hydrophilic groups such as saccharide moieties in flavonoid glycosides reduces the level of hydrophobic interactions with the CD cavity. However, less hydrophilic moieties of flavonoid glycosides or flavonolignans interact with CDs (i.e., 4-hydroxyphenyl, 3,4-dihydroxyphenyl- and 3-methoxy-4-hydroxyphenyl moieties in the hesperidin, naringin, and rutin aglycones or silibinin). There are many studies revealing the interaction of flavonoids, flavonoid glycosides, and flavonolignans with CDs, especially for obtaining binary complexes [42-49].

In a ternary complex, considering the vegetable oil as a single component, an on-site antioxidant can protect labile FA glycerides by co-nanoencapsulation into a CD cavity. However, it is very difficult to evaluate the way of interaction in such multicomponent systems. There are some studies on the CD-based ternary complexes, but they do not deal with triglyceride-based vegetable oils or with flavonoid glycosides/flavonolignans. Most of these studies are related to controlled release of various drugs from the CD complexes such as diosmin and polyethylene glycol, haloperidol and lactic acid, cyclosporine A and polyvinyl alcohol, ketoprofen and phospholipids, dihydroartemisinin and lecithin, cefixime and L-arginine, flurbiprofen and naproxen/ketoprofen/ethenzamide [50-59].

Fourier-transform infrared spectroscopy (FTIR) is a very fast, nondestructive and cheap method suitable for the evaluation of such ternary complexes. The coupling of FTIR or other spectroscopic or chromatographic techniques with a multivariate statistical analysis method (e.g., principal component analysis, PCA) allows the evaluation of the similarity/dissimilarity of complexes, as well as the identification of the variables that have significance for these classifications. FTIR–PCA was successfully applied for the discrimination of raw and thermally processed chicken lipid/β-CD complexes [16]. Moreover, raw and recrystallized β-CD samples (from water and alcohol–water solutions) were successfully classified by the FTIR–PCA technique [4]. In other studies, PCA was coupled with GC–MS for the classification of β-CD/*Ocimum basilicum* L. essential oil complexes and raw and thermally processed Mangalitza (*Sus scrofa domesticus*) lipid fractions, as well as for the discrimination of organic apples (*Malus domestica* Borkh.) on the basis of antioxidant properties and radical scavenging kinetics [27,60,61]. However, only few studies have been published on the discrimination of CD-based complexes using multivariate statistical analysis. They are especially related to the retention behavior of various biologically active molecules on CD-coated polymers used in chromatography [62]. PCA was used for the evaluation of the similarity/dissimilarity of some pesticides, especially fungicides and herbicides, using the effect of a water-soluble β-CD polymer on the apparent pesticide's lipophilicity [63]. Also, partial least square (PLS) modeling was used for the determination of the composition of solutions containing tryptophan methyl ester, phenylalanine, norephedrine, *N*,*N*'-bis-(α-methylbenzyl)sulfamide, sulfaguanidine or sulfamethoxazole using the spectral data of the corresponding CD host–guest complexes [64-66].

The goal of this study was the synthesis of β-CD/hazelnut (*Corylus avellana* L.) oil/flavonoid glycoside or flavonolignan ternary complexes (Figure 1) and the discrimination of these complexes by FTIR–PCA. These innovative ternary complexes were synthesized for the first time and can provide the on-site protection of hazelnut oil components against oxidative degra-

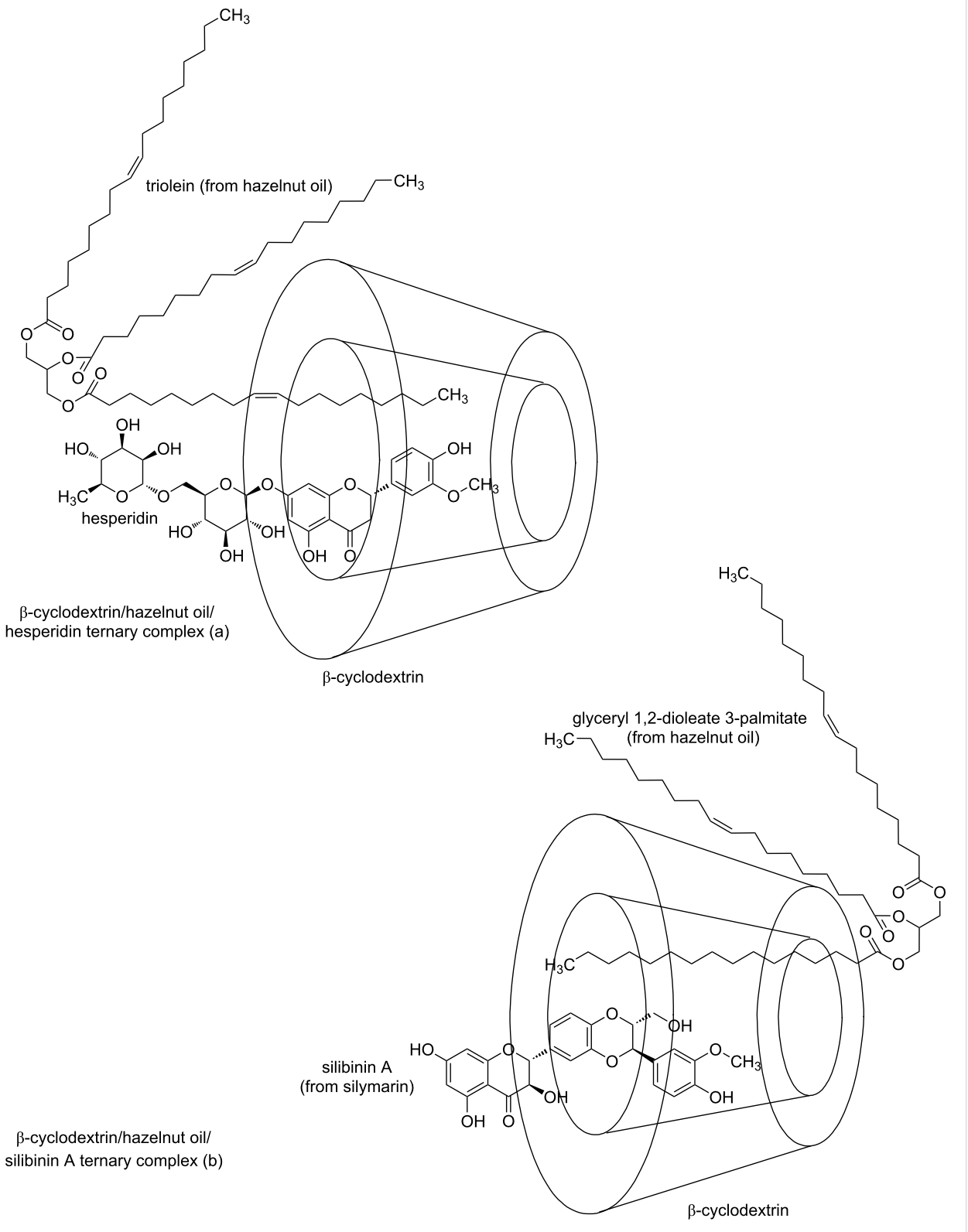


Figure 1: Hypothetical interactions between the β-cyclodextrin host and guest molecules (flavonoid glycoside/flavonolignan and a fatty acid triglyceride from the hazelnut oil), not explicitly proven in this study. (a) Both triolein from hazelnut oil and hesperidin interact with β-cyclodextrin from the secondary face; (b) glyceryl 1,2-oleate 3-palmitate from hazelnut oil interacts with the β-cyclodextrin from the primary face, while silibinin A, the main component of silymarin, interacts with β-cyclodextrin from the secondary face.

dation, in combination with a protection/stabilization through CD nanoencapsulation. Moreover, the apparent water solubility, bioaccessibility, bioavailability, and controlled release of the guest bioactive compounds can also be enhanced by ternary complexation.

Results and Discussion

Synthesis and thermal analysis of the ternary complexes

The complexity of the starting materials, especially that of hazelnut oil, as well as the differences among their characteristics (hydrophobicity and water solubility) suggest the kneading method as the most appropriate one for obtaining β-CD/hazelnut (*Corylus avellana* L.) oil/flavonoid glycoside or flavonolignan ternary complexes. Kneading allows for higher recovery yields of complexes in comparison with the co-crystallization method because only small amounts of solvent are needed for preparation. On the other hand, similar methods such as spray-drying do not provide intimate contact between the three types of components for a sufficient period of time to reach the association–dissociation equilibrium [1,27,67]. In this study, the recovery yields were in the range of 51.5–85.3%, and significantly higher for the 3:1:1 complexes. Equimolar X1H, X1N, X1R and X1S ternary complexes were obtained with yields of 57.7 (± 8.8), 54.6 (± 1.9), 74.3 (± 1.8), and 64.7 (± 2.6)%, respectively. For the 3:1:1 ternary complexes (single samples) these yields were in the range of 74.5–85.3%. The difference in the yield can be explained by the level of hydration, as was determined by TG (see below). For the 1:1:1 complexes, the mass loss is half in comparison with the water content of β-CD (6.4–7.4% for complexes and 14% for β-CD hydrate). On the other hand, the mass loss of the 3:1:1 complexes is much higher (e.g., 11.8% for X3N complex). As a consequence, the 1:1:1 complexes lose relatively more hydration water than the corresponding 3:1:1 complexes. This can be explained by the high level of complexation for the 1:1:1 complexes. This aspect could be confirmed by thermal analysis, especially by DSC.

Both TG–DTG and DSC thermal analyses provide information about the molecular inclusion of guest molecules into the β-CD cavity. Unfortunately, these methods cannot differentiate between the encapsulated components and their entrapment efficiency. However, the goal of the study was the discrimination of such ternary complexes on the basis of FTIR. The evaluation of the encapsulation competitiveness of such multicomponent mixtures is very challenging (highly hydrophobic FA triglycerides, mono- and diglycerides, free FAs, as well as more hydrophilic flavonoid glycoside, namely hesperidin, naringin and rutin, or flavonolignan – silibinins). According to TG-DTG and DSC analyses, the ternary complexes are highly stable up to 200 °C. The TG and DTG plots were similar for ternary complexes at a 1:1:1 molar ratio, in comparison with the β-CD hydrate at temperatures up to ≈200 °C. The only significant difference was observed for the mass loss corresponding to water/moisture release up to ≈110 °C, with values of 6.37–7.38% and 9.45% for β-CD hydrate, respectively. A lower mass loss was observed for β-CD hydrate in comparison with the water content provided by the manufacturer (maximum 14% by oven drying). This could be due to the TG protocol, which assumes the pre-equilibration of the microbalance prior to analysis. Consequently, loss of surface water could have taken place before the start of the analysis. However, the difference of 2–3% for the ternary complexes at 1:1:1 molar ratios can be explained by a partial replacement of water molecules during the molecular encapsulation of the FA triglyceride and flavonoid guest molecules. On the other hand, the mass loss for the 3:1:1 ternary complexes was similar to the one observed of β-CD hydrate or even higher (see Supporting Information File 1, Figures S1–S4 and Tables S1 and S2). This means that a significant amount of β-CD is not involved in the formation of complexes and remains as β-CD hydrate in the mixture. These observations are in agreement with other studies on the complexation of vegetable (common bean lipids) and fish oil (common barbel, Pontic shad, European wels catfish, common bleak) by CDs [11,17]. Moreover, this TG behavior does not depend on the method of synthesis (kneading or co-crystallization) or the method of water determination (TG as mass loss or Karl Fischer water titration, KFT) [6,68]. It was observed that the difference between the water content or TG mass loss up to ≈110 °C is lower for binary complexes of CD/flavonoids in comparison with CD/fish oil (Atlantic salmon or European anchovy) [12,14,43]. The TG results are in agreement with the DSC data, where the calorimetric effect corresponding to water/moisture release is lower for the ternary complexes (378 J/g for X1N and 432 J/g for β-CD hydrate, Supporting Information File 1, Figure S5 and Table S3). There are two aspects that can be observed in the DSC but not in the TG–DTG analyses. The first aspect is the presence of two types of water molecules in the ternary complexes. They appear at two specific DSC peak temperatures of 44.5 °C for surface water and 82.0 °C for the stronger retained water molecules. While the surface water-related temperature is quite similar to β-CD hydrate, the stronger retained water has a higher DSC peak temperature value for β-CD (94.7 °C). This observation confirms the partial replacement of strongly retained water molecules during the complexation process. The second observation on DSC results is related to the absence of an endothermal–exothermal calorimetric peak in the case of the X1N ternary complex. This peak appears at 218.9 °C for β-CD hydrate and means that the complex obtained by kneading has an amorphous structure, in comparison with crys-

talline β-CD hydrate. The calorimetric peak observed for β-CD hydrate at this temperature is due to the transition of anhydrous β-CD (after water release) from the crystalline to the amorphous state [6]. Finally, TG analysis indicates a mass loss of 1.4–4.0% in the temperature range of 110–275 °C for the 1:1:1 ternary complexes and only 1.25% for the 3:1:1 complexes, whereas almost no mass loss was observed for β-CD hydrate (0.05%). The degradation of β-CD appears above 275 °C, with a maximum degradation rate at 299.4–326.0 °C as determined by DTG (the highest for β-CD) and at ≈322 °C by DSC. The degradation of the encapsulated hazelnut oil – of the triglyceride components – appears at a higher temperature of 394–407 °C (DTG and DSC).

Fourier-transform infrared spectroscopy (FTIR) of ternary complexes

FTIR is a fast method that allows the evaluation of the presence of a compound in a complex through specific absorption bands. β-CD consists of seven 1→4-linked α-D-glucopyranose units forming a macrocycle. As a consequence, the FTIR specific bands especially appear for OH, CC and CH/CH_2 bonds and groups. However, CD specific bands also appear for CH groups in the CD ring and α-type glycosidic bonds. Thus, a broad FTIR band corresponding to the stretching vibration of the O–H bonds in β-CD and hydration water molecules appears at ≈3301 cm^{-1}. A weak band for the asymmetric stretching vibrations of the C–H groups appears at 2924.8 (± 1.4) cm^{-1}, while the bending vibrations (in-plane, asymmetric, and symmetric) of the OH and CH groups appear as weak bands in the range of 1205–1643 cm^{-1}. The stretching vibrations of the C–O and C–C groups in the glucoside moieties appear as medium-strong bands in the range of 998–1152 cm^{-1}. A specific band for CD appears at 939.2 (± 1.8) cm^{-1} and is assigned to the stretching vibrations of the C–H groups from the β-CD ring. Also, the band at 852.9 (± 0.8) cm^{-1} is attributable to the bending vibrations of the C–C–H groups related to the α-type glycosidic bonds in the CD. Other bands appear at wavenumbers lower than 800 cm^{-1} and were tentatively assigned to the bending vibrations of the CH and OCC groups (574–754 cm^{-1}), as well as to the stretching vibrations of the CC bonds at 526.3 (± 1.3) cm^{-1} [69,70]. Relevant data from the FTIR analysis of β-CD is presented in Figure 2 and Figure 3 and in Supporting Information File 1 (Figures S6–S11 and Table S4).

Vegetable oils and animal fat especially contain FA triglycerides, but mono-, diglycerides and free FAs also exist. As a consequence, the broad band corresponding to the stretching vibrations of the O–H groups is attributable to free fatty acids,

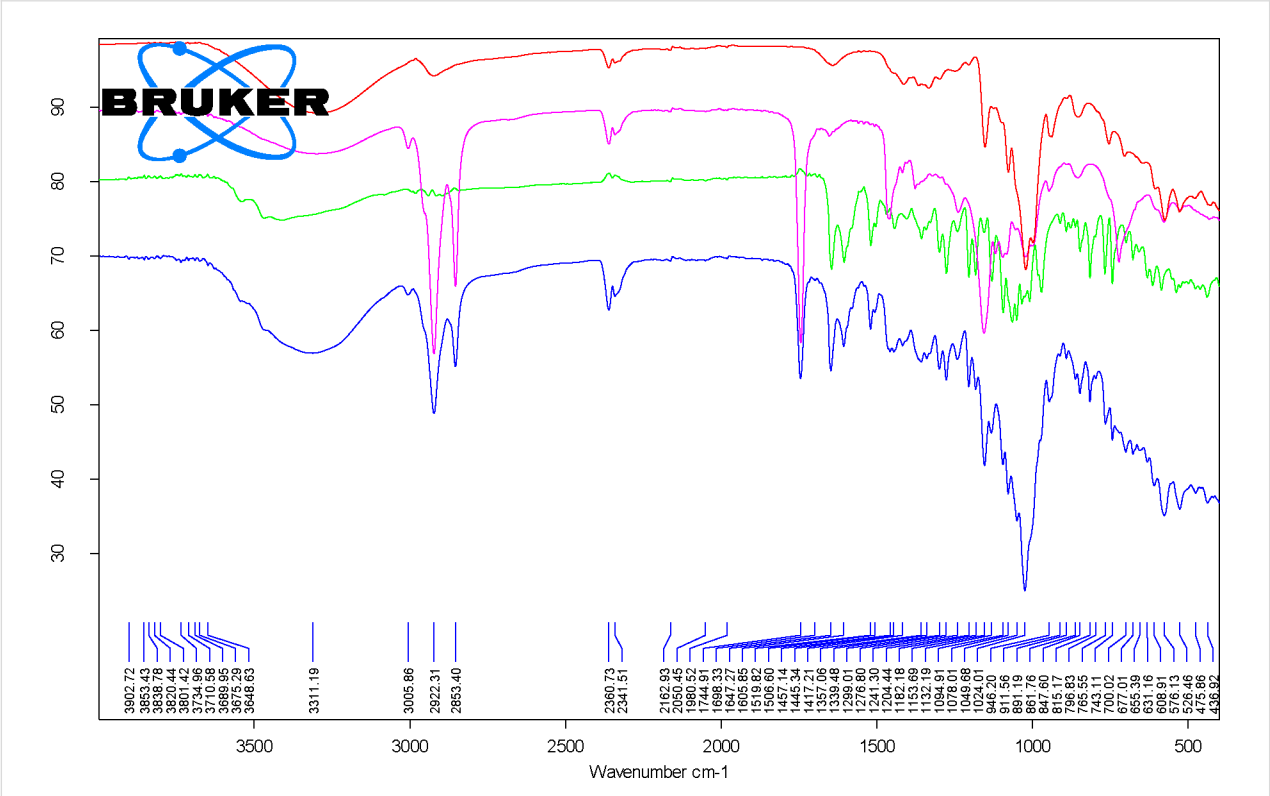


Figure 2: Superposition of the FTIR spectra for the β-cyclodextrin/*Corylus avellana* oil/hesperidin ternary complex at a 1:1:1 molar ratio (blue), β-cyclodextrin hydrate (red), *C. avellana* oil (pink), and hesperidin (green).

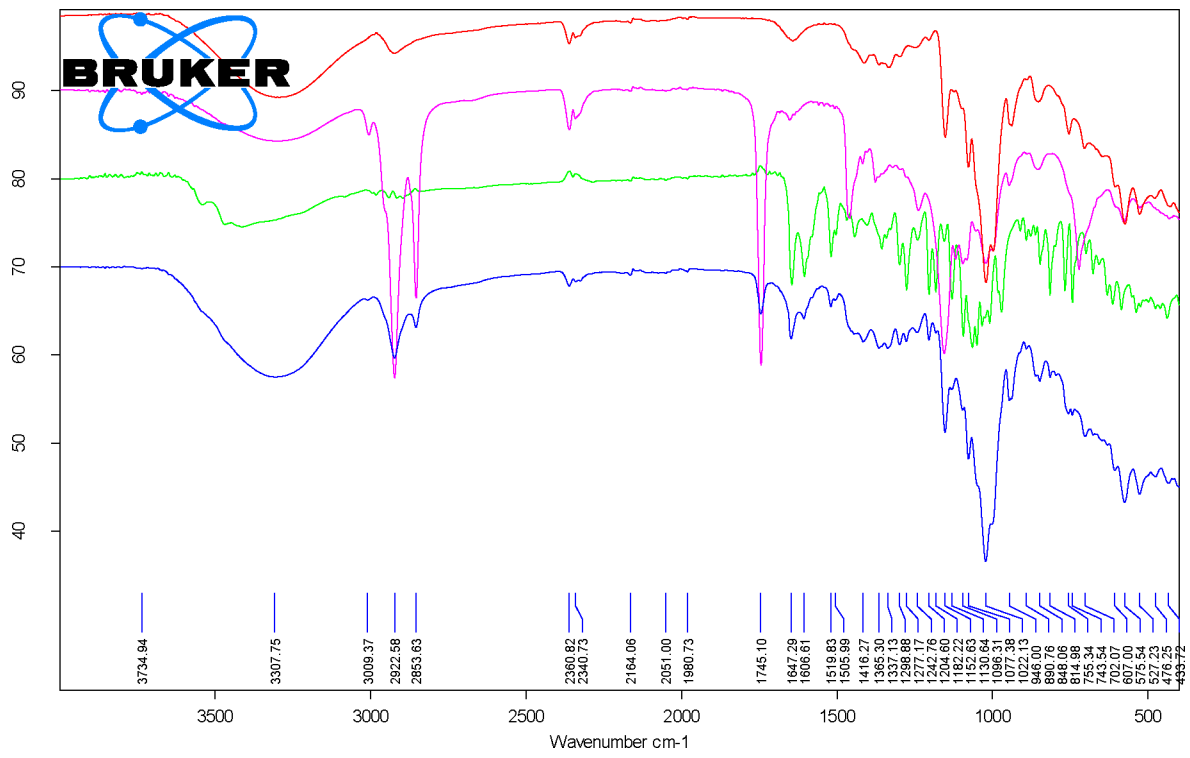


Figure 3: Superposition of the FTIR spectra for the β-cyclodextrin/*Corylus avellana* oil/hesperidin ternary complex at a 3:1:1 molar ratio (blue), β-cyclodextrin hydrate (red), *C. avellana* oil (pink), and hesperidin (green).

monoglycerides, diglycerides and water. In the hazelnut samples, this band was observed at 3287.8 (± 10) cm^{-1}. In this study, very useful was the weak band at 3005 (± 0.2) cm^{-1}, which corresponds to the symmetric stretching vibrations of the =CH groups from the mono- and polyunsaturated FA moieties (especially oleic acid, but also palmitoleic and linoleic acids). The asymmetric and symmetric stretching vibrations of the CH groups provide strong bands at 2952.5 (± 0.3), 2922.5 (± 0), and 2853.2 (± 0) cm^{-1} due to the high number of CH_2 and CH_3 groups in the triglyceride structures. Another important and characteristic FTIR band for glycerides is that corresponding to the stretching vibrations of the ester C=O groups that appears as very strong band at 1744 (± 0) cm^{-1} for hazelnut oil. The stretching vibration of the *cis*-RHC=CHR' group is observed as a weak band at 1652.7 (± 0.3) cm^{-1}. Medium and strong bands are those related to the bending vibrations of the CH_2 and CH_3 groups at 1458.7 (± 0.2) cm^{-1}, bending vibrations of the CH_2 groups at 1236.8 (± 1.3) and 1158.1 (± 2.3) cm^{-1}, the stretching vibrations of the C–O groups at 1027.9 (± 5.7) cm^{-1}, as well as the out-of-plane bending vibrations in the C–H groups at 722 (± 0.1) cm^{-1}. Degradation/isomerization of oil components (low level) can be observed at 956.7 (± 8.7) cm^{-1}, where the band corresponding to the bending vibrations of the C=C groups in *trans*-RHC=CHR' groups appears (sometimes at slightly higher values). Details of the FTIR analysis of hazelnut oil samples can be seen in Figure 2 and Figure 3 and in Supporting Information File 1 (Figures S6–S11 and Table S5) [71].

Hesperidin, naringin, and rutin are flavonoid glycosides derived from the corresponding flavanones hesperetin and naringenin and the flavonol quercetin, respectively. These compounds have a disaccharide moiety connected to the aglycones through an ether linkage with the hydroxy groups in the 7 and 3 positions (Figure 1a). On the other hand, silibinins (the main components of silymarin) are flavanonol derivatives, having a coniferyl alcohol moiety connected through the hydroxy groups in the 3' and 4' positions of the aglycone (Figure 1b). FTIR analysis of these flavonoids revealed stretching and bending vibrations corresponding to OH bonds (phenolic or alcoholic, glycosidic and OH groups from water molecules), CH bonds (especially from the CH_2 and CH_3 groups), bands corresponding to the aromatic CC bonds, and the carbonyl C=O bond. The most relevant FTIR band for these compounds is the asymmetric stretching vibration of the C=O bonds, $\nu^{as}{}_{C=O}$, which appears around 1633–1651 cm^{-1}. The lowest value for this band was observed for silymarin at 1634.1 (± 0.4) cm^{-1} and the highest one for rutin at 1651 (± 0.1) cm^{-1}. For hesperidin and naringin this band appears at approximately the same value (≈1645 cm^{-1}).

The stretching vibrations of phenolic, glycosidic or water O–H bonds appear as broad bands in the range of 3263–3541 cm^{-1}. Asymmetric and symmetric stretching vibrations of the C–H bonds in CH_3 and CH_2 groups appear at 2931–2941 cm^{-1}. Similar FTIR bands also appear at 2982, 2907–2914, and 2876–2897 cm^{-1} in flavonoid glycosides. In the spectra of these compounds the bending vibrations of the aromatic CC groups appear at 1583–1604 cm^{-1} and ≈1518 cm^{-1}, some of them being superimposed by the stretching vibrations of the C–C group in the ring C of aglycones. The stretching of a C–C group also appears in silymarin/silibinins at 1509.9 (± 0.6) cm^{-1}, while this value is significantly lower for flavonoid glycosides (1502–1504 cm^{-1}). Other bending vibrations were observed for CH bonds in the range of 1393–1468 cm^{-1}, while the stretching vibrations for CC and CO bonds and the bending vibrations for HOC, OCH, an HCC groups were superimposed in the range of 1011–1364 cm^{-1}. The stretching vibration of the O–C groups in all flavonoids appears at 968–995 cm^{-1}. Finally, out-of-plane bending vibrations of CH groups and twisting bending vibrations of COH and HCCC groups appear in the range of 742–921 cm^{-1} [72-77]. All wavenumber values corresponding to the specific FTIR bands as well as the superimposed FTIR spectra of flavonoids with the other components of the ternary complexes are presented in Figure 2 and Figure 3 and in Supporting Information File 1 (Figures S6–S11 and Tables S6–S9).

The synthesized ternary complexes reveal the medium and strong FTIR bands of the above-mentioned host and guest components. However, FTIR bands that appear in specific regions where no interference occurs can also be relevant for the presence of individual compounds in the complex. This is the case for the weak band corresponding to the symmetric stretching vibrations of =CH groups from unsaturated glycerides in the hazelnut oil, which appear at 3006.5 (± 1), 3006.4 (± 0.6), 3006.3 (± 1.1), and 3006.6 (± 1.6) cm^{-1} for the X1H, X1N, X1R, and X1S ternary complexes at 1:1:1 molar ratios, respectively. These values are slightly higher by 1.1–3.1 cm^{-1} for all 3:1:1 ternary complexes (see Figure 2 and Figure 3 and Supporting Information File 1, Figures S6–S11 and Tables S6–S9). The strong bands corresponding to the asymmetric and symmetric stretching vibrations of the C–H bonds in the aliphatic CH_3 and CH_2 groups, as well as to the stretching vibrations of the ester C=O groups in triglycerides from hazelnut oil are clearly visible in all ternary complexes at 2922–2924, 2853–2854, and 1744–1745 cm^{-1}, respectively. These values are very close to those corresponding to the starting hazelnut oil. Among other glyceride-related bands, those at 1453–1458 cm^{-1} originating from bending vibrations of the CH_2 and CH_3 groups, and 1236–1244 and 1152–1153 cm^{-1} from bending vibrations of the CH_2 groups are also representative in the ternary complexes. They generally appear at lower values in the first case and at significantly higher values in the latter case in comparison with the starting hazelnut oil (see Supporting Information File 1, Figures S6–S11).

The most relevant flavonoid-related FTIR bands for the ternary complexes are those corresponding to the asymmetric stretching vibrations of the C=O groups. They occur in the range of 1637–1652 cm^{-1} for ternary complexes. The stretching vibrations of the C–C group in the ring C of the flavonoid glycosides or the bending vibrations of the aromatic CC groups occur in the range of 1598–1608 cm^{-1}, but without specific variations in comparison with the starting compounds. The same is true for the band correlated to the in-plane bending vibrations of CH and OCH groups that appears at 1268–1299 cm^{-1}. Also, the stretching vibrations of the C–C groups in the flavonoid glycosides or the stretching vibrations of the C–O groups in silymarin components (lower values) are observed in the same region. Another band that is present in all ternary complexes and is assigned to flavonoids is found at 807–821 cm^{-1}, and corresponds to the out-of-plane bending vibrations of the C–H groups. This band appears at significantly lower values in rutin and rutin-related complexes.

β-CD was selected as the host for the formation of ternary complexes with the above-mentioned biologically active compounds and its content varies in complexes at 1:1:1 and 3:1:1 molar ratios. In the FTIR spectra of β-CD as a host, besides the wavenumbers corresponding to characteristic bands of β-CD, their intensities are relevant for the discrimination of the ternary complexes. However, many β-CD-related bands are weak or have at least medium intensities in the range of 1200–4000 cm^{-1}. The most relevant bands for ternary complexes were the medium-strong intensity bands at 1152–1154 cm^{-1} (stretching vibrations of the C–O–C groups in the glucoside moieties), 1077–1080 cm^{-1} (stretching vibrations of the C–C groups), 1022–1026 cm^{-1} (stretching vibrations of the C–O groups), 944–947 cm^{-1} (stretching vibrations of the C–H groups from the β-CD ring), and two other medium intense bands at 574–576 and 522–529 cm^{-1}, which were tentatively assigned as bending vibrations of the O–C–C groups and stretching vibrations of the C–C groups, respectively (see Figure 2 and Figure 3 and Supporting Information File 1, Figures S6–S11 and Tables S4, and S6–S9).

Discrimination of ternary complexes by Fourier-transform infrared spectroscopy coupled with principal component analysis (FTIR–PCA)

Taking into account the differences between the wavenumbers and intensities of specific stretching and bending vibrations of

β-CD hydrate, raw hazelnut oil, and flavonoids in the pure form and as ternary complexes, a multivariate statistical analysis technique was applied for the discrimination of these samples and identification of the important FTIR variables for such classifications. PCA is a widely used multivariate statistical analysis technique that can extract valuable information from a large dataset. It is the case of FTIR data (both wavenumbers and intensities), where were assigned 20, 17, 34, and 33 FTIR bands for β-CD hydrate, hazelnut oil, flavonoids, and ternary complexes, respectively (see Supporting Information File 1, Tables S4–S9). On the other hand, not all FTIR bands corresponding to the starting compounds can be observed and assigned for the ternary complexes. PCA works with a complete variable matrix. As a consequence, only the FTIR bands that were identified in both the starting materials and the ternary complexes were considered for PCA analysis (see Table 1 and Supporting Information File 1, Tables S10–S12). This matrix is transformed in order to obtain the maximum variance of the data. The new axes are denominated Factors or Principal Components (PCs). The translation coordinates will provide the scores plots that reveal the similarities/dissimilarities between cases (samples), while the representation of the rotation coordinates of the axes (direction cosines) will give information about the influence of variables to the classification of cases. Only few PCs will extract the useful information from the dataset. As a consequence, the large number of variables will be reduced to only 2–4 PCs that will explain the variance of the data.

Discrimination of flavonoid glycosides and flavonolignans

Twenty-two variables were considered for the discrimination of flavonoids (flavonoid glycosides – hesperidin, “H”, naringin, “N”, rutin, “R”, and flavonolignans – silymarin, “S”). They correspond to wavenumbers and intensities of the FTIR bands identified for all flavonoids (Supporting Information File 1, Table S10). The flavonoid samples were clearly grouped, according to the PC_2 vs PC_1 or PC_3 vs PC_1 scores plot (Supporting Information File 1, Figures S12 and S13). Better results were obtained when only wavenumbers were used as PCA variables (Figure 4). All flavonoid glycosides are classified in the positive region of the PC_1, in comparison with flavonolignans (silymarin components). According to FTIR–PCA analysis, hesperidin, naringin, and rutin are more similar and all of them are dissimilar to silymarin. This classification is especially due to the bands corresponding to stretching vibrations of the C=O groups and bending vibrations for the CH groups for the positive region of PC_1, as well as to the stretching vibrations of the CO and CC bonds for the negative part (Table 1 and Support-

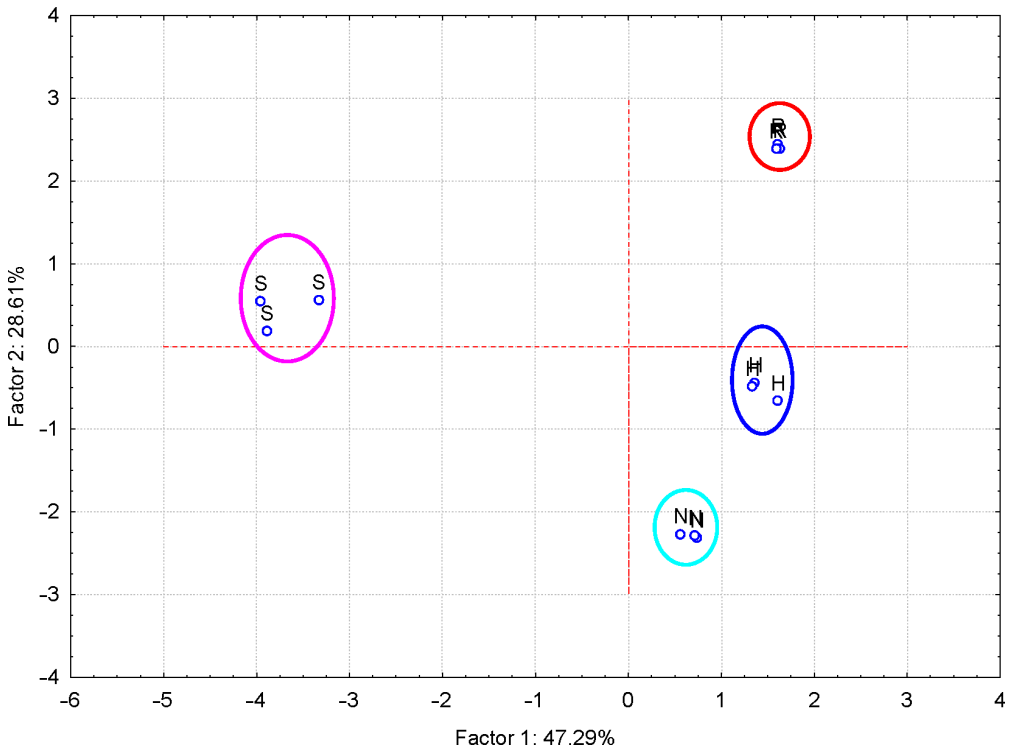


Figure 4: PC_2 versus PC_1 scores plot from the FTIR–PCA analysis of the flavonoid glycoside and flavonolignan antioxidants (codes: “H” – hesperidin, “N” – naringin, “R” – rutin and “S” – silymarin); only wavenumbers of the FTIR bands were used as input variables.

Table 1: Factor coordinates (principal components, PCs) of the variables, based on correlations from the FTIR–PCA analysis of the flavonoid glycoside and flavonolignan antioxidants; only wavenumbers ("v" – for stretching vibrations, "d" – for bending vibrations) of the FTIR bands were used as input variables.

	PC_1	PC_2	PC_3
v(OH)	0.763	−0.616	−0.182
vas(CH)	−0.090	0.565	−0.780
vs(CH)	0.233	−0.781	−0.563
d(OH)/vas(C=O/C=C)	0.930	0.323	0.165
d(arC#C)	0.595	0.714	0.353
d1(CH2/3)	−0.350	0.026	−0.931
v1(CO)/d1(CO)	−0.416	0.797	−0.435
d1(CH)	0.986	−0.142	−0.061
v(CO)/v(CC)	0.937	0.128	−0.321
v(CO)/v(CC/CO)	−0.940	0.077	0.302
d4(CH)	−0.557	−0.739	0.049

ing Information File 1, Figures S14–S18 and Table S10). In this latter case, only the first three PCs explain 97.41% of the variance of the FTIR data, with the highest value for PC_1 (47.29%; see the eigenvalues greater than 1 in Figure S19, Supporting Information File 1).

Discrimination of ternary complexes and β-CD hydrate samples

In the same way, ternary complexes and native β-CD hydrate samples were classified according to specific FTIR wavenumbers and intensities of the bands identified in all samples. β-CD hydrate samples were classified in the top-right region of the PC_2 vs PC_1 scores plot (codes "Y"), in comparison with the ternary complexes in the center-left and bottom of the plot. Moreover, such grouping can also be observed for some ternary complexes types (e.g., "X1H" in the left and "X3R" in the top-left of the plot, Figure 5). Few FTIR variables are responsible for the discrimination of ternary complexes and β-CD samples, especially those related to band intensities corresponding to bending vibrations of CH_2 groups and stretching vibrations of various bonds including those from CCO, CCC, CO and COC systems (PCA results are not presented).

Discrimination of ternary complexes and flavonoids

More interesting were the results obtained for the FTIR–PCA analysis of ternary complexes and flavonoids. A total of 18 FTIR variables (both wavenumbers and intensities, Supporting Information File 1, Tables S11 and S12) were identified in all ternary complexes and flavonoids. They were used as input

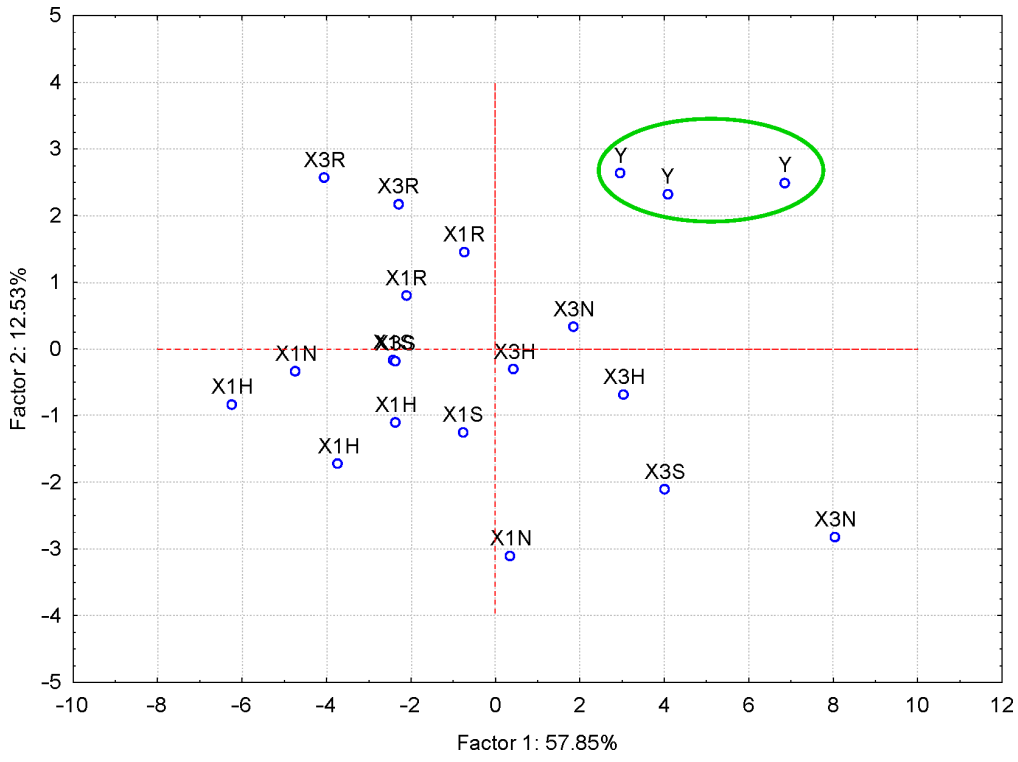


Figure 5: PC_2 versus PC_1 scores plot from the FTIR–PCA analysis of the β-CD/hazelnut oil/flavonoid ternary complexes (codes: "X1H/N/R/S" and "X3H/N/R/S" for the 1:1:1 and 3:1:1 ternary complexes with hesperidin/naringin/rutin/silymarin, respectively) and β-CD hydrate (code: "Y"); all wavenumbers and intensities of the FTIR bands were used as input variables.

variables for the discrimination of complexes and guest compounds. Also, the wavenumbers and intensities sets were used separately for the discrimination. Flavonoids were clearly classified in the left side of the PC_2 vs PC_1 scores plot (Figure 6). Wavenumbers of the bands corresponding to the stretching vibrations of the CO and CC bonds for the positive side, as well as the intensity of the band corresponding to the asymmetric stretching vibration of the CH bond for the negative side of the PC_1 were the most important for this classification (see also Supporting Information File 1, Figure S20 for the PC_3 vs PC_1 scores plot, Figures S21and S22 for the corresponding loadings plots, and Table S11 for the influence of variables on the classification). Better results were obtained if only wavenumbers were used as input variables for the FTIR–PCA analysis of ternary complexes and the starting flavonoids. All flavonoids were grouped in the right side of the PC_2 vs PC_1 scores plot, with higher similarity for hesperidin, naringin, and rutin (Figure 7). On the other hand, all ternary complexes were located in the left side of this plot, also sub-classified according to the presence of specific flavonoids. In a similar manner, ternary complexes based on silymarin are dissimilar with the other complexes, which have a high level of similarity. These observations are also sustained by the other scores plots, all with very good classifications of the samples (Figure 8 and Figure 9). Responsible for these classifications are the variables corresponding to the FTIR bands related to symmetric and asymmetric stretching vibrations of the CH bonds (positive PC_1), stretching vibrations of the CC and CO bonds (negative PC_1), stretching and bending of C=O and OH/CH, respectively (negative PC_2) (Figure 10 and Figure 11, Supporting Information File 1, Table S12). Only the first three PCs were used for obtaining these valuable discrimination results. They explain almost all variances of the FTIR data, as is presented in Figure 12 (85.69%).

Conclusion

The β-CD/hazelnut oil/flavonoid ternary complexes are innovative materials synthesized for the first time, which combine the valuable properties of the specific components, the host – β-CD and the guests – the antioxidant and the essential FA glyceride compounds. β-CD encapsulation enhances the apparent water solubility of both hazelnut triglyceride components (e.g., triolein) and flavonoid glycosides/flavonolignans. They both have significantly lower water solubility and thus low bioaccessibility and bioavailability. They are enhanced by β-CD co-encapsulation. On the other hand, the encapsulated flavonoid molecule can act as on-site antioxidant and protect the labile

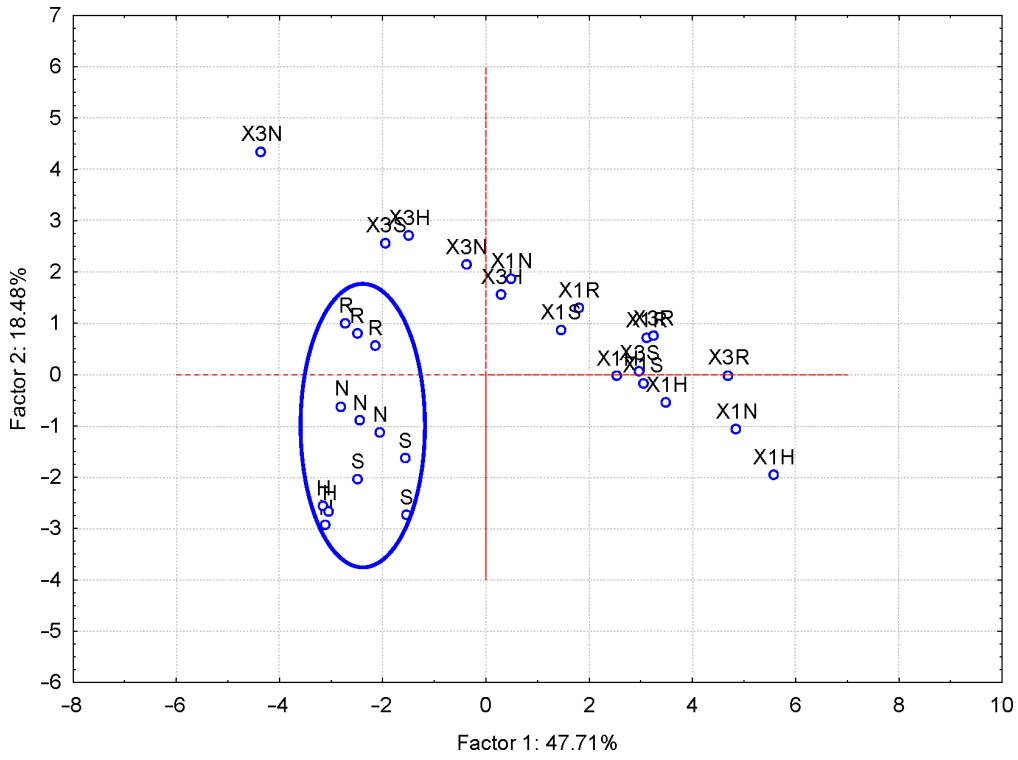


Figure 6: PC_2 versus PC_1 scores plot from the FTIR–PCA analysis of the β-CD/hazelnut oil/flavonoid ternary complexes (codes: "X1H/N/R/S" and "X3H/N/R/S" for the 1:1:1 and 3:1:1 ternary complexes with hesperidin/naringin/rutin/silymarin, respectively) and flavonoids (codes: "H" – hesperidin, "N" – naringin, "R" – rutin and "S" – silymarin); all wavenumbers and intensities of the FTIR bands were used as input variables.

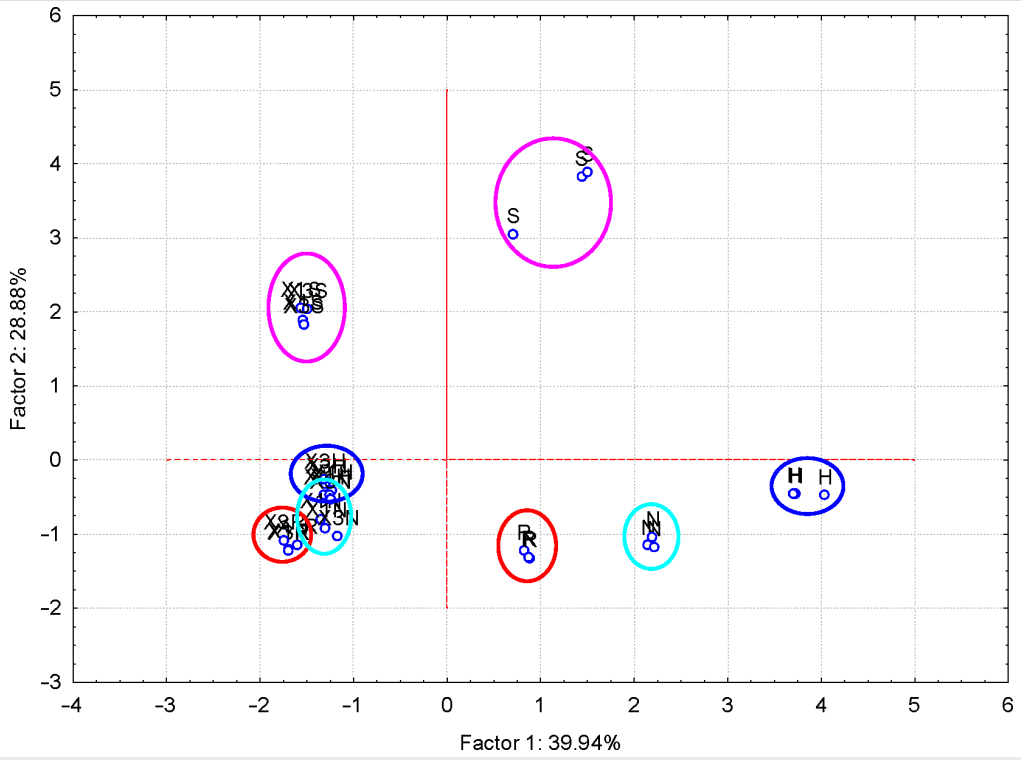


Figure 7: PC_2 versus PC_1 scores plot from the FTIR–PCA analysis of the β-CD/hazelnut oil/flavonoid ternary complexes (codes: "X1H/N/R/S" and "X3H/N/R/S" for the 1:1:1 and 3:1:1 ternary complexes with hesperidin/naringin/rutin/silymarin, respectively) and flavonoids (codes: "H" – hesperidin, "N" – naringin, "R" – rutin and "S" – silymarin); only wavenumbers of the FTIR bands were used as input variables.

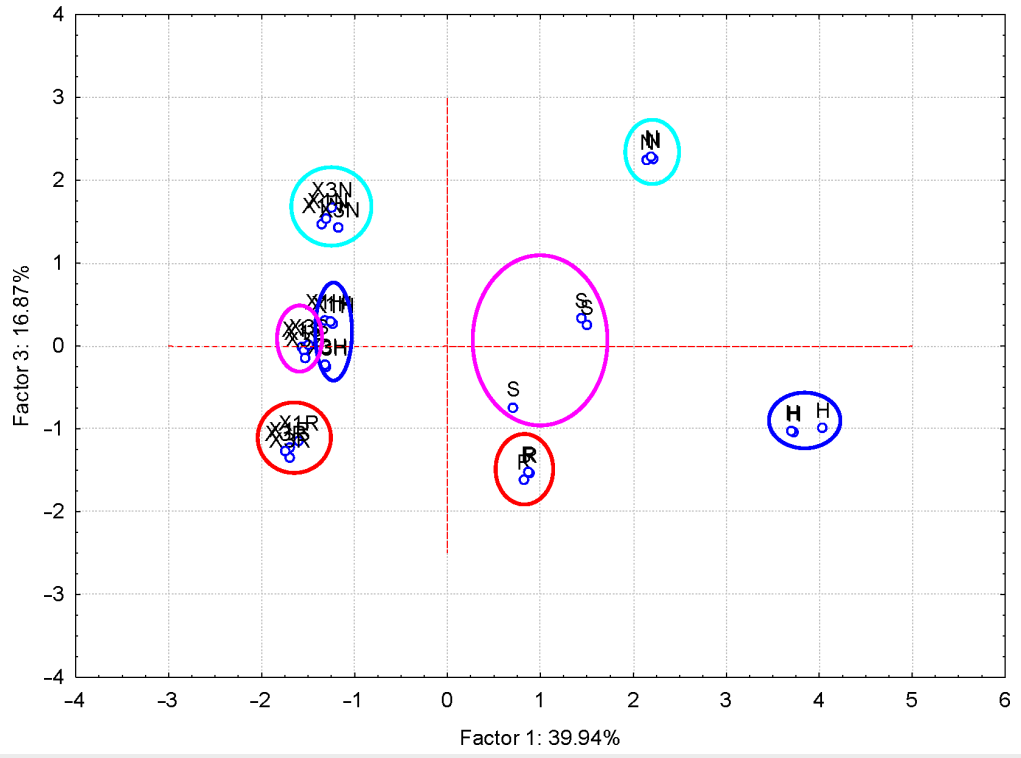


Figure 8: PC_3 versus PC_1 scores plot from the FTIR-PCA analysis of the β-CD/hazelnut oil/flavonoid ternary complexes (codes: "X1H/N/R/S" and "X3H/N/R/S" for the 1:1:1 and 3:1:1 ternary complexes with hesperidin/naringin/rutin/silymarin, respectively) and flavonoids (codes: "H" – hesperidin, "N" – naringin, "R" – rutin and "S" – silymarin); only wavenumbers of the FTIR bands were used as input variables.

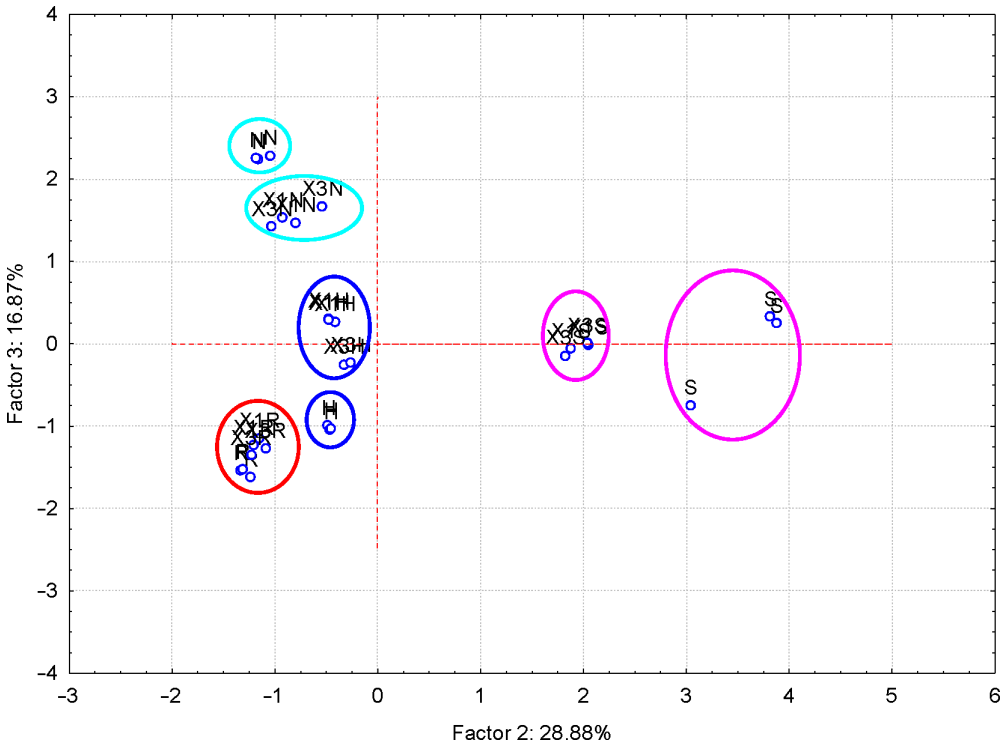


Figure 9: PC_3 versus PC_2 scores plot from the FTIR–PCA analysis of the β-CD/hazelnut oil/flavonoid ternary complexes (codes: "X1H/N/R/S" and "X3H/N/R/S" for the 1:1:1 and 3:1:1 ternary complexes with hesperidin/naringin/rutin/silymarin, respectively) and flavonoids (codes: "H" – hesperidin, "N" – naringin, "R" – rutin and "S" – silymarin); only wavenumbers of the FTIR bands were used as input variables.

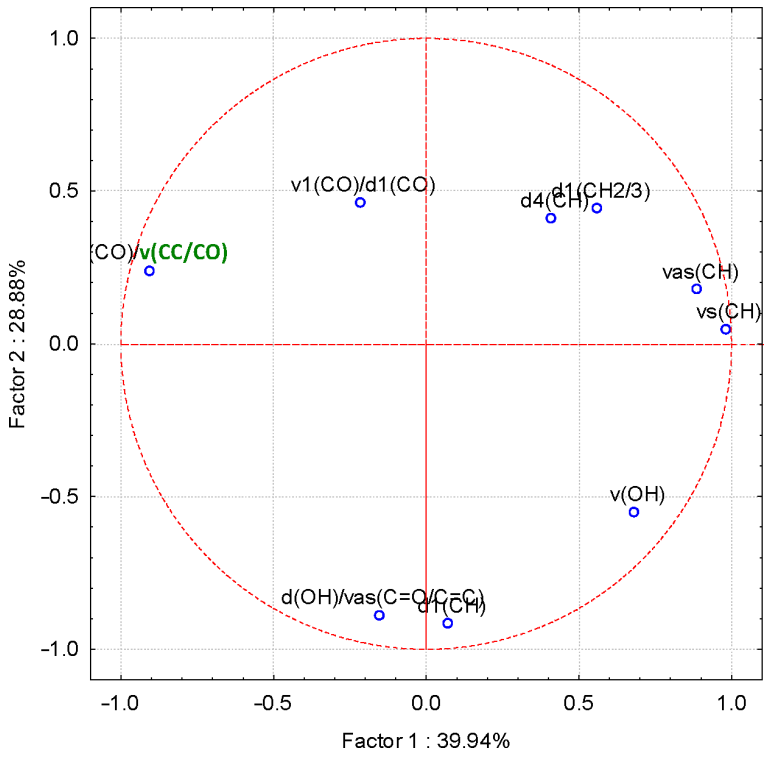


Figure 10: PC_2 versus PC_1 loadings plot from the FTIR–PCA analysis of the β-CD/hazelnut oil/flavonoid ternary complexes and flavonoids; only wavenumbers of the FTIR bands were used as input variables (see Table S12 in Supporting Information File 1 for codes).

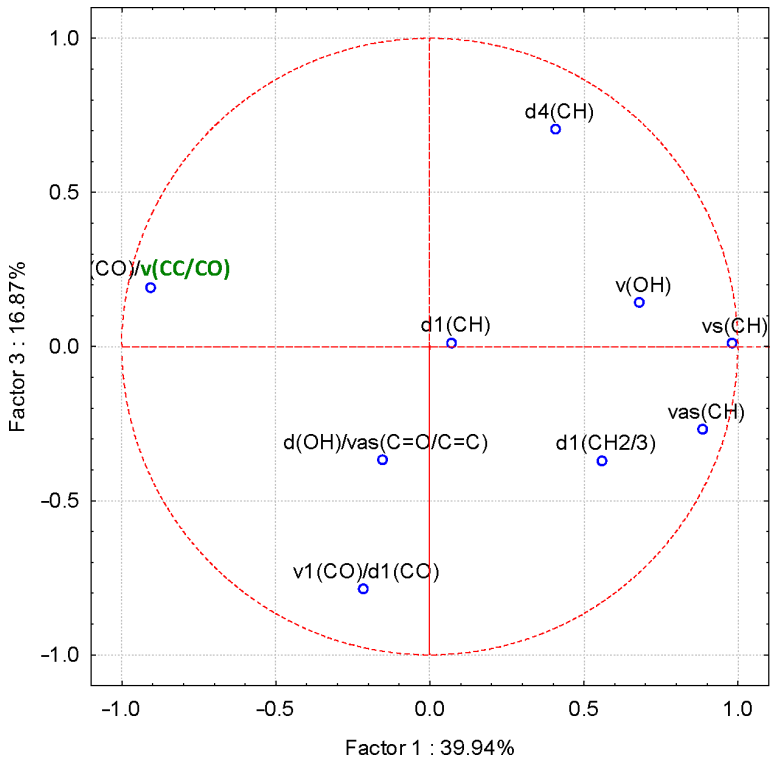


Figure 11: PC_3 versus PC_1 loadings plot from the FTIR–PCA analysis of the β-CD/hazelnut oil/flavonoid ternary complexes and flavonoids; only wavenumbers of the FTIR bands were used as input variables (see Table S12 in Supporting Information File 1 for codes).

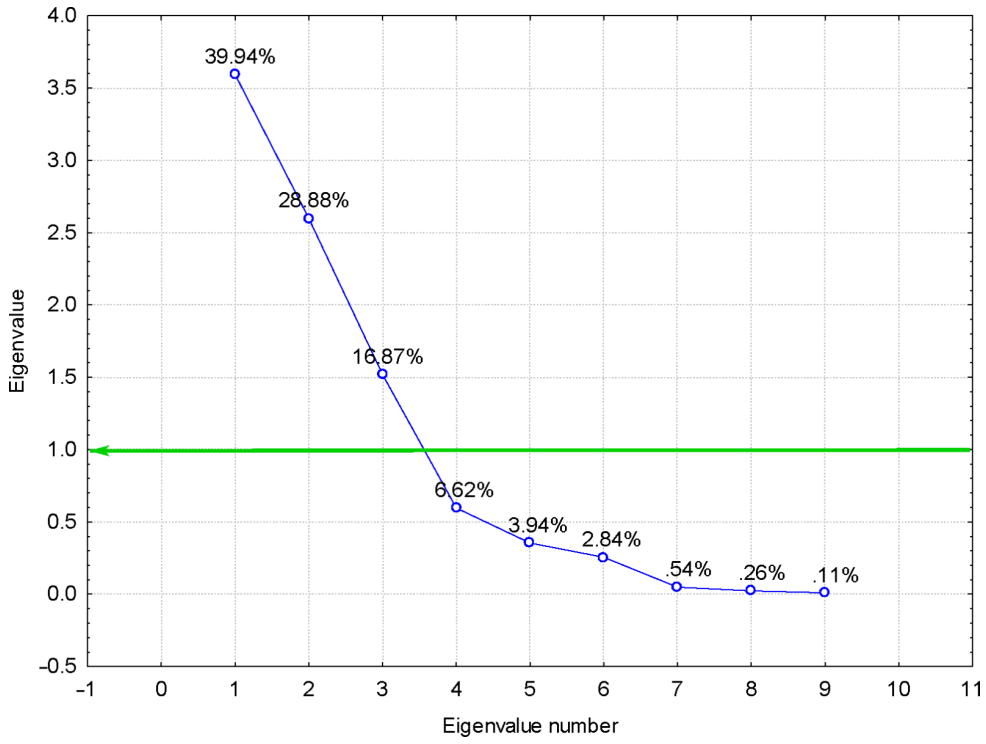


Figure 12: Eigenvalues of the correlation matrix from the FTIR–PCA analysis of the β-CD/hazelnut oil/flavonoid ternary complexes and flavonoids; only wavenumbers of the FTIR bands were used as input variables (see Table S12 in Supporting Information File 1 for codes); the first three PCs can be retained, which explain 85.69% from the variance of the data.

hazelnut oil components that contain unsaturated FA moieties. The thermal/oxidative stability of ternary complexes is similar to β-CD hydrate, as was evaluated by TG and DSC. Moreover, the formation of the molecular inclusion complexes is supported by thermal analysis (partial replacing of the hydration water by biologically active molecules and disappearance of the DSC peak corresponding to crystalline–amorphous transition). In the present study, an appropriate synthesis method for ternary complexes (from the applicative point of view) was used. Also, a very fast, cheap and nondestructive technique, namely FTIR–PCA, was used for discrimination between ternary complexes (by the antioxidant used or by the molar ratio) and the starting components. β-CD/hazelnut oil/flavonoid ternary complexes at a 3:1:1 ratio had spectroscopic and thermal behavior more close to the native β-CD hydrate, in comparison with the 1:1:1 complexes. This observation indicates that not all FA moieties interact with the β-CD host molecules. This was the reason to use such non-equimolar ratios. If a theoretical 3:1 interaction can be considered, the formation of such β-CD/triglyceride supramolecular system in practice is limited by the steric hindrance. On the other hand, ternary complexes and flavonoids were very well classified and discriminated by FTIR–PCA, especially through the type of antioxidant used. However, further synthesis methods and analyses (slow co-crystallization, single-crystal X-ray diffraction, ^{1}H and ^{13}C nuclear magnetic resonance analyses) are needed for the elucidation of the interactions in such complex supramolecular systems.

Experimental

Vegetable samples and chemicals

Hazelnut (*Corylus avellana* L.) oil was obtained from nut kernel by Soxhlet extraction. Wild hazelnuts were collected from the Apuseni Mountains (Transylvania, Romania, 46°22'46" N and 23°16'47" E) between September and October 2018 and were kept at room temperature, in the dark, and dry atmosphere for six months. Then, the kernels were manually separated, finely ground, and subjected to Soxhlet extraction using a 250 mL equipment. One hundred of hazelnut kernels were extracted five times with 300 mL of anhydrous petroleum ether (ACS reagent, 40–60 °C boiling range, Sigma-Aldrich, St. Louis, MO, USA). The extract was distilled and evaporated to dryness until no petroleum ether remained. The oil separation yield was ≈50%. The hazelnut oil was kept at −20 °C until further analyses and β-CD complexation.

β-CD hydrate, Kleptose®, was kindly donated by Roquette Frères S.A. (Lestrem, France) and had a purity of >98%, a water content of 14.0%, and maximum 0.5% α-CD and γ-CD. Flavonoid glycosides and flavonolignans used in the complexation process were hesperidin (code "H", $C_{28}H_{34}O_{15}$, M = 610.56 g/mol, purity ≥80%, other flavonoid glycosides as impurities), naringin hydrate (code "N", $C_{27}H_{32}O_{14}{\cdot}2H_2O$, M = 580.50 g/mol, purity ≥95%), rutin hydrate (code "R", $C_{27}H_{30}O_{16}{\cdot}xH_2O$, M = 610.52 g/mol, purity ≥94%), and silymarin (code "S", $C_{25}H_{22}O_{10}$, M = 482.44 g/mol, ≈70% silibinin A, other flavonolignans as impurities) and were purchased from Sigma-Aldrich, St. Louis, MO, USA. Ethanol used for complex synthesis was of 96% concentration (v/v) and was purchased from ChimReactiv (Bucharest, Romania). The analysis of the FA profile of the hazelnut oil required the derivatization (transesterification) of the FA glycerides to the corresponding FA methyl esters (FAMEs) [11,13]. The derivatization involved methanol–boron trifluoride (20% BF_3), hexane (GC grade) and anhydrous sodium sulfate, all purchased from Merck & Co., Inc., Rahway, NJ, USA. Sodium chloride (reagent grade) used for the separation of FAMEs was purchased from Reactivul (Bucharest, Romania). The identification of the FAME components of the hazelnut oil involved FAME37 standard mixture, as well as C_8–C_{20} linear alkane standard mixture for the determination of the specific retention index (RI) of compounds (both purchased from Sigma-Aldrich, St. Louis, MO, USA). Finally, 2-propanol (ACS reagent, Reag. Ph. Eur.) used for FTIR cleaning was obtained from Merck & Co., Inc., Rahway, NJ, USA.

Gas chromatography–mass spectrometry (GC–MS)

The FA profile of the hazelnut oil was determined by GC–MS, after derivatization to FAMEs. Derivatization was performed by quantitative transesterification in a 100 mL one-necked flask equipped with reflux condenser. 5 mL of BF_3·MeOH 20% and ≈100 mg of hazelnut oil were used for derivatization. The mixture was refluxed for at least 30 min, until no oil remained. Then, 2 mL of hexane was added and the mixture refluxed for another 15 min for completing the transesterification. The organic layer was separated in the neck region by adding a sufficient amount of saturated sodium chloride solution. The organic layer was transferred into a GC vial with ≈0.5 g of anhydrous sodium sulfate and stored at 4 °C until GC–MS analysis. GC–MS analysis was performed on a GC Hewlett Packard 6890 Series equipment, coupled with a Hewlett Packard 5973 Mass Selective Detector. The following GC conditions were used: Zebron 5-MS column (30 m length, 0.25 mm i.d., 0.25 μm film thickness), temperature program of 50–300 °C (heating rate 6 °C/min), injector temperature 300 °C, detector temperature 300 °C, carrier gas He (99.9999% purity), injected sample volume 2 μL, delay time 4 min. The MS conditions were: energy source EI 70 eV, temperature 150 °C, scan range 50–300 amu, scan rate 1/s. RI values were determined using a C_8–C_{20} alkane standard mixture and a RI vs RT correlation equation of $RI = 672.792 + 73.268{\cdot}RT - 3.287{\cdot}RT^2 + 0.148{\cdot}RT^3 - 0.00201{\cdot}RT^4$ [16]. On the other hand, the identifi-

cation of the main FAMEs from the derivatized hazelnut oil was performed by comparing the experimental RI values with those for the FAME standard mixture. Moreover, the experimental MS spectra were compared with those from the NIST/EPA/NIH Mass Spectral Library 2.0 (2011). Acquisition and handling of the GC–MS data were performed using the Enhanced MSD ChemStation D.02.00.275 (Agilent Technologies, Santa Clara, CA, USA), while the MS identification was performed with the NIST Mass Spectral Search Program for the NIST/EPA/NIH Mass Spectral Library 2.0 (Gaithersburg, MD, USA). Determinations were performed in duplicate and the main findings reveal a high oleic acid relative content (as methyl ester) of 69.91(± 4.14) % at a RI of 2096.4. The other important FAs, as methyl esters, were palmitoleic, palmitic, linoleic, elaidic/vaccenic, and stearic acids with concentrations of 0.13, 7.54, 15.51, 2.85 and 2.73%, respectively (a total of 98.68% identified FAMEs in the hazelnut oil).

Synthesis of ternary complexes by the kneading method

The synthesis of β-CD/hazelnut oil/flavonoid glycoside or flavonolignan ternary complexes was performed using the kneading method, which is the most appropriate for such type of complexes [13,14,50]. In this study, two β-CD:hazelnut oil:flavonoid molar ratios of 1:1:1 and 3:1:1 were used. Particularly, 1322 (± 5) or 3959 (± 10) mg of β-CD hydrate (for 1:1:1 and 3:1:1 molar ratios, respectively), 909 (± 5) mg hazelnut oil, 613 (± 3) mg hesperidin, 628 (± 5) mg naringin hydrate, 656 (± 5) mg rutin hydrate and 488 (± 1) mg silymarin were weighted, taking into account the water content and purity of compounds. The mean molar mass for the hazelnut oil of M = 900 g/mol was determined as triolein, according to GC–MS data and a purity of ≈97% [33,78]. The following ternary complexes were obtained: β-CD/hazelnut oil/hesperidin at 1:1:1 and 3:1:1 molar ratios (codes "X1H" and "X3H"), β-CD/hazelnut oil/naringin at 1:1:1 and 3:1:1 molar ratios (codes "X1N" and "X3N"), β-CD/hazelnut oil/rutin at 1:1:1 and 3:1:1 molar ratios (codes "X1R" and "X3R") and β-CD/hazelnut oil/silymarin at 1:1:1 and 3:1:1 molar ratios (codes "X1S" and "X3S"). The amounts of β-CD, hazelnut oil, and flavonoid, corresponding to 1:1:1 or 3:1:1 were mixed in a preheated mortar at 60 °C. Then, 4 mL water and 1 mL ethanol for 1:1:1 complexes or 6 mL water and 1.5 mL ethanol for 3:1:1 complexes were added. The mixture was kneaded for at least 30 min, until a viscous paste is obtained. The mortar temperature decreases to the room temperature during kneading. The wet complex was dried until constant mass at room temperature in the dark. The dried complex was then grinded in the same mortar, recovered and weighted. The recovering yield was determined as the percent ratio of the recovered dried complex and the sum of starting compounds. The 1:1:1 ternary complexes were obtained as duplicate samples, while the 3:1:1 ternary complexes were obtained as unique samples.

Fourier-transform infrared spectroscopy (FTIR)

FTIR analysis of the ternary complexes and the starting compounds was performed using a Bruker Vertex 70 FTIR equipment (Bruker Optik GmbH, Ettlingen, Germany), equipped with an ATR (single-reflection Platinum diamond attenuated total reflectance) system. The following FTIR conditions were set up: acquisition range 4000–400 cm^{-1}, resolution 4 cm^{-1}, number of scans 128, sample mass 10–20 mg, spectrum range for the DLaTGS detector 12000–250 cm^{-1} and sensibility D* > 2108 $cm \cdot Hz^{1/2} \cdot W^{-1}$. OPUS ver. 7.2 software (Bruker Optik GmbH 2012, Ettlingen, Germany) was used for the acquisition and handling of the FTIR spectra. All determinations were performed as triplicates for the starting compounds and as duplicates for the ternary complexes.

Thermal analyses

The thermal and oxidative stability of complexes can be evaluated through thermal analyses. TG–DTG and DSC techniques were used for both the complexes and starting compounds. TG–DTG analysis was performed on a Netzsch TG 209F1 Libra equipment, while DSC analysis was conducted on a Netzsch 204 F1 Phoenix apparatus (both from Netzsch Group, Selb, Germany). The TG–DTG and DSC conditions were similar: temperature program of 25–500 °C, with a heating rate of 10 °C/min, nitrogen purge and protection flow of 40 mL/min, the data acquisition and handling by Netzsch Proteus-Thermal Analysis ver. 6.1 software (Netzsch Group, Selb, Germany). Only representative ternary complexes were evaluated by thermal analyses.

Statistical analysis and principal component analysis (PCA)

Means (± standard deviations, SD) of the values were obtained for the replicate determinations using Basic Statistics&Tables and One-way ANOVA modules in Statistica 7.1 software (StatSoft, Inc., Tulsa, OK, USA). PCA for the FTIR data was performed with the Principal Components & Classification Analysis module from the above-mentioned package. The discrimination between samples was based on the scores plot, while the importance of variables to the classification was based on the loadings plot in PCA analysis. Both FTIR wavenumber (WN) and intensity (I) of the specific bands identified in all analyzed samples were used as input data. PCA was performed with both FTIR variable types (both WN and I) or as separated variable types (only WN or only I). PCA analysis was based on correlations, a computed variance as SS/(N-1), with centered factor coordinates of the variables (or principal components, coded as "PC"). All significant PCA results are also presented in the

Supporting Information File 1 (Figures S12–S23 and Tables S10–S12).

Supporting Information

Supporting Information File 1

Thermal analysis, FTIR and FTIR–PCA data for ternary complexes.
[https://www.beilstein-journals.org/bjoc/content/supplementary/1860-5397-19-30-S1.pdf]

Acknowledgements

The authors want to thank Simona Funar-Timofei ("Coriolan Drăgulescu" Institute of Chemistry, Romanian Academy) for the help with Statistica 7.1 software. The authors also want to thank G.-E. Decan for the help in preparing the complexes.

Funding

The authors thank the "Program to increase performance and innovation in doctoral and postdoctoral research excellence - PROINVENT", Contract No. 62487/03.06.2022, POCU/993/6/13, SMIS Code 153299 for support.

ORCID® iDs

Daniel Ioan Hădărugă - https://orcid.org/0000-0002-6326-413X

Preprint

A non-peer-reviewed version of this article has been previously published as a preprint: https://doi.org/10.3762/bxiv.2023.3.v1

References

1. Kurkov, S. V.; Loftsson, T. *Int. J. Pharm.* **2013,** *453,* 167–180. doi:10.1016/j.ijpharm.2012.06.055
2. Duchêne, D.; Bochot, A. *Int. J. Pharm.* **2016,** *514,* 58–72. doi:10.1016/j.ijpharm.2016.07.030
3. Crini, G. *Chem. Rev.* **2014,** *114,* 10940–10975. doi:10.1021/cr500081p
4. Medeleanu, M. A.; Hădărugă, D. I.; Muntean, C. V.; Popescu, G.; Rada, M.; Hegheş, A.; Zippenfening, S. E.; Lucan (Banciu), C. A.; Velciov, A. B.; Bandur, G. N.; Hădărugă, N. G.; Riviş, M. *Carbohydr. Polym.* **2021,** *265,* 118079. doi:10.1016/j.carbpol.2021.118079
5. Del Valle, E. M. M. *Process Biochem. (Oxford, U. K.)* **2004,** *39,* 1033–1046. doi:10.1016/s0032-9592(03)00258-9
6. Hădărugă, N. G.; Bandur, G. N.; David, I.; Hădărugă, D. I. *Environ. Chem. Lett.* **2019,** *17,* 349–373. doi:10.1007/s10311-018-0806-8
7. Carrier, R. L.; Miller, L. A.; Ahmed, I. *J. Controlled Release* **2007,** *123,* 78–99. doi:10.1016/j.jconrel.2007.07.018
8. Szente, L.; Fenyvesi, É. *Struct. Chem.* **2017,** *28,* 479–492. doi:10.1007/s11224-016-0884-9
9. Paramita, V.; Fitri Novia, S.; Dwi Ariyanto, H.; Pramudono, B.; Yoshii, H.; Kusumayanti, H.; Amalia, R. *Mater. Today: Proc.* **2022,** *63,* S312–S317. doi:10.1016/j.matpr.2022.03.156
10. Hădărugă, N. G.; Hădărugă, D. I.; Păunescu, V.; Tatu, C.; Ordodi, V. L.; Bandur, G.; Lupea, A. X. *Food Chem.* **2006,** *99,* 500–508. doi:10.1016/j.foodchem.2005.08.012
11. Hădărugă, D. I.; Birău (Mitroi), C. L.; Gruia, A. T.; Păunescu, V.; Bandur, G. N.; Hădărugă, N. G. *Food Chem.* **2017,** *236,* 49–58. doi:10.1016/j.foodchem.2017.03.093
12. Hădărugă, D. I.; Ünlüsayin, M.; Gruia, A. T.; Birău (Mitroi), C.; Rusu, G.; Hădărugă, N. G. *Beilstein J. Org. Chem.* **2016,** *12,* 179–191. doi:10.3762/bjoc.12.20
13. Hădărugă, N. G.; Szakal, R. N.; Chirilă, C. A.; Lukinich-Gruia, A. T.; Păunescu, V.; Muntean, C.; Rusu, G.; Bujancă, G.; Hădărugă, D. I. *Food Chem.* **2020,** *303,* 125419. doi:10.1016/j.foodchem.2019.125419
14. Ünlüsayin, M.; Hădărugă, N. G.; Rusu, G.; Gruia, A. T.; Păunescu, V.; Hădărugă, D. I. *LWT-Food Sci. Technol.* **2016,** *68,* 135–144. doi:10.1016/j.lwt.2015.12.017
15. Lee, C.-M.; Kim, M.-H.; Na, H.-S.; Kim, J.; Lee, K.-Y. *Biotechnol. Bioprocess Eng.* **2013,** *18,* 507–513. doi:10.1007/s12257-012-0752-4
16. Hădărugă, N. G.; Chirilă, C. A.; Szakal, R. N.; Gălan, I. M.; Simandi, M. D.; Bujancă, G. S.; David, I.; Riviş, A.; Stanciu, S. M.; Hădărugă, D. I. *Foods* **2022,** *11,* 3632. doi:10.3390/foods11223632
17. David, I.; Orboi, M. D.; Simandi, M. D.; Chirilă, C. A.; Megyesi, C. I.; Rădulescu, L.; Drăghia, L. P.; Lukinich-Gruia, A. T.; Muntean, C.; Hădărugă, D. I.; Hădărugă, N. G. *PLoS One* **2019,** *14,* e0225474. doi:10.1371/journal.pone.0225474
18. Hamoudi, M. C.; Bourasset, F.; Domergue-Dupont, V.; Gueutin, C.; Nicolas, V.; Fattal, E.; Bochot, A. *J. Controlled Release* **2012,** *161,* 861–867. doi:10.1016/j.jconrel.2012.05.032
19. Trichard, L.; Chaminade, P.; Grossiord, J.-L.; Le Bas, G.; Huang, N.; Durand, D.; Fattal, E.; Bochot, A. *J. Drug Delivery Sci. Technol.* **2011,** *21,* 189–194. doi:10.1016/s1773-2247(11)50021-8
20. Sun, X.; Li, W.; Li, J.; Zu, Y.; Zhao, X. *Int. J. Food Sci. Technol.* **2017,** *52,* 2352–2361. doi:10.1111/ijfs.13519
21. Yoshikiyo, K.; Takahashi, M.; Narumiya, Y.; Honda, M.; Iwasaki, K.; Ishigaki, M.; Nagato, E. G.; Noothalapati, H.; Shimizu, H.; Murota, K.; Yamamoto, T. *Food Hydrocolloids Health* **2023,** *3,* 100116. doi:10.1016/j.fhfh.2023.100116
22. Benyacoub, A.; Skender, A.; Boutemak, K.; Hadj-Ziane-Zafour, A. *Chem. Pap.* **2019,** *73,* 525–534. doi:10.1007/s11696-018-0600-x
23. Chew, S. C.; Tan, C. P.; Nyam, K. L. *J. Food Eng.* **2018,** *237,* 78–85. doi:10.1016/j.jfoodeng.2018.05.016
24. Adel, A. M.; Ibrahim, A. A.; El-Shafei, A. M.; Al-Shemy, M. T. *Food Packag. Shelf Life* **2019,** *20,* 100307. doi:10.1016/j.fpsl.2019.100307
25. Azzi, J.; Danjou, P.-E.; Landy, D.; Ruellan, S.; Auezova, L.; Greige-Gerges, H.; Fourmentin, S. *Beilstein J. Org. Chem.* **2017,** *13,* 835–844. doi:10.3762/bjoc.13.84
26. Kfoury, M.; Landy, D.; Ruellan, S.; Auezova, L.; Greige-Gerges, H.; Fourmentin, S. *Food Chem.* **2017,** *236,* 41–48. doi:10.1016/j.foodchem.2016.12.086
27. Hădărugă, D. I.; Hădărugă, N. G.; Costescu, C. I.; David, I.; Gruia, A. T. *Beilstein J. Org. Chem.* **2014,** *10,* 2809–2820. doi:10.3762/bjoc.10.298
28. Hădărugă, N. G.; Hădărugă, D. I.; Isengard, H.-D. *Food Chem.* **2012,** *132,* 1741–1748. doi:10.1016/j.foodchem.2011.11.003

29. Menezes, P. P.; Serafini, M. R.; Quintans-Júnior, L. J.; Silva, G. F.; Oliveira, J. F.; Carvalho, F. M. S.; Souza, J. C. C.; Matos, J. R.; Alves, P. B.; Matos, I. L.; Hădărugă, D. I.; Araújo, A. A. S. *J. Therm. Anal. Calorim.* **2014,** *115,* 2429–2437. doi:10.1007/s10973-013-3367-x
30. Yoshikiyo, K.; Yoshioka, Y.; Narumiya, Y.; Oe, S.; Kawahara, H.; Kurata, K.; Shimizu, H.; Yamamoto, T. *Food Chem.* **2019,** *294,* 56–59. doi:10.1016/j.foodchem.2019.04.093
31. Alasalvar, C.; Amaral, J. S.; Satır, G.; Shahidi, F. *Food Chem.* **2009,** *113,* 919–925. doi:10.1016/j.foodchem.2008.08.019
32. Ciemniewska-Żytkiewicz, H.; Verardo, V.; Pasini, F.; Bryś, J.; Koczoń, P.; Caboni, M. F. *Food Chem.* **2015,** *168,* 615–622. doi:10.1016/j.foodchem.2014.07.107
33. Köksal, A. İ.; Artik, N.; Şimşek, A.; Güneş, N. *Food Chem.* **2006,** *99,* 509–515. doi:10.1016/j.foodchem.2005.08.013
34. Başyiğit, Z. Ö. *Res. Eng. Struct. Mater.* **2019,** *5,* 33–41. doi:10.17515/resm2018.84ma1226
35. Hădărugă, N. G.; Hădărugă, D. I. Hydroxycinnamic acids. In *Handbook of Food Bioactive Ingredients: Properties and Applications;* Jafari, S. M.; Rashidinejad, A.; Simal-Gandara, J., Eds.; Springer: Cham, Switzerland, 2022; pp 1–51. doi:10.1007/978-3-030-81404-5_3-1
36. Pedro, A. C.; Maurer, J. B. B.; Zawadzki-Baggio, S. F.; Ávila, S.; Maciel, G. M.; Haminiuk, C. W. I. *Ind. Crops Prod.* **2018,** *112,* 90–97. doi:10.1016/j.indcrop.2017.10.052
37. Guitard, R.; Paul, J.-F.; Nardello-Rataj, V.; Aubry, J.-M. *Food Chem.* **2016,** *213,* 284–295. doi:10.1016/j.foodchem.2016.06.038
38. Iqbal, R.; Mehmood, Z.; Baig, A.; Khalid, N. *Food Bioprod. Process.* **2020,** *123,* 304–311. doi:10.1016/j.fbp.2020.07.013
39. Roedig-Penman, A.; Gordon, M. H. *J. Am. Oil Chem. Soc.* **1998,** *75,* 169–180. doi:10.1007/s11746-998-0029-4
40. Tańska, M.; Mikołajczak, N.; Konopka, I. *Food Chem.* **2018,** *240,* 679–685. doi:10.1016/j.foodchem.2017.08.007
41. Viskupicova, J.; Danihelova, M.; Ondrejovic, M.; Liptaj, T.; Sturdik, E. *Food Chem.* **2010,** *123,* 45–50. doi:10.1016/j.foodchem.2010.03.125
42. Ficarra, R.; Tommasini, S.; Raneri, D.; Calabrò, M. L.; Di Bella, M. R.; Rustichelli, C.; Gamberini, M. C.; Ficarra, P. *J. Pharm. Biomed. Anal.* **2002,** *29,* 1005–1014. doi:10.1016/s0731-7085(02)00141-3
43. Hădărugă, D. I.; Hădărugă, N. G.; Bandur, G. N.; Isengard, H.-D. *Food Chem.* **2012,** *132,* 1651–1659. doi:10.1016/j.foodchem.2011.06.004
44. Liu, B.; Li, W.; Nguyen, T. A.; Zhao, J. *Food Chem.* **2012,** *134,* 926–932. doi:10.1016/j.foodchem.2012.02.207
45. Nguyen, T. A.; Liu, B.; Zhao, J.; Thomas, D. S.; Hook, J. M. *Food Chem.* **2013,** *136,* 186–192. doi:10.1016/j.foodchem.2012.07.104
46. Pham, T. L.; Usacheva, T. R.; Kuz'mina, I. A.; Nguyen, T. N.; Thai, H.; Volkova, M. A.; Le, H. K.; Nguyen, T. D.; Volynkin, V. A.; Tran, D. L. *J. Mol. Liq.* **2020,** *318,* 114308. doi:10.1016/j.molliq.2020.114308
47. Pinho, E.; Grootveld, M.; Soares, G.; Henriques, M. *Carbohydr. Polym.* **2014,** *101,* 121–135. doi:10.1016/j.carbpol.2013.08.078
48. Purewal, S. S.; Sandhu, K. S. *Sci. Hortic. (Amsterdam, Neth.)* **2021,** *276,* 109750. doi:10.1016/j.scienta.2020.109750
49. You, G.-J.; Sun, L.-L.; Cao, X.-X.; Li, H.-H.; Wang, M.; Liu, Y.-N.; Ren, X.-L. *LWT-Food Sci. Technol.* **2018,** *94,* 172–177. doi:10.1016/j.lwt.2018.04.035
50. Anwer, M. K.; Jamil, S.; Ansari, M. J.; Al-Shdefat, R.; Ali, B. E.; Ganaie, M. A.; Abdel-Kader, M. S.; Shakeel, F. *J. Mol. Liq.* **2014,** *199,* 35–41. doi:10.1016/j.molliq.2014.08.012
51. Chantasart, D.; Rakkaew, P. *J. Drug Delivery Sci. Technol.* **2019,** *52,* 73–82. doi:10.1016/j.jddst.2019.04.011
52. Chaudhari, P.; Birangal, S.; Mavlankar, N.; Pal, A.; Mallela, L. S.; Roy, S.; Kodoth, A. K.; Ghate, V.; Nampoothiri, M.; Lewis, S. A. *Carbohydr. Polym.* **2022,** *297,* 120007. doi:10.1016/j.carbpol.2022.120007
53. Cirri, M.; Maestrelli, F.; Mennini, N.; Mura, P. *J. Pharm. Biomed. Anal.* **2009,** *50,* 683–689. doi:10.1016/j.jpba.2008.11.003
54. Cirri, M.; Maestrelli, F.; Mennini, N.; Mura, P. *J. Pharm. Biomed. Anal.* **2009,** *50,* 690–694. doi:10.1016/j.jpba.2008.11.002
55. Jadhav, P.; Petkar, B.; Pore, Y.; Kulkarni, A.; Burade, K. *Carbohydr. Polym.* **2013,** *98,* 1317–1325. doi:10.1016/j.carbpol.2013.07.070
56. Li, J.; Gao, H.; Ye, Z.; Deng, J.; Ouyang, D. *Carbohydr. Polym.* **2022,** *275,* 118712. doi:10.1016/j.carbpol.2021.118712
57. Liu, N.; Higashi, K.; Ueda, K.; Moribe, K. *Int. J. Pharm.* **2017,** *531,* 543–549. doi:10.1016/j.ijpharm.2017.04.049
58. Mura, P.; Bettinetti, G. P.; Cirri, M.; Maestrelli, F.; Sorrenti, M.; Catenacci, L. *Eur. J. Pharm. Biopharm.* **2005,** *59,* 99–106. doi:10.1016/j.ejpb.2004.05.005
59. Wang, D.; Li, H.; Gu, J.; Guo, T.; Yang, S.; Guo, Z.; Zhang, X.; Zhu, W.; Zhang, J. *J. Pharm. Biomed. Anal.* **2013,** *83,* 141–148. doi:10.1016/j.jpba.2013.05.001
60. Iordănescu, O. A.; Băla, M.; Iuga, A. C.; Gligor (Pane), D.; Dascălu, I.; Bujancă, G. S.; David, I.; Hădărugă, N. G.; Hădărugă, D. I. *Plants* **2021,** *10,* 1957. doi:10.3390/plants10091957
61. Petroman, C.; Popescu, G.; Szakal, R.-N.; Păunescu, V.; Drăghia, L. P.; Bujancă, G. S.; Chirilă, C. A.; Hădărugă, D. I.; Văduva, L.; Hădărugă, N. G.; Petroman, I. *Foods* **2021,** *10,* 242. doi:10.3390/foods10020242
62. Cserháti, T.; Forgács, E. *J. Chromatogr. A* **1996,** *728,* 67–73. doi:10.1016/0021-9673(95)01015-7
63. Forgacs, E.; Darwish, Y.; Oros, G.; Illes, Z. *J. Inclusion Phenom. Macrocyclic Chem.* **2002,** *42,* 235–240. doi:10.1023/a:1016020615251
64. Fakayode, S. O.; Busch, M. A.; Busch, K. W. *Talanta* **2006,** *68,* 1574–1583. doi:10.1016/j.talanta.2005.08.018
65. Ingle, J. R.; Busch, K. W.; Busch, M. A. *Talanta* **2008,** *75,* 572–584. doi:10.1016/j.talanta.2007.11.056
66. Mora Diez, N.; Muñoz de la Peña, A.; Mahedero García, M. C.; Gil, D. B.; Cañada-Cañada, F. *J. Fluoresc.* **2007,** *17,* 309–318. doi:10.1007/s10895-007-0174-4
67. Santos, C. I. A. V.; Teijeiro, C.; Ribeiro, A. C. F.; Rodrigues, D. F. S. L.; Romero, C. M.; Esteso, M. A. *J. Mol. Liq.* **2016,** *223,* 209–216. doi:10.1016/j.molliq.2016.08.035
68. Margolis, S. A.; Huang, P. H.; Hădărugă, N. G.; Hădărugă, D. I. Water determination. *Encyclopedia of Analytical Science,* 3rd ed.; Elsevier: Oxford, UK, 2019; Vol. 10, pp 382–390. doi:10.1016/b978-0-12-409547-2.14505-6
69. Ge, X.; He, J.; Qi, F.; Yang, Y.; Huang, Z.; Lu, R.; Huang, L. *Spectrochim. Acta, Part A* **2011,** *81,* 397–403. doi:10.1016/j.saa.2011.06.028
70. Chen, L.-F.; Shen, Q.; Shen, J.-P.; Shi, D.-T.; Chen, T.; Yu, H.-R. *Colloids Surf., A* **2012,** *411,* 69–73. doi:10.1016/j.colsurfa.2012.07.003
71. Sim, S. F.; Ting, W. *Talanta* **2012,** *88,* 537–543. doi:10.1016/j.talanta.2011.11.030
72. Tsirigotis-Maniecka, M.; Gancarz, R.; Wilk, K. A. *Colloids Surf., A* **2017,** *532,* 48–56. doi:10.1016/j.colsurfa.2017.07.001
73. Puri, M.; Kaur, A.; Schwarz, W. H.; Singh, S.; Kennedy, J. F. *Int. J. Biol. Macromol.* **2011,** *48,* 58–62. doi:10.1016/j.ijbiomac.2010.09.012

74. Gera, S.; Pooladanda, V.; Godugu, C.; Swamy Challa, V.; Wankar, J.; Dodoala, S.; Sampathi, S. *Pharm. Dev. Technol.* **2020,** *25,* 971–988. doi:10.1080/10837450.2020.1765378
75. Qian, B.-J.; Wu, C.-F.; Lu, M.-M.; Xu, W.; Jing, P. *Food Chem.* **2017,** *232,* 545–551. doi:10.1016/j.foodchem.2017.04.010
76. Wu, W.; Zu, Y.; Wang, L.; Wang, L.; Li, Y.; Liu, Y.; Wu, M.; Zhao, X.; Zhang, X. *RSC Adv.* **2017,** *7,* 54379–54390. doi:10.1039/c7ra10242a
77. Pooja, D.; Babu Bikkina, D. J.; Kulhari, H.; Nikhila, N.; Chinde, S.; Raghavendra, Y. M.; Sreedhar, B.; Tiwari, A. K. *Int. J. Biol. Macromol.* **2014,** *69,* 267–273. doi:10.1016/j.ijbiomac.2014.05.035
78. Oliveira, I.; Sousa, A.; Morais, J. S.; Ferreira, I. C. F. R.; Bento, A.; Estevinho, L.; Pereira, J. A. *Food Chem. Toxicol.* **2008,** *46,* 1801–1807. doi:10.1016/j.fct.2008.01.026

License and Terms

This is an open access article licensed under the terms of the Beilstein-Institut Open Access License Agreement (https://www.beilstein-journals.org/bjoc/terms), which is identical to the Creative Commons Attribution 4.0 International License (https://creativecommons.org/licenses/by/4.0). The reuse of material under this license requires that the author(s), source and license are credited. Third-party material in this article could be subject to other licenses (typically indicated in the credit line), and in this case, users are required to obtain permission from the license holder to reuse the material.

The definitive version of this article is the electronic one which can be found at:
https://doi.org/10.3762/bjoc.19.30

BEILSTEIN JOURNAL OF ORGANIC CHEMISTRY

Cyclodextrins permeabilize DPPC liposome membranes: a focus on cholesterol content, cyclodextrin type, and concentration

Ghenwa Nasr[1,2], Hélène Greige-Gerges[1], Sophie Fourmentin[3], Abdelhamid Elaissari[2] and Nathalie Khreich[*1]

Full Research Paper

Open Access

Address:
[1]Bioactive Molecules Research Laboratory, Faculty of Sciences, Lebanese University, Jdeidet el-Metn 90656, Lebanon, [2]University Lyon, University Claude Bernard Lyon 1, CNRS, ISA-UMR 5280, 69622, Villeurbanne, France, and [3]Unité de Chimie Environnementale et Interactions sur le Vivant (UCEIV, UR 4492), SFR Condorcet FR CNRS 3417, Université du Littoral Côte d'Opale, 145 Av. M.Schumann, 9140 Dunkirk, France

Email:
Nathalie Khreich[*] - nathalie.khreich@ul.edu.lb

* Corresponding author

Keywords:
cholesterol; cyclodextrins; liposome; membrane permeability

Beilstein J. Org. Chem. **2023,** *19,* 1570–1579.
https://doi.org/10.3762/bjoc.19.115

Received: 24 July 2023
Accepted: 06 October 2023
Published: 17 October 2023

This article is part of the thematic issue "Cyclodextrins as building blocks for new materials".

Associate Editor: N. Sewald

© 2023 Nasr et al.; licensee Beilstein-Institut.
License and terms: see end of document.

Abstract

Cyclodextrins (CDs) are known for their ability to extract lipid components from synthetic and biological membranes and therefore to induce an increase of membrane permeability. However, the effect of cholesterol (CHOL) content in the membrane on the CD permeabilizing effect was not considered yet. Given that an increase in CHOL content reduces the membrane permeability, the aim of this work was to reveal how CHOL would modulate the CDs effect on the membrane. Hence, liposomes made of dipalmitoyl phosphatidylcholine (DPPC) and various CHOL contents (DPPC/CHOL 100:10, 100:25, 100:50, and 100:100) encapsulating the hydrophilic fluorophore, sulforhodamine B (SRB), were prepared and exposed to the native CDs (α-CD, β-CD, γ-CD) and four β-CD derivatives: the randomly methylated-β-CD (RAMEB), the low methylated-β-CD (CRYSMEB), the hydroxypropyl-β-CD (HP-β-CD) and the sulfobutyl ether-β-CD (SBE-β-CD) at different CD/DPPC molar ratios (1:1, 10:1, and 100:1). The membrane permeability was monitored following the release of SRB with time. The results demonstrated that the CDs effect on the membrane depends on the CD type, CD concentration, and membrane CHOL content. The investigated CDs exhibited an instantaneous permeabilizing effect promoting vesicle leakage of SRB from the various membranes; this effect increased with CDs concentration. Among the studied CDs, α-CD, β-CD, and RAMEB were the most permeabilizing CDs on the different membranes. Similar modifications of SRB release from the various liposomal formulations were obtained with HP-β-CD, CRYSMEB, and SBE-β-CD. γ-CD was the less potent CD in affecting the membrane permeability. The CDs effect also depended on the CHOL content: at the CD/DPPC molar ratio (100:1), RAMEB and β-CD considerably permeabilized the membrane of high CHOL content (50%, 100%) while the remaining CDs showed a decreasing permeabilizing effect upon CHOL content membrane increase.

Introduction

Cyclodextrins (CDs) are a family of cyclic oligosaccharides made of glucopyranose units connected by α-1,4-glycosidic bonds. They possess a cone-shaped molecular structure with a hydrophobic internal cavity and a hydrophilic outer surface [1]. The common CDs are the native α-CD, β-CD, and γ-CD consisting of 6, 7, and 8 D-glucopyranose units, respectively. Due to their limited water solubility (especially β-CD), native CDs can be chemically or enzymatically modified (by e.g., alkylation, arylation, hydroxypropylation, amination, etherification, etc.) giving rise to synthetic CD derivatives with greater water solubility [2]. Thanks to their unique structure, CDs can offer exclusive advantages by allowing the entrapment of lipophilic molecules inside their inner cavities. This inclusion improves the chemical stability and aqueous solubility of the guest molecule and results in most of the cases in the formation of a water-soluble CD–guest complex [3]. Being recognized as non-toxic, biodegradable, and sustainable carriers, CDs have attracted wide interest as potential carriers in different fields, mainly in drug delivery where they are used as pharmaceutical excipients to increase the drug permeability through biological membranes improving drug bioavailability and efficacy [2,4,5]. Furthermore, the CDs peculiarities helped to develop a combined system in which CD–guest complexes are encapsulated in the aqueous core of liposomes which is generally known as "drug-in-cyclodextrin-in-liposomes" (DCL) [6]. This novel delivery system has gained popularity in the past few decades and many publications proved its importance and significance. Actually, the use of the two delivery systems (liposomes and CDs) was shown to combine the advantages of each separate system and to circumvent the drawbacks of liposomes and the problems associated with CDs: for instance, studies reported that the DCL increased the entrapment of hydrophobic drugs in liposomes and enhanced the vesicle stability. The DCL avoids a burst release of the drug from the carrier resulting in an ameliorated controlled release [6,7].

Nevertheless, CDs are known to induce considerable damages in the membrane structure and composition. In fact, CDs can alter the biophysical properties of the membrane by increasing its fluidity and permeability [8]. They are even able to extract the lipid membrane components leading the membrane to lose its integrity [8]. This behavior was attributed to the hemolytic activity of CDs previously observed on erythrocytes and other cell membranes [9].

Numerous reports highlighting the CDs-mediated lipid extraction demonstrated that some CDs displayed a higher affinity towards phospholipids such as α-CD for phosphatidylinositol (PI), phosphatidylserine (PS), and dipalmitoyl phosphatidylcholine (DPPC) [10,11], etc., while other CDs preferentially extracted cholesterol (CHOL) from membranes such as β-CD and its methylated derivatives [12,13]. Consequently, CDs are classified as permeabilizing agents for being able to promote the leakage of liposomal membranes [14]. Although a great number of reports demonstrated the membrane-damaging effect induced by several CDs, the CHOL content in the membrane was not considered in the literature despite the remarkable effect of CHOL on the stability of the lipid bilayer. In fact, CHOL can greatly modulate the membrane permeability: a previous work showed that increasing the CHOL content in the membrane results in a decrease in the membrane permeability in a dose-dependent manner [15]. Additionally, the CHOL content was demonstrated to reduce and sometimes to inhibit the permeability of DPPC vesicles induced by bioactive agents [16,17]. Given the condensing and ordering effect that CHOL exerts on the membrane, the presence of CHOL in the lipid bilayer introduced a new phase to the membrane referred to as "the liquid-ordered" (Lo) alongside with the gel phase and the liquid-disordered phase [18].

Besides, CHOL is a major component of the so-called "lipid rafts" which are perceived as membrane domains rich in CHOL and sphingomyelin and involved in various cellular processes, (e.g., signaling transduction, proteins trafficking, etc.) [19]. However, many discrepancies could be found in the literature regarding the existence of lipid rafts in synthetic membranes, especially CHOL–lipid binary mixtures. Studies of DPPC:CHOL bilayers have elucidated the formation of nanodomains enriched in CHOL within the membrane displaying a fluid-like structure as manifested in the Lo phase [20].

Different types of CDs were considered in this study; these include the native CDs: α-CD, β-CD, γ-CD, and four β-CD derivatives: the randomly methylated-β-CD (RAMEB), the low methylated-β-CD (CRYSMEB), the hydroxypropyl-β-CD (HP-β-CD), and the sulfobutyl ether-β-CD (SBE-β-CD). A schematic representation of the chemical structure of the native CDs and their dimensions is depicted in Figure 1, reprinted with permission from [21]. The structures of β-CD derivatives and their degrees of substitution are represented in Figure 2. The effect of the CDs on the membrane permeability was monitored by following the release of a hydrophilic fluorophore, sulforhodamine B (SRB), from liposomes composed of DPPC and different CHOL content upon exposure to different concentrations of CDs.

To the best of our knowledge, this work is the first study investigating the effect of CDs on the permeability of DPPC liposome membranes of various CHOL content. The CDs effect was examined at various CD/DPPC molar ratios. This work will

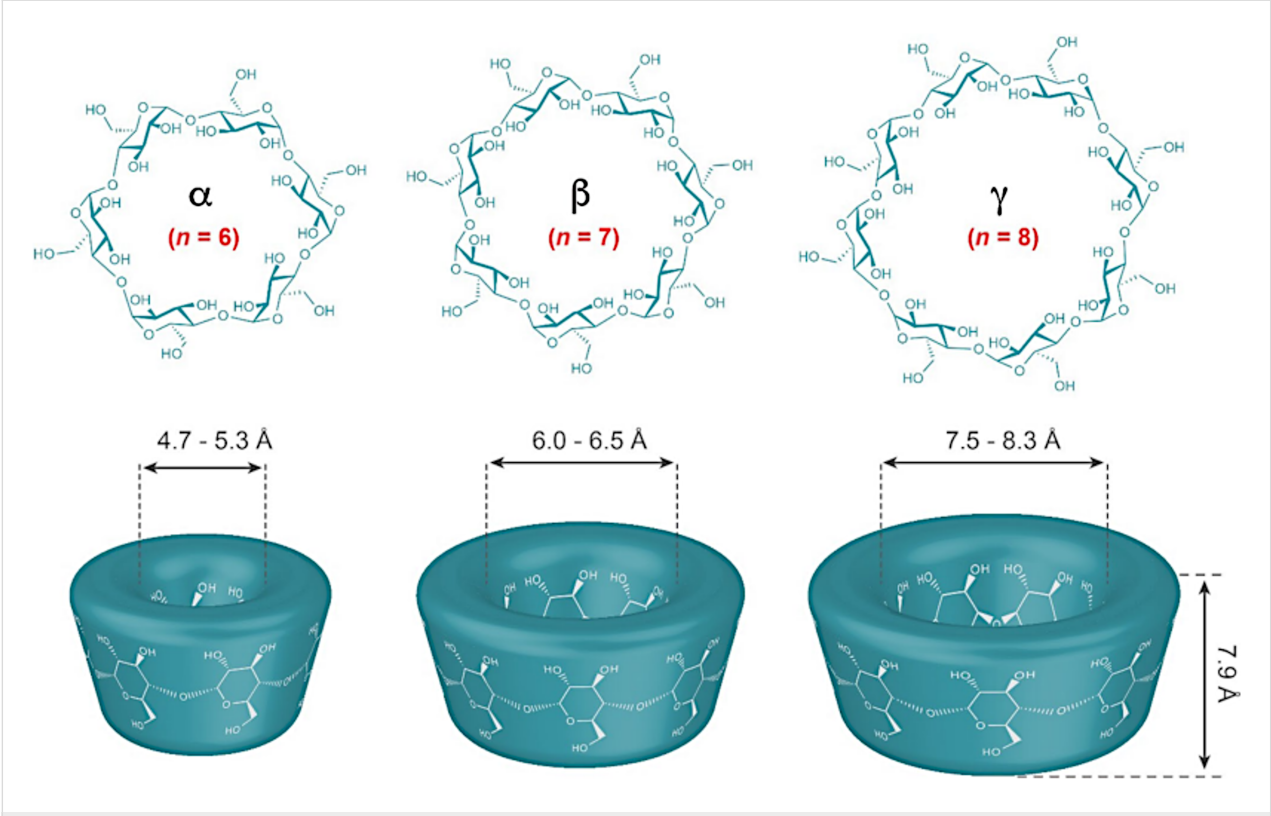
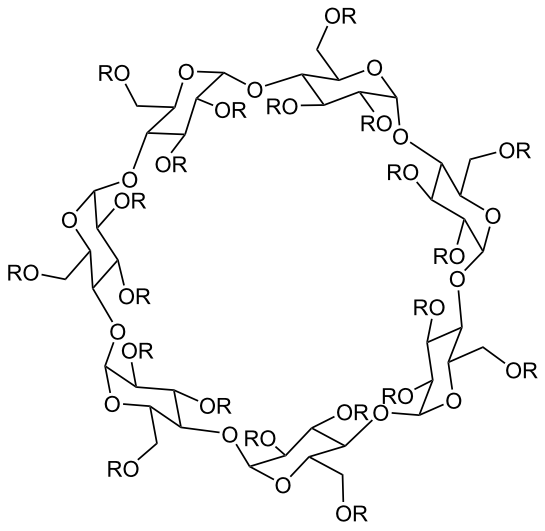


Figure 1: The chemical structure of the native CDs, their three-dimensional structure, and their dimensions (*n* = 6, 7, and 8 glucopyranose units for α-, β-, and γ-CD, respectively). This figure was reused by permission from Springer Nature from [21]. ("130 years of cyclodextrin discovery for health, food, agriculture, and the industry: a review" by N. Morini-Crini; S. Fourmentin; É. Fenyvesi; E. Lichtfouse; G. Torri; M. Fourmentin; G. Crini, Environmental Chemistry Letters, Vol. 19, pp 2581–2617, 2021), Copyright 2021 Springer Nature. Journal home page: https://www.springer.com/journal/10311. This content is not subject to CC BY 4.0.



HP-β-CD: R = -H or -CH_2-CH(OH)-CH_3; DS = 5.6
RAMEB: R = -H or -CH_3; DS = 12.9
CRYSMEB: R = -H or -CH_3 ; DS = 4.9
SBE-β-CD: R = -H or -$(CH_2)_4$-SO_3^- Na^+ ; DS = 6.5

Figure 2: Structures of β-CD derivatives and their degrees of substitution (DS).

provide a better understanding of the influence of CHOL content on the CDs effect with regards to their affinity to lipid membrane components. It will also allow us to point out if the CDs-induced lipid extraction may occur in "lipid rafts".

Results and Discussion

In this study, liposome membranes made of DPPC and various CHOL contents were prepared (10%, 25%, 50%, and 100% CHOL). It is relevant to note that the percentage of CHOL in the formulations represents the amount of CHOL added to the fixed amount of DPPC not the sum of the total lipids. Thus, a formulation of 100% CHOL comprises a number of moles of CHOL equal to that of DPPC. These formulations were individually treated with 0.15 mM, 1.5 mM, and 15 mM of CDs (CD/DPPC molar ratios 1:1, 10:1 and 100:1, respectively). Following the exposure of liposomes to CDs, the samples were incubated at 37 °C and the fluorescence signals were measured at time 0, 4, and 24 h. For each formulation, the effect of CDs was obtained by subtracting the SRB release from vesicles in the presence of CDs from that obtained in their absence as explained earlier. Results are presented in Figures 3, 4, and 5.

The obtained data are also reported in Tables S1–S4 (Supporting Information File 1) in which the vertical reading points out the effect of the CD concentration on the SRB release for a specific membrane composition, while the horizontal reading of the tables highlights the impact of CHOL content on the permeability of membranes at various intervals of time.

The SRB release kinetics for blank liposomes (untreated with CDs) obtained in our study were consistent with a previous work conducted by Kaddah et al. [15]. Indeed, the study focused on following the SRB release from liposomes composed of DPPC and various CHOL contents. The previous results showed that the SRB release from liposomes incorporating 10% CHOL was 6.1% after 1 h of incubation whereas those from membranes containing higher CHOL contents did not exceed 5% after the same time. After 4 h of incubation, the SRB release reached 16.41% for 10% CHOL liposomal membranes and less than 10% for vesicles composed of higher CHOL content. After 48 h of incubation, 63% of SRB was released from 10% CHOL membranes while less than 20% of SRB leakage was obtained with the formulations of 50 and 100% CHOL [15]. Similar findings were noted in this work (Tables S1–S4 in Supporting Information File 1) showing that increasing the CHOL content in the membrane reduces its permeability and increases its rigidity and stability.

1 The instantaneous effect of CDs at t_0

CD/DPPC molar ratio (1:1). As shown in Figure 3, the studied CDs barely modified the membrane permeability of the different liposome membranes where the percentage of SRB release did not exceed 4% when compared to the blank of each formulation.

CD/DPPC molar ratio (10:1). α-CD, β-CD, and RAMEB were the most effective CDs inducing an increase in the permeability of the different membranes. Their maximum effect reaching 15% of SRB release was observed at the lowest CHOL content and their permeabilizing effect decreased with CHOL content increase (13.08, 8.94, 4.20, and 2.95% of SRB release from α-CD-treated liposomes composed of 10, 25, 50, and 100% CHOL, respectively).

HP-β-CD, CRYSMEB, and SBE-β-CD were less effective than α-CD, β-CD, and RAMEB on the membranes since the instantaneous SRB release values did not exceed 7% regardless the membrane composition at t_0. Their highest effect was observed at a low CHOL content (7.11% of SRB release from SBE–β-CD-treated liposomes composed of 10% CHOL) with a noticeable decrease (SRB release less than 4%) with membranes of high CHOL content. γ-CD demonstrated the weakest effect on the membrane regardless its composition.

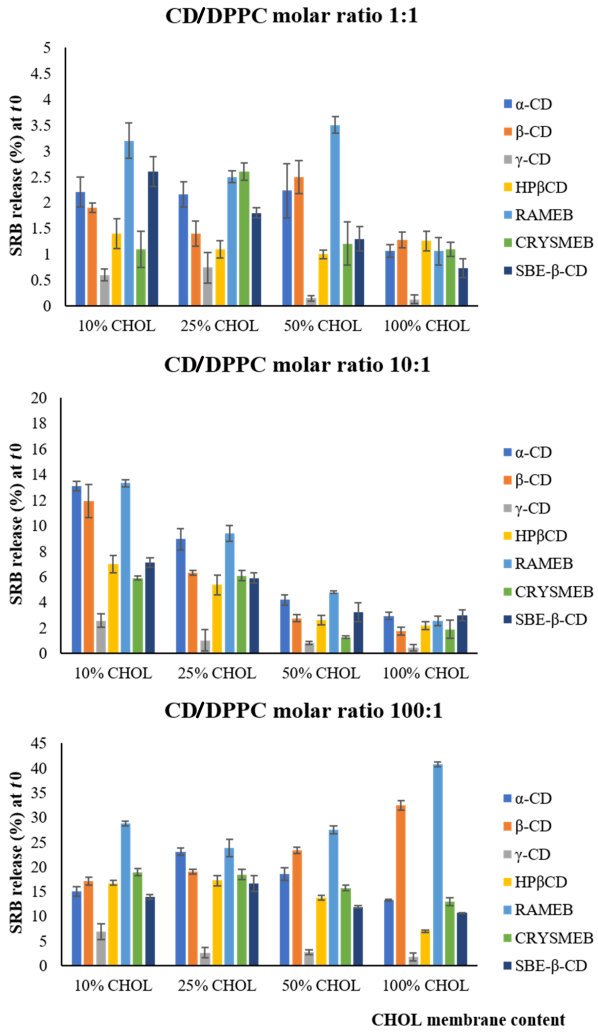


Figure 3: The instantaneous effect of CDs on the various liposome membranes at different CD/DPPC molar ratios (1:1, 10:1, and 100:1) at t_0. Values are expressed as the means of three different measurements ± SD.

CD/DPPC molar ratio (100:1). At this molar ratio, RAMEB was the most effective CD acting on both CHOL-poor and -rich membranes. Remarkably, the SRB release values reached around 42.00% with membranes containing 100% CHOL which draws attention to the ability of RAMEB to extract CHOL from membranes rich in CHOL. β-CD showed a similar effect at 10% CHOL but it remained lower than that obtained with RAMEB.

Although α-CD and β-CD demonstrated the same ability to affect the permeability of membranes of CHOL content 10, 25, and 50% (with SRB release values ranging from 15 to 25%), their effect was not the same at 100% CHOL where β-CD (SRB release of 32.37%) was more potent than α-CD (SRB release of 13.29%). HP-β-CD, CRYSMEB, and SBE-β-CD similarly

affected the liposome membranes of different CHOL content; their permeabilizing effect was higher on low CHOL content membranes 10 and 25% (SRB release values varying between 14 and 20%) compared to high CHOL membranes 50 and 100% (SRB release values ranging from 7 to 14%). Among these CDs, HP-β-CD exerted the lowest effect at 100% CHOL (6.9% of SRB release). As for γ-CD, it increased the SRB release from 10% CHOL membranes at this high CD concentration, though, its effect decreased with the other membrane types. Overall, we observed that increasing the CDs concentration increased their permeabilizing effects regardless the membrane composition and the CD type.

2 The permeabilizing effect of CDs at 4 h

CD/DPPC molar ratio (1:1). As depicted in Figure 4, the effect of CDs at the molar ratio 1:1 on the various membrane types did not strongly differ from the blank or untreated liposomes; less than 4% of SRB release (compared to blank) was obtained with the different CDs. Surprisingly, all CDs seem to produce a slight decrease of membrane permeability (less than 6%) when compared to the blank for the membranes of CHOL content 10, 50, and 100% whereas a slight increase (3% of release) was noticed after CDs exposure to 25% CHOL membranes.

CD/DPPC molar ratio (10:1). The same trends obtained at the CD/DPPC molar ratio 1:1 seem to be maintained at the CD/DPPC molar ratio 10:1. α-CD and RAMEB were the only CDs that induce an increase in SRB release higher than 5% with the membranes containing 25 and 50% CHOL. β-CD kept a weak permeabilizing effect on 25% CHOL membrane.

CD/DPPC molar ratio (100:1). α-CD, β-CD, and RAMEB produced a permeabilizing effect on the membranes composed of 25, 50 and 100% CHOL where the SRB release values varied between 25 and 50%. The effect of β-CD and RAMEB increased with CHOL content; this was not obtained with α-CD. HP-β-CD, CRYSMEB, and SBE-β-CD increased the permeability of 25, 50, and 100% CHOL membranes (with SRB release values 10 to 20%) with a better effect at 25 and 50% CHOL.

3 The permeabilizing effect of CDs at 24 h

CD/DPPC molar ratio (1:1). As we can see in Figure 5, the data obtained at 24 h are similar to those collected at 4 h. Effectively, at the CD/DPPC molar ratio (1:1), the investigated CDs did not exhibit a permeabilizing effect on 10% CHOL membranes. Even though some CDs showed an effect at 25, 50, and 100% CHOL, their effect remained weak and unsignificant (SRB release values less than 4% compared to blank).

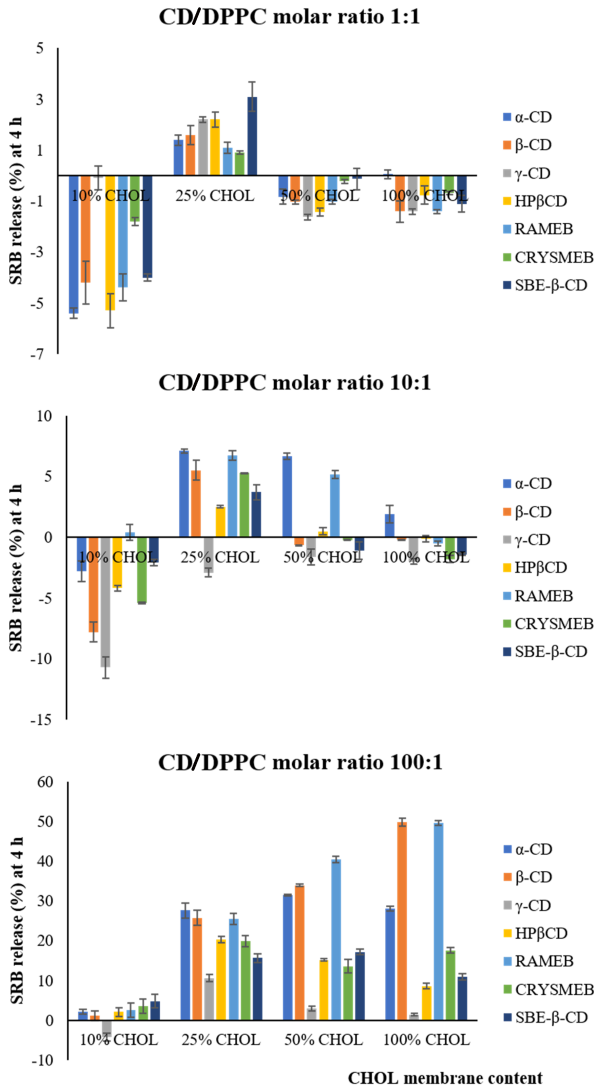


Figure 4: The permeabilizing effect of CDs on the various liposome membranes at different CD/DPPC molar ratios (1:1, 10:1, and 100:1) obtained at 4 h. Values are expressed as the means of three different measurements ± SD.

CD/DPPC molar ratio (10:1). At the CD/DPPC molar ratio (10:1), α-CD and RAMEB were able to permeabilize 25 and 50% CHOL membranes. β-CD exerted a slight effect when compared to that of α-CD and RAMEB.

CD/DPPC molar ratio (100:1). A strong permeabilizing effect was induced by α-CD, β-CD, and RAMEB with SRB release values ranging from 25 to 55%. The remaining β-CD derivatives showed a lower effect at 25 and 50% CHOL.

Discussion

The CD–membrane interaction was broadly studied in the past few decades. The ability of CDs to induce membrane permeabi-

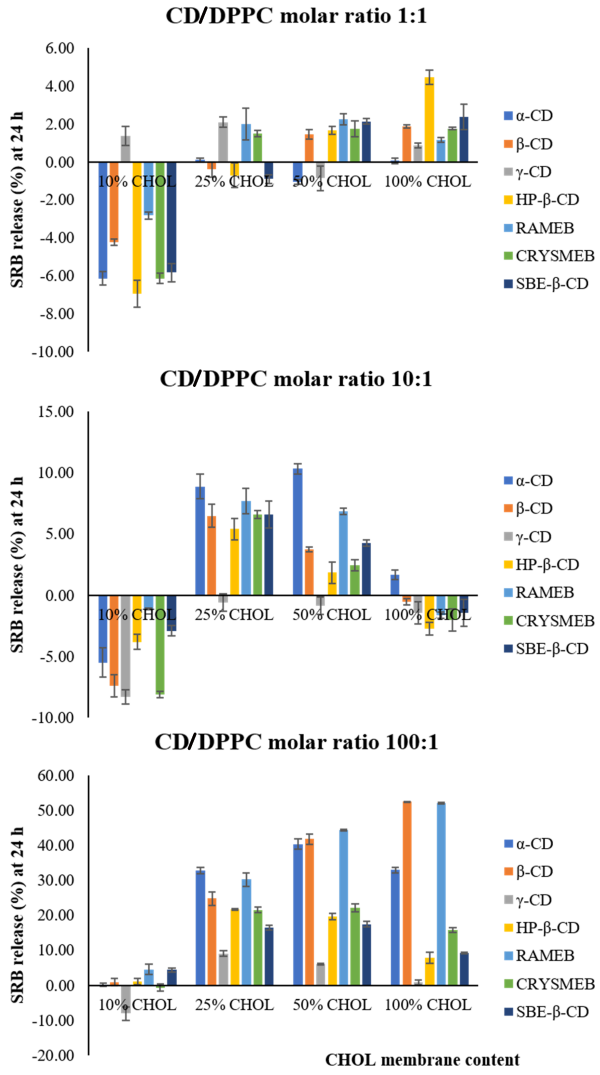


Figure 5: The permeabilizing effect of CDs on the various liposome membranes at different CD/DPPC molar ratios (1:1, 10:1, and 100:1) obtained at 24 h. Values are expressed as the means of three different measurements ± SD.

lization was also proved in numerous reports. This effect was dose dependent which is consistent with the obtained results where the permeabilizing effect of CDs increased with CDs concentration: at the CD/DPPC molar ratio (1:1), the CDs did not promote considerable vesicle leakage whereas at the CD/DPPC molar ratio (10:1), the CDs affected the membrane permeability and their effect was enhanced at the CD/DPPC molar ratio (100:1).

In addition, we can notice that the CDs potency in permeabilizing the membrane was not the same: among the studied CDs, and α-CD, β-CD, and RAMEB were the most potent CDs acting on both low and high CHOL content membranes, particularly at the highest CDs concentration. However, they did not behave similarly at high CHOL content: the permeabilizing effect of β-CD and RAMEB was enhanced at 100% CHOL compared to α-CD whose release effect was reduced at high CHOL content. Additionally, α-CD presented the highest effect at 25% CHOL at the highest CD concentration. The main reason behind these observations is the preferential lipid membrane extraction exhibited by the CDs. As a matter of fact, α-CD can remove phospholipids from membranes. A previous work reported that α-CD can extract DPPC through a special complex formation between the acyl chains of the phospholipid and the CD molecules where many α-CD units string along the nonpolar chains of DPPC forming a rotaxane-like ring [11]. DSC studies have also proved that α-CD forms an insoluble complex with DPPC [22]. Besides, α-CD has previously demonstrated the strongest destabilizing effect on the DPPC liposome membranes among the native CDs [11]. In our study, being more abundant in phospholipids than CHOL, the 10 and 25% CHOL liposome membranes were more sensitive to α-CD (at a CD/DPPC molar ratios above 10:1) compared to the remaining formulations (50 and 100% CHOL) which explains the highest permeabilizing effect instantly exerted by α-CD at low CHOL content. With increasing CHOL content (at 50 and 100% CHOL), CHOL might be clustered into microdomains which may hinder the α-CD's effect and reduce its effect on the membrane.

According to literature, the effect of β-CD and RAMEB is mainly attributed to the ability of these CDs to remove CHOL from membranes [8]. This explains the increase of their permeabilizing effect with CHOL addition at the CD/DPPC molar ratio 100:1 as more CHOL molecules are extracted from the membrane leading to the disruption of the membrane continuity and its subsequent leakage [14]. Though, this effect was not seen at the CD/DPPC molar ratio of (10:1). This leads to suppose that the CHOL extraction mediated by β-CD is probably achieved at a CD/DPPC molar ratio larger than 10:1. Comparing the α-CD-induced permeability to that of β-CD and RAMEB, it is possible to state that CHOL-rich membranes are sensitive to β-CD and RAMEB at the highest ratio (100:1). Hence, β-CD and RAMEB are active on CHOL-rich membranes (50 and 100% CHOL) where the raft domains may be present. We suggest therefore that β-CD and RAMEB at high concentration would extract CHOL from raft domains, as previously reported for RAMEB [8,23].

As mentioned earlier, HP-β-CD, CRYSMEB, and SBE-β-CD were less effective on the membrane than α-CD, β-CD, and RAMEB. They displayed a better permeabilizing effect at low CHOL content (10 and 25% CHOL membranes) with a decrease in their effect upon CHOL content increase at the CD/DPPC molar ratios 10:1 and 100:1.

Despite that CRYSMEB is a methylated β-CD derivative, its behavior was different from that of RAMEB whose effects were enhanced with CHOL increase at the CD/DPPC molar ratio 100:1. Our result for CRYSMEB is in agreement with the work of Piel et al., who showed that CRYSMEB is less potent than RAMEB and other methylated CDs in promoting calcein leakage from liposomes comprising 30% CHOL [13]. The authors stated that the low degree of substitution of CRYSMEB decreased its affinity to the lipid membrane components and resulted in a weaker disturbing effect compared to RAMEB and other methylated CDs. Consequently, CRYSMEB is active on CHOL-poor membranes (25% CHOL) at a CD/DPPC molar ratio above 10:1.

HP-β-CD and SBE-β-CD showed similar behavior to CRYSMEB. According to a recent biophysical study, HP-β-CD demonstrated an increase in the fluidity of DPPC liposomes through the interaction of HP-β-CD with the polar head group region and the acyl chains of DPPC [24]. Although the complex between HP-β-CD and CHOL has been previously characterized [25], this complex seems to be unstable. Thus, a better interaction would occur between HP-β-CD and DPPC rather than with CHOL which explains the obtained results. As for SBE-β-CD, it was reported that charged CDs could not interact with CHOL molecules and form inclusion complexes due to charge repulsion [26]. This could explain the results obtained for these two CDs. Hence, HP-β-CD and SBE-β-CD are active on CHOL-poor membranes.

The effects of β-CD derivatives obtained in this study present a good correlation with biological membranes studies: the methylated β-CD derivatives with high degree of substitution (RAMEB in our study) possess the strongest CHOL extraction capacity and can subsequently achieve the highest solubilization of CHOL [27], while the low-substituted derivatives (CRYSMEB in our case) were less cytotoxic and maintained the integrity of endothelial cells assuming a lower affinity to CHOL membrane compared to the other derivatives [23]. Furthermore, the hydroxypropyl substituents are bulkier and less hydrophobic than the methyl groups resulting in a lower CHOL solubilizing capacity and a weaker hemolytic activity for HP-β-CD [28]. Besides, the ionic β-CD derivatives are less effective in promoting CHOL extraction given that the charge decreases the affinity of CDs towards CHOL [27].

With regards to the native γ-CD, it exerted the weakest effect among all CDs. A slight permeabilizing effect was instantly obtained on the various membranes at the highest CD concentration and it disappeared with time. These observations are in agreement with published data where γ-CD always exhibited low vesicle leakage [29]. Actually, γ-CD was found to be less lipid specific than the remaining native CDs (α-CD and β-CD) [8], which implies that the interaction of γ-CD with DPPC would be not favorable. Considering its large cavity in comparison to α and β-CD, γ-CD is not able to extract properly lipid membrane components. This result confirms that the mechanism of CDs-induced permeability is mainly attributed to the lipid extraction mediated by CDs resulting in the formation of a complex between the CD and the lipid membrane components, as reviewed by Nasr et al. in 2020 [14]. Based on our results, γ-CD was active on CHOL-poor membranes. Yet, its effect remains very weak compared to the studied CDs.

Moreover, the instantaneous permeabilizing effect of CDs on 10% CHOL membranes disappeared at 4 and 24 h regardless the CD type and the CD/DPPC molar ratio (Supporting Information File 1). The instantaneous effect of CDs on other membranes was similarly obtained. This may be due to the rapid equilibrium that could be established at 10% CHOL between the membrane and the CD. In fact, CD can instantly interact with the liposome membrane constituents and the extraction of lipid molecules takes place resulting in membrane destabilization. This is illustrated by the rapid leakage of SRB loaded liposomes upon CDs exposure to membranes of different CHOL contents. After this initial effect, the CD would not influence the stability of the bilayer supposing that the membrane is re-organized and the equilibrium between the CD and the membrane is established. Our result for 10% CHOL liposomes is in accordance with that of Hatzi et al. showing an instant calcein release from CHOL-free liposomes (PC and H-PC vesicles) exposed to CDs with no further leakage with time [12]. It is worthy to note, that the 10% CHOL membranes are less stable than the remaining formulations and evidenced the same SRB release pattern as CHOL-free liposomes [15]. Nonetheless, the rapid equilibrium between the CDs and the membrane cannot alone explain the reason behind the disappearance of the CDs effect with time because it does not fully consider the complexation process between the CDs and the membrane components. Another finding obtained by Nishijo and his co-workers [30] may further clarify this idea. The authors studied the interaction of various CDs with CHOL: heptakis(2,6-di-*O*-methyl)-β-CD (DOM-β-CD) was able to form two types of soluble complexes, with molar ratios of 1:1 and 1:2 (CHOL/DOM-β-CD). The latter (1:2 inclusion complex) occurred much more easily than that of the 1:1 complex showing a much higher equilibrium constant. At low CDs concentration, the formation of the 1:1 inclusion complex dominated with low equilibrium constant (109 M^{-1}) suggesting that the unstable complex would rapidly decompose into its components. With time elapsing and with increasing CDs concentration, the 1:1 inclusion complex was transformed into the more stable 1:2 complex with greater equilibrium constant (5.68×10^4 M^{-1}). Therefore, we can

suggest that at high CDs concentration, more of the lipid membrane components would enter the cavity of CDs to form a stable complex instead of refluxing back to the liposomes. Based on these studies, we can assume that the disappearance of the CDs permeabilizing effect with time is additionally accounted for the complexation process occurring between the CDs and the membrane components [30].

Interestingly, a decrease in the permeability was reported with various CDs after t_0 (Figure 2 and Figure 3). This result could be in line with the ability of CDs to stabilize the biological membranes during freeze-drying [8].

Considering the above discussed results, we can assume the dependency of the CDs effect on the membrane permeability on three main parameters: the CHOL content, the CD concentration, and type or more precisely its affinity towards lipid membrane components. At the CD/DPPC molar ratio 1:1, the studied CDs had no effect on the membrane regardless the CHOL content. Their effect occurred above this ratio and was thereafter strongly modulated by the CHOL content depending on the CD's affinity or interaction with lipid membrane components. CHOL-poor membranes were mainly sensitive to the CDs displaying a preferential phospholipids membrane extraction such as α-CD and the β-CD derivatives: HP-β-CD, CRYSMEB, and SBE-β-CD with α-CD being the most potent, whereas CHOL-rich membranes were sensitive to β-CD and its methylated derivative, RAMEB.

Conclusion

In this work, we investigated the effect of CDs on the membrane permeability of DPPC liposomes composed of different CHOL contents at different CD/DPPC molar ratios. The obtained data revealed the dependency of the CD's induced permeability on three main factors: the CHOL content, the CD concentration, and the CD type interpreted by their ability to extract lipid membrane components. No effect was observed for the CD/DPPC molar ratio 1:1 on the membrane permeability for all the CDs. At the ratio 10:1 and 100:1, CDs exhibited different behaviors towards the membrane depending on the CHOL content and the CDs' affinity to the lipid membrane components. Among the studied CDs, α-CD, β-CD, and RAMEB can be classified as the most effective CDs acting on both CHOL-rich and -poor membranes with β-CD and RAMEB showing an enhanced effect at high CHOL content. Hence, β-CD and RAMEB may extract CHOL from raft domains at high CHOL content. The remaining β-CD derivatives (HP-β-CD, CRYSMEB, and SBE-β-CD) showed a lower effect that was mainly observed instantaneously at low CHOL content and it decreased with CHOL content increase. γ-CD showed the weakest effect on the membrane. Increasing time of incubation did not affect the CD permeabilizing effect on the various liposomal membranes.

These results contribute to the better understanding of the CD–membrane interaction and may be very useful in the choice of these CDs as a delivery system. Furthermore, these results may help in the development of the combined delivery system "drug-in-cyclodextrin-in-liposomes" (DCL) where CD–drug inclusion complexes are in contact with the membrane. The choice of CD in such a system does not only depend on the drug affinity towards the CD cavity, but should also take into consideration the affinity of the selected CD towards membrane lipids, the CD–phospholipid molar ratio, and the CHOL content in the membrane.

Experimental

Materials and methods

Materials

α-CD, β-CD, γ-CD, and randomly methylated-β-CD (RAMEB, DS = 12.9), were provided by Wacker Chemie (Germany). Low methylated-β-CD (CRYSMEB, DS = 4.9) and hydroxypropyl-β-CD (HPBCD, DS = 5.6) were provided by Roquette Frères (Lestrem, France). Sulfobutyl ether-β-CD (SBE-β-CD, DS = 6.5) was provided by LIGAND Pharmaceuticals (San Diego, CA, USA). Dipalmitoylphosphatidylcholine (DPPC) and trizma base (buffer reagent) were purchased from Sigma-Aldrich, Switzerland. Triton X-100, sodium chloride (NaCl), and Sephadex G25 gel were purchased from Sigma-Aldrich, Belgium. Ammonium molybdate, hydrogen peroxide, potassium dihydrogen phosphate, sodium sulfite, sodium bisulfite, chloroform, and methanol were purchased from Sigma-Aldrich, Germany. Cholesterol and sulforhodamine B were purchased from Sigma-Aldrich, USA. 4-Amino-3-hydroxy-1-naphthalene sulfonic acid was purchased from Fluka, India. Sulfuric acid was purchased from ACROS Organics, Belgium and diethyl ether was purchased from VWR-Prolabo Chemicals, Belgium.

Liposomes preparation, extrusion, and purification

The SRB-loaded liposomes were prepared, extruded, and purified following the same method described by Nasr et al. [17]. Briefly, the lipid mixture of DPPC and CHOL at the different molar ratios (DPPC/CHOL 100:10, 100:25, 100:50, and 100:100) was dissolved in an organic phase made of chloroform/diethyl ether/methanol 6:6:1 (v/v/v). After a short sonication, the aqueous phase made of SRB (150 mM) dissolved in Tris HCl buffer (0.1 M, pH 7.4) was added to the lipid solution and the mixture was sonicated at 60 °C under a nitrogen stream. The removal of organic solvents was achieved by evaporation at 45 °C using a rotary vacuum evaporator (Heidolph, Germany). Then, the aqueous phase (SRB containing buffer) was added to

the dry film and the mixture was sonicated at 60 °C under a nitrogen stream to generate vesicles. The SRB-loaded liposomes were subjected to extrusion through polycarbonate filter membranes (Avanti Polar Lipids, Switzerland) of decreasing pore sizes resulting in a homogenous mixture of LUVs (large unilamellar vesicles).

Finally, the purification of the SRB-loaded LUVs to eliminate unencapsulated SRB and lipid molecules from liposomes was carried out via a centrifugation (2 hours, 15 000 rpm, 4 °C) and a molecular sieves chromatography (using a Sephadex G25 gel filtration column). A Tris HCl buffer (0.1 M, pH 7.4) containing 150 mM NaCl was used for elution and liposome storage.

Exposure of SRB-loaded liposomes to CDs

The concentration of DPPC was determined for each formulation according to Bartlett method, as previously described by Habib et al. [31]. Then, the liposomal suspensions were all diluted to obtain solutions with a DPPC concentration of 0.15 mM. At time of incubation, the CDs were individually added to the liposomes so that the concentration of CD in the final volume of CD treated liposomes is equal to 0.15 mM, 1.5 mM, and 15 mM in respect to the CD/DPPC molar ratios: 1:1, 10:1, and 100:1, respectively. The fluorescence signal was measured for each sample immediately after the exposure of LUVs to CDs and the samples were incubated at 37 °C during 24 h. For each formulation, a solution containing only liposomes was used as the blank solution.

The membrane permeability study by fluorescence spectroscopy

The membrane permeability is commonly evaluated by following the leakage of self-quenching probes such as SRB from liposomes [14]. Indeed, a fluorescence auto-quenching effect is observed when SRB is encapsulated at a high concentration inside the liposomes. The recovery of the fluorescence signal is achieved upon the release of the dye from liposomes and its dilution in the external medium. Thus, the effect of CDs on the permeability of liposomal membranes was studied by measuring the fluorescence signal of liposomes treated with CDs and incubated at 37 °C. An enhanced membrane permeability is detected when the fluorescence signal is increased demonstrating the permeabilizing effect of the tested agents.

As described in the previous section, the SRB-loaded liposomes of each formulation treated or not with CDs were incubated in a water bath at 37 °C. Aliquots were taken from each sample at 0, 4, and 24 h and the fluorescence signal was measured after a dilution of 100 times in the Tris HCl (0.1 M, pH 7.4) buffer containing 150 mM NaCl.

The measurements were carried out on a spectrophotometer (Hitashi F-7000 Spectrofluorometer) at an excitation wavelength of 535 nm and an emission wavelength of 590 nm. The emission spectrum was recorded in the range 540–700 nm. The results of the permeability study were expressed as the percentage of the fluorophore released from LUVs obtained using Equation 1:

$$\text{SRB release percentage} = \frac{\left(F_t - F_{0,\text{blank}}\right)}{F_{\max}} \times 100, \qquad (1)$$

where F_t is the fluorescence intensity measured at time t for each sample, $F_{0,\text{blank}}$ is the fluorescence intensity measured at time 0 for the blank liposomes of each formulation and $F_{\max}$ is the maximum fluorescence indicating a complete release of SRB from vesicles and obtained in the presence of the nonionic detergent, Triton X-100 (1%) in a Tris HCl buffer (0.1 M, pH 7.4) containing 150 mM NaCl. The results are expressed as the means of three independent experiments ± SD.

To highlight the effect of CDs on the membrane, results are presented by subtracting the SRB release obtained in the presence of CDs from that obtained in their absence.

Statistical analysis

To assess significant differences between values, statistical analysis was carried out using the Student's t-test. A value of $p < 0.05$ was considered statistically significant.

Supporting Information

Supporting Information File 1

Supporting tables.
[https://www.beilstein-journals.org/bjoc/content/supplementary/1860-5397-19-115-S1.pdf]

Funding

The authors thank the Research Funding Program at the Lebanese University for supporting the project (2019–2021).

ORCID® iDs

Sophie Fourmentin - https://orcid.org/0000-0002-4334-0051
Abdelhamid Elaissari - https://orcid.org/0000-0002-2151-9894
Nathalie Khreich - https://orcid.org/0000-0002-2667-2126

References

1. Crini, G. *Chem. Rev.* **2014,** *114,* 10940–10975. doi:10.1021/cr500081p

2. Sharma, N.; Baldi, A. *Drug Delivery* **2016,** *23,* 729–747. doi:10.3109/10717544.2014.938839
3. Duchêne, D.; Bochot, A. *Int. J. Pharm.* **2016,** *514,* 58–72. doi:10.1016/j.ijpharm.2016.07.030
4. Arima, H.; Motoyama, K.; Higashi, T. *Chem. Pharm. Bull.* **2017,** *65,* 341–348. doi:10.1248/cpb.c16-00779
5. Bonnet, V.; Gervaise, C.; Djedaïni-Pilard, F.; Furlan, A.; Sarazin, C. *Drug Discovery Today* **2015,** *20,* 1120–1126. doi:10.1016/j.drudis.2015.05.008
6. Gharib, R.; Greige-Gerges, H.; Fourmentin, S.; Charcosset, C.; Auezova, L. *Carbohydr. Polym.* **2015,** *129,* 175–186. doi:10.1016/j.carbpol.2015.04.048
7. Chen, J.; Lu, W.-L.; Gu, W.; Lu, S.-S.; Chen, Z.-P.; Cai, B.-C.; Yang, X.-X. *Expert Opin. Drug Delivery* **2014,** *11,* 565–577. doi:10.1517/17425247.2014.884557
8. Hammoud, Z.; Khreich, N.; Auezova, L.; Fourmentin, S.; Elaissari, A.; Greige-Gerges, H. *Int. J. Pharm.* **2019,** *564,* 59–76. doi:10.1016/j.ijpharm.2019.03.063
9. Irie, T.; Otagiri, M.; Sunada, M.; Uekama, K.; Ohtani, Y.; Yamada, Y.; Sugiyama, Y. *J. Pharmacobio-Dyn.* **1982,** *5,* 741–744. doi:10.1248/bpb1978.5.741
10. Debouzy, J. C.; Fauvelle, F.; Crouzy, S.; Girault, L.; Chapron, Y.; Göschl, M.; Gadelle, A. *J. Pharm. Sci.* **1998,** *87,* 59–66. doi:10.1021/js970180j
11. Puskás, I.; Csempesz, F. *Colloids Surf., B* **2007,** *58,* 218–224. doi:10.1016/j.colsurfb.2007.03.011
12. Hatzi, P.; Mourtas, S.; Klepetsanis, P. G.; Antimisiaris, S. G. *Int. J. Pharm.* **2007,** *333,* 167–176. doi:10.1016/j.ijpharm.2006.09.059
13. Piel, G.; Piette, M.; Barillaro, V.; Castagne, D.; Evrard, B.; Delattre, L. *Int. J. Pharm.* **2007,** *338,* 35–42. doi:10.1016/j.ijpharm.2007.01.015
14. Nasr, G.; Greige-Gerges, H.; Elaissari, A.; Khreich, N. *Int. J. Pharm.* **2020,** *580,* 119198. doi:10.1016/j.ijpharm.2020.119198
15. Kaddah, S.; Khreich, N.; Kaddah, F.; Charcosset, C.; Greige-Gerges, H. *Food Chem. Toxicol.* **2018,** *113,* 40–48. doi:10.1016/j.fct.2018.01.017
16. Kaddah, S.; Khreich, N.; Kaddah, F.; Khrouz, L.; Charcosset, C.; Greige-Gerges, H. *Biochimie* **2018,** *153,* 33–45. doi:10.1016/j.biochi.2018.06.011
17. Nasr, G.; Greige-Gerges, H.; Elaissari, A.; Khreich, N. *J. Membr. Biol.* **2021,** *254,* 381–395. doi:10.1007/s00232-021-00180-3
18. Sankaram, M. B.; Thompson, T. E. *Proc. Natl. Acad. Sci. U. S. A.* **1991,** *88,* 8686–8690. doi:10.1073/pnas.88.19.8686
19. Simons, K.; Sampaio, J. L. *Cold Spring Harbor Perspect. Biol.* **2011,** *3,* a004697. doi:10.1101/cshperspect.a004697
20. Toppozini, L.; Meinhardt, S.; Armstrong, C. L.; Yamani, Z.; Kučerka, N.; Schmid, F.; Rheinstädter, M. C. *Phys. Rev. Lett.* **2014,** *113,* 228101. doi:10.1103/physrevlett.113.228101
21. Morin-Crini, N.; Fourmentin, S.; Fenyvesi, É.; Lichtfouse, E.; Torri, G.; Fourmentin, M.; Crini, G. *Environ. Chem. Lett.* **2021,** *19,* 2581–2617. doi:10.1007/s10311-020-01156-w
22. Nishijo, J.; Mizuno, H. *Chem. Pharm. Bull.* **1998,** *46,* 120–124. doi:10.1248/cpb.46.120
23. Castagne, D.; Fillet, M.; Delattre, L.; Evrard, B.; Nusgens, B.; Piel, G. *J. Inclusion Phenom. Macrocyclic Chem.* **2009,** *63,* 225–231. doi:10.1007/s10847-008-9510-9
24. Gharib, R.; Fourmentin, S.; Charcosset, C.; Greige-Gerges, H. *J. Drug Delivery Sci. Technol.* **2018,** *44,* 101–107. doi:10.1016/j.jddst.2017.12.009
25. Williams, R. O., III; Mahaguna, V.; Sriwongjanya, M. *Eur. J. Pharm. Biopharm.* **1998,** *46,* 355–360. doi:10.1016/s0939-6411(98)00033-2
26. Stella, V. J.; Rajewski, R. A. *Int. J. Pharm.* **2020,** *583,* 119396. doi:10.1016/j.ijpharm.2020.119396
27. Szente, L.; Fenyvesi, É. *Struct. Chem.* **2017,** *28,* 479–492. doi:10.1007/s11224-016-0884-9
28. Malanga, M.; Szemán, J.; Fenyvesi, É.; Puskás, I.; Csabai, K.; Gyémánt, G.; Fenyvesi, F.; Szente, L. *J. Pharm. Sci.* **2016,** *105,* 2921–2931. doi:10.1016/j.xphs.2016.04.034
29. Nishijo, J.; Shiota, S.; Mazima, K.; Inoue, Y.; Mizuno, H.; Yoshida, J. *Chem. Pharm. Bull.* **2000,** *48,* 48–52. doi:10.1248/cpb.48.48
30. Nishijo, J.; Moriyama, S.; Shiota, S. *Chem. Pharm. Bull.* **2003,** *51,* 1253–1257. doi:10.1248/cpb.51.1253
31. Habib, L.; Khreich, N.; Jraij, A.; Abbas, S.; Magdalou, J.; Charcosset, C.; Greige-Gerges, H. *Int. J. Pharm.* **2013,** *448,* 313–319. doi:10.1016/j.ijpharm.2013.03.027

License and Terms

This is an open access article licensed under the terms of the Beilstein-Institut Open Access License Agreement (https://www.beilstein-journals.org/bjoc/terms), which is identical to the Creative Commons Attribution 4.0 International License (https://creativecommons.org/licenses/by/4.0). The reuse of material under this license requires that the author(s), source and license are credited. Third-party material in this article could be subject to other licenses (typically indicated in the credit line), and in this case, users are required to obtain permission from the license holder to reuse the material.

The definitive version of this article is the electronic one which can be found at:
https://doi.org/10.3762/bjoc.19.115